# THE EVALUATION OF *IN VIVO* RELEASE RATES OF PHARMACEUTICAL PREPARATIONS

by

Frances Stewart

Thesis submitted for the Degree of Doctor of Philosophy in the University of London

The School of Pharmacy

University of London

29/39 Brunswick Square

November 1991

ProQuest Number: U053256

All rights reserved

INFORMATION TO ALL USERS
The quality of this reproduction is dependent upon the quality of the copy submitted.

In the unlikely event that the author did not send a complete manuscript and there are missing pages, these will be noted. Also, if material had to be removed, a note will indicate the deletion.

ProQuest U053256

Published by ProQuest LLC (2017). Copyright of the Dissertation is held by the Author.

All rights reserved.
This work is protected against unauthorized copying under Title 17, United States Code
Microform Edition © ProQuest LLC.

ProQuest LLC.
789 East Eisenhower Parkway
P.O. Box 1346
Ann Arbor, MI 48106 – 1346

# ABSTRACT

Traditional methods for the assessment of drug delivery concentrate on the analysis of the absorption process, however, more recent techniques have enabled the actual release rates of the drugs to be determined. Direct evaluation of the release rate *in vivo* is not practical, as such an approach would be excessively invasive, therefore information about the *in vivo* release process must come from the manipulation of other data. Two methods in particular (Maximum Entropy and Deconvolution) have the ability to provide information about the whole time course of release and can separate the *in vivo* release process from that of absorption.

The Maximum Entropy approach and various deconvolution algorithms were examined for stability to data noise and their ability to predict correctly both the form and values of unknown release rates. This examination was made using pseudo-experimental data, so that the true form of the unknown release rate was known prior to analysis, and using clinical data arising from the administration of controlled release metoprolol tablets. A comparison was made of all the methods tested to find the optimal method for the assessment of *in vivo* release.

The results obtained showed that no one method is optimal for all aspects of the assessment of drug release, but that the method of choice is dependent on the information required. The Maximum Entropy method was shown to be preferred when the aim of the assessment was the study of the *in vivo* release rate as a function of time. However, if a less in depth assessment is required (eg the calculation of MDT or the fraction of dose released vs time) then there was no advantage shown to the use of the more complex methods and one of the simpler deconvolution algorithms becomes the method of choice.

For my Parents

## ACKNOWLEDGEMENTS

Firstly, I would like to thank both London University and the Science and Engineering Research Council who between them, at different stages, funded this research.

I would also like to thank all those in the Pharmaceutics Department at the School of Pharmacy who have provided me not only with endless help and support over the last few years, but also with friendship.

My thanks to Graham, Curt and Sue from the computer unit for being so generous with their time and paper and to all my friends for being just that, but especially Una, Nicky, Aneeta and Rhoda for their sense of humour which made the last three years pass so quickly.

Lastly I would like to thank my parents for giving me the opportunities to be where I am now and for their frequent offers of financial assistance in the firm conviction that all students have no money!

# TABLE OF CONTENTS


ABSTRACT 2

ACKNOWLEDGEMENTS 4

TABLE OF CONTENTS 5

LIST OF FIGURES 14

LIST OF TABLES 20

LIST OF SYMBOLS 28

**1 INTRODUCTION** 34

1.1 THE IMPORTANCE OF THE RATE OF DRUG DELIVERY 34

1.1.1 The Definition of Drug Delivery 34

1.1.2 Controlled Release Products and Drug delivery 34

1.1.3 Evaluation of the Delivery Process 35

1.1.3.1 Single Point Values 35

1.1.3.2 Time Course Analysis 37

1.2 THE USE OF DECONVOLUTION IN PHARMACOKINETICS 39

1.2.1 Linear Systems Approaches 39

1.2.2 Definition of a Linear Systems Approach 40

1.2.3 Definition of Deconvolution 40

1.2.4 The Superposition Principle 42

1.2.5 Applications of Deconvolution 42

1.2.5.1 Calculation of Absorption Rates 42

1.2.5.2 Calculation of *in vivo* Release Rates 43

1.2.5.3 Calculation of Bioavailability 43

1.2.5.4 Calculation of *in vivo* Metabolic Rates 44

1.2.6 The Advantages of Deconvolution Techniques 44

1.2.7 The Disadvantages of Deconvolution Techniques 44

1.3 DECONVOLUTION ALGORITHMS 45

1.3.1 Numerical Methods 45

1.3.1.1 Point-Point Method 45

1.3.1.2 Area-Area Method 47

1.3.1.3 Point-Area Method 48

1.3.1.4 Linear Trapezoidal Method 49

1.3.1.5 Inequality Constrained Least Squares Deconvolution 51

1.3.2 Non-Numerical Methods 52

1.3.2.1 Cutler's Prescribed Input Method 52

1.3.2.2 Cutlers's Method of Orthogonal Polynomials 52

1.3.2.3 Veng-Pederson's Polyexponential Method 53

1.3.2.4 Veng-Pederson's Polynomial Method 54

1.3.2.5 System Identification Methods 54

1.4 AIMS AND OBJECTIVES 55

**2 METHODS** 58

2.1 REGRESSION SUBROUTINES 58

2.1.1 Non-Linear Least Squares Curve Fitting 58

2.1.2 Linear Least Squares Regression 60

2.2 DECONVOLUTION ALGORITHMS 61

2.2.1 Numerical Deconvolution 61

2.2.2 Semi-Numerical Deconvolution 62

2.2.3 Polynomial Deconvolution 63

2.2.4 Polyexponential Deconvolution 66

2.3 GENERATION OF PSEUDO-EXPERIMENTAL DATA 69

2.3.1 Equations Assigned to the Weighting and Input Functions 70

2.3.2 Calculation of the Response Function 70

2.3.2.1 Input Form (a) 70

2.3.2.2 Input Form (b) 71

2.3.2.3 Input Form (c) 72

2.3.3 Addition of Noise to the Data 73

2.4 STATISTICAL METHODS 73

2.4.1 F Test 73

2.4.2 t Test 74

2.5 STATISTICAL MOMENTS 74

2.5.1 Mean Dissolution Time (MDT) 74

**3 COMPARISON OF DECONVOLUTION METHODS USING PSEUDO-EXPERIMENTAL DATA** 77

3.1 MONOEXPONENTIAL INPUT FUNCTION 79

3.1.1 Increasing Levels of Added Noise 79

3.1.1.1 Method 79

3.1.1.2 Results 81

3.1.1.3 Percentage Difference between Predicted and True Values 87

3.1.2 Constant Level of Noise Added to Ten Data Sets 89

3.1.2.1 Method 89

3.1.2.2 Results 92

3.1.2.3 Estimated Fraction Released $F_R$ 97

3.1.2.4 Mean Dissolution Times 99

3.1.3 Discussion 100

3.2 ZERO ORDER RELEASE FUNCTION 101

3.2.1 Increasing Levels of Added Noise 102

3.2.1.1 Method 102

3.2.1.2 Results 105

3.2.1.3 Percentage Difference between Predicted and True Values 111

3.2.2 Constant Level of Noise Added to Ten Data Sets 113

3.2.2.1 Method 113

3.2.2.2 Results 116

3.2.2.3 Estimated Fraction Released $F_R$ 122

3.2.2.4 Mean Dissolution Times 123

3.2.3 Discussion 125

3.3 CONTROLLED RELEASE INPUT FUNCTION 128

3.3.1 Increasing Levels of Added Noise 129

3.3.1.1 Method 129

3.3.1.2 Results 131

3.3.1.3 Percentage Difference between Predicted and True Values 137

3.3.2 Constant Level of Noise Added to Ten Data Sets 139

3.3.2.1 Method 139

3.3.2.2 Results 141

3.3.2.3 Estimated Fraction Released $F_R$ 147

3.3.2.4 Mean Dissolution Times 149

3.3.3 Discussion 150

3.4 CONCLUSIONS 151

**4 *IN VIVO* RELEASE CHARACTERISTICS OF CONTROLLED RELEASE METOPROLOL** 153

4.1 DETAILS OF THE CLINICAL DATA 154

4.2 DETAILS OF THE CONTROLLED RELEASE TABLETS 154

4.3 *IN VITRO* DISSOLUTION STUDIES 154

4.4 JUSTIFICATION OF LINEARITY 155

4.5 METHOD 155

4.5.1 Deconvolution Details 156

4.5.1.1 Numerical Deconvolution 157

4.5.1.2 Semi-Numerical Deconvolution 157

4.5.1.3 Polynomial Deconvolution 158

4.5.1.4 Polyexponential Deconvolution 158

4.5.2 Calculation of the Fraction of Dose Released, $F_R$ 160

4.5.3 Calculation of Mean Dissolution Time *in vivo* , MDT 160

4.6 RESULTS 160

4.6.1 Mean *in vivo* Release Rates 160

4.6.1.1 Similarities 160

4.6.1.2 Differences 165

4.6.2 Mean Cumulative Fraction Released Profiles 165

4.6.2.1 Similarities 165

4.6.2.2 Differences 167

4.6.3 Estimated Fraction of Dose Released, $F_R$ 167

4.6.4 Mean Dissolution Time, $MDT_{30}$ 169

4.6.5 *In vivo* - *in vitro* Correlation using MDT values 171

4.7 DISCUSSION 173

4.8 CONCLUSIONS 174

**5 MAXIMUM ENTROPY IN THE ESTIMATION OF *IN VIVO* DRUG RELEASE / ABSORPTION RATES** 176

5.1 THE APPLICATION OF BAYESIAN METHODS 177

5.1.1 Basis of Probability Theory 177

5.1.2 Inference and Inverse Probability 177

5.2 MAXIMUM ENTROPY 179

5.2.1 The Origins of the Maximum Entropy Equation 179

5.2.2 Assigning Probability Distributions with Maximum Entropy 180

5.2.3 Application of Maximum Entropy to other Distributions 181

5.2.4 Positive Additive Distributions in Pharmacokinetics 182

5.3 COMBINING MAXIMUM ENTROPY AND BAYESIAN INFERENCE 182

5.3.1 Representing the Prior Probability Distribution 182

5.3.2 Representing the Likelihood 184

5.3.3 Combining The Prior and Likelihood 184

5.3.4 The Regularising Parameter $\alpha_R$ 185

5.3.5 Historic vs Classic Maximum Entropy 185

5.4 MAXIMUM ENTROPY TECHNIQUES IN PHARMACOKINETICS 185

5.4.1 A Statement of the Problem 185

5.4.2 Calculation of the Entropy 186

5.4.3 Calculation of the Likelihood 187

5.4.4 Calculation of Predicted Data 187

5.4.4.1 Prediction of the Input Rate from f 187

5.4.4.2 Calculation of Predicted Data from Input Rate 187

5.4.5 The Intrinsic Correlation Function 188

5.5 PRACTICAL IMPLEMENTATION 188

**6 EVALUATION OF MAXENT USING PSEUDO-EXPERIMENTAL DATA** 190

6.1 MONOEXPONENTIAL INPUT FUNCTION 190

6.1.1 Increasing Levels of Added Noise 191

6.1.1.1 Method 191

6.1.1.2 Results 191

6.1.1.3 Percentage Difference between Predicted and True Values 193

6.1.2 Constant Level of Noise Added to Ten Data Sets 194

6.1.2.1 Method 194

6.1.2.2 Results 195

6.1.2.3 Estimated Fraction Released $F_R$ 197

6.1.2.4 Mean Dissolution Times 198

6.1.3 Discussion 198

6.2 ZERO ORDER INPUT FUNCTION 199

6.2.1 Increasing Levels of Added Noise 199

6.2.1.1 Method 199

6.2.1.2 Results 200

6.2.1.3 Percentage Difference between Predicted and True Values 202

6.2.2 Constant Level of Noise Added to Ten Data Sets 203

6.2.2.1 Method 203

6.2.2.2 Results 204

6.2.2.3 Estimated Fraction Released $F_R$ 206

6.2.2.4 Mean Dissolution Times 207

6.2.3 Discussion 208

6.3 CONTROLLED RELEASE INPUT FUNCTION 209

6.3.1 Increasing Levels of Added Noise 209

6.3.1.1 Method 209

6.3.1.2 Results 210

6.3.1.3 Percentage Difference between Predicted and True Values 212

6.3.2 Constant Level of Noise Added to Ten Data Sets 213

6.3.2.1 Method 213

6.3.2.2 Results 214

6.3.2.3 Estimated Fraction Released $F_R$ 216

6.3.2.4 Mean Dissolution Times 217

6.3.3 Discussion 218

6.4 CONCLUSIONS 218

**7 *IN VIVO* RELEASE OF CR METOPROLOL TABLETS PREDICTED BY MAXENT** 221

7.1 METHOD 222

7.1.1 Calculation of *In vivo* Dissolution Rates 222

7.1.2 Calculation of *In vitro* Dissolution Rate 223

7.1.3 Calculation of the Fraction of Dose Released, $F_R$ 223

7.1.4 Calculation of Mean Dissolution Time *in vivo*, MDT 223

7.2 RESULTS 223

7.2.1 *In vivo* Release Characteristics for Individual Subjects 223

7.2.1.1 Metoprolol CR A 228

7.2.1.2 Metoprolol CR B 228

7.2.1.3 Metoprolol CR C 229

7.2.2 Mean *in vivo* Dissolution Rates 229

7.2.3 Estimated Fraction of Dose Released, $F_R$ 231

7.2.4 Mean Dissolution Time, $MDT_{30}$ 235

7.2.5 *In vivo* - *in vitro* Correlation 238

7.2.5.1 $MDT_{in\ vivo}$ vs $_{in\ vitro}$ Correlation 238

7.2.5.2 Comparison of *In vivo* and *In vitro* Dissolution Rates 241

7.3 DISCUSSION 241

7.4 CONCLUSIONS 243

**8 GENERAL DISCUSSION AND CONCLUSIONS** 244

8.1 GENERAL DISCUSSION 244

8.1.1 Stability to Data Noise 244

8.1.2 The Input Rate Profiles 245

8.1.3 Cumulative Fraction Input Profiles 246

8.1.4 Fraction of Dose Released, $F_R$ 246

8.1.5 Mean Dissolution Time, MDT 246

8.1.6 Analysis of Metoprolol Data 247

8.1.7 Some other Observations 249

8.2 SUGGESTIONS FOR FURTHER WORK 250

8.3 CONCLUSIONS 252

REFERNECES 254

APPENDIX A 262

APPENDIX B 268

APPENDIX C 272

APPENDIX D 281

APPENDIX E 288

# LIST OF FIGURES

Figure 1 : Input Rates produced by Numerical Deconvolution for the Monoexponential Input Function with Increasing Levels of Error added to both the Weighting and Response Functions 83

Figure 2 : Cumulative Input produced by Numerical Deconvolution for the Monoexponential Input Function with Increasing Levels of Error added to both Weighting and Response Functions. 83

Figure 3 : Input Rate produced by Semi-Numerical Deconvolution for the Monoexponential Input Function with Increasing Levels of Error added to both the Weighting and Response Functions. 84

Figure 4 : Cumulative Input produced by Semi-numerical Deconvolution for the Monoexponential Input Function with Increasing Levels of Error added to both Weighting and Response Functions. 84

Figure 5 : Input Rates produced by Polynomial Deconvolution for the Monoexponential Input Function with Increasing Levels of Error added to both the Weighting and Response Functions. 85

Figure 6 : Cumulative Input produced by Polynomial Deconvolution for the Monoexponential Input Function with Increasing Levels of Error added to both the Weighting and Response Functions. 85

Figure 7 : Input Rates produced by Polyexponential Deconvolution for the Monoexponential Input Function with Increasing Levels of Error added to both Weighting and Response Functions. 86

Figure 8 : Cumulative Input produced by Polyexponential Deconvolution for the Monoexponential Input Function with Increasing Levels of error added to both Weighting and Response Functions. 86

Figure 9 : Mean results produced by Numerical Deconvolution for the Monoexponential Input Function on 10 Data Sets with 10% Error added to both the Weighting and Response Functions 93

Figure 10 : Mean results produced by Semi-Numerical Deconvolution for the Monoexponential Input Function on 10 Data Sets with 10% Noise added to both the Weighting and Response Functions 94

Figure 11 : Mean results produced by Polynomial Deconvolution for the Monoexponential Input Function on 10 Data Sets with 10% Error added to both the Weighting and Response Functions 95

Figure 12 : Mean results produced by Polyexponential Deconvolution for the Monoexponential Input Function on 10 Data Sets with 10% Error added to both the Weighting and Response Functions 96

Figure 13 : Input Rates produced by Numerical Deconvolution for the Zero Order Input Function with Increasing Levels of Error added to both the Weighting and Response Functions 106

Figure 14 : Cumulative Input produced by Numerical Deconvolution for the Zero Order Input Function with Increasing Levels of Error added to both Weighting and Response Functions. 106

Figure 15 : Input Rate produced by Semi-Numerical Deconvolution for the Zero Order Input Function with Increasing Levels of Error added to both the Weighting and Response Functions. 108

Figure 16 : Cumulative Input produced by Semi-numerical Deconvolution for the Zero Order Input Function with Increasing Levels of Error added to both Weighting and Response Functions. 108

Figure 17 : Input Rates produced by Polynomial Deconvolution for the Zero Order Input Function with Increasing Levels of Error added to both the Weighting and Response Functions. 109

Figure 18 : Cumulative Input produced by Polynomial Deconvolution for the Zero Order Input Function with Increasing Levels of Error added to both the Weighting and Response Functions. 109

Figure 19 : Input Rates produced by Polyexponential Deconvolution for the Zero Order Input Function with Increasing Levels of Error added to both Weighting and Response Functions. 110

Figure 20 : Cumulative Input produced by Polyexponential Deconvolution for the Zero Order Input Function with Increasing Levels of error added to both Weighting and Response Functions. 110

Figure 21 : Mean results produced by Numerical Deconvolution for the Zero Order Input Function on 10 Data Sets with 10% Noise added to the Weighting and Response Functions 117

Figure 22 : Mean results produced by Semi-Numerical Deconvolution for the Zero Order Input Function on 10 Data Sets with 10% Noise added to both the Weighting and Response Functions 119

Figure 23 : Mean results produced by Polynomial Deconvolution for the Zero Order Input Function on 10 Data Sets with 10% Error added to both the Weighting and Response Functions 120

Figure 24 : Mean results produced by Polyexponential Deconvolution for the Zero Order Input Function on 10 Data Sets with 10% Error added to both the Weighting and Response Functions 121

Figure 25 : Input Rates produced by Numerical Deconvolution for the Controlled Release Input Function with Increasing Levels of Error added to both the Weighting and Response Functions 132

Figure 26 : Cumulative Input produced by Numerical Deconvolution for the Controlled Release Input Function with Increasing Levels of Error added to both Weighting and Response Functions. 132

Figure 27 : Input Rate produced by Semi-Numerical Deconvolution for the Controlled Release Input Function with Increasing Levels of Error added to both the Weighting and Response Functions. 134

Figure 28 : Cumulative Input produced by Semi-numerical Deconvolution for the Controlled Release Input Function with Increasing Levels of Error added to both Weighting and Response Functions. 134

Figure 29 : Input Rates produced by Polynomial Deconvolution for the Controlled Release Input Function with Increasing Levels of Error added to both the Weighting and Response Functions. 135

Figure 30 : Cumulative Input produced by Polynomial Deconvolution for the Controlled Release Input Function with Increasing Levels of Error added to both the Weighting and Response Functions. 135

Figure 31 : Input Rates produced by Polyexponential Deconvolution for the Controlled Release Input Function with Increasing Levels of Error added to both Weighting and Response Functions. 136

Figure 32 : Cumulative Input produced by Polyexponential Deconvolution for the Controlled Release Input Function with Increasing Levels of error added to both Weighting and Response Functions. 136

Figure 33 : Mean results produced by Numerical Deconvolution for the Controlled Release Input Function on 10 Data Sets with 10% Noise added to the Weighting and Response Functions 143

Figure 34 : Mean results produced by Semi-Numerical Deconvolution for the Controlled Release Input Function on 10 Data Sets with 10% Noise added to both the Weighting and Response Functions 144

Figure 35 : Mean results produced by Polynomial Deconvolution for the Controlled Release Input Function on 10 Data Sets with 10% Error added to both the Weighting and Response Functions 145

Figure 36 : Mean results produced by Polyexponential Deconvolution for the Controlled Release Input Function on 10 Data Sets with 10% Error added to both the Weighting and Response Functions 146

Figure 37 : Mean Results (n=10) produced by Numerical Deconvolution of Three Controlled Release Metoprolol 95mg Tablets 161

Figure 38 : Mean Results (n=10) produced by Semi-Numerical Deconvolution of Three Controlled Release Metoprolol 95mg Tablets 162

Figure 39 : Mean Results (n=10) produced by Polynomial Deconvolution of Three Controlled Release Metoprolol 95mg Tablets 163

Figure 40 : Release Rate and Cumulative Fraction Released for Three Metoprolol CR Tablets predicted by Polyexponential Deconvolution 164

Figure 41 : Fraction of Dose Released predicted by Four Deconvolution Methods for Three Metoprolol CR Tablets 166

Figure 42 : Input Rates produced by MAXENT for the Monoexponential Input Function with Increasing Levels of Error added to both the Weighting and Response Functions 192

Figure 43 : Cumulative Input produced by MAXENT for the Monoexponential Input Function with Increasing Levels of Error added to both Weighting and Response Functions. 192

Figure 44 : Mean results (n=10) produced by MAXENT for the Monoexponential Input Function with 10% Error added to both the Weighting and Response Functions 196

Figure 45 : Input Rates produced by MAXENT for the Zero Order Input Function with Increasing Levels of Error added to both the Weighting and Response Functions 201

Figure 46 : Cumulative Input produced by MAXENT for Zero Order Input Function with Increasing Levels of Error added to both Weighting and Response Functions. 201

Figure 47 : Mean results (n=10) produced by MAXENT for the Zero Order Input Function with 10% Error added to both the Weighting and Response Functions 205

Figure 48 : Input Rates produced by MAXENT for Controlled Release Input Function with Increasing Levels of Error added to both the Weighting and Response Functions 211

Figure 49 : Cumulative Input produced by MAXENT the Controlled Release Input Function with Increasing Levels of Error added to both Weighting and Response Functions. 211

Figure 50 : Mean results (n=10) produced by MAXENT for the Controlled Release Input Function with 10% Error added to both the Weighting and Response Functions 215

Figure 51 : Results from MAXENT for Metoprolol CR A, Subject 1 225

Figure 52 : Results from MAXENT for Metoprolol CR B, Subject 1 226

Figure 53 : Results from MAXENT for Metoprolol CR C, Subject 1 227

Figure 54 : Mean Results (n=10) produced by MAXENT for Three Controlled Release Metoprolol 95mg Tablets 230

Figure 55 : Mean *in vivo* (n=10) and *in vitro* (n=6) Dissolution Rates produced by MAXENT for Three Controlled Release Metoprolol 95mg Tablets 239

Figure 56 : Mean *in vivo* (n=10) CFI profiles produced by MAXENT and mean *in vitro* (n=6) CFI profiles for 3 Controlled Release Metoprolol 95mg Tablets 240

Figures E(1)-E(10) : Results from MAXENT for Metoprolol CR A, Subjects 1-10 288

Figures E(11)-E(20) : Results from MAXENT for Metoprolol CR B, Subjects 1-10 298

Figures E(21)-E(30) : Results from MAXENT for Metoprolol CR C, Subjects 1-10 308

# LIST OF TABLES

Table 1 : Weighting Function data produced by $W(t) = -2e^{-10t} + e^{-5t} + e^{-t}$ , Input Function Data produced from $I(t) = 1.2e^{-2t}$ and Response Data produced from Convolution of the Weighting and Input Functions 78

Table 2(a) : Parameters obtained following Curve-fitting of Weighting Data, shown in Table C(1a), to a Polyexponential with Constants $A_i$ and Exponents $\alpha_i$. 80

Table 2(b) : Parameters obtained following Curve-fitting of Response Data, shown in Table C(1b), to a Polyexponential with Constants $A_i$ and Exponents $\alpha_i$. 80

Table 3 : Selected Polynomials produced by Polynomial Deconvolution on Data (from Table C(1)) with Increasing Levels of Added Noise 81

Table 4 : Mean Percentage Difference for Input Rate Values shown in Figures 1,3,5 and 7 for Increasing Levels of Added Noise. The S.E.M. values are shown in Parentheses (n=39). 88

Table 5 : Mean Percentage Difference for Cumulative Fraction Input Values shown in Figures 2,4,6 and 8 for Increasing Levels of Added Noise. The S.E.M. values are shown in Parentheses (n=39). 88

Table 6 : Parameters Obtained following Curve-fitting of the Weighting Data, shown in Table C(2), to a Polyexponential with Constants $A_i$ and Exponents $\alpha_i$. 90

Table 7 : Parameters obtained following Curve-fitting of Response Data, shown in Table C(3), to a Polyexponential with Constants $A_i$ and Exponents $\alpha_i$. 90

Table 8 : Selected Polynomials produced by Polynomial Deconvolution on Data from Tables C(2) and C(3). 91

Table 9 : Fraction of Dose Released predicted by Four Deconvolution Algorithms for a Release Rate of $I(t) = 1.2e^{-2t}$ with 10% Noise added to both Weighting and Response Functions 98

Table 10 : Mean Dissolution Times Estimated for the Input Rates produced by Four Deconvolution Algorithms for a Release Rate of $I(t) = 1.2e^{-2t}$ with 10% Noise added to both Weighting and Response Functions. 99

Table 11 : Weighting Function data produced by $W(t) = -2e^{-10t} + e^{-5t} + e^{-t}$ , Input Function Data produced from $I(t) = 0.5$ for $t \leq 0.8$ and $0.5e^{-2.5(t-0.8)}$ for $t > 0.8$ and Response Data produced from Convolution of the Weighting and Input Functions 102

Table 12(a) : Parameters obtained following Curve-fitting of Weighting Data, shown in Table C(4a), to a Polyexponential with Constants $A_i$ and Exponents $\alpha_i$. 103

Table 12(b) : Parameters obtained following Curve-fitting of Response Data, shown in Table C(4b), to a Polyexponential with Constants $A_i$ and Exponents $\alpha_i$. 103

Table 13 : Selected Polynomials produced by Polynomial Deconvolution on Data (from Table C(4)) with Increasing Levels of Added Noise 104

Table 14 : Mean Percentage Difference for Input Rate Values shown in Figures 13,15,17 and 19 for Increasing Levels of Added Noise. The S.E.M. values are shown in Parentheses (n=39). 112

Table 15 : Mean Percentage Difference for Cumulative Fraction Input Values shown in Figures 14,16,18 and 20 for Increasing Levels of Added Noise. The S.E.M. values are shown in Parentheses (n=39). 113

Table 16 : Parameters Obtained following Curve-fitting of the Weighting Data, shown in Table C(5), to a Polyexponential with Constants $A_i$ and Exponents $\alpha_i$. 114

Table 17 : Parameters obtained following Curve-fitting of Response Data, shown in Table C(6), to a Polyexponential with Constants $A_i$ and Exponents $\alpha_i$. 115

Table 18 : Selected Polynomials produced by Polynomial Deconvolution on Data from Tables C(5) and C(6). 115

Table 19 : Fraction of Dose Released predicted by Four Deconvolution Algorithms for a Release Rate of $I(t) = 0.5$ for $t \leq 0.8$ and $I(t) = 0.5e^{-2.5(t-0.8)}$ with 10% Noise added to both Weighting and Response Functions 123

Table 20 : Mean Dissolution Times Estimated for the Input Rates produced by Four Deconvolution Algorithms for a Release Rate of $I(t) = 0.5$ for $t \leq 0.8$ and $I(t) = 0.5e^{-2.5(t-0.8)}$ for $t > 0.8$ with 10% Noise added to both Weighting and Response Functions. 124

Table 21 : Weighting Function data produced by $W(t) = -2e^{-10t} + e^{-5t} + e^{-t}$ , Input Function Data represented by the controlled release input function and Response Data produced from Convolution of the Weighting and Input Functions 128

Table 22(a) : Parameters obtained following Curve-fitting of Weighting Data, shown in Table C(7a), to a Polyexponential with Constants $A_i$ and Exponents $\alpha_i$. 129

Table 22(b) : Parameters obtained following Curve-fitting of Response Data, shown in Table C(7b), to a Polyexponential with Constants $A_i$ and Exponents $\alpha_i$. 130

Table 23 : Selected Polynomials produced by Polynomial Deconvolution on Data (from Table C(7)) with Increasing Levels of Added Noise 131

Table 24 : Mean Percentage Difference for Input Rate Values shown in Figures 25,27,29 and 31 for Increasing Levels of Added Noise. The S.E.M. values are shown in Parentheses (n=39). 137

Table 25 : Mean Percentage Difference for Cumulative Fraction Input Values shown in Figures 26,28,30 and 32 for Increasing Levels of Added Noise. The S.E.M. values are shown in Parentheses (n=39). 138

Table 26 : Parameters Obtained following Curve-fitting of the Weighting Data, shown in Table C(8), to a Polyexponential with Constants $A_i$ and Exponents $\alpha_i$. 139

Table 27 : Parameters obtained following Curve-fitting of Response Data, shown in Table C(9), to a Polyexponential with Constants $A_i$ and Exponents $\alpha_i$. 140

Table 28 : Selected Polynomials produced by Polynomial Deconvolution on Data from Tables C(8) and C(9). 141

Table 29 : Fraction of Dose Released predicted by Four Deconvolution Algorithms for the Controlled Release Input Rate with 10% Noise added to both Weighting and Response Functions 148

Table 30 : Mean Dissolution Times Estimated for the Input Rates produced by Four Deconvolution Algorithms for the Controlled Release Input Rate with 10% Noise added to both Weighting and Response Functions. 149

Table 31 : Parameters obtained by Curve Fitting Plasma Concentrations following administration of Metoprolol Solution 95mg(shown in Table D(1)) to a polyexponential equation (shown in equation (4.1)). 156

Table 32 : Parameters obtained following Curve Fitting of Plasma Concentrations from Metoprolol CR A (Table D(2)) to a polyexponential (equation 4.1) 158

Table 33 : Parameters obtained following Curve Fitting of Plasma Concentrations from Metoprolol CR B (Table D(3)) to a polyexponential (equation 4.1) 159

Table 34 : Parameters obtained following Curve Fitting of Plasma Concentrations from Metoprolol CR C (Table D(4)) to a polyexponential (equation 4.1) 159

Table 35 : Estimated Fraction of Dose Released, $F_R$, in ten subjects, predicted for Three CR Metoprolol Tablets (CR A,CR B and CR C) by Four Deconvolution Methods. 168

Table 36 : ANOVA table for log Transforms of the Estimated Fraction Released data (shown in Table 35) for different Metoprolol CR tablets and Deconvolution methods. (Model I - two way) 169

Table 37 : Estimated Mean Dissolution Time $MDT_{30}$, in ten subjects, predicted for Three CR Metoprolol Tablets (CR A,CR B and CR C) by Four Deconvolution Methods. 170

Table 38 : ANOVA table for the Mean Dissolution Time data (shown in Table 37) for different Metoprolol CR tablets and Deconvolution methods. (Model I - two way) 171

Table 39 : *In vitro* MDT (hrs) calculated for three Metoprolol CR Tablets from data shown in Tables D(5)-D(7) 172

Table 40 : Parameters obtained following Linear Regression of $MDT_{in\ vivo}$ against the $MDT_{in\ vitro}$ for Three Metoprolol CR Tablets. 172

Table 41 : Mean Percentage Difference for Input Rate Values shown in Figure 42 for Increasing Levels of Added Noise. 193

Table 42 : Mean Percentage Difference for Cumulative Fraction Input Values shown in Figure 43 for Increasing Levels of Added Noise. 194

Table 43 : Fraction of Dose Released predicted by MAXENT for a Release Rate of I(t) = $1.2e^{-2t}$ with 10% Noise Added to both Weighting and Response Functions 197

Table 44 Mean Dissolution Times Estimated for the Input Rates predicted by MAXENT for a Release Rate of I(t) = $1.2e^{-2t}$ with 10% Noise Added to both Weighting and Response Functions 198

Table 45 : Mean Percentage Difference for Input Rate Values shown in Figure 45 for Increasing Levels of Added Noise. 202

Table 46 : Mean Percentage Difference for Cumulative Fraction Input Values shown in Figure 46 for Increasing Levels of Added Noise. 203

Table 47 : Fraction of Dose Released predicted by MAXENT for a Release Rate of I(t) = 0.5 for $t \leq 0.8$ and $I(t) = 0.5e^{-2.5(t-0.8)}$ for $t > 0.8$ with 10% Noise Added to both Weighting and Response Functions 206

Table 48 Mean Dissolution Times Estimated for the Input Rates predicted by MAXENT for a Release Rate of I(t) = 0.5 for $t \leq 0.8$ and $I(t) = 0.5e^{-2.5(t-0.8)}$ with 10% Noise Added to both Weighting and Response Functions 207

Table 49 : Mean Percentage Difference for Input Rate Values shown in Figure 48 for Increasing Levels of Added Noise. 212

Table 50 : Mean Percentage Difference for Cumulative Fraction Input Values shown in Figure 49 for Increasing Levels of Added Noise. 213

Table 51 : Fraction of Dose Released predicted by MAXENT for the Controlled Release Input Function with 10% Noise Added to both Weighting and Response Functions 216

Table 52 Mean Dissolution Times Estimated for the Input Rates predicted by MAXENT for the Controlled Release Input Function with 10% Noise Added to both Weighting and Response Functions 217

Table 53 : Estimated Fraction of Dose Released, $F_R$, in ten subjects, predicted for Three CR Metoprolol Tablets (CR A, CR B and CR C) by MAXENT 232

Table 54 : Calculated $F_{diff}$ values, in ten subjects, predicted for Three CR Metoprolol Tablets (CR A,CR B and CR C) by MAXENT 233

Table 55 : Values of the $t_s$ statistic, calculated for a Paired t-test between the values of $F_R$ produced by MAXENT and those Produced by Four Deconvolution Methods 234

Table 56 : Mean $F_R$ values predicted for Three Metoprolol CR Tablets by MAXENT and Four Deconvolution Algorithms. 234

Table 57 : Estimated Mean Dissolution Time / hours, $MDT_{30}$, in ten subjects, predicted for Three CR Metoprolol Tablets (CR A, CR B and CR C) by MAXENT 235

Table 58 : Calculated $MDT_{diff}$ values for 10 subjects, predicted for Three CR Metoprolol Tablets (CR A,CR B and CR C) by MAXENT. 236

Table 59 : Values of the $t_s$ statistic, calculated for a Paired t-test between the values of $MDT_{30}$ produced by MAXENT and those Produced by Four Deconvolution Methods 237

Table 60 : Parameters obtained following Linear Regression of $MDT_{in\ vivo}$ (produced by MAXENT) against $MDT_{in\ vitro}$ for Three Metoprolol CR Tablets 238

Table C(1a) : Pseudo-Experimental Weighting Function Values used in Chapter 3 with Increasing Levels of Added Noise and Generated from the Equation $W(t) = -2e^{-10t} + e^{-t} + e^{-5t}$. 272

Table C(1b) : Pseudo-Experimental Response Function Values used in Chapter 3 with Increasing Levels of Added Noise and Generated from the Equations $W(t) = -2e^{-10t} + e^{-t} + e^{-5t}$ and $I(t) = 1.2e^{-2t}$ according to the Method Described in Section 2.3.2 272

Table C(2) : Pseudo-Experimental Weighting Function Values used in Chapter 3 with a Noise Level of 10% and Generated from the Equation $W(t) = -2e^{-10t} + e^{-t} + e^{-5t}$ 273

Table C(3) : Pseudo-Experimental Response Function Values used in Chapter 3 (section 3.1) with a Noise Level of 10% and Generated from the Equations $W(t) = -2e^{-10t} + e^{-t} + e^{-5t}$ and $I(t) = 1.2e^{-2t}$ according to the Method Described in Section 2.3.2 274

Table C(4a) : Pseudo-Experimental Weighting Function Values used in Chapter 3 with Increasing Levels of Added Noise and Generated from the Equation $W(t) = -2e^{-10t} + e^{-t} + e^{-5t}$. 275

Table C(4b) : Pseudo-Experimental Response Function Values used in Chapter 3 with Increasing Levels of Added Noise and Generated from the Equations $W(t) = -2e^{-10t} + e^{-t} + e^{-5t}$ and $I(t) = 0.5$ for $t \leq 0.8$ and $I(t) = 0.5e^{-2.5(t-0.8)}$ for $t > 0.8$ according to the Method Described in Section 2.3.2 275

Table C(5) : Pseudo-Experimental Weighting Function Values used in Chapter 3 with a Noise Level of 10% and Generated from the Equation $W(t) = -2e^{-10t} + e^{-t} + e^{-5t}$ 276

Table C(6) : Pseudo-Experimental Response Function Values used in Chapter 3 (section 3.1) with a Noise Level of 10% and Generated from the Equations $W(t) = -2e^{-10t} + e^{-t} + e^{-5t}$ and $I(t) = 0.5$ for $t \leq 0.8$ and $I(t) = 0.5e^{-2.5(t-0.8)}$ according to the Method Described in Section 2.3.2 277

Table C(7a) : Pseudo-Experimental Weighting Function Values used in Chapter 3 with Increasing Levels of Added Noise and Generated from the Equation $W(t) = -2e^{-10t} + e^{-t} + e^{-5t}$. 278

Table C(7b) : Pseudo-Experimental Response Function Values used in Chapter 3 with Increasing Levels of Added Noise and Generated from the Equations $W(t) = -2e^{-10t} + e^{-t} + e^{-5t}$ and the Controlled Release Input Function according to the Method Described in Section 2.3.2 278

Table C(8) : Pseudo-Experimental Weighting Function Values used in Chapter 3 with a Noise Level of 10% and Generated from the Equation

$W(t) = -2e^{-10t} + e^{-t} + e^{-5t}$ 279

Table C(9) : Pseudo-Experimental Response Function Values used in Chapter 3 (section 3.1) with a Noise Level of 10% and Generated from the Equations $W(t) = -2e^{-10t} + e^{-t} + e^{-5t}$ and the Controlled Release Input Function according to the Method Described in Section 2.3.2 280

Table D(1) : Individual Plasma Concentrations (μmol/l) after Oral Administration of Metoprolol Succinate Solution 95mg. 281

Table D(2) : Individual Plasma Concentrations (μmol/l) after Oral Administration of CR A ; Metoprolol Succinate CR Tablet 95mg. 282

Table D(3) : Individual Plasma Concentrations (μmol/l) after Oral Administration of CR B ; Metoprolol Succinate CR Tablet 95mg. 283

Table D(4) : Individual Plasma Concentrations (μmol/l) after Oral Administration of CR C ; Metoprolol Succinate CR Tablet 95mg. 284

Table D(5) : Mean and SD (n=6) per cent Metoprolol released *in vitro* at Different Times for CR A ; Metoprolol Succinate CR 95mg 285

Table D(6) : Mean and SD (n=6) per cent Metoprolol released *in vitro* at Different Times for CR B ; Metoprolol Succinate CR 95mg 286

Table D(7) : Mean and SD (n=6) per cent Metoprolol released *in vitro* at Different Times for CR C ; Metoprolol Succinate CR 95mg 287

# LIST OF SYMBOLS

| | |
|---|---|
| $\alpha$ | probability level |
| $\alpha_i$ | exponent of the polyexponential used to represent the weighting function |
| $\alpha_R$ | a regularising parameter |
| $\beta_i$ | exponent of the polyexponential used to represent the response function |
| $\beta_L$ | a Lagrange multiplier |
| $\gamma_i$ | the roots of polynomial Q(x) |
| $\delta(t-t_i)$ | the delta function |
| $\Delta m_i$ | mass released during the interval $\Delta t$ |
| $\Delta t$ | a short time interval |
| $\theta_j$ | complex function used to represent part of the response function for the polynomial deconvolution method |
| $\varphi(t)$ | function of $g_i$, $\gamma_i$ and t |
| $\Phi(S)$ | a monotonically increasing function of the entropy S |
| $\chi^2$ | chi-squared value |
| $\psi(t)$ | function of $g_i$, $\gamma_i$ and t |
| a | the number of separate samples in Hartley's $F_{max}$ test |
| $A_i$ | coefficient of the polyexponential use to represent the weighting function |
| ANOVA | analysis of variance |
| AUC | the area under a plasma concentration - time curve |
| $b_i$ | coefficient of the polyexponential used to represent the response function |
| $B_i$ | function of $b_i$ and $\beta_i$ |
| C | matrix of coefficients |
| C(t) | plasma concentration at time t |

| | |
|---|---|
| $C_{max}$ | the maximum plasma concentration reached following administration of an extravascular dose |
| C(x,t) | intrinsic correlation function |
| CFI | cumulative fraction input |
| $C_i$ | coefficient of a polynomial |
| CR | controlled release |
| **d** | the default value for the distribution h |
| **D** | experimental data |
| D | extravascular dose administered |
| df | degrees of freedom |
| $d_i$ | default value for the hypothesis value $h_i$ |
| DILS | direct integral least squares |
| $D_O$ | dose administered to produce the response function |
| $D_r$ | the dose remaining at $t_c$ |
| E | a vector containing error values $E_i$ |
| $E^T$ | transpose of vector E |
| F | value calculated for the F test |
| **f** | vector related to the input function I |
| f(t) | probability density function of a random variable |
| F(t) | cumulative distribution of a random variable |
| f(x) | an arbitrary function of x |
| $F_b$ | bioavailability |
| $f_i$ | cumulative amount input over a time interval $t_{i-1}$ to $t_i$ |
| $F_{max}$ | value of Hartley's $F_{max}$ test |
| $F_R$ | fraction of dose released |

$\bar{F}_R$ mean fraction of dose released

$g_i$ a set of values obtained from $\gamma_i$

**h** vector representing the distribution h(x)

h(x) distribution h as a function of x, where x is any variable

h hypothesis

H(t-tlag) Heaviside unit step function

I a vector representing the input rate, with elements $I_i$

I(s) the Laplace transform of the input function

I(t) input function

ICF intrinsic correlation function

$I_f$ previous known information

$I_i$ $I(i.\Delta t)$ the value of the input rate at $i.\Delta t$

$I^T$ transpose of vector I

IV intravenous

k first order rate constant for the monoexponential input function

$k_0$ zero order rate constant for the zero order input function

$k_a$ absorption rate constant

L an integer

L(h) the likelihood

**logprob** a value returned from the MAXENT program

MAT mean absorption time

MAXENT the application of the principle of maximum entropy

MDT mean dissolution time

$MDT_t$ the mean dissolution time calculated up to a time t

| | |
|---|---|
| $M_i$ | represents the message in Shannon's Entropy Equation |
| MRT | mean residence time |
| MS | mean sum of squares , SS/df |
| MT | mean time associated with a random variable |
| $m_t$ | mass dissolved at time t |
| $M\bar{D}T$ | mean value of MDT |
| $m_\infty$ | mass dissolved at $t=\infty$ |
| NAG | Nottingham Algorithms Group |
| P | probability |
| p | vector of parameters |
| P(A + B) | the probability that either A or B is true |
| P(A) | the probability that A is true |
| P(A,B) | the joint probability of A and B being true |
| P(A\|B) | the probability of A given that B is true |
| P(B) | the probability that B is true |
| P(B\|A) | the probability of B given that A is true |
| PAD | positive additive distribution |
| PCT | cumulative percentage input |
| PCT($\infty$) | cumulative percentage input at $t=\infty$ |
| Q | an unknown function of $\alpha_R$, the entropy S and the likelihood |
| Q(x) | a polynomial of x |
| R | a vector containing elements of the response function $R_i$ |
| r | correlation coefficient |
| $R'(t)$ | first derivative of the response function |

| | |
|---|---|
| R(s) | the Laplace transform of the response function |
| R(t) | response function |
| $R_e$ | predicted plasma concentration |
| $R_i$ | $R(i.\Delta t)$ the value of the response function at $i.\Delta t$ |
| $R^T$ | transpose of vector R |
| S(h) | the entropy of a distribution h |
| SD | standard deviation |
| SEM | standard error of the mean |
| SS | sum of squares |
| SVD | singular value decomposition |
| $t_0$ | lag time associated with the response function |
| $t_c$ | the time at which the zero order input ceases |
| $\bar{t}_i$ | the mid-point of the time interval $t_{i-1}$ to $t_i$ |
| $t_i$ | the time corresponding to the ith time interval |
| tlag | time lag |
| $T_{max}$ | the time at which the maximum plasma concentration is reached following administration of an extravascular dose |
| $t_s$ | value of the t statistic used in the t-test |
| $u_i$ | a complex function of $\beta_i$, $g_i$, $B_i$ and $\gamma_i$ |
| V | covaraince matrix |
| $v_i$ | a complex function of $\gamma_i$ or $\beta_i$ |
| W | a matrix containing elements of the weighting function $W_{ij}$ |
| W(s) | the Laplace transform of the weighting function |
| W(t) | weighting function |
| $W_e(t)$ | the weighting function produced from a non-unit dose |

| | |
|---|---|
| $W_i$ | $W(i.\Delta t)$ the value of the weighting function at $i.\Delta t$ |
| $\bar{w}_i$ | the value of w(t) at the mid-point of the time interval $t_{i-1}$ to $t_i$ |
| WSS | weighted sum of squares |
| $wt_i$ | the weight assigned to data point i |
| x | percentage of noise added to data |
| $\bar{Y}$ | sample mean |
| y(x,p) | estimated value of y at the same point x as $y_i$ |
| $Y_0$ | standard value used in the t test |
| $y_i$ | experimental value at data point i |
| $Z_L$ | a complex function of the likelihood |
| $Z_S(\alpha_R)$ | a complex function of $\alpha_R$ and the entropy S |

# 1 INTRODUCTION

## 1.1 THE IMPORTANCE OF THE RATE OF DRUG DELIVERY

### 1.1.1 The Definition of Drug Delivery

The process of drug delivery can be represented in two different ways. Firstly, the delivery process can be regarded as the rate at which drug, from an extravascular source, reaches the systemic circulation (normally referred to as the absorption rate) or secondly it can be regarded as the rate at which drug is released from the extravascular source, which, in the case of an oral dosage form would represent the *in vivo* drug release rate. The term drug delivery can therefore be used to represent both the rate of drug absorption and the rate of *in vivo* drug release.

Frequently the absorption rate of a drug has been used to correlate *in vivo* drug release characteristics with *in vitro* drug release characteristics for a particular dosage form. However this implies that the release rate of drug from the dosage form is the rate limiting step and hence the absorption rate is an accurate reflection of the *in vivo* release rate. This may not always be the case and if the desired result of the evaluation of drug delivery is an *in vivo-in vitro* correlation then the *in vivo* release rate is the ideal function to use for that correlation.

### 1.1.2 Controlled Release Products and Drug delivery

There has been an increasing number of specialised pharmaceutical dosage forms developed with the specific aim of controlling the rate of entry of the drug they contain into the systemic circulation, these are known as Controlled Release (CR) dosage forms. These products are designed to retard the absorption rate to produce a low, steady concentration-time profile, by controlling the rate at which the drug is released from the dosage form. Because of this, the overall quality of a CR dosage form is critically dependant on its ability to control drug release *in vivo*. Therefore in their assessment, the biopharmaceutical characteristics of a CR product are very important.

Drugs for which it is desirable to produce a CR product are those which have a narrow therapeutic window, those with a short half life or those whose administration is likely to be long term. For the first of these the CR product will minimise the difference

between peak and trough concentrations which will not only minimise the occurrence of side-effects, but will also provide better clinical control for the patient. For the second, a CR product will enable the frequency of dosage required to be reduced and will therefore increase patient compliance, ideally by enabling the dosage form to be administered on a once daily basis.

### 1.1.3 Evaluation of the Delivery Process

Traditional methods of assessment of delivery rates concentrate on the analysis of the absorption process, however more recent techniques have enabled the actual release rates of drugs *in vivo* to be estimated. Several reviews of methods for calculating the delivery rates of drugs have been published (Tucker 1983 , Cutler 1986, Firsov and Piotrovskii 1986a,b and Tucker and Jackson 1989) and provide a good overview of current methods available.

Direct evaluation of either the absorption rate or release rate of the drug *in vivo* is not practical, as such an approach would be excessively invasive, therefore information about the delivery process must come from manipulation of other data. Assessment of the absorption/release process falls into two categories, those which give a single piece of information about the processes being considered (point values) and those which provide information about the whole time course of the process.

#### 1.1.3.1 Single Point Values

The traditional point values used in the assessment of the biopharmaceutical characteristics of dosage forms are $C_{max}$ , $T_{max}$ , AUC and $F_b$. More recently moments have been used to describe the mean transit/residence characteristics of a dosage form and a further modification of this in the form of the Centre of Gravity of concentration curves has been proposed.

**(a) AUC and $F_b$**

The AUC (Area under the curve) gives a value for the total amount of drug absorbed during the whole absorption process. The bioavailability $F_b$ is a dimensionless term which expresses the fraction of the administered extravascular

dose which is absorbed. The bioavailability can be expressed as an absolute value, $F_b = \frac{Cl}{AUC/D}$, (where D is the extravascular dose administered) or as a relative value when the performances of two dosage forms are being compared. The main drawback to the calculation of the bioavailability by this method lies in the accuracy of calculating the area under the curve.

**(b) $C_{max}$ and $T_{max}$**

Following an extravascular dose of a drug the plasma concentration will pass through a maximum some time after the dose is administered. The magnitude of the concentration at this maximum is $C_{max}$ and the time at which it occurs is $T_{max}$. These two values can give some indication of the rate of absorption as the earlier $T_{max}$ occurs the greater the absorption rate.

Although extremely simple there are two disadvantages involved in the use of $C_{max}$ and $T_{max}$. These are that

a) they depend to some extent on the disposition process of the drug and

b) when applied to CR products, problems occur as the exact position and value of $C_{max}$ is often difficult to determine.

This problem occurs because the desired consequence of the dosage form design is to produce plasma concentration- time profiles that are both low and steady.

**(c) Moments**

A more recent advance in the use of single values in pharmaceutical analysis are statistical moments. These have been extensively reviewed in the literature (Yamaoka et al. 1978, Cutler 1987, Gillespie and Veng-Pederson 1985a and Wagner 1988), although there has been some confusion between the definition of the terms used and the equations used in their evaluation in linear systems. The statistical moments are used to estimate the mean transit times of a drug for various processes, eg the Mean Residence Time (MRT) or the Mean Absorption Time (MAT). The advantage of using moments instead of $C_{max}$ and $T_{max}$ are twofold, they provide more information about the delivery process than $C_{max}$ and $T_{max}$ and their values are independent of the disposition process.

More recently it has been proposed (Veng-Pederson and Tillman 1989) that a fuller description of the bioavailability of a drug in the body could be provided if the Centre of Gravity of the blood level curve was used instead of just the Mean Residence Time. The Centre of Gravity consists of two values one of which is the Mean Residence Time the other is a corresponding co-ordinate on the concentration axis. Taken together they form a more complete characterisation of the absorption rate.

#### 1.1.3.2 Time Course Analysis

There are many more possible approaches when the evaluation of the whole time course of drug delivery is considered. These include mass balance methods, prescribed forms to represent the absorption process, deconvolution methods and the most recent method proposed - the maximum entropy approach. Of these various approaches only the deconvolution and maximum entropy methods can separate the release process from that of absorption.

##### (a) Mass Balance Methods

These methods are based on the assumption that the cumulative amount of drug absorbed is equal to the sum of the cumulative amount excreted and the amount remaining in the body. The well known Wagner-Nelson method (Wagner and Nelson 1963) assumes that there is no distribution of drug to the tissues (ie a one compartment model) and this assumption restricts the usefulness of the method. Wagner (Wagner 1974) adapted his original method for use with a two compartment model in certain prescribed situations dependant on the relative values of the rate constants in the two compartment model.

The Loo-Riegelman method (Loo and Riegelman 1968) was originally proposed for a two compartment model, but data from an intravenous dose was mandatory for its evaluation (Wagner 1975). It was later shown (Vaughan and Dennis 1980) that the method was not restricted to a two compartment model but was valid for any multi-compartmental model.

Despite the limitations imposed by the simplicity of the approach and the confinement into compartmental modelling the mass balance methods do offer one advantage, they make no assumptions about the form of the absorption process itself.

**(b) Prescribed Form for the Absorption Process**

These include a variety of methods ranging from curve fitting in which the form of the absorption is set (maybe as a result of *in vitro* dissolution studies) and included into the disposition equations which are known. The parameters of the absorption process are then optimised by least squares fitting.

In other methods the absorption rate is assumed to be first order, and the absorption rate constant $k_a$ is estimated. In one method $k_a$ is estimated based on a fitting around the maximum point of the concentration time profile (Saunders and Natunen 1973).

**(c) Deconvolution Techniques**

Deconvolution as a method of calculating absorption rates was proposed as early as 1961 (Silverman and Burgen 1961) since which time a wide variety of differing algorithms have been proposed for the deconvolution process. Unlike the previous methods discussed deconvolution can be made to differentiate between the absorption process as a whole and the process of *in vivo* drug release from the dosage form. However at least one other set of data, from either an iv or oral bolus dose, is mandatory for use as a reference in the deconvolution process.

**(d) Maximum Entropy Technique**

This is the most recent of all the techniques proposed for the evaluation of the delivery process. It is a technique which has been widely used in other fields eg for image resolution, and has been adapted for use in pharmacokinetics (Charter and Gull 1987). It the most conceptually complex of all the techniques mentioned here and there has been much scepticism about its potential use in pharmacokinetics. The theory behind this approach will be discussed more fully in chapter 5.

## 1.2 THE USE OF DECONVOLUTION IN PHARMACOKINETICS

Deconvolution algorithms have been used in the analysis of pharmacokinetics as early as 1961 (Silverman & Burden 1961), Rescigno and Segre (Rescigno & Segre 1966) were already using one method of deconvolution before Loo and Riegelman proposed their 'novel' method for calculating the absorption rates of drugs (Loo & Riegelman 1968). Despite the fact that the method has been in existence for so many years deconvolution is still not regarded as a routine tool for pharmacokinetic analysis. This may be because of the numerical complexity of many of the algorithms proposed for the evaluation of deconvolution or perhaps because the previous needs of biopharmaceutical analysis have been met by the more simple methods discussed in previous sections, and there has therefore been no incentive to develop its use.

However, with the increasing number of Controlled Release products becoming available a much greater depth of knowledge about the release process is required and deconvolution methods have been increasingly used to analyze the biopharmaceutical characteristics of new dosage forms.

Deconvolution is only one example of what is called a Linear Systems Approach to the analysis of pharmacokinetic data. Although the emphasis used in the previous section implied the use of deconvolution as a tool to evaluate the *in vivo* drug delivery rate, it should be stressed that the Linear Systems Approach to pharmacokinetic analysis, and deconvolution itself, are much more versatile and can be used to evaluate a wide range of other pharmacokinetic properties.

### 1.2.1 Linear Systems Approaches

Linear Systems Theory, like many other techniques used in pharmacokinetics, is not native to the subject. It originated approximately 100 years ago (Siegel 1988), when it was developed by Oliver Heaviside to describe the behaviour of electrical circuits and transmission lines. A review of Linear and Non-linear Systems Approaches was presented by Veng-Pederson (Veng-Pederson 1988a,b) in which he discussed the advantages of the approach, the definitions on which it is based, various misconceptions involved in its use

and the variety of uses to which it could be applied in pharmacokinetics. His review was met with various levels of reception (Siegel 1988, Boxenbaum 1988 and Metzler 1988) but still provides a good overview of the use of Linear Systems Approaches in pharmacokinetics.

A review of Linear Systems Analysis presented by Cutler (Cutler 1978c) is more specific for the applications of deconvolution than system approaches in general. Linear Systems Approaches have also been used in the analysis of pharmacodynamic data and several papers have been published to this effect (Veng-Pederson and Gillespie 1988 and Smolen 1976a,b). Its use in this direction may eventually lead to effective correlation of drug release directly to its pharmacological action.

### 1.2.2 Definition of a Linear Systems Approach

The definition given by Veng-Pederson in his review (Veng-Pederson 1988a) is that a Linear System Approach is one which models the general linear property of a system without modelling specifically any pharmacokinetic processes involved in that property. Although this seems a cumbersome definition it is useful to demonstrate the basic philosophy of the system approach, which is to use the fewest, least restrictive assumptions necessary to reach a specific objective.

This philosophy applies to the deconvolution technique as well and most of the advantages and disadvantages of deconvolution as a tool for pharmacokinetic analysis stem from this philosophy. With regard to the use of deconvolution to evaluate release rates this means that the disposition processes of the drug in question need not be modelled specifically (unlike the Loo-Riegelman method in which the micro-constants of the disposition process must be known in advance and the model is assumed to be compartmental) as long as the overall disposition effect can be represented accurately.

### 1.2.3 Definition of Deconvolution

The definition of deconvolution is based on an equation known as the convolution integral (1.1).

$$R(t) = \int_0^t W(t-\theta)I(\theta)d\theta \qquad (1.1)$$

R(t) = The Response Function

W(t) = The Weighting Function

I(t) = The Input Function

I(t) The Input rate is defined as the rate at which the substance of interest enters the system being studied at a point P. This input could derive not only from an extravascular source (a drug delivery system) but could also represent the production of a metabolite *in vivo*.

R(t) The Response function is the response produced at a point Q in response to the input I(t) at point P. The response function could be a plasma concentration time profile, a urinary excretion rate or even a pharmacological action which has been shown to be linearly related to the input rate.

W(t) The Weighting function is the response produced at point Q when a unit amount of the substance of interest is introduced to point P at t=0 (ie a bolus unit dose).

The process of convolution is the prediction of the response function when the input and weighting functions are known. Deconvolution is the inverse process, it is the prediction of the input rate when the response and the weighting functions are known (or the prediction of the weighting function when the response and input functions are known).

What precisely the three functions just defined will represent will depend on where the point P is situated. If the point P is the venous circulation the input function will represent the rate at which the substance appears in the general circulation, if the point P is the gastrointestinal tract then the input rate is the rate at which the substance becomes available for absorption. Therefore by changing the point of administration of the weighting function the input function could represent either the absorption rate or the *in vivo* drug release rate.

Before deconvolution can be used as a tool, the system in question must be shown to be linear in the property to be analyzed. The verification of system linearity is performed using the superposition principle.

### 1.2.4 The Superposition Principle

The superposition principle can be stated as follows (Thron 1974) :

---

*...if* $R_1(t)$ *is the system response to* $I_1(t)$ *and*
$R_2(t)$ *is the system response to* $I_2(t)$ *and*
*a and b are arbitrary constants then*
$aR_1(t) + bR_2(t)$ *is the response to input* $aI_1(t) + bI_2(t)$

---

The implication of this principle in pharmacokinetics is that the input must not affect the characteristic behaviour of the system (the weighting function). Non-linearity in pharmacokinetic processes will be introduced by the presence of such features as Michaelis-Menten kinetics, extensive plasma protein binding or induced enzymatic metabolism. Time-dependant processes will not actually introduce non-linearity into the system, however the amount of data required to enable the time-dependant processes to be modelled exactly would be prohibitive in a practical situation. Therefore, the time-independence of the system becomes a practical, if not theoretical, requirement.

The principle of superposition can be easily tested by plotting the dose-normalised concentration curves of several different doses (with the same release characteristics). If the system is linear the curves will superimpose. A second way of testing for non-linearity is to compare the sum of plasma profiles following different inputs (eg. iv and oral) with the plasma profile produced when the two inputs are given simultaneously, once again the curves should superimpose.

Deconvolution can still be applied to systems which are known to be non-linear if it can be shown that they obey the principle of superposition over the dose ranges considered.

### 1.2.5 Applications of Deconvolution

#### 1.2.5.1 Calculation of Absorption Rates

If the weighting function is determined by administration of a unit iv bolus dose and the response function is obtained by the administration of an oral dosage form then, by definition, the input function obtained by deconvolution will be the absorption rate as a function of time.

#### 1.2.5.2 Calculation of *in vivo* Release Rates

If instead of using an iv bolus dose to generate the characteristic behaviour of the system (weighting function), an oral bolus (ie solution) is used instead then the input function obtained following deconvolution of the response to an oral dosage form will represent the *in vivo* drug release rate. This could then be used to correlate *in vivo* and *in vitro* drug release rates which would be especially valuable for Controlled Release products.

#### 1.2.5.3 Calculation of Bioavailability

If the input rate obtained by deconvolution represents the absorption rate then the integral of this rate with respect to time will be the cumulative amount of drug absorbed. The asymptote of this curve, divided by the dose administered will represent the bioavailability of the dosage form.

The traditional method of calculating the bioavailability is to use the AUC value, however there are several disadvantages to using this method.

(1) A large number of points are needed in the post-absorptive phase and, since the number of samples which can be taken in pharmacokinetic studies is usually restricted, this leads to few points in the absorption stage where the best information about the absorption process will be found.

(2) The tail-end points used to calculate the elimination rate constant, and hence the tail area of the curve, are always the lowest and will therefore contain the largest degree of measurement error. This makes determination of the correct elimination rate more difficult.

(3) The tail-end samples may still contain some absorption processes, especially for products which have slow absorption rates, therefore the elimination rate constant obtained from these points may not be the true value.

When deconvolution is used to estimate the bioavailability most of these disadvantages are avoided. Few data points are required in the post-absorptive phase, and once the absorption is complete then the cumulative input profile will level off and the bioavailability can be calculated. No estimate of the elimination rate is

needed and less reliance is placed on the later time points.

#### 1.2.5.4 Calculation of *in vivo* Metabolic Rates

If the concentration of metabolite in the body following the introduction of a unit amount of that metabolite is used to represent the weighting function, and the concentration of metabolite following the administration of an oral dosage form is measured, then deconvolution of these two functions will give the rate of formation of the metabolite *in vivo* ie. the rate of metabolism of the parent drug.

These are only some of the possible uses of deconvolution and, with the exception of the last example, are those which are pertinent to the evaluation of drug delivery. Others are mentioned in the review articles quoted previously (Veng-Pederson 1988a,b and Cutler 1978c).

### 1.2.6 The Advantages of Deconvolution Techniques

(1) The techniques are based on as few assumptions about the system as possible and should therefore be intrinsically more simple to use that other methods. The functions involved are represented in the most general way possible and when the function has to be represented by a model an empirical equation such as a polynomial or polyexponential is usually chosen.

(2) The use of specific models has the drawback that, the more a model is expanded to be as realistic as possible , the more insignificant the values of the individual parameters become. Because the aim of any modelling involved in deconvolution is function approximation rather than parameter estimation, then, the statistical significance assigned to individual parameters is unimportant.

### 1.2.7 The Disadvantages of Deconvolution Techniques

(1) In representing a system in the simplest possible way the total effect of individual processes are lumped together and differentiation of the individual underlying kinetics processes is often not possible.

(2) Although the function approximations have fairly simple mathematical forms the deconvolution algorithms used to evaluate the data may themselves be mathematically very complex.

## 1.3 DECONVOLUTION ALGORITHMS

Deconvolution methods can be broadly divided into two categories, numerical deconvolution and non-numerical deconvolution. The non-numerical methods involve approximation of the unknown input function with some form of empirical equation while the numerical methods impose little or no structure on the form of the input function.

### 1.3.1 Numerical Methods

The numerical methods are typified by their simplicity of approach. They can be used solely on experimental data provided that the data is supplied with a common time interval. All the methods included in this section are based on a numerical approximation of the convolution integral and vary only slightly from one another with the exception of the linear trapezoidal method.

#### 1.3.1.1 Point-Point Method

This method was originally described as an empirical formula (Chiou 1980) but was shown to be an actual deconvolution method and to be identical to that used by Rescigno and Segre (Vaughan 1981). In the point-point method the input function I(t), instead of being a continuous function, is represented by a series of instantaneous impulses so that any input which occurs in the interval $t_{i-1}$- $t_i$ is assumed to take place at $\bar{t}_i$ where $\bar{t}_i = (t_{i-1} + t_i)/2$. The input function is now represented by a delta function (equation (1.2)) where $f_i$ is the cumulative amount of input over the interval $t_{i-1}$- $t_i$ and $\delta(t-\bar{t}_i)$ is a delta function.

If the equation for the input function is substituted in equation (1.1) (the convolution integral) equation (1.3) is obtained, where $R(t_n)$ is the value of the response function

$$I(t) = \sum_{i=1}^{n} f_i \delta(t - \bar{t}_i)$$

$$\text{where} \quad \delta(t - \bar{t}_i) = 0 \quad \text{for} \quad t \neq \bar{t}_i \qquad (1.2)$$

$$= 1 \quad \text{for} \quad t = \bar{t}_i$$

$$n = \text{number of impulse inputs}$$

at $t = t_n$.

The response at $t_n$ is equal to the sum of the responses due to the preceding n-1 impulses plus the response due to the nth impulse. If equation (1.3) is re-written to express this, then $f_n$ can be separated from the rest of the summation (equation (1.4)) and re-arrangement of this gives an expression for $f_n$, the amount of input in the nth interval (equation (1.5)).

$$R(t_n) = \sum_{i=1}^{n} \int_0^{t_n} f_i \delta(\theta - \bar{t}_i) W(t_n - \theta)\, d\theta$$

$$\text{where} \quad \delta(\theta - \bar{t}_i) W(t_n - \theta) = 0 \quad \text{for} \quad \theta \neq \bar{t}_i \qquad (1.3)$$

$$\therefore \quad R(t_n) = \sum_{i=1}^{n} f_i W(t_n - \bar{t}_i)$$

$$R(t_n) = \sum_{i=1}^{n-1} f_i W(t_n - \bar{t}_i) + f_n W(t_n - \bar{t}_n) \qquad (1.4)$$

$$f_n = \frac{R(t_n) - \sum_{i=1}^{n-1} f_i W(t_n - \bar{t}_i)}{W(t_n - \bar{t}_n)} \qquad (1.5)$$

The input rate can be represented by a staircase function $I(t) = \Sigma_{i=1}^{n} I_i$ where $I_i = f_i/(t_{i-1} - t_i)$, one advantage is that if the analytical form of the weighting function is known then the method can be used on data which do not have a common time interval.

### 1.3.1.2 Area-Area Method

In this method the input function $I_i$ is assumed to be constant over the time interval $t_{i-1}$ - $t_i$ and therefore the input function is again represented by a staircase function. If there are n of these time intervals then the response function at $t=t_n$ can be calculated using equation (1.6) (Firsov and Piotrovskii 1986a), which is a modification of the convolution integral for a staircase input function.

$$R(t_n) = \sum_{i=1}^{n} I_i \int_{t_{i-1}}^{t_i} W(t_n - \theta)d\theta \tag{1.6}$$

Re-arrangement of equation (1.6) to solve for $I(t_n)$ will give equation (1.7), which is very similar to equation (1.5) used in the point-point method.

$$\text{let } W_{ni} = \int_{t_{i-1}}^{t_i} W(t_n - \theta)d\theta = \int_{t_n - t_i}^{t_n - t_{i-1}} W(\tau)d\tau$$

$$\therefore \quad R(t_n) = \sum_{i=1}^{n} I_i W_{ni} = \sum_{i=1}^{n-1} I_i W_{ni} + I_n W_{nn}$$

$$\therefore \quad I_n = \frac{R(t_n) - \sum_{i=1}^{n-1} I_i W_{ni}}{W_{nn}} \tag{1.7}$$

The input rate at any interval $I_n$ is dependant on the input rate calculated for the preceding n-1 intervals, this is true for all the numerical methods in this section. The difference between the area-area method and the point-area method lies in the method of calculating the integral $W_{ni}$. For the area-area method the integral $W_{ni}$ is approximated by a rectangular function, centred about the mid-point of the integration interval. The formula used to calculate the integral is given in equation (1.8). When this formula is substituted into the expression for $I_n$ given by equation (1.7), equation (1.9) is produced.

$$W_{ni} = (t_i - t_{i-1})W\left(t_n - \frac{(t_{i-1} + t_i)}{2}\right)$$

$$\text{if} \quad \frac{t_{i-1} + t_i}{2} = \overline{t_i} \quad \text{then} \tag{1.8}$$

$$W_{ni} = (t_i - t_{i-1})W(t_n - \overline{t_i})$$

$$I(t_n) = \frac{R(t_n) - \sum_{i=1}^{n-1} I_i W(t_n - \overline{t_i})(t_i - t_{i-1})}{W(t_n - \overline{t_n})(t_n - t_{n-1})} \tag{1.9}$$

If $f_i$ is the amount of input in the interval $t_{i-1}$- $t_i$ then $I_i = f_i / (t_i - t_{i-1})$. Substituting $I_n$ for $f_n$ and $I_i$ for $f_i$ in equation (1.9) then re-arranging will give an expression for $f_n$ (equation (1.10)) which is identical to the equation produced for the point-point method.

$$f_n = \frac{R(t_n) - \sum_{i=1}^{n-1} f_i W(t_n - \overline{t_i})}{W(t_n - \overline{t_n})} \tag{1.10}$$

Therefore the point-point and area-area methods are equivalent when the integral, $W_{ni}$, is represented by a rectangular function.

### 1.3.1.3 Point-Area Method

Like the area-area method the input function is assumed to be constant over the time intervals $t_{i-1}$- $t_i$. The original method (Vaughan and Dennis 1978) was essentially similar to the area-area method, and like it was based on equation (1.4). The real difference between the two methods lies in the way in which the integral $W_{ni}$ is estimated. Unless the integral $W_{ni}$ is approximated in some way then the weighting function must be known analytically so the integral $W_{ni}$ can be calculated for any i and any n, and this is the point-area method. A method using a known polyexponential to represent the weighting function was developed (Iga et al 1986) so that equation (1.7) could be evaluated for experimental data at non-equal time intervals.

If the data have a common time interval, $\Delta t$, then equation (1.7) can be modified accordingly to give equation (1.11). Where $R_n$ is the value of the response function at $n.\Delta t$. However some method for calculating the integral is still required.

$$I_n = \frac{R_n - \sum_{i=1}^{n-1} I_i W_{ni}}{W_{nn}} \tag{1.11}$$

When the integrals are approximated by a rectangular function then the method becomes equivalent to the area-area and point-point methods. This is the approach used by Langenbucher in his applications of the point-area algorithm (Langenbucher 1982). He used the value of the function at the mid-point of the time interval multiplied by the time interval to represent the integral $W_{ni}$. If $\bar{W}_i$ is the value of W(t) at the mid-point of the interval $t_{i-1}$ - $t_i$ then the integral $W_{ni} = \bar{W}_{n-i+1}.\Delta t$. This integral can be substituted into equation (1.11) to give equation (1.12) which is that initially proposed by Langenbucher. When a common time interval is used then $W_{nn} = \bar{W}_1$ and this can also be substituted into equation (1.12).

$$I_n = \frac{R_n/\Delta t - \sum_{i-1}^{n-1} I_i \bar{W}_{n-i+1}}{\bar{W}_1} \tag{1.12}$$

### 1.3.1.4 Linear Trapezoidal Method

In a later method (Langenbucher and Möller 1983a,b) proposed that the linear trapezoidal method for numerical deconvolution was preferable to the point area method. He stated that the accuracy of this method was comparable with the point-area algorithm but, although the formulae were more complicated , the fact that the method could be applied directly to the data points without having to transpose them to their mid-point or area values made the method preferable.

In this method the value of the response function at $t=t_n$ is calculated using equation (1.13) where $I_i = I(i.\Delta t)$ , $W_i = W(i.\Delta t)$ and $R_i = R(i.\Delta t)$. $\Delta t$ is the common time interval for the data points of the functions. Re-arranging equation (1.13) gives

an expression for $I_n$ (equation (1.14)).

$$R_n = \Delta t \left( \frac{I_0 W_n + I_n W_0}{2} + \sum_{i=1}^{n-1} I_i W_{n-i} \right) \tag{1.13}$$

$$I_n = \frac{2R_n/\Delta t - I_0 W_n - 2\sum_{i=1}^{n-1} I_i W_{n-i}}{W_0} \tag{1.14}$$

Using equation (1.14) it is impossible to evaluate $I_0$ at n=1. The method of estimating this initial value depends on the initial value of the weighting function at t=0. If W(0) > 0 (eg iv bolus) then $I_0$ is calculated from the initial slope of the response functions according to equation (1.15) and subsequent values of $I_i$ calculated using equation (1.14).

$$I_0 = \frac{R_0}{W_0} \qquad \text{where} \quad R_0 = \frac{(2R_1 - R_2/2)}{\Delta t} \tag{1.15}$$

If the initial value of the weighting function is W(0) = 0 (eg oral bolus dose) then a different equation must be used to calculate all the $I_i$ (equation (1.16)) and in this case only n-1 of the data points can be transformed into their equivalent $I_i$.

$$I_{n-1} = \frac{R_n/\Delta t - I_0 W_n/2 - \sum_{i=1}^{n-2} I_i W_{n-i}}{W_1} \qquad \text{where} \quad I_0 = \frac{2R_1}{\Delta t W_1} \tag{1.16}$$

Therefore, depending on the form of the weighting function (either iv or oral bolus dose), one of two sets of formulae are used to calculate the deconvolved input function.

### 1.3.1.5 Inequality Constrained Least Squares Deconvolution

This method is much more computationally complex than the other numerical

deconvolution methods but is based on the point-area method and equation (1.7) is again the basic equation for the method (Verotta 1989) but constraints are placed on the possible values of $I_n$. Possible constraints include conditions such as $I_n$ be non-negative and monotonically decreasing. If equation (1.6) is rewritten as a matrix equation where R is a vector with elements $R_i$ containing the experimental response values, I is a vector with elements $I_i$ containing the estimated values of the input rate, E is a vector of errors between the experimental response function and the estimated response function from the current vector I and W is the matrix of the weighting function, then equation (1.17) is obtained.

$$R = WI + E \qquad \therefore \qquad E = R - WI$$

$$\text{where} \quad W = \begin{bmatrix} W_{11} & 0 & 0 & . & 0 \\ W_{21} & W_{22} & 0 & . & . \\ . & . & . & . & . \\ W_{n1} & W_{n2} & . & . & W_{nn} \end{bmatrix} \tag{1.17}$$

The optimal value for the vector I can be found by minimising the sum of squares criterion (SS) according to equation (1.18), where T represents the transpose of the matrix or vector in question.

$$\begin{aligned} SS &= E^T E \\ &= (R - WI)^T (R - WI) \\ &= R^T R - 2R^T WI + I^T W^T WI \end{aligned} \tag{1.18}$$

Because the SS criterion is only dependant on I through the last two terms, the least squares problem can be re-stated as follows - Minimise the quadratic function - $2R^TWI + I^TW^TWI$ subject to $CI \geq 0$ , where the n x m matrix C contains the coefficient corresponding to the m linear inequality constraints.

The method is computationally very complex but, with the exception of the constraints, it imposes no structure on the unknown input function.

## 1.3.2 Non-Numerical Methods

### 1.3.2.1 Cutler's Prescribed Input Method

The method was originally developed (Cutler 1978a) in an attempt to produce a deconvolution method which was more stable for use with noisy data than the numerical methods mentioned previously. It is based on the following theory. The form of the input function is assumed to be known, perhaps from *in vitro* dissolution studies or from a theoretical model. This equation for the input rate is incorporated into the convolution equation and its parameters optimised according to a least squares criterion.

The current best guess for the parameters of the input function are convolved with the known weighting function to give estimated values for the response function at times corresponding to the experimental data points obtained for the response function. The degree of closeness of these estimated parameters is found through the residual sum of squares, which is the sum of the squared differences between the actual and estimated response function values. As the parameters of the input function approach the true values the residual sum of squares decreases and the best estimate of the parameters is found by minimising the residual sum of squares.

The method is much more stable to noisy data than the numerical methods and if parameter optimisation is the aim of the deconvolution process then the method is valuable. However, if the desired outcome is to obtain information about the form and value of the input function itself, then the use of this method is limited as it imposes a pre-defined form upon the input function.

### 1.3.2.2 Cutlers's Method of Orthogonal Polynomials

In this method, the input function I(t) is represented by a polynomial of unknown degree, but is still based on the least squares criterion of the previous method (Cutler 1978a). In order to avoid the ill-conditioning often associated with the fitting of functions to polynomials a method involving the use of orthogonal polynomials was introduced (Cutler 1978b).

In this method, both the weighting and the input functions are represented by

polynomials. The degree of the polynomial representing the input function is increased until the improvement seen in the residual sum of squares is not large enough to justify the inclusion of an extra term. Cutler intended this method to be a preliminary method of identifying the possible form of the input function since polynomials can be used to approximate a wide range of functions. The form identified from this method could be used as the prescribed input form in the previous method.

#### 1.3.2.3 Veng-Pederson's Polyexponential Method

All the various deconvolution methods proposed by Veng-Pederson are based on an equation which is an exact mathematical solution to the deconvolution problem of determining the input rate when the weighting function is represented by a polyexponential and the response function is approximated by an arbitrary function (Veng-Pederson 1980a).

The first method proposed approximated the response function with an adaptive least squares cubic spline technique (Veng-Pederson 1980b). The method was compared with Cutlers method of orthogonal polynomials using the data proposed by Cutler (Cutler 1978b) and no significant difference was found between the two methods except when the form of the input function was the cube root dissolution equation. In the latter case the cubic spline technique was shown to be superior.

The cubic spline method was later adapted (Veng-Pederson 1980c) to a simple, more easily implemented approach, since the cubic spline approach was regarded as being computationally very complex. This adaptation was based on the approximation of **both** the weighting and response functions by polyexponential functions. A condition of the method was that all the coefficients of the polyexponential describing the weighting function were positive, i.e. the weighting function had to be from an iv bolus dose. A computer program was given to evaluate the input function based on these approximations.

This new method was again compared with Cutler's orthogonal polynomial method and no significant difference was found between the two methods.

A later modification of the program (Gillespie and Veng-Pederson 1985b)

extended its range so that there were no restrictions on the sign of the coefficients of the polyexponential representing the weighting function, enabling an oral bolus solution to be used as the weighting function.

#### 1.3.2.4 Veng-Pederson's Polynomial Method

This method is also based on the equation derived to evaluate the input function when the weighting function is represented by a polyexponential. However, in this method, the unknown input function is represented by a polynomial, whose coefficients are linearly related to the values of the response function (Veng-Pederson 1980d).

Because of this linear relationship the values of these coefficients can be found easily by linear regression when the equation of the weighting function is known. The unknown input is fitted to polynomials of increasing degree until no improvement of fit is found, judged by some statistical criterion. The input function is then represented by that polynomial.

Veng-Pederson again compared his method with that of Cutler's orthogonal polynomials and found no significant difference between them on the data tested.

#### 1.3.2.5 System Identification Methods

The method presented by Vajda et al (1988) is similar to that presented by Veng-Pederson, representing both the weighting and response functions by polyexponentials. Instead of fitting polyexponentials to the functions using non-linear fitting techniques, the response and input functions are approximated by differential equations whose parameters are estimated by a direct integral (DILS) method which involves only linear regression.

The process involves two steps, system identification and input evaluation. System identification involves fitting differential equations of increasing order until no significant improvement is seen. The weighting function is then obtained from this equation. The input evaluation step uses the weighting function previously evaluated to represent an input function in identifying a second linear system, whose weighting function represents the original unknown input function.

The method has a supposed advantage over Veng-Pederson's method in that it involves only two evaluation steps not three and it uses linear instead of non-linear regression.

## 1.4 AIMS AND OBJECTIVES

There is a wide range of deconvolution algorithms available, as can be seen from the preceding sections, but little information about which method is to be preferred if deconvolution is to be used as a tool to assess drug delivery rates. Generally numerical algorithms, although very simple both to apply and to understand, are extremely sensitive to noise in the data. This could in theory, limit their use in practical situations. The non-numerical methods are computationally very complex and a greater effort is required to understand the underlying principles. However the extra effort may be compensated by an increase in stability to data noise.

One great advantage of deconvolution as a tool in the evaluation of drug release is its ability not only to give information about the whole time course of the delivery process but also its ability, with a suitable weighting function, to evaluate the rate of *in vivo* drug release.

If deconvolution can be shown to predict accurately both the form and the values of the *in vivo* release rate, then deconvolution would become the ideal method for quantifying the *in vivo* release characteristics of controlled release products. This prompts the following questions :

- To what degree is the output of the deconvolution process a good reflection of the true input rate ?
- To what extent does the predicted input rate, achieved through deconvolution, depend on the quality of the initial data ?
- What criteria affect the choice of the deconvolution algorithm ?
- What additional complications to the use of deconvolution are encountered when the algorithms are used to evaluate real clinical data ?

- Can deconvolution be used to provide an *in vivo-in vitro* correlation in the evaluation of clinical data ?
- Is the method of Maximum Entropy in any way superior to the deconvolution methods for estimating the release characteristics of a dosage form ?

With these questions in mind the following objectives were set.

(1) To investigate a range of deconvolution algorithms for their stability to data noise.

(2) To investigate a range of deconvolution algorithms for their ability to predict correctly the form of unknown input functions, and the effect of data noise on this ability.

(3) To investigate the accuracy of various deconvolution algorithms at predicting the bioavailability or the fraction of dose released from a dosage form.

(4) To use the various algorithms selected to analyze actual clinical data to highlight any problems to the use of the various algorithms in a practical situation.

(5) To investigate the stability of the maximum entropy method to increasing levels of data noise.

(6) To investigate the ability of the maximum entropy method to predict the form of unknown input functions.

(7) To evaluate actual clinical data using the maximum entropy method for comparison with the various deconvolution techniques.

Four deconvolution algorithms were selected, from those described previously, to cover a range from the numerically very simple to the computationally complex.

From the numerical methods, the trapezium method proposed by Langenbucher was chosen. This method was selected because its output is a set of point values at the end of each time interval, making comparison with other methods easier. It has also already been used in the evaluation of drug delivery of oxprenolol Oros preparations (Langenbucher and Mysicka 1985) and bacampicillin microcapsule suspensions (Nicklasson et al 1984).

The second method chosen is an adaptation of the first, in which the weighting function is smoothed, by curve fitting, prior to deconvolution. This method was chosen to examine the possibility that smoothing one function would improve the performance

of the numerical algorithm, and has been termed the semi-numerical method.

The third method chosen was one of the polynomial methods. The Veng-Pederson method was chosen instead of the Cutler method simply because it represented the weighting function with a polyexponential, which is considered preferable when approximating drug concentration curves.

The fourth method was Veng-Pederson's method of polyexponentials, which was considered similar to the system identification method, but was selected because it was simpler to implement and had already been used for the analysis of cimetidine (Veng-Pederson 1981).

Cutler's method of prescribed inputs was excluded by its definition as it imposes, prior to deconvolution, a known form on an unknown input function.

The four deconvolution algorithms mentioned above were used in the stated objectives and further details of these four algorithms are given in chapter 2.

The clinical data used for evaluation came from administration of three different Metoprolol CR tablets which were deconvolved with an oral solution.

# 2 METHODS

The various methods presented in this chapter are tools with which the objectives, set out at the end of the previous chapter, can be undertaken. Because many of the methods are used repeatedly, but often in differing circumstances, this chapter is designed as a reference section, to be used in conjunction with the later chapters.

The chapter includes a much more detailed description of the four chosen deconvolution methods (section 2.2), some of which require the use of either linear or non-linear regression, the details of which are given in section 2.1.

In order to examine the accuracy of the release rates predicted by the deconvolution algorithms, and the stability of these algorithms to noise, the true release rate must be known *a priori*. Therefore the true release rate must be used as a starting point in the generation of pseudo-experimental data, which when deconvolved will (if the deconvolution is perfect) yield the original release rate. The methods for the calculation of the response function from the desired release rate and weighting function are described in section 2.3, together with the means of adding noise to the data generated in this fashion.

The various other methods included here are used in different places throughout the following chapters and should be referred to as the need arises. The theory of the Maximum Entropy technique and details of the method are presented in a separate chapter.

## 2.1 REGRESSION SUBROUTINES

### 2.1.1 Non-Linear Least Squares Curve Fitting

The method used for non-linear curve fitting was that proposed by Marquardt and is known as the Levenburg-Marquardt method.

It is based on finding the parameters of a user defined function which minimise the $\chi^2$ merit function (Press et al 1988a) as shown in equation (2.1).

$$\chi^2(p) = \sum_{i=1}^{n} \left( \frac{y_i - y(x,p)}{wt_i} \right)^2 \qquad (2.1)$$

where p is the vector of parameters to be estimated

$y_i$ is the experimental value at data point i

y(x,p) is the estimated value of y at the same point x as $y_i$ using the current best estimate of the parameters

n is the number of data points

$wt_i$ is the weight assigned to data point i.

The method is based on combining two well known non-linear parameter estimation techniques - that involving inversion of the Hessian matrix (the Hessian matrix holds the second derivatives of the $\chi^2$ value w.r.t. each estimated parameter value at each data point) and the steepest descent method. When the $\chi^2$ value is far from the minimum then the steepest descent method is used but this is changed to the inverse-Hessian method when the $\chi^2$ value is close to the minimum, thus making the method converge more rapidly.

The method was implemented using two subroutines mrqmin() and mrqcof() (Press et at 1988a). The program required a user supplied subroutine to evaluate the function whose parameters were to be estimated, and that function's first derivatives w.r.t. its parameters. The subroutine expon() was used to calculate any polyexponential of degree ma/2 and its first derivatives.

```
expon(x, a, y, dyda, ma)
float x, a[], *y, dyda[];
int ma;
{
        int i;
        *y = 0.0;
        for(i=1 ; i<=ma ; i +=2){
                *y = a[i]*exp(-a[i+1]*x);
                dyda[i] = exp(-a[i+1]*x);
                dyda[i+1] = -a[i]*x*exp(-a[i+1]*x);
        }
}
```

The weights assigned to each data point should be the standard deviation of that data point so that the squared value is weighted inversely as its variance. However, with experimental data the true variance is rarely known, so the squared value was weighted

inversely with the square of the experimental value, i.e. $wt_i = y_i$ (Boxenbaum et al 1973). This assumes that the variance of $y_i$ is proportional to $y_i^2$, and although not the only weighting scheme for pharmacokinetic data it is one of the most common.

### 2.1.2 Linear Least Squares Regression

The basic requirement of parameter estimation by linear regression is that the equation to be fitted is linear in the parameters to be estimated i.e. it is in the form of the equation given below.

$$y(x) = \sum_{k=1}^{m} p_k f_k(x) \tag{2.2}$$

where $p_k$ are the parameters to be estimated and $f_k(x)$ are arbitrarily fixed functions of x known as the basis functions. Like the non-linear curve fitting methods the values of the parameters chosen are those which minimise the $\chi^2$ merit function as given by equation (2.1).

When the $\chi^2$ value is at a minimum the first derivatives of $\chi^2$ w.r.t each of the parameters p will be 0. This gives a series of normal equations for $\delta\chi^2/\delta p_1$, $\delta\chi^2/\delta p_2$,....$\delta\chi^2/\delta p_m$ which can be solved by Gauss-Jordan elimination (Press et al 1988b). In order to avoid the problems associated when normal equations become close to singular a technique called Singular Value Decomposition (SVD) was used (Press et al 1988c) to find the minimum $\chi^2$ value. Although SVD can be slower than solving linear equations by Gauss-Jordan elimination, its great advantage is that it theoretically cannot fail.

Like the non-linear least squares method the weights chosen are the experimental values $y_i$ for each data point. The subroutines used require only one user supplied routine to evaluate the basis functions at any value x. For a general polynomial the following subroutine fpoly() was used, where np is the degree of polynomial.

```
void fpoly( x, p, np)
float x, p[];
int np;
{
        int j;
        p[1] = 1.0;
        for(j=2 ; j<=np ; j++) p[j] = p[j-1]*x;
}
```

## 2.2 DECONVOLUTION ALGORITHMS

### 2.2.1 Numerical Deconvolution

The input function was calculated directly from the data according to the algorithms given for the linear trapezoidal method (Langenbucher and Möller 1983a). The algorithms are based on equations (1.14), (1.15) and (1.16) of section 1.3.1.4 and are designed to give a stepwise progression through the calculation (equations (2.3) and (2.4)).

$$
\begin{aligned}
&\textit{If} \quad W(0) = 0 \\
&I_0 = (2R_1/\Delta t)/W_1 \\
&I_1 = (R_2/\Delta t - I_0W_2/2)/W_1 \\
&I_2 = (R_3/\Delta t - I_0W_3/2 - I_1W_2)/W_1 \\
&I_{n-1} = (R_n/\Delta t - I_0W_n/2 - I_1W_{n-1} - \ldots - I_{n-2}W_2)/W_1
\end{aligned}
\tag{2.3}
$$

$$
\begin{aligned}
&\textit{If} \quad W(0) > 0 \\
&I_0 = (2R_1 - R_2/2)/W_0\Delta t \\
&I_1 = 2(R_1/\Delta t - I_0W_1/2)/W_0 \\
&I_2 = 2(R_2/\Delta t - I_0W_2/2 - I_1W_1)/W_0 \\
&I_n = 2(R_n/\Delta t - I_0W_n/2 - I_1W_{n-1} - \ldots - I_{n-1}W_1)/W_0
\end{aligned}
\tag{2.4}
$$

The weighting and response function data was required to be at a constant time interval, $\Delta t$, prior to deconvolution. Any data not already having a constant time interval was interpolated using a cubic spline interpolation subroutine (Press et al 1988d) which has been shown to give a better function approximation than linear or log-linear interpolation methods (Yeh and Kwan 1978), especially for data with rapid changes in curvature or widely spaced data points.

If the weighting function did not arise from the administration of a unit dose then the values of the weighting function were normalised (by division by the dose administered) prior to deconvolution. The interpolated data was then processed according to equations (2.3) and (2.4) to give a vector I, whose elements hold the values $I_i$, where $I_i$ is the value

of the input function at $t_i$=i.Δt.

The cumulative input was calculated from the vector $I_i$ by numerical integration using the trapezoid formula to estimate the area under the input function - time curve. This gives an equation for the cumulative fraction input ($CFI_i$ = CFI(i.Δt)) shown by equation (2.5) and the cumulative percentage input ($PCT_i$ = PCT(i.Δt)) shown by equation (2.6) where $D_o$ is the dose administered to produce the response function.

$$CFI_n = CFI(n\Delta t) = \frac{1}{D_0}\sum_{i=1}^{n}\frac{(I_i + I_{i-1})}{2}.\Delta t \qquad (2.5)$$

$$PCT_n = PCT(n\Delta t) = \frac{100}{D_0}\sum_{i=1}^{n}\frac{(I_i + I_{i-1})}{2}.\Delta t \qquad (2.6)$$

### 2.2.2 Semi-Numerical Deconvolution

Prior to deconvolution the experimental data for the weighting function, $W_e(t)$, was fitted to a polyexponential equation of the form given in equation (2.7), where tlag is the time lag associated with the data and $A_i$ and $\alpha_i$ are the coefficients and exponents of the polyexponential ( if W(0) = 0 then $\Sigma_{i=1}^{n}A_i = 0$). The curve fitting was performed using a non-linear least squares curve fitting routine described previously (section 2.1.1).

$$W(t) = \sum_{i=1}^{n} A_i e^{-\alpha_i (t - tlag)_+}$$

$$\text{where} \quad (t - tlag)_+ = 0 \quad \text{for } t < tlag \qquad (2.7)$$

$$= (t - tlag) \quad \text{for } t \geq tlag$$

$$\text{and} \quad \alpha_i > 0$$

If the data for the weighting function was obtained by administration of a non-unit dose then the weighting function was normalised prior to deconvolution by dividing by the actual dose administered, D, to give equation (2.8).

$$W(t) = \frac{1}{D}\sum_{i=1}^{n} A_i e^{-\alpha_i(t - tlag)}. \tag{2.8}$$

The equation for the weighting function (2.8) was used to generate data at constant intervals, Δt, for use in the deconvolution process. The experimental data for the response function was interpolated at the same interval, Δt, (using the cubic spline interpolation routine described previously) prior to deconvolution with the weighting data produced by equation (2.8). The estimated input function produced was a vector I, with elements $I_i$, which represent the values of I(t) at t = i.Δt. The cumulative fraction input and cumulative percentage input were calculated according to equations (2.5) and (2.6) respectively.

### 2.2.3 Polynomial Deconvolution

Prior to deconvolution, the experimental data for the weighting function, $W_e(t)$, following administration of a dose D, was fitted to a polyexponential equation given by equation (2.9) using a non-linear least-squares curve fitting routine (section 2.1.1 ). Equation (2.9) was normalised to give equation (2.10) by division by the dose administered, D.

$$W_e(t) = \sum_{i=1}^{n} A_i e^{-\alpha_i t} \tag{2.9}$$

$$W(t) = \frac{1}{D}\sum_{i=1}^{n} A_i e^{-\alpha_i t} \tag{2.10}$$

The unknown input function, I(t), was represented by a polynomial of unknown degree, m+1, and unknown coefficients $C_j$ (equation (2.11)).

$$I(t) = \sum_{j=0}^{m} C_j t^j \tag{2.11}$$

If the Laplace transform of the convolution integral is taken then equation (2.12) is the result, where R(s) is the Laplace transform of the response function R(t), W(s) is the Laplace transform of the weighting function W(t) and I(s) is the Laplace transform of the

input function I(t).

If the Laplace transforms of the equations representing the weighting function (equation (2.10)) and the input function (equation (2.11)) are taken, then equations (2.13) and (2.14) are obtained respectively.

$$R(s) = W(s).I(s) \tag{2.12}$$

$$W(s) = \frac{1}{D}\sum_{i=1}^{n}\frac{A_i}{(s+\alpha_i)} \tag{2.13}$$

$$I(s) = \sum_{j=0}^{m}\frac{C_j j!}{s^{j+1}} \tag{2.14}$$

Multiplication of equations (2.13) and (2.14) give the Laplace transform of the response function (equation (2.15)) and the inverse transformation of this equation gives

$$R(s) = \frac{1}{D}\sum_{i=1}^{n}\frac{A_i}{(s+\alpha_i)}.\sum_{j=0}^{m}\frac{C_j j!}{s^{j+1}} \tag{2.15}$$

$$R(t) = \frac{1}{D}\sum_{j=0}^{m}C_j j!\sum_{i=1}^{n}\frac{A_i}{\alpha_i^{j+1}}\left((-1)^{j+1}e^{-\alpha_i t} + \sum_{k=0}^{k=j}(-1)^{j-k}\frac{\alpha_i^k t^k}{k!}\right) \tag{2.16}$$

an algebraic expression (equation (2.16)) for the response function R(t). A full derivation of equation (2.16) is given in Appendix A.

Equation (2.16) forms the basis of Veng-Pederson's polynomial method of deconvolution, however, it is unable to accommodate for any time lag present in the weighting function data. In theory, the weighting function is the response to an instantaneous input and there, therefore, should be no time lag. However, in practical situations there may often be a small, but distinct, delay especially when an oral solution is being used to produce the weighting function, as the drug must be absorbed from the GI tract and pass through the liver before its presence will be noticed. Because of the need to accommodate for a time lag in the weighting function equation (2.16) was re-

derived using equation (2.7) to represent the weighting function.

The experimental data for the weighting function $W_e(t)$ was therefore fitted to equation (2.7) using the non-linear curve fitting routine described in section 2.1.1. The equation was then normalised to give equation (2.8) by division by the dose administered, D. Equation (2.8) can be re-written (2.17) to include a unit step function whose purpose is to 'turn on' the weighting function after t=tlag.

$$W(t) = \frac{1}{D} H(t - tlag) \sum_{i=1}^{n} A_i e^{-\alpha_i (t - tlag)}$$
$$\text{where} \quad H(t - tlag) = 0 \quad \text{for} \quad t < tlag$$
$$= 1 \quad \text{for} \quad t \geq tlag \tag{2.17}$$

The Laplace transform of this new weighting function, W(s), is shown in equation (2.18). When equation (2.18) is multiplied by the Laplace transform of the input function (equation (2.14)) a revised expression for the Laplace transform of the response function is obtained (2.19) and inverse transformation of this gives a new expression for the response function R(t) which can accommodate a time lag in the weighting function (equation (2.20)).

$$W(s) = \frac{e^{-tlag\, s}}{D} \sum_{i=1}^{n} \frac{A_i}{(s + \alpha_i)} \tag{2.18}$$

$$R(s) = \frac{e^{-tlag\, s}}{D} \sum_{i=1}^{n} \frac{A_i}{(s + \alpha_i)} \sum_{j=0}^{m} \frac{C_j j!}{s^{j+1}} \tag{2.19}$$

$$R(t) = \frac{1}{D} H(t - tlag) \sum_{j=0}^{m} C_j j! \sum_{i=1}^{n} \frac{A_i}{\alpha_i^{j+1}} \left( (-1)^{j+1} e^{-\alpha_i (t - tlag)} + \sum_{k=0}^{k=j} (-1)^{j-k} \frac{\alpha_i^k (t - tlag)^k}{k!} \right) \tag{2.20}$$

A full derivation of equation (2.20) is given in Appendix A. It can be seen that equation (2.20) is linear in the coefficients $C_j$ and can therefore be re-written in a simplified form as equation (2.21).

(2.21)

$$R(t) = \sum_{j=0}^{m} C_j \theta_j \qquad \text{where}$$

$$\theta_j = \frac{1}{D} H(t - tlag)\, j! \sum_{i=1}^{n} \frac{A_i}{\alpha_i^{j+1}} \left( (-1)^{j+1} e^{-\alpha_i (t - tlag)} + \sum_{k=0}^{k=j} (-1)^{j-k} \frac{\alpha_i^k (t - tlag)^k}{k!} \right)$$

The linear regression program (Press et al 1988e) based on singular value decomposition, described previously, (section 2.1.2 ) was used to solve for the unknown coefficients $C_j$. Starting at m=1, the coefficients $C_j$ were solved for using linear regression, m was then increased and the process repeated until the decrease in the residual sum of squares for the regression was insufficient to justify the inclusion of an additional term in the polynomial, as judged by the F Test (section 2.4.1).

The cumulative fraction input and the cumulative percentage input were calculated from the algebraic integration of the selected polynomial, according to equations (2.22) and (2.23) respectively, where $D_o$ is the dose given to produce the response function.

$$CFI(t) = \frac{1}{D_o} \sum_{j=0}^{m} \frac{C_j t^{j+1}}{j+1} \tag{2.22}$$

$$PCT(t) = \frac{100}{D_o} \sum_{j=0}^{m} \frac{C_j t^{j+1}}{j+1} \tag{2.23}$$

### 2.2.4 Polyexponential Deconvolution

The experimental data for the weighting function obtained after administration of a bolus dose D was fitted to equation (2.9) by a non-linear least squares fitting routine (section 2.1.1). Analytical deconvolution, if the weighting function is represented by a polyexponential, as in equation (2.9), has been shown to lead to equations (2.24) and (2.25) (Gillespie and Veng-Pederson 1985b).

$$PCT(t) = K_4 \left[ K_1 R(t) + K_3 \int_0^t R(u)\, du + \psi * R(t) \right] \tag{2.24}$$

$$I(t) = D\,[K_1 R'(t) + K_2 R(t) + \varphi(t) * R(t)] \tag{2.25}$$

R(t) is the response function, R'(t) is the first derivative of the response function and D is the dose administered to produce the weighting function. All the other expressions within the two equations are constants derived from the values of the coefficients and exponents of the equation fitted to the weighting function.

In order to make the equations applicable to oral weighting functions, alternative definitions of certain terms must be used when the initial value of the weighting function is zero (i.e. when the weighting function used arises from an oral bolus dose). The definitions of the terms used in equations (2.24) and (2.25) are given in equation (2.26), (2.27) and (2.28). $D_o$ is the dose given to produce the response function.

$$K_1 = \frac{1}{\sum_{i=1}^{n} a_i} \qquad K_2 = K_1^2 \sum_{i=1}^{n} a_i \alpha_i$$

$$K_3 = K_2 - \sum_{i=1}^{n-1-i_o} \frac{g_i}{\gamma_i} \qquad K_4 = \frac{100\,D}{D_o} \tag{2.26}$$

$$R(t) = \begin{cases} R(t) & W(0) \neq 0 \\ R'(t) & W(0) = 0 \end{cases} \qquad a_i = \begin{cases} A_i & W(0) \neq 0 \\ -A_i \alpha_i & W(0) = 0 \end{cases}$$

The parameters { $g_i$, $\gamma_i$ } for {i=1 to i= n-1} are obtained from the n-1 roots of the polynomial Q(x) shown in equation (2.27), where $\gamma_i$ are the n-1 roots of the polynomial. These parameters are then used to calculate $\varphi(t)$ and $\psi(t)$ as shown in equation (2.28).

$$Q(x) = \sum_{i=1}^{n} A_i \prod_{\substack{j=1 \\ j \neq i}}^{n} (\alpha_j + x)$$

$$\textit{and} \quad g_i = K_1 \prod_{j=1}^{n} (\gamma_j + \alpha_j) \Big/ \prod_{\substack{j=1 \\ j \neq i}}^{n-1} (\gamma_i - \gamma_j) \tag{2.27}$$

The roots of the polynomial Q(x) were calculated using two subroutines, laguer() and zroots(),which are based on Laguerr's root finding methods (Press et al 1988f). The subroutines used needed to be able to converge for both real and complex roots since it

$$\varphi(t) = g_0 + \sum_{i=1}^{n-1-i_0} g_i e^{\gamma_i t} \qquad \psi(t) = g_0 t + \sum_{i=1}^{n-1-i_0} \frac{g_i e^{\gamma_i}}{\gamma_i}$$

$$\text{where} \quad i_0 = \begin{cases} 0 & W(0) \neq 0 \\ 1 & W(0) = 0 \end{cases} \quad \textit{and} \quad g_0 = \begin{cases} 0 & W(0) \neq 0 \\ g_{n-1} & W(0) = 0 \end{cases} \tag{2.28}$$

was possible that the roots of Q(x) could be complex, and $u_i$ and $v_i$ in equations (2.30) and (2.31) are complex numbers. The advantage of Laguerr's method is that it is computationally very simple and is guaranteed to converge from any starting point.

$$R(t) = \sum_{i=1}^{m} b_i e^{-\beta_i (t - t_0)} \qquad t \geq 0 \tag{2.29}$$

The experimental data representing the response function is fitted to equation (2.29) using the non-linear least-squares method described in section 2.1.1. Incorporation of equation (2.29) into equations (2.24) and (2.25) results in expressions for the input rate, I(t), and the cumulative percentage input, PCT(t), given by equations (2.30) and (2.31).

$$PCT(t) = u_0 + \sum_{i=1}^{L-i_0} u_i e^{-v_i (t - t_0)} \qquad t \geq t_0 \tag{2.30}$$

$$I(t) = \frac{D}{100} \sum_{i=1}^{L-i_0} u_i(-v_i) e^{-v_i (t - t_0)} \qquad t \geq t_0$$

$$\text{where} \quad L = m + n - 1 \tag{2.31}$$

$$v_i = \begin{cases} \beta_i & i = 1, 2, \ldots, m \\ -\gamma_{i-m} & i = m+1, m+2, \ldots, L - i_0 \end{cases}$$

$$B_i = \begin{cases} b_i & W(0) \neq 0 \\ -b_i \beta_i & W(0) = 0 \end{cases}$$

$$u_i = \begin{cases} K_4 B_i \left( K_1 - \dfrac{K_3}{\beta_i} - \displaystyle\sum_{j=1}^{n-1-i_0} \dfrac{g_j}{\gamma_j(\gamma_j + \beta_i)} + \dfrac{g_0}{\beta_i^2} \right) & i = 1, 2, \ldots, m \\ K_4 \dfrac{g_{i-m}}{\gamma_{i-m}} \displaystyle\sum_{j=1}^{m} \dfrac{B_j}{\gamma_{i-m} + \beta_j} & i = m+1, m+2, \ldots, L - i_0 \end{cases}$$

(2.31) cont.

$$u_0 = PCT(\infty) = \frac{K_4 \sum_{i=1}^{m} (b_i/\beta_i)}{\sum_{i=1}^{n} (a_i/\alpha_i)}$$

Once all the constants in equations (2.30) and (2.31) have been calculated from the constants and coefficients of the polyexponentials used to represent the weighting and response functions then the input function (I(t)) and the cumulative percentage input (PCT(t)) can be calculated directly from equations (2.30) and (2.31).

## 2.3 GENERATION OF PSEUDO-EXPERIMENTAL DATA

Based on the convolution integral (equation (2.32)), different equations were assigned to the weighting (W(t)) and input (I(t)) functions and these were used to calculate the response function R(t). Once the response function had been calculated, noise was then added to both the weighting and response functions, which were then used as input data for the various deconvolution algorithms, to produce a predicted value for the input function, I(t).

$$R(t) = \int_0^t W(t-\theta) I(\theta) d\theta \qquad (2.32)$$

### 2.3.1 Equations Assigned to the Weighting and Input Functions

The weighting function was always represented by a polyexponential of the form shown in equation (2.33).

The input function was assigned one of three forms :

$$W(t) = \sum_{i=1}^{n} A_i e^{-\alpha_i t} \tag{2.33}$$

(a) A first order release process as shown in equation (2.34)

$$I(t) = Dke^{-kt} \tag{2.34}$$

Where D is the dose given, k is the first order rate constant and t is time.

(b) A zero order release process which becomes first order after time $t_c$ as shown in equation (2.35).

$$I(t) = k_0 - H(t - t_c)k_0 + H(t - t_c)D_r ke^{-k(t - t_c)} \tag{2.35}$$

Where $D_r$ is the dose remaining at $t_c$, $k_0$ is the zero order rate constant, k is the first order rate constant and $H(t-t_c)$ is the unit step function which has a value of 0 at $t < t_c$ and 1 at $t \geq t_c$.

(c) An input function, defined not by an equation, but only by a set of points to allow greater flexibility in representing the input function for more unusual profiles.

### 2.3.2 Calculation of the Response Function

When the input function is in the form (a) or (b) specified in section (2.3.1), then the response function can be calculated algebraically by evaluation of the convolution integral. However, when the input function is numerical, as for (c) in section (2.3.1), the response function must also be calculated numerically.

#### 2.3.2.1 Input Form (a)

When the input function is represented by a monoexponential, as shown in equation (2.34) and the weighting function is represented by a polyexponential as shown on equation (2.33), then the response function can be calculated through evaluation of the convolution integral (equation (2.32)). This is done by taking Laplace transforms of the weighting and input functions to give equations (2.36) and (2.37), where W(s) is the Laplace transform of the weighting function and I(s) is the

Laplace transform of the input function. Multiplication of these equations according to the equation R(s) = W(s).I(s) gives the Laplace transform of the response function (equation (2.38)).

$$W(s) = \sum_{i=1}^{n} \frac{A_i}{s + \alpha_i} \tag{2.36}$$

$$I(s) = \frac{Dk}{s + k} \tag{2.37}$$

$$R(s) = \frac{Dk}{s + k} \sum_{i=1}^{n} \frac{A_i}{s + \alpha_i} \tag{2.38}$$

Taking the inverse transformation of equation (2.38) gives an expression for the response function, R(t), shown in equation (2.39), a full derivation of this equation is given in Appendix B.

$$R(t) = kD \sum_{i=1}^{n} A_i \frac{(e^{-\alpha_i t} - e^{-kt})}{(k - \alpha_i)} \tag{2.39}$$

Equation (2.39) can then used to generate values for the response function, for any set of parameters, at any time t.

### 2.3.2.2 Input Form (b)

The weighting function was again represented by a polyexponential as given by equation (2.33) and the Laplace transform of the weighting function W(s) is shown in equation (2.36). The input function I(t) was represented by equation (2.35) and its Laplace transformation shown in equation (2.40).

$$I(s) = \frac{k_0}{s} - e^{-t_c s}.\frac{k_0}{s} + e^{-t_c s} \frac{kD_r}{s + k} \tag{2.40}$$

Multiplication of equation (2.40) with equation (2.36) give an expression for the Laplace transform of the response function R(s) as shown in equation (2.41).

$$R(s) = \frac{k_0}{s}\sum_{i=1}^{n}\frac{A_i}{s+\alpha_i} - e^{-t_c s}.\frac{k_0}{s}\sum_{i=1}^{n}\frac{A_i}{s+\alpha_i} + e^{-t_c s}.\frac{kD_r}{s+k}\sum_{i=1}^{n}\frac{A_i}{s+\alpha_i} \tag{2.41}$$

Inverse transformation of equation (2.41) gives an expression for the response function R(t) as shown in equation (2.42), see Appendix B for a more detailed derivation.

$$R(t) = k_0\sum_{i=1}^{n}\frac{A_i}{\alpha_i}(1 - e^{-\alpha_i t}) - k_0 H(t - t_c)\sum_{i=1}^{n}\frac{A_i}{\alpha_i}(1 - e^{-\alpha_i(t - t_c)})$$
$$+ H(t - t_c)kD\sum_{i=1}^{n}\frac{A_i}{k - \alpha_i}(e^{-\alpha_i(t - t_c)} - e^{-k(t - t_c)}) \tag{2.42}$$

This equation can be used to produce values for the response function at any time t and for any set of parameters chosen.

### 2.3.2.3 Input Form (c)

In this form, the input function is represented solely by a set of data and the response function can therefore not be calculated algebraically. Instead the discrete form of the convolution integral was used to calculate the response data, which was presented in its iterative form by Langenbucher and Möller 1983 (equation (2.43)), where $W_i$ is the value of the weighting function at t= i.Δt, $I_i$ is the value of the input function at t = i.Δt and $R_i$ is the value of the response function at t = i.Δt.

$$\begin{aligned} R_0 &= 0 \\ R_1 &= (I_0 W_1/2 + I_1 W_0/2)\Delta t \\ R_n &= (I_0 W_n/2 + I_1 W_{n-1} + \ldots + I_{n-1} W_1 + I_n W_0/2)\Delta t \end{aligned} \tag{2.43}$$

The weighting function was again represented by a polyexponential and this equation was used to generate the weighting function at the required interval, Δt, for input into equation (2.43).

### 2.3.3 Addition of Noise to the Data

Noise was added to the required data sets using a subroutine G05DDF from the NAG libraries. This subroutine returns a random number from a normal distribution, with a mean and standard deviation specified by the user. In this case the mean was set to zero and the standard deviation (SD) set as shown below :

$$SD = x.y_i / 100$$

where $x$ = the percentage noise required

$y_i$ = the experimental value to which the noise is added

The value returned by G05DDF was added to the experimental value to create the new value which contained the desired amount of noise.

## 2.4 STATISTICAL METHODS

The statistical tables used for all statistical tests are those by Rohlf and Sokal, 1981.

### 2.4.1 F Test

The F test was used to test whether or not the weighted sum of squares was sufficiently different between two models, with p and q parameters, to justify the inclusion of additional terms in the equation (Boxenbaum et al 1973).

$$F = ((WSS_p - WSS_q).\ df_q) / (WSS_q .(df_p - df_q)) \quad df_p > df_q$$

where $WSS_p$ = weighted sum of squares obtained with p parameters

$WSS_q$ = weighted sum of squares obtained with q parameters

$df_p$ = n-p (n = number of data points)

$df_q$ = n-q degrees of freedom in the numerator

$df_p - df_q$ = degrees of freedom in the denominator

The value of F calculated from the equation above was compared with a value taken from a table of F values at $p = 0.05$, with $df_q$ degrees of freedom in the numerator and $df_p - df_q$ degrees of freedom in the denominator.

If the calculated value of F was less than that obtained from the table then there was no significant difference between the two models and the model with p parameters was accepted.

### 2.4.2 t Test

The t test can be used to test the significance of the deviation of a sample parameter from a standard value (Sokal and Rohlf 1981a). The $t_s$ value for a sample is determined according to equation (2.44) where $\bar{Y}$ is the sample mean, $Y_0$ is the standard value to which the mean is to be compared and SEM is the standard error of the sample mean.

$$t_s = \frac{\bar{Y} - Y_0}{SEM} \tag{2.44}$$

The null hypothesis for the test is that the sample mean is equal to the standard value. The value of $t_s$ is compared to the critical value of $t_{\alpha(n-1)}$ from the tables, where $\alpha$ is the probability level chosen to be significant (in most case $\alpha = 0.05$) and n is the number of samples. If $t_s < t_{\alpha(n-1)}$ then the null hypothesis is accepted.

## 2.5 STATISTICAL MOMENTS

### 2.5.1 Mean Dissolution Time (MDT)

The Statistical Moment theory is based on the primary assumption that the movement of drug molecules within the body is a stochastic process and therefore the time any one drug molecule takes to complete a process is a random variable. If the cumulative distribution function of this variable is represented by the function, F(t), then F(t) is the probability that a molecule has completed the process being studied by time t. The Probability Density function of a random variable, whose cumulative distribution function is represented by F(t), is f(t) (Cutler 1987), where f(t) is the differential of F(t), (equation (2.45)).

$$f(t) = \frac{dF(t)}{dt} \tag{2.45}$$

The mean value of the random variable is given by the integral of the first moment of its probability density function (equation (2.46)). The Mean Dissolution time can be calculated as follows.

$$MT = \int_{-\infty}^{\infty} t.f(t)\,dt = \int_{-\infty}^{\infty} t\frac{dF(t)}{dt}\,dt \qquad (2.46)$$

where MT is the Mean Time of the variable

The dissolution-time curve represents a statistical cumulative distribution process, therefore the probability, P, that at a time t any one particle has dissolved is equal to the fraction dissolved at time t divided by the total fraction which will dissolve (Tanigawara et al. 1982) and this is shown in equation (2.47).

$$P = F(t) = \frac{m_t}{m_\infty} \qquad (2.47)$$

$m_\infty$ = mass dissolved at time t = ∞ $m_t$ = mass dissolved at t = t

Substituting this equation for F(t) in equation (2.46) gives equation (2.48), the integral from -∞ to 0 in equation (2.48) will be zero since the dissolution process is assumed to start at t=0.

$$MDT = \int_{-\infty}^{\infty} t.f(t)\,dt = \frac{1}{m_\infty}\int_{-\infty}^{\infty} t.\frac{dm_t}{dt}\,dt = \frac{1}{m_\infty}\int_{0}^{\infty} t.\frac{dm_t}{dt}.dt = \frac{\int_{o}^{m_\infty} t.dm}{m_\infty} \qquad (2.48)$$

Equation (2.48) can be expressed as a discrete summation which can be used to evaluate both the *in vitro* and *in vivo* Mean Dissolution Time. This summation is shown in equation (2.49), where $t_i$ is the mid-point of two successive time intervals, $\Delta m_i$ is the amount released during this interval and $m_\infty$ is the total quantity released.

$$MDT = \frac{\sum (t_i.\Delta m_i)}{m_\infty} \qquad (2.49)$$

Equation (2.49) can be used to calculate the values of the Mean Dissolution Time for the *in vivo* dissolution rate from the input rate provided by the deconvolution algorithms, and for the *in vitro* dissolution rate from the cumulative fraction released as a function of time. If the input rate itself is used, then equation (2.49) has to be adapted slightly to give

equation (2.50) and this is used instead.

$$MDT = \frac{\sum t_i(I_{i-1} + I_i).\Delta t/2}{m_\infty} \qquad (2.50)$$

where $I_i$ is the input rate at t = i.$\Delta$t

To obtain the correct MDT value the upper limit in the summation must be infinity. In practice this is not possible and the MDT can only be determined up to the last time point used, without some form of extrapolation. It has been shown that, when the final value of the dissolution rate is 5% of its maximum value, then the difference between the true MDT and that determined up to this last time point, is 10% (Yamaoka et al 1978). Therefore in the following chapters the MDT will always be shown as $MDT_{(t)}$, where t is the time up to which it has been calculated. In this case $m_\infty$ in equations (2.49) and (2.50) will become $m_z$, where $m_z$ is the mass dissolved at $t_z$ and the summations in these equations will have an upper limit of $t_z$.

# 3 COMPARISON OF DECONVOLUTION METHODS USING PSEUDO-EXPERIMENTAL DATA

In this chapter each of the four deconvolution algorithms were tested with pseudo-experimental data , the aim being to examine the ability of the four algorithms (described in detail in section 2.2) to predict the true form and values of an input function whose form and values were set prior to deconvolution.

Three different forms of input functions were used, and these were chosen to reflect plausible release rate profiles which might arise following the administration of a dosage form.

The first form chosen was to let the input function represent a first order release process, in which the rate of drug release is dependant on the amount of drug remaining in the dosage form. First order release is assumed to occur with most "normal" tablets, once disintegration of the tablet has occurred.

The second form chosen was to use an input function comprising of two parts. An initial zero order process during which the release rate is constant and independent of all other factors and this continues up until a time $t_c$, after which the release rate becomes first order. This input function represents an idealised release profile for a controlled release product, the majority of which aim to produce zero order release over a specified time period. As a further test of the deconvolution algorithms the transition from zero to first order release occurs suddenly at $t=t_c$ producing a sharp change in the release profile (input rate) which would not be seen *in vivo* . In subsequent sections this input form will be designated as the **zero order release function.**

The third form chosen for the input function was a more realistic release rate profile for a controlled release product in which the initial rate of release is zero, then rises rapidly to reach a plateau phase during which release is zero order. After a certain time interval this plateau phase decays slowly into a first order process. In subsequent sections this form of the input function will be designated as the **controlled release input function.**

The input function, in one of these three forms, was convolved with a triexponential weighting function represented by equation (3.1), to produce values for the response

function (see section 2.3.2). The weighting function was given one negative coefficient, (-2), in order to mimic the type of profile which would arise after administration of an oral bolus solution, i.e. it would have an initial value of zero. In this way the input function produced by the deconvolution represents a hypothetical release rate and not an absorption rate.

$$W(t) = -2e^{-10t} + e^{-t} + e^{-5t} \tag{3.1}$$

Various levels of noise were added to the values of both the weighting and response data (section 2.3.3) to produce pseudo-experimental data which were then processed by each of the four deconvolution algorithms. For each of the different forms of input function two separate examinations were made. Firstly the effect on the predicted input rate, from one data set, due to increasing levels of added noise and secondly the effect on the mean predicted input rate produced by deconvolution of multiple data sets containing a constant level of noise.

| Time | True Input Function I(t) | True Weighting Function W(t) | True Response Function R(t) |
|---|---|---|---|
| 0.05 | 1.0858 | 0.5170 | 0.0166 |
| 0.10 | 0.9825 | 0.7756 | 0.0530 |
| 0.15 | 0.8890 | 0.8868 | 0.0959 |
| 0.20 | 0.8044 | 0.9159 | 0.1386 |
| 0.30 | 0.6586 | 0.8644 | 0.2110 |
| 0.40 | 0.5392 | 0.7690 | 0.2615 |
| 0.60 | 0.3614 | 0.5936 | 0.3081 |
| 0.80 | 0.2423 | 0.4670 | 0.3100 |
| 1.00 | 0.1624 | 0.3745 | 0.2899 |
| 1.20 | 0.1089 | 0.3037 | 0.2607 |
| 1.40 | 0.0730 | 0.2475 | 0.2287 |
| 1.60 | 0.0489 | 0.2022 | 0.1973 |
| 2.00 | 0.0220 | 0.1354 | 0.1422 |

**Table 1 :** Weighting Function data produced by $W(t) = -2e^{-10t} + e^{-5t} + e^{-t}$, Input Function Data produced from $I(t) = 1.2e^{-2t}$ and Response Data produced from Convolution of the Weighting and Input Functions

## 3.1 MONOEXPONENTIAL INPUT FUNCTION

The input function was represented by the following equation (3.2) where $D_O$ is the dose administered and k is the first order rate constant.

$$I(t) = kD_O e^{-kt} \tag{3.2}$$

The values used for the constants were k = 2.0 and D = 0.6 so that the equation for the input function becomes $I(t) = 1.2e^{-2t}$. The weighting function used was that shown in equation (3.1), and these two equations were used to produce the values shown in Table 1 where the response function data was produced by convolving the weighting and input functions according to the procedure given in section 2.3.2.

### 3.1.1 Increasing Levels of Added Noise

#### 3.1.1.1 Method

Noise levels of 1, 5 and 10% were added to the values of the weighting and response functions shown in Table 1 using the NAG subroutine G05DDF (see section 2.3.4). The data sets produced following the addition of noise are shown in Tables C(1a) and C(1b) in appendix C.

The true data and the data sets containing the added noise were then processed through each of the four deconvolution algorithms (section 2.2) according to the details for each given in the sections below. The weighting and response data were fitted to polyexponentials of the form shown in equation (3.3) using the non-linear curve-fitting routine described in section 2.1.1. The number of terms in the exponential was increased sequentially and the data re-fitted until there was no significant reduction in the residual

$$W(t) = \sum_{i=1}^{n} A_i e^{-\alpha_i t} \tag{3.3}$$

sum of squares as judged by the F test (section 2.4.1) at P=0.05 and n=13. The parameters obtained from the curve fitting of the weighting and response data are shown in Tables 2(a) and 2(b) respectively.

| Parameters | True Values | 0% Noise Added | 1% Noise Added | 5% Noise Added | 10% Noise Added |
|---|---|---|---|---|---|
| $A_1$ | -2.0000 | -2.0006 | -1.5478 | -2.1365 | -3.5620 |
| $A_2$ | 1.0000 | 1.0006 | 0.5573 | 1.0487 | 2.9420 |
| $A_3$ | 1.0000 | 1.0000 | 0.9905 | 1.0878 | 0.6220 |
| $\alpha_1$ | 10.0000 | 9.9982 | 11.6021 | 9.2226 | 6.1112 |
| $\alpha_2$ | 5.0000 | 5.0004 | 3.9029 | 5.3127 | 3.6964 |
| $\alpha_3$ | 1.0000 | 1.0000 | 0.9972 | 1.0388 | 0.6943 |

**Table 2(a) :** Parameters obtained following Curve-fitting of Weighting Data, shown in Table C(1a), to a Polyexponential with Constants $A_i$ and Exponents $\alpha_i$.

### (a) Numerical Deconvolution

An interpolation interval of 0.05 was used for the spline interpolation of both weighting and response data prior to deconvolution.

| Parameters | 0% Noise Added | 1% Noise Added | 5% Noise Added | 10% Noise Added |
|---|---|---|---|---|
| $A_1$ | -1.0261 | -1.0414 | -1.1477 | -1.9246 |
| $A_2$ | 0.2119 | 0.2000 | 0.3069 | 1.0314 |
| $A_3$ | 0.8142 | 0.8414 | 0.8408 | 0.8932 |
| $\alpha_1$ | 2.9260 | 2.8465 | 3.0684 | 3.5102 |
| $\alpha_2$ | 10.7707 | 11.2968 | 8.8962 | 5.5215 |
| $\alpha_3$ | 0.8589 | 0.8696 | 0.86020 | 0.9224 |

**Table 2(b) :** Parameters obtained following Curve-fitting of Response Data, shown in Table C(1b), to a Polyexponential with Constants $A_i$ and Exponents $\alpha_i$.

### (b) Semi-Numerical Deconvolution

The response data was interpolated as for the numerical deconvolution. The parameters in Table 2(a) were used to generate the data for the weighting function at a time interval of 0.05 and these were used together with the interpolated response function for input into the semi-numerical deconvolution algorithm.

**(c) Polynomial Deconvolution**

The parameters from Table 2(a) were used to represent the weighting function data, the dose administered was 0.6 (see equation (3.2)), and together with the response data, these formed the input for the polynomial deconvolution method (see section 2.2.3).

The optimal polynomial to represent the input function was selected using the F test (section 2.4.1) on the residual sum of squares associated with that polynomial at P= 0.05 and n=13. The selected polynomials for each data set are shown in Table 3. These were then used to generate the values of the input function, and the integrals of these polynomials were used to generate the values of the cumulative fraction input (CFI).

| % Noise Added to Data | Selected Polynomial for the Input Rate I(t) |
|---|---|
| 0% | $I(t) = 1.199 - 2.380t + 2.282t^2 - 1.306t^3 + 0.428t^4 - 0.061t^5$ |
| 1% | $I(t) = 1.155 - 1.933t + 1.186t^2 - 0.254t^3$ |
| 5% | $I(t) = 1.093 - 1.454t + 0.500t^2$ |
| 10% | $I(t) = 1.104 - 1.517t + 0.535t^2$ |

**Table 3 :** Selected Polynomials produced by Polynomial Deconvolution on Data (from Table C(1)) with Increasing Levels of Added Noise

**(d) Polyexponential Deconvolution**

The parameters from Table 2(a) were used to represent the weighting function and those from Table 2(b) used to represent the response function and these two sets of parameters were used as input into the polyexponential deconvolution algorithm (section 2.2.4).

### 3.1.1.2 Results

For all the deconvolution methods the input rates and the cumulative fraction input (CFI) produced with data for 1% added noise were so close to those produced with the error free data that they were indistinguishable and have therefore been omitted from the graphs shown in Figures 1-8.

**(a) Numerical Deconvolution**

The input rates produced by numerical deconvolution with increasing levels of added noise are shown in Figure 1 and the cumulative input as a fraction of the total dose administered are shown in Figure 2.

As can be seen from the graphs the numerical deconvolution methods works well on error free data, and the results produced are indistinguishable from the true input rate and the cumulative fraction input. However, as the level of noise increases, the input rate produced by the numerical deconvolution begins to oscillate widely achieving considerable negative values, which, if the input function truly represented the *in vivo* drug release rate, would be physiologically impossible. At some points the oscillations produce estimated input rate values which are triple the true values.

The picture presented by the cumulative fraction input, (CFI),is slightly different, as the level of added noise is increased the input rates produced at the 5 and 10% noise level do show some oscillation but to a much lower degree than the input rate itself. The estimations of the total fraction released for all error levels are close to the true value.

**(b) Semi-Numerical Deconvolution**

The input rates produced by semi-numerical deconvolution are very similar to those produced by numerical deconvolution and, like the numerical method, the semi-numerical algorithm works very well on error free data (Figure 3) producing values indistinguishable from the true values. However, the method (like the numerical method) produces severe oscillations with higher levels of noise.

The CFI's (Figure 4) are also very similar to those produced for the numerical deconvolution. The CFI produced with 0% and 1% noise are indistinguishable from the true CFI, but as the level of added noise increases the CFI produced begins to oscillate. Like the numerical deconvolution the oscillations are much less than for the input rate values themselves and the final estimation of the total fraction released is very close to the true value.

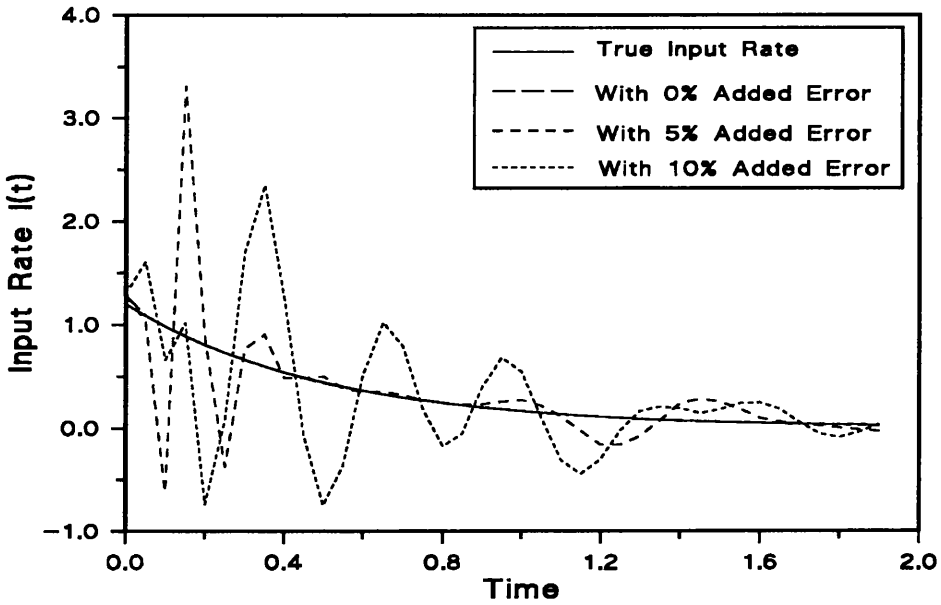


**Figure 1** : Input Rates produced by Numerical Deconvolution for the Monoexponential Input Function with Increasing Levels of Error added to both the Weighting and Response Functions

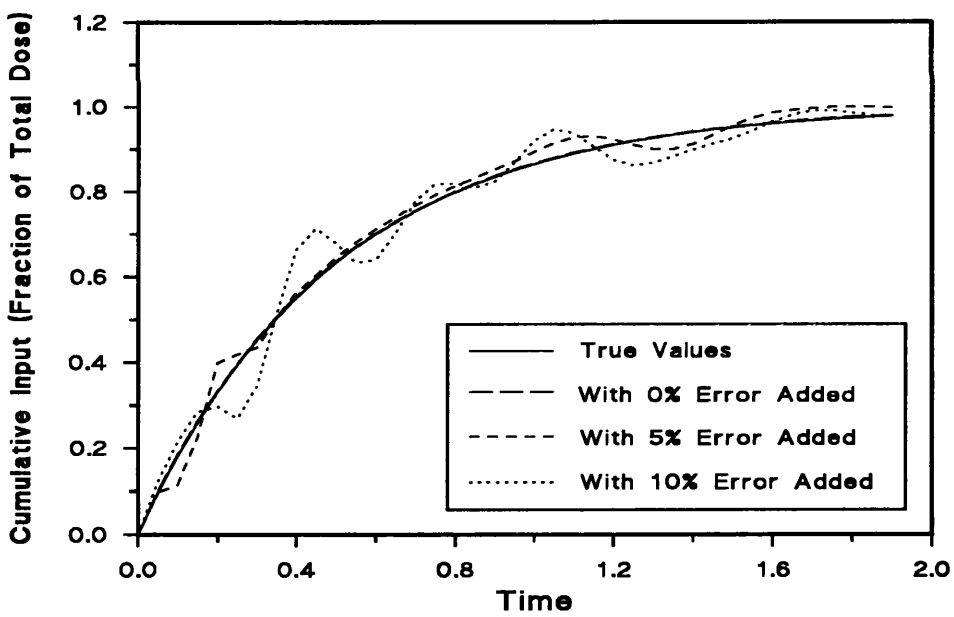


**Figure 2** : Cumulative Input produced by Numerical Deconvolution for the Monoexponential Input Function with Increasing Levels of Error added to both the Weighting and Response Functions

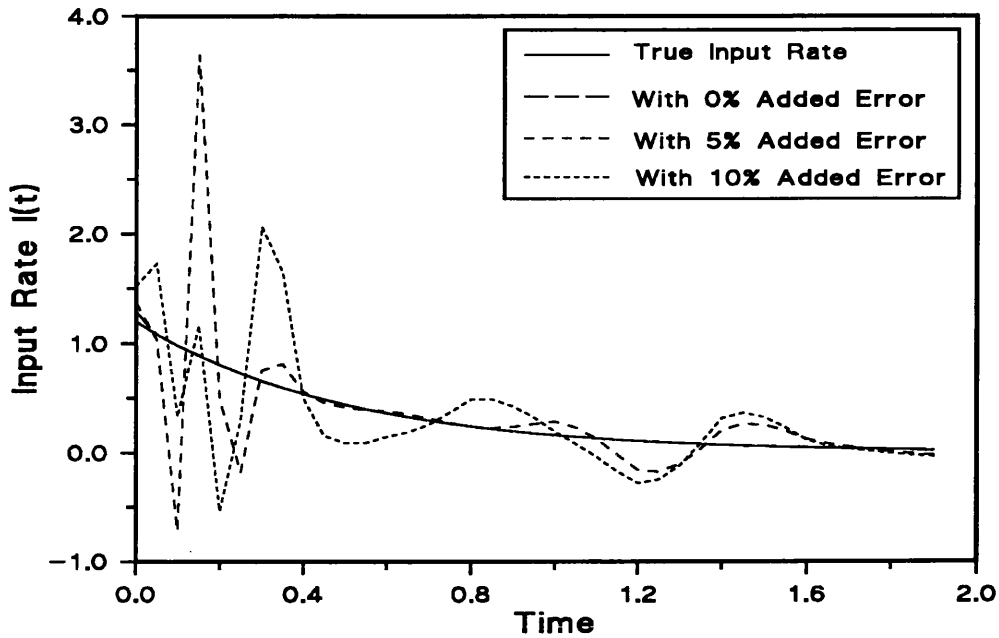


**Figure 3** : Input Rate produced by Semi-Numerical Deconvolution for the Monoexponential Input Function with Increasing Levels of Error added to both the Weighting and Response Functions.

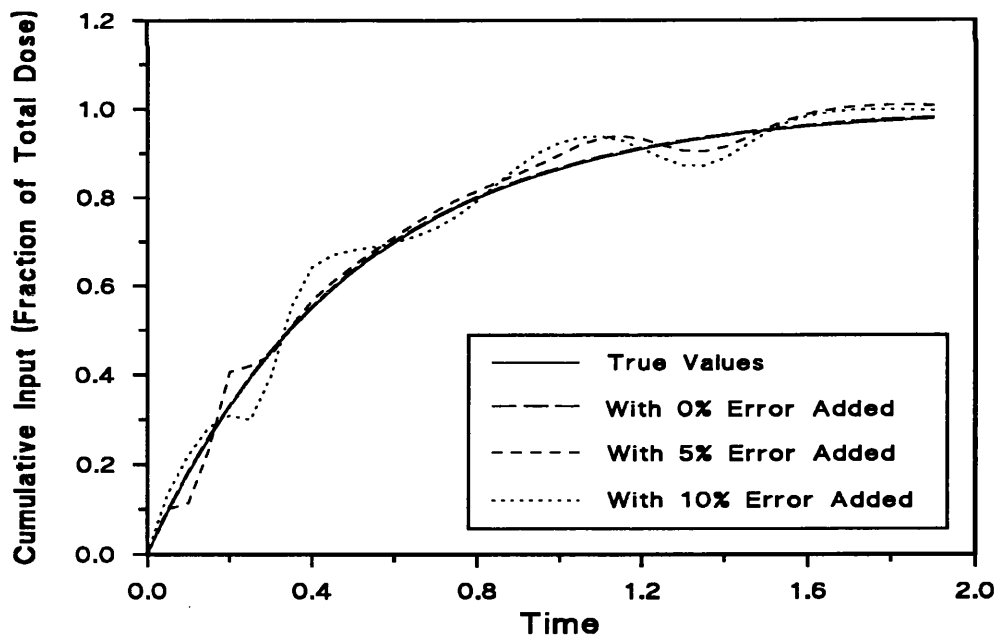


**Figure 4** : Cumulative Input produced by Semi-numerical Deconvolution for the Monoexponential Input Function with Increasing Levels of Error added to both Weighting and Response Functions.

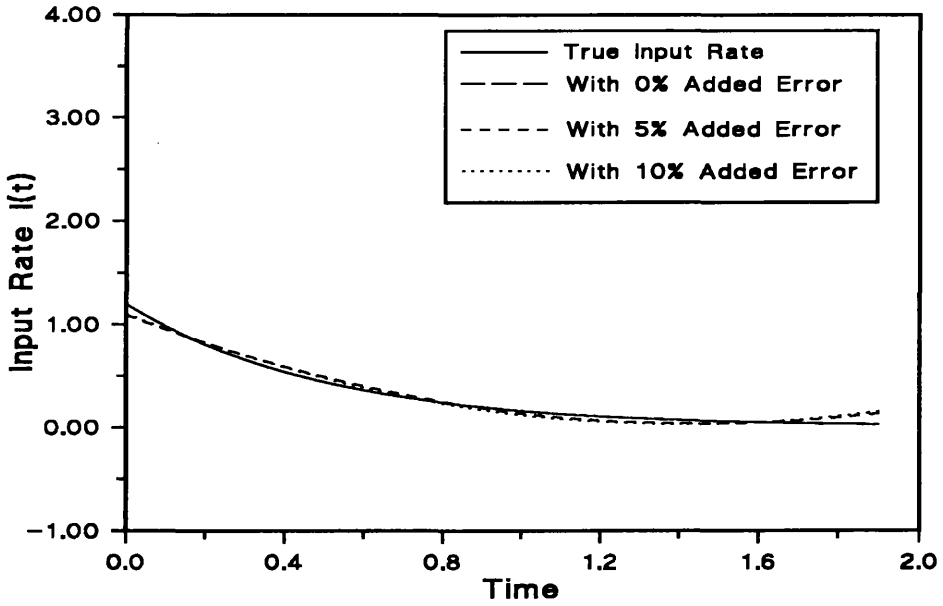


**Figure 5** : Input Rates produced by Polynomial Deconvolution for the Monoexponential Input Function with Increasing Levels of Error added to both the Weighting and Response Functions.

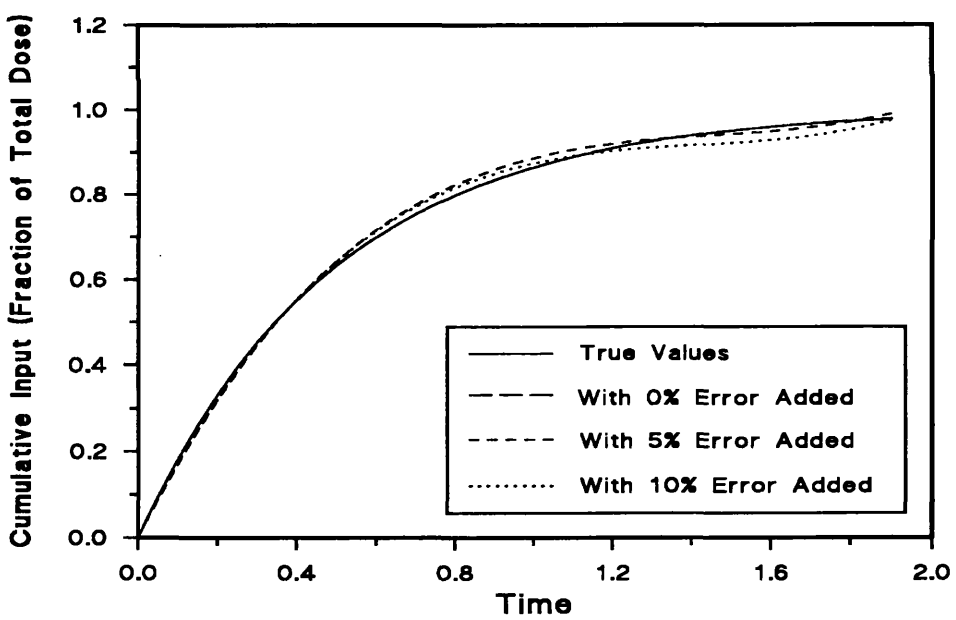


**Figure 6** : Cumulative Input produced by Polynomial Deconvolution for the Monoexponential Input Function with Increasing Levels of Error added to both the Weighting and Response Functions.

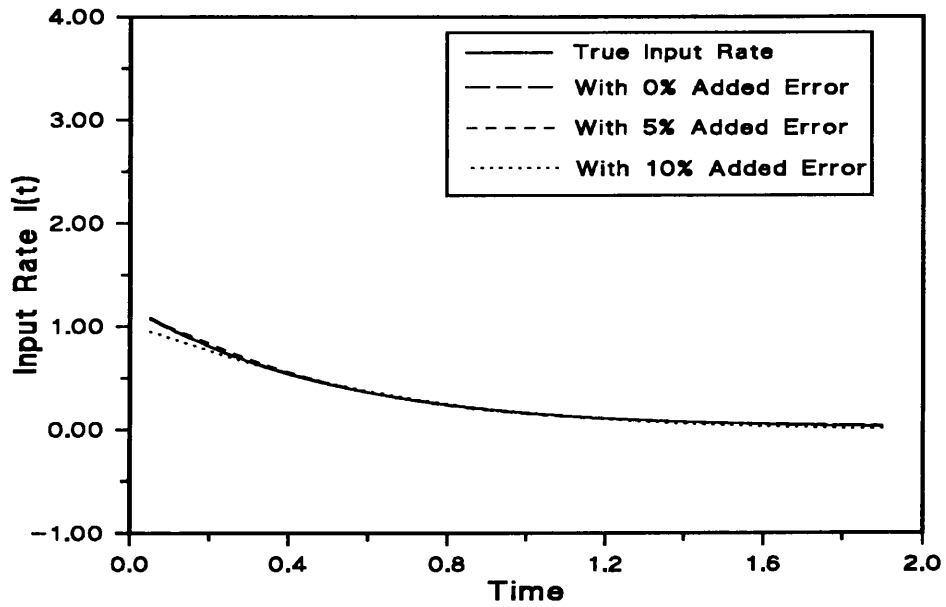


**Figure 7** : Input Rates produced by Polyexponential Deconvolution for the Monoexponential Input Function with Increasing Levels of Error added to both Weighting and Response Functions.

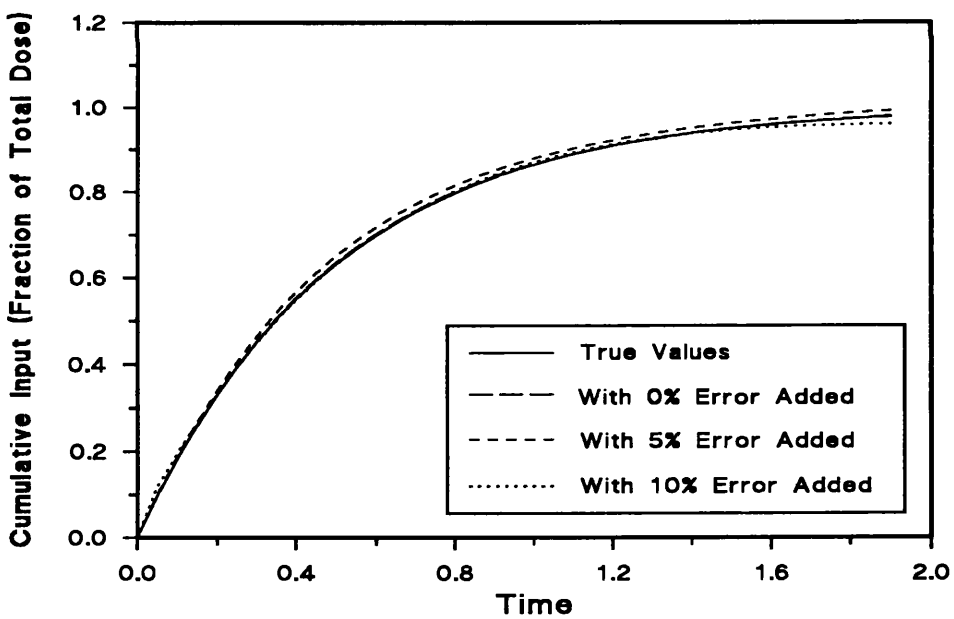


**Figure 8** : Cumulative Input produced by Polyexponential Deconvolution for the Monoexponential Input Function with Increasing Levels of error added to both Weighting and Response Functions.

**(c) Polynomial Deconvolution**

The input rates and CFI's (Figures 5 and 6 respectively) produced by this method show little variation with increasing levels of data noise and at all levels of noise the predicted input rate is very close to the true value. With error free data the input rate produced is indistinguishable from the true input rate and even at higher noise levels there is little divergence. At no point does the input rate become negative and there is no oscillation in the rate predicted, however the input rate does begin to diverge at the extremes of the time range over which deconvolution was performed.

The predicted CFI's exhibit the same features as the predicted input rates. The CFI produced with error free data are indistinguishable from the true CFI, and all the predicted CFI's are very close to the true values and little variation is seen with increasing levels of noise.

**(d) Polyexponential Deconvolution**

In both the estimated input rate and CFI there is little change in the predicted values with increasing levels of noise (Figures 7 and 8) and all the results produced are very close to the true values. The input rate and CFI produced with error free data are almost identical to the true values. There is no oscillation in the estimated input rate and at no time does this rate become negative. The estimation of the total fraction released for all noise levels is very close to the true value.

### 3.1.1.3 Percentage Difference between Predicted and True Values

For each of the data sets shown in Figures 1-8 the percentage difference between the true value and the predicted value for each point was calculated in the following way.

The percentage difference for the input rate was calculated as the absolute value of the difference between the calculated input and the true input, divided by the true input at t=0 and multiplied by 100, i.e.

$$\%\text{diff } I(t) = \left| \text{Calc. } I(t) - \text{True } I(t) \right| * 100 / 1.2$$

where 1.2 is the exact value of the input rate at t=0

The percentage difference for the cumulative fraction input was calculated as the calculated fraction minus the true fraction multiplied by 100.

$$\%\text{diff fraction input} = |\text{calc. value} - \text{true value}| * 100$$

Each data set comprised 39 values over a time range of 0 to 1.9 at intervals of 0.05, which was the output from the deconvolution algorithms. The percentage differences, once calculated, were averaged for each data set and the mean and standard error of the means for these values are shown in Table 4 for the estimated input rate values and Table 5 for the estimated fraction input values.

| | Noise Level in original Data | | | |
|---|---|---|---|---|
| Type of Deconvolution | 0% | 1% | 5% | 10% |
| Numerical | 0.31 (0.177) | 1.57 (0.261) | 17.1 (6.30) | 32.8 (5.50) |
| Semi-Numerical | 0.30 (0.180) | 2.48 (0.401) | 18.2 (6.84) | 24.0 (4.40) |
| Polynomial | 0.03 (0.005) | 0.72 (0.105) | 3.04 (0.33) | 3.25 (0.36) |
| Polyexponential | 0.30 (0.030) | 0.36 (0.053) | 0.68 (0.092) | 1.65 (0.03) |

**Table 4 :** Mean Percentage Difference for Input Rate Values shown in Figures 1,3,5 and 7 for Increasing Levels of Added Noise. The S.E.M. values are shown in Parentheses (n=39).

| | Noise Level in original Data | | | |
|---|---|---|---|---|
| Type of Deconvolution | 0% | 1% | 5% | 10% |
| Numerical | 0.212 (0.012) | 0.85 (0.073) | 2.15 (0.237) | 3.72 (0.518) |
| Semi-Numerical | 0.285 (0.010) | 1.05 (0.111) | 2.35 (0.259) | 3.41 (0.370) |
| Polynomial | 0.008 (0.001) | 0.35 (0.032) | 1.15 (0.121) | 1.39 (0.146) |
| Polyexponential | 0.161 (0.020) | 0.495 (0.020) | 1.50 (0.198) | 1.74 (0.217) |

**Table 5 :** Mean Percentage Difference for Cumulative Fraction Input Values shown in Figures 2,4,6 and 8 for Increasing Levels of Added Noise. The S.E.M. values are shown in Parentheses (n=39).

The mean values shown in the tables reflect what has already been shown in Figures 1-8. The mean percentage difference values for the input rates for all of the deconvolution algorithms are very small when there is little or no noise present in the data, however as the level of noise is increased the mean percentage difference jumps dramatically for the numerical and semi-numerical methods at the 5 and 10% noise levels (see Table 4) and

is much greater than the level of noise originally added to the data. The mean %difference for the polynomial and polyexponential methods at these higher noise levels remains low and is always lower than the level of noise added to the original data, indicating that these methods are much more stable to data noise.

The mean percentage differences obtained for the CFI's are much lower for all deconvolution methods, at all noise levels, than those obtained for the input rate. All of these mean values are of the same order as the level of noise added to the original data (see Table 5). The numerical and semi-numerical methods have slightly higher mean values than the polynomial and polyexponential methods at the greater noise levels, but these are still well below the level of noise added.

### 3.1.2 Constant Level of Noise Added to Ten Data Sets

#### 3.1.2.1 Method

In this second part the level of added noise was set at 10% and ten different random data sets were generated by using the addition of noise to the true weighting and response values shown in Table 1 using the NAG subroutine G05DDF (section 2.1.1). The ten data sets thus produced are shown in Tables C(2) and C(3) in Appendix C.

Each of the data sets was fitted to an equation of the form given in equation (3.3) using the non-linear least-squares fitting routine (section 2.1.1). The number of terms in the polyexponential was sequentially increased until there was no significant improvement in the residual sum of squares as judged by the F test at P=0.05 and n=13 (n is the number of data points). The parameters produced from this fitting are shown in Tables 6 (Weighting Function) and 7 (Response Function).

The ten data sets produced were then processed through each of the four deconvolution algorithms (section 2.2) according to the details given below.

**(a) Numerical Deconvolution**

The interpolation time used was again 0.05, and both weighting and response data was interpolated prior to deconvolution.

| Parameters / Subject | $A_1$ | $A_2$ | $A_3$ | $\alpha_1$ | $\alpha_2$ | $\alpha_3$ |
|---|---|---|---|---|---|---|
| 1 | -1.0583 | 1.0583 | | 14.7831 | 1.0103 | |
| 2 | -1.2167 | 1.2167 | | 13.1451 | 1.1509 | |
| 3 | -1.2764 | 1.2764 | | 11.3284 | 1.2370 | |
| 4 | -1.2244 | 1.2244 | | 14.8374 | 1.1877 | |
| 5 | -1.2888 | 1.2888 | | 12.6102 | 1.1787 | |
| 6 | -1.4136 | 1.4136 | | 13.6901 | 1.2980 | |
| 7 | -2.2218 | 0.7759 | 1.4459 | 10.2161 | 0.7469 | 5.3961 |
| 8 | -1.2805 | 1.2805 | | 14.2763 | 1.2403 | |
| 9 | -1.1364 | 1.1364 | | 16.2309 | 1.1238 | |
| 10 | -1.2704 | 1.2704 | | 12.5863 | 1.18836 | |

**Table 6 :** Parameters Obtained following Curve-fitting of the Weighting Data, shown in Table C(2), to a Polyexponential with Constants $A_i$ and Exponents $\alpha_i$.

| Parameters / Subject | $A_1$ | $A_2$ | $A_3$ | $\alpha_1$ | $\alpha_2$ | $\alpha_3$ |
|---|---|---|---|---|---|---|
| 1 | -1.8094 | 1.1699 | 0.6365 | 4.3187 | 6.1635 | 0.7038 |
| 2 | -1.1629 | 0.1900 | 0.9729 | 2.8527 | 15.4793 | 1.0416 |
| 3 | -10.0574 | 10.0574 | | 1.3925 | 1.2853 | |
| 4 | -10.0259 | 10.0259 | | 1.4518 | 1.3307 | |
| 5 | -3.2794 | 1.2192 | 2.0602 | 2.4069 | 3.8828 | 1.2581 |
| 6 | -5.0043 | 5.0043 | | 1.3878 | 1.1899 | |
| 7 | -0.9191 | 0.1920 | 0.7271 | 3.1552 | 15.9445 | 0.7938 |
| 8 | -1.7884 | 1.0874 | 0.7010 | 3.7424 | 5.3098 | 0.7360 |
| 9 | -10.0691 | 10.0691 | | 1.3254 | 1.2230 | |
| 10 | -10.0368 | 10.0368 | | 1.3911 | 1.2831 | |

**Table 7 :** Parameters obtained following Curve-fitting of Response Data, shown in Table C(3), to a Polyexponential with Constants $A_i$ and Exponents $\alpha_i$.

**(b) Semi-Numerical Deconvolution**

The parameters from Table 6 were used to generate values for the weighting function at intervals of 0.05 and these, together with the response function data (interpolated at t=0.05), were used as input into the semi-numerical deconvolution algorithm.

**(c) Polynomial Deconvolution**

The parameters from Table 6 were used to represent the weighting function, the dose administered for the response function was 0.6 (see equation 3.2) and the values in Table C(3) were used for the response function. The data were then processed according to the polynomial deconvolution method (section 2.2.3) and the optimal polynomial to represent the input function was selected using the F Test (section 2.4.1) at P=0.05 and n=13. The selected polynomials are shown in Table 8 and these were used to calculate the input rate, I(t), and their integrals used to calculate the cumulative fraction input.

| Subject | Selected Polynomial for the Input Rate |
|---|---|
| 1 | $I(t) = 1.1807 - 1.6038t + 0.5571t^2$ |
| 2 | $I(t) = 1.1020 - 1.5061t + 0.5130t^2$ |
| 3 | $I(t) = 1.2915 - 2.7201t + 2.1382t^2 - 0.5610t^3$ |
| 4 | $I(t) = 1.0592 - 1.2708t + 0.3924t^2$ |
| 5 | $I(t) = 0.9961 - 1.1645t + 0.3482t^2$ |
| 6 | $I(t) = 0.8132 - 0.9638t + 0.3208t^2$ |
| 7 | $I(t) = 1.1428 - 1.4920t + 0.4864t^2$ |
| 8 | $I(t) = 1.0750 - 1.7373t + 1.1332t^2 - 0.2675t^3$ |
| 9 | $I(t) = 1.0508 - 1.3739t + 0.4794t^2$ |
| 10 | $I(t) = 1.4164 - 3.5604t + 3.2853t^2 - 0.9767t^3$ |

**Table 8 :** Selected Polynomials produced by Polynomial Deconvolution on Data from Tables C(2) and C(3).

**(d) Polyexponential Deconvolution**

The parameters from Table 6 were used to represent the weighting function and

those from Table 7 used to represent the response function and together these formed the input into the polyexponential deconvolution algorithm.

Following deconvolution the mean and standard error of the mean over the ten data sets were calculated for the input rate and the cumulative fraction input (CFI) for each deconvolution method. The estimated fraction of dose released ($F_R$) produced for each data set was calculated by taking the maximum value reached in the cumulative fraction input profile. For each input rate produced the Mean Dissolution Time (MDT) was calculated according to the method described in section (2.5.1).

#### 3.1.2.2 Results

For each deconvolution method the mean input rate and mean cumulative fraction input for the ten data sets were plotted together with the standard error of the mean values (S.E.M.) and these are shown in Figures 9-12.

**(a) Numerical Deconvolution**

The mean input rate (n=10) produced for the numerical deconvolution shows considerable oscillation and the SEM values associated with it are very large (Figure 9). The oscillations are smaller than those shown by individual data sets, but are still unacceptably high.

The mean CFI is much closer to the true value, showing little oscillation. The SEM values are much smaller than those for the mean input rate.

**(b) Semi-Numerical Deconvolution**

The results produced for the semi-numerical deconvolution method (Figure 10) are very similar to those produced for the numerical deconvolution method (Figure 9). The mean input rate (n=10) still shows a marked degree of oscillation although to a lesser extent than the individual data and the SEM values are still large especially at the earlier time points.

The mean CFI is very close to the true value and the SEM values associated with the cumulative profile are much smaller than those for the mean input rate.

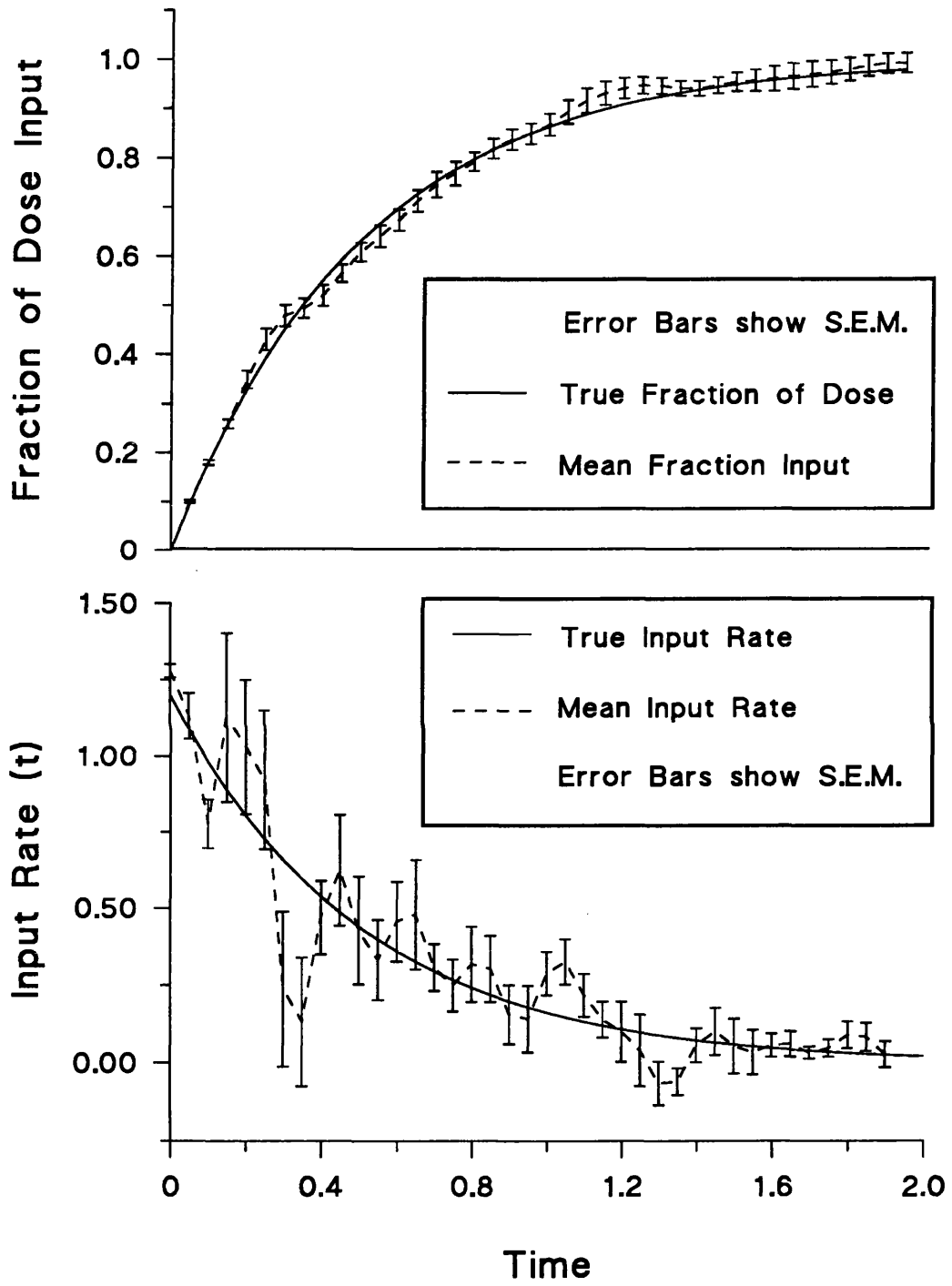


**Figure 9** : Mean results produced by Numerical Deconvolution for the Monoexponential Input Function on 10 Data Sets with 10% Error added to both the Weighting and Response Functions

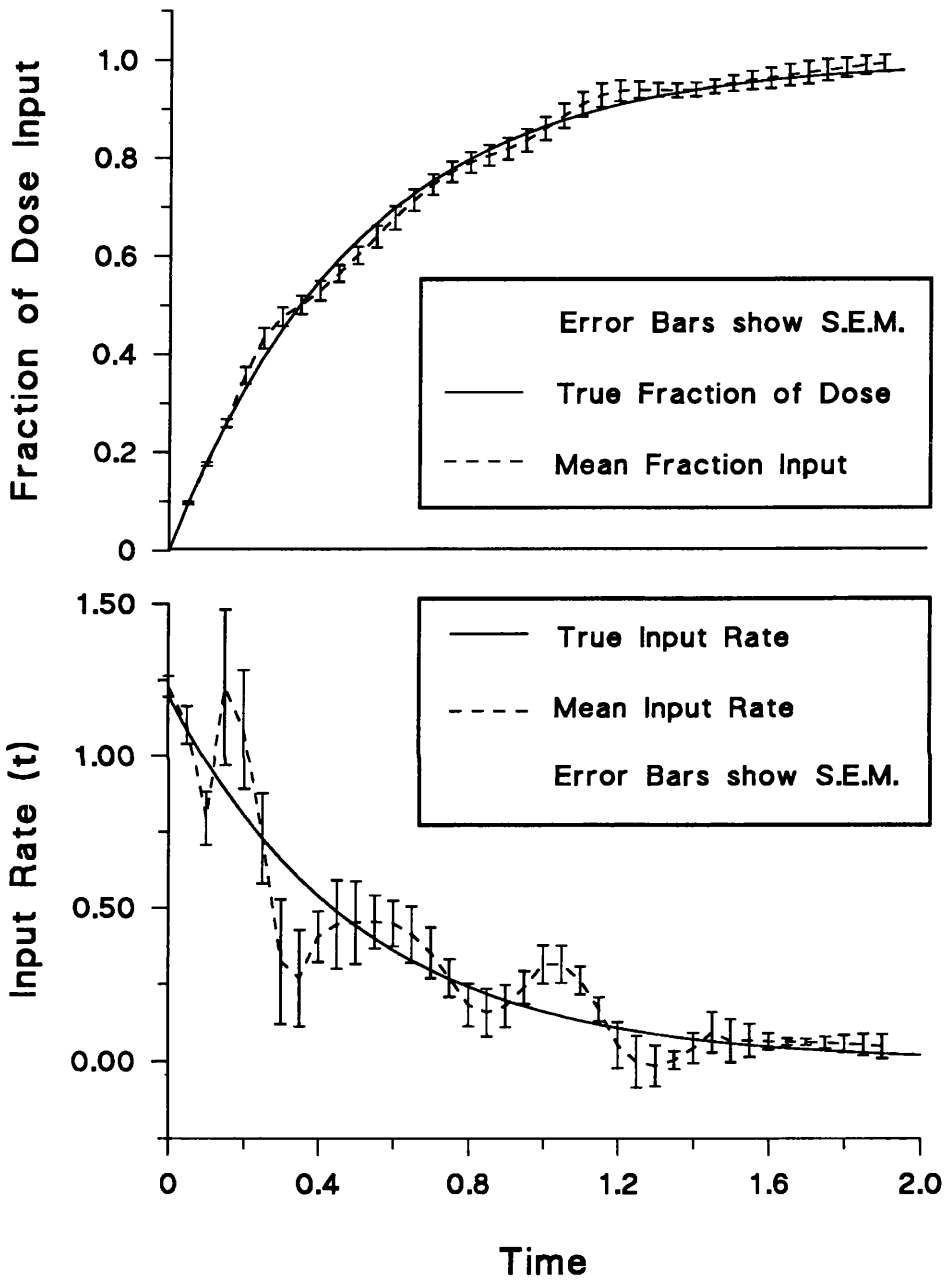


**Figure 10** : Mean results produced by Semi-Numerical Deconvolution for the Monoexponential Input Function on 10 Data Sets with 10% Noise added to both the Weighting and Response Functions

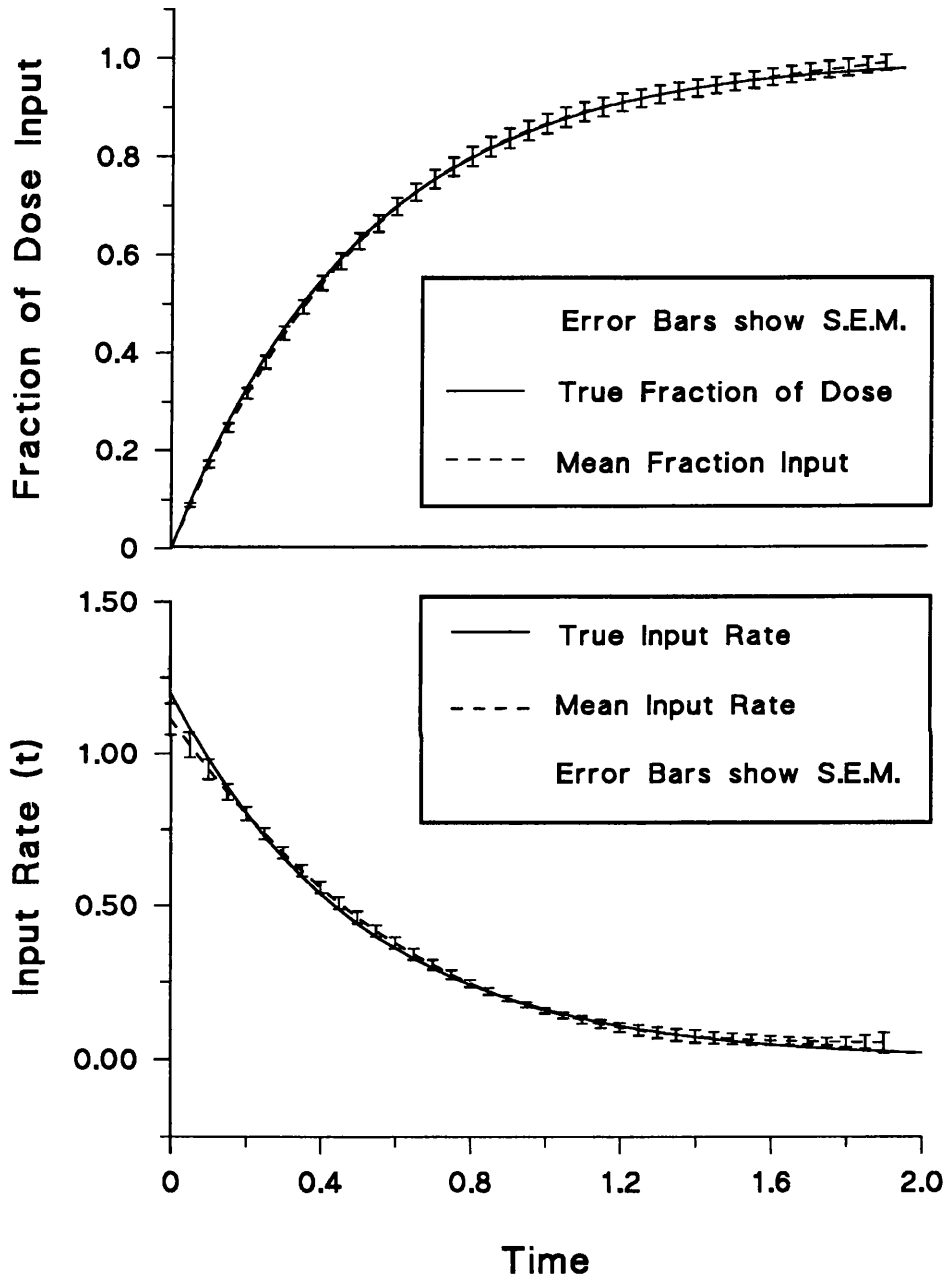


**Figure 11** : Mean results produced by Polynomial Deconvolution for the Monoexponential Input Function on 10 Data Sets with 10% Error added to both the Weighting and Response Functions

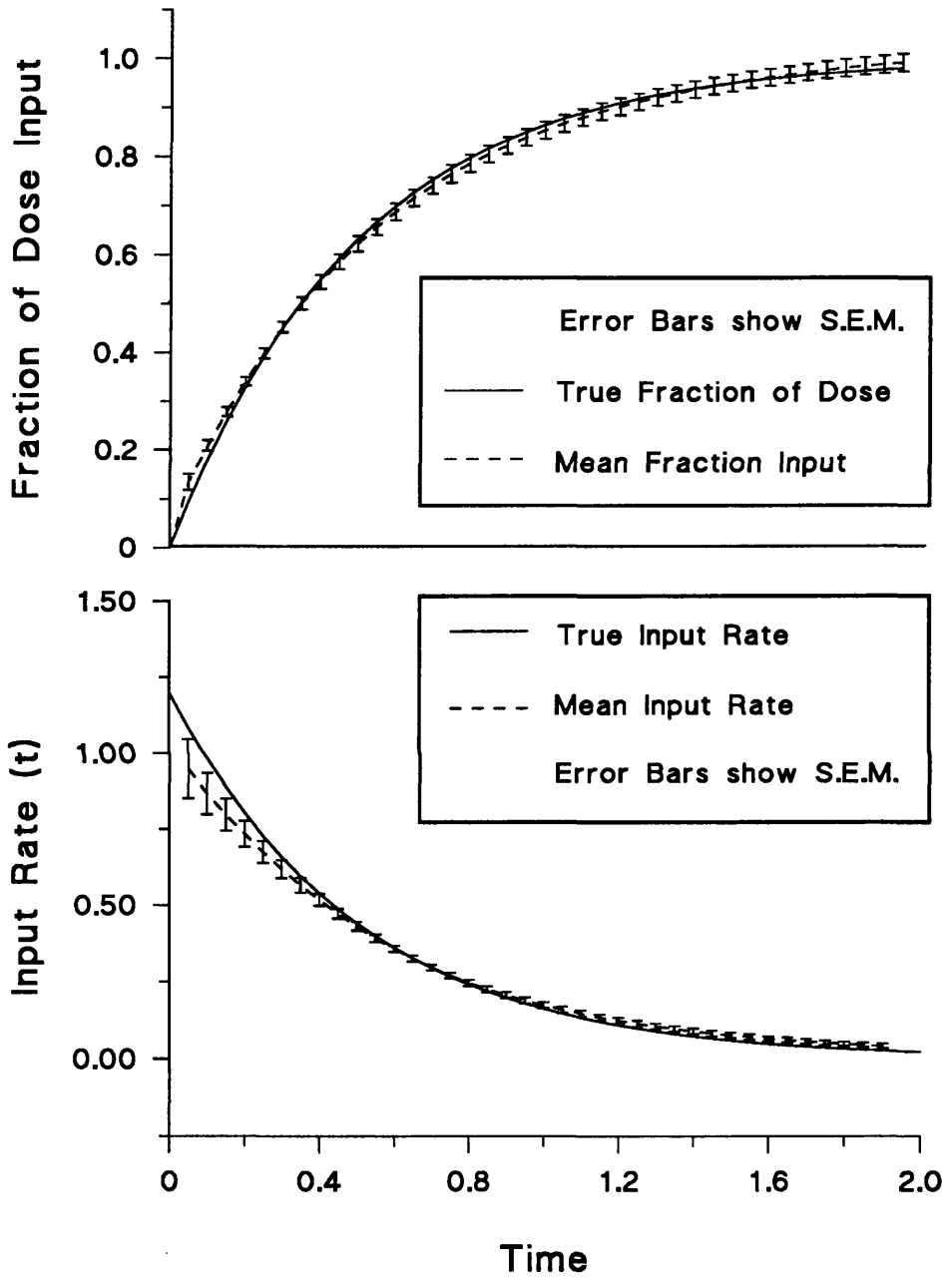


**Figure 12** : Mean results produced by Polyexponential Deconvolution for the Monoexponential Input Function on 10 Data Sets with 10% Error added to both the Weighting and Response Functions

**(c) Polynomial Deconvolution**

The mean input rate and mean cumulative fraction input (n=10) produced by polynomial deconvolution are shown in Figure 11. The mean input rate is very close to the true value with the greatest difference between the two occurring at either end of the interval over which deconvolution was performed. The SEM values associated with the mean input rate are small showing that the method produces consistently good estimates of the true input rate.

The mean CFI is very close to the true value and the SEM values associated with it are small.

**(d) Polyexponential Deconvolution**

The mean input rate and mean cumulative fraction input produced by polyexponential deconvolution are shown in Figure 12. The mean input rate produced is very close to the true rate at the later time points, however the input rate estimated for the initial time points is consistently underestimated by the method. The deviation from the true values is still not large, compared with the numerical and semi-numerical methods, but it is apparent.

The mean CFI is very close to the true value and the SEM values associated with it is very small, showing the consistency of the estimates produced by this method.

### 3.1.2.3 Estimated Fraction Released $F_R$

The estimated fraction of dose released for each subject and each deconvolution method are shown in Table 9, together with the mean fraction released ($\bar{F}_R$), the standard deviation (SD) and the standard error of the mean (SEM) for each deconvolution method.

The mean fraction released produced for each of the deconvolution methods was compared with the true value of 0.978 using the t-test (section 2.4.2) at a probability level of P=0.05 and 9 degrees of freedom. The value of 0.978 is the fraction of dose released at t=1.9 calculated form the integral of $I(t) = 1.2e^{-2t}$. The $t_s$ values were calculated according to the equation given below, the mean and SEM values were taken from Table 9 :

$$t_s = \bar{F}_R - 0.978 / SEM$$

where $\bar{F}_R$ is the mean fraction released.

The values of $t_s$ calculated for each of the four deconvolution methods were as follows

| | |
|---|---|
| Numerical Deconvolution | $t_s = 1.238$ |
| Semi-Numerical Deconvolution | $t_s = 1.129$ |
| Polynomial Deconvolution | $t_s = 1.301$ |
| Polyexponential Deconvolution | $t_s = 0.694$ |

| Subject | Numerical | Semi-Numerical | Polynomial | Poly-exponential |
|---|---|---|---|---|
| 1 | 1.063 | 1.033 | 1.052 | 1.042 |
| 2 | 0.917 | 0.935 | 0.923 | 0.908 |
| 3 | 0.993 | 1.005 | 1.008 | 1.033 |
| 4 | 1.077 | 1.062 | 1.032 | 0.925 |
| 5 | 0.962 | 0.980 | 0.982 | 0.988 |
| 6 | 0.908 | 0.882 | 0.910 | 0.920 |
| 7 | 0.993 | 0.992 | 0.992 | 0.987 |
| 8 | 1.028 | 1.032 | 1.045 | 1.045 |
| 9 | 1.110 | 1.060 | 1.040 | 1.075 |
| 10 | 1.002 | 1.010 | 1.010 | 0.992 |
| Mean | 1.005 | 0.999 | 0.999 | 0.992 |
| SD | 0.0662 | 0.0561 | 0.0494 | 0.0584 |
| SEM | 0.0221 | 0.0187 | 0.0165 | 0.0195 |

**Table 9 :** Fraction of Dose Released predicted by Four Deconvolution Algorithms for a Release Rate of $I(t) = 1.2e^{-2t}$ with 10% Noise added to both Weighting and Response Functions

The value of $t_s$ taken from the tables at P=0.05 and 9 degrees of freedom ($t_{0.05(9)}$) is 2.26. All the $t_s$ values calculated for the deconvolution methods are less than the critical value taken from the table, therefore there is no significant difference between the mean fraction released predicted by any of the deconvolution algorithms and the true value.

### 3.1.2.4 Mean Dissolution Times

The Mean Dissolution Times (MDT) calculated, from the input rates predicted by the deconvolution methods, according to the method described in section 2.5.1, were calculated for each subject and each method. These MDT values, together with the mean, standard deviation (SD), and standard error of the mean (SEM) for each method, are shown in Table 10.

| Subject | Numerical | Semi-Numerical | Polynomial | Poly-Exponential |
|---|---|---|---|---|
| 1 | 0.483 | 0.456 | 0.481 | 0.467 |
| 2 | 0.382 | 0.424 | 0.420 | 0.402 |
| 3 | 0.502 | 0.497 | 0.491 | 0.498 |
| 4 | 0.427 | 0.459 | 0.496 | 0.544 |
| 5 | 0.469 | 0.477 | 0.470 | 0.460 |
| 6 | 0.548 | 0.573 | 0.608 | 0.537 |
| 7 | 0.428 | 0.404 | 0.417 | 0.407 |
| 8 | 0.490 | 0.535 | 0.540 | 0.550 |
| 9 | 0.492 | 0.528 | 0.557 | 0.522 |
| 10 | 0.453 | 0.443 | 0.419 | 0.491 |
| Mean | 0.467 | 0.480 | 0.488 | 0.490 |
| SD | 0.0468 | 0.0533 | 0.0634 | 0.0559 |
| SEM | 0.0156 | 0.0178 | 0.0213 | 0.0186 |

**Table 10 :** Mean Dissolution Times Estimated for the Input Rates produced by Four Deconvolution Algorithms for a Release Rate of $I(t) = 1.2e^{-2t}$ with 10% Noise added to both Weighting and Response Functions.

The mean MDT produced for each of the deconvolution methods was compared with the true value using the t-test (section 2.4.2) at a probability level of P=0.05 and 9 degrees of freedom. The MDT of a monoexponential release is the reciprocal of the rate constant (Yamaoka et al 1978) therefore the MDT of the input rate should be 0.5. However, the MDT value is only calculated up to t=1.9 and therefore the true $MDT_{t=1.9}$ is 0.4634, calculated according to equation (2.49) in section 2.5.1. The $t_s$ values were calculated

according to the equation given below, the mean and SEM values were taken from Table 10 :

$$t_s = \bar{M}DT - 0.4634 / SEM$$

where $\bar{M}DT$ is the mean MDT.

The values of $t_s$ calculated for each of the four deconvolution methods were as follows

| | |
|---|---|
| Numerical Deconvolution | $t_s = 0.231$ |
| Semi-Numerical Deconvolution | $t_s = 0.933$ |
| Polynomial Deconvolution | $t_s = 1.155$ |
| Polyexponential Deconvolution | $t_s = 1.430$ |

The value of $t_s$ taken from the table $t_{0.05(9)}$ for P=0.05 and 9 degrees of freedom was 2.26. All the $t_s$ values calculated for the MDT values of the four deconvolution methods were less than the critical value of 2.26. Therefore there is no significant difference between the estimates of MDT calculated from the input rates produced from the four deconvolution methods and the true value at the 0.95 probability level.

### 3.1.3 Discussion

Using data with no added noise, or very low levels of added noise, all the deconvolution methods were able to predict accurately both the shape and the values of the true input function.

When data containing a greater degree of noise was used the input rate predicted by the polynomial and polyexponential methods was still very close to the true values and showed the correct shape. However, the numerical and semi-numerical methods fail, at the higher noise levels, to show any form at all in the input rate. Instead, the predicted values oscillated widely about the true input rate, even becoming negative at some points.

The cumulative fraction released (CFI) profiles produced by the deconvolution methods are very close to the true values. The polynomial and polyexponential methods show little change in CFI with increasing noise levels, but the numerical and semi-numerical methods show a small degree of oscillation at the higher noise levels.

At the higher noise levels the best approximations to the form and value of the true

input function are shown by the polynomial and polyexponential deconvolution algorithms, with very little difference apparent between these two methods. This picture is confirmed when the mean results (n=10) at a noise level of 10% are considered.

The polyexponential and polynomial deconvolution algorithms both correctly predict the true form of the input function and show very small SEM values, indicating that these algorithms are not influenced by the fluctuations in the data which are due to the added noise. Of these two algorithms the polynomial method approximated the true input rate at the earlier time points better than the polyexponential.

In this case representing the input function by an empirical function (polynomial or polyexponential) enables the predicted rate to be smooth while still reflecting the form of the true input function.

For all the deconvolution algorithms the mean CFI's show a form that is very close to the true form, although those produced by the polynomial and polyexponential methods are smoother. Despite the apparent differences in the input rate produced by the different algorithms there is no significant difference between the estimated values of either the fraction of dose released ($F_R$) or the Mean Dissolution Time (MDT) and their true values, as judged by the t test at P=0.05 with 9 degrees of freedom.

## 3.2 ZERO ORDER RELEASE FUNCTION

The input function was represented by the following equation (3.4)

$$\begin{aligned} I(t) &= k_0 && t \le t_c \\ &= D_r k e^{-k(t-t_c)} && t > t_c \end{aligned} \qquad (3.4)$$

where $t_c$ is the point of change from zero to first order

$D_r$ is the dose remaining at $t = t_c$

$k_0$ is the zero order rate constant and

k is the first order rate constant

The values used were k = 2.5, $k_0$ = 0.5, $t_c$ = 0.8 and $D_r$ = 0.2, so that equation (3.4)

becomes $I(t) = 0.5$ for $t \leq t_c$ and $I(t) = 0.5e^{-2.5(t-0.8)}$ for $t > t_c$. The weighting function used was that used in the previous sections and shown in equation (3.1). Equations (3.4) and (3.1) were used to produce values for the input and weighting functions respectively. Equation (3.4) was convolved with equation (3.1), according to the procedure given in section 2.3.2., to produce values for the response function.

| Time | True Input Function I(t) | True Weighting Function W(t) | True Response Function R(t) |
|---|---|---|---|
| 0.05 | 0.5000 | 0.5170 | 0.0072 |
| 0.10 | 0.5000 | 0.7756 | 0.0237 |
| 0.15 | 0.5000 | 0.8868 | 0.0447 |
| 0.20 | 0.5000 | 0.9159 | 0.0674 |
| 0.30 | 0.5000 | 0.8644 | 0.1123 |
| 0.40 | 0.5000 | 0.7690 | 0.1531 |
| 0.60 | 0.5000 | 0.5936 | 0.2209 |
| 0.80 | 0.5000 | 0.4670 | 0.2735 |
| 1.00 | 0.3033 | 0.3745 | 0.3037 |
| 1.20 | 0.1839 | 0.3037 | 0.2967 |
| 1.40 | 0.1116 | 0.2475 | 0.2696 |
| 1.60 | 0.0677 | 0.2022 | 0.2356 |
| 2.00 | 0.0249 | 0.1354 | 0.1698 |

**Table 11 :** Weighting Function data produced by $W(t) = -2e^{-10t} + e^{-5t} + e^{-t}$ , Input Function Data produced from $I(t) = 0.5$ for $t \leq 0.8$ and $0.5e^{-2.5(t-0.8)}$ for $t > 0.8$ and Response Data produced from Convolution of the Weighting and Input Functions

The values produced for the input, weighting and response functions are shown in Table 11.

### 3.2.1 Increasing Levels of Added Noise

#### 3.2.1.1 Method

Noise levels of 1,5 and 10% were added to the true values of the weighting and response functions, shown in Table 11, using the NAG subroutine G05DDF (see section

2.3.3). The data sets produced following the addition of noise are shown in Table C(4a) and C(4b) in Appendix C.

The true data and the data sets containing the different levels of noise were processed through each of the four deconvolution algorithms according to the details given below. The weighting and response data were fitted to a polyexponential of the form shown in equation (3.3) according to the details given in section 3.1.1.1. The parameters obtained following the curve-fitting of the data in Tables C(4a) and C(4b) are shown in Tables 12(a) and 12(b).

| Parameters | True Values | 0% Noise Added | 1% Noise Added | 5% Noise Added | 10% Noise Added |
|---|---|---|---|---|---|
| $A_1$ | -2.0000 | -2.0006 | -2.0116 | -1.2420 | -1.4030 |
| $A_2$ | 1.0000 | 1.0006 | 1.0109 | 1.2420 | 1.4030 |
| $A_3$ | 1.0000 | 1.0000 | 1.0007 | | |
| $\alpha_1$ | 10.0000 | 9.9982 | 9.9882 | 14.0558 | 13.7110 |
| $\alpha_2$ | 5.0000 | 5.0004 | 5.1283 | 1.1856 | 1.2974 |
| $\alpha_3$ | 1.0000 | 1.0000 | 1.0073 | | |

**Table 12(a) :** Parameters obtained following Curve-fitting of Weighting Data, shown in Table C(4a), to a Polyexponential with Constants $A_i$ and Exponents $\alpha_i$.

| Parameters | 0% Noise Added | 1% Noise Added | 5% Noise Added | 10% Noise Added |
|---|---|---|---|---|
| $A_1$ | -28.1615 | -23.3057 | -26.8012 | -18.5205 |
| $A_2$ | 13.8768 | 16.6959 | 16.6498 | 8.9789 |
| $A_3$ | 14.2847 | 6.6090 | 10.1514 | 9.5416 |
| $\alpha_1$ | 1.9151 | 1.8063 | 1.9047 | 1.9783 |
| $\alpha_2$ | 2.2861 | 1.5470 | 1.6032 | 1.5100 |
| $\alpha_3$ | 1.5500 | 2.4516 | 2.3923 | 2.4061 |

**Table 12(b) :** Parameters obtained following Curve-fitting of Response Data, shown in Table C(4b), to a Polyexponential with Constants $A_i$ and Exponents $\alpha_i$.

**(a) Numerical Deconvolution**

An interpolation interval of 0.05 was used for the spline interpolation of both weighting and response data prior to deconvolution.

**(b) Semi-Numerical Deconvolution**

The response data was interpolated as for the numerical deconvolution. The parameters in Table 12(a) were used to generate the data for the weighting function at a time interval of 0.05 and these were used together with the interpolated response function for input into the semi-numerical deconvolution algorithm.

**(c) Polynomial Deconvolution**

The parameters from Table 12(a) were used to represent the weighting function data, and together with the response data, this formed the input for the polynomial deconvolution method (see section 2.2.3).

The optimal polynomial to represent the input function was selected using the F test (section 2.4.1) on the residual sum of squares associated with that polynomial at P= 0.05 and n=13. The selected polynomials for each data set are shown in Table 13. These were then used to generate the values of the input function, and the integrals of these polynomials were used to generate the values of the cumulative fraction input (CFI).

| % Noise Added to Data | Selected Polynomial for the Input Rate I(t) |
|---|---|
| 0% | $I(t) = 0.5538 - 1.0238t + 4.4847t^2 - 6.9707t^3 + 4.1013t^4 - 0.8248t^5$ |
| 1% | $I(t) = 0.5687 - 1.1447t + 4.9884t^2 - 7.7548t^3 + 4.6082t^4 - 0.9394t^5$ |
| 5% | $I(t) = 0.3863 + 1.0067t - 1.7035t^2 + 0.5881t^3$ |
| 10% | $I(t) = 0.4294 + 0.4382t - 0.8772t^2 + 0.2882t^3$ |

**Table 13 :** Selected Polynomials produced by Polynomial Deconvolution on Data (from Table C(4)) with Increasing Levels of Added Noise

**(d) Polyexponential Deconvolution**

The parameters from Table 12(a) were used to represent the weighting function and those from Table 12(b) used to represent the response function and these two sets of parameters were used as input into the polyexponential deconvolution algorithm (section 2.2.4).

### 3.2.1.2 Results

The input rates and the cumulative fraction input's (CFI) produced for each level of added noise and each deconvolution method are shown in Figures 13-20.

**(a) Numerical Deconvolution**

The input rates produced by numerical deconvolution are shown in Figure 13 and the cumulative fraction released shown in Figure 14. When the data is error free the input rate produced follows the true input rate very closely, coping very well with the abrupt change from zero to first order at t=0.8, however, when noise is added to the data oscillations begin to appear in the input rates produced.

At the 1% noise level these oscillations are small and the profile still reflects the zero order and first order portions of the input rate, also the point of change from zero to first order is shown clearly. With 5% noise in the data the oscillations are even more pronounced and the deconvolution method fails to show the true form of the input rate. At the 10% noise level these oscillations become even more severe and more frequent enabling little structure at all to be seen in the input rate profile and very little information to be derived from it.

When the CFI profiles are examined, the picture presented is much more stable. Both the error free data and that containing 1% noise produce profiles which are very close (if not identical in the case of the error free data) to the true CFI.

The CFI produced from data containing 5% noise agrees well with the true CFI up until t=1.2 where it begins to diverge before rejoining the true profile at the later time points. The CFI produced from data containing 10% noise agrees well with the true CFI at the early time points but begins to diverge from the true profile at t=0.7. The CFI remains lower than the true profile by a considerable margin for the rest of

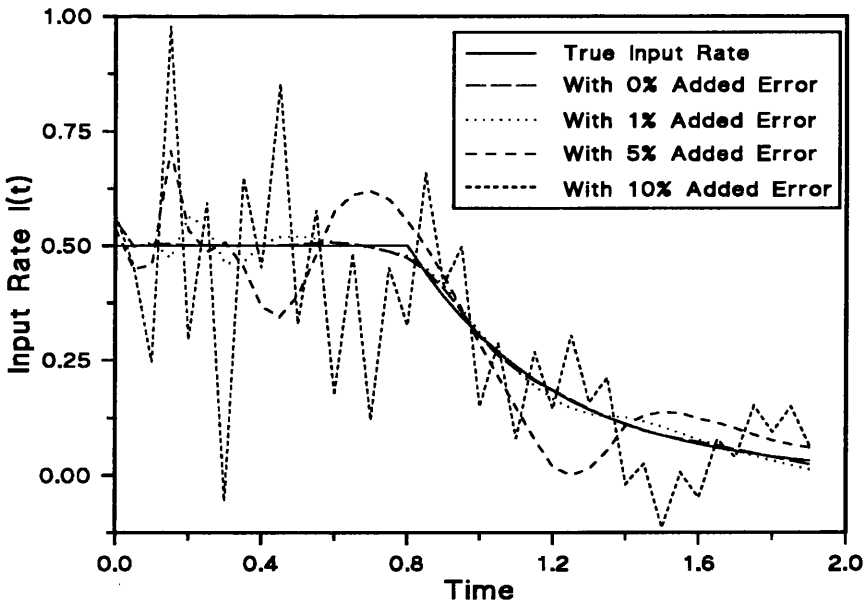


**Figure 13** : Input Rates produced by Numerical Deconvolution for the Zero Order Input Function with Increasing Levels of Error added to both the Weighting and Response Functions

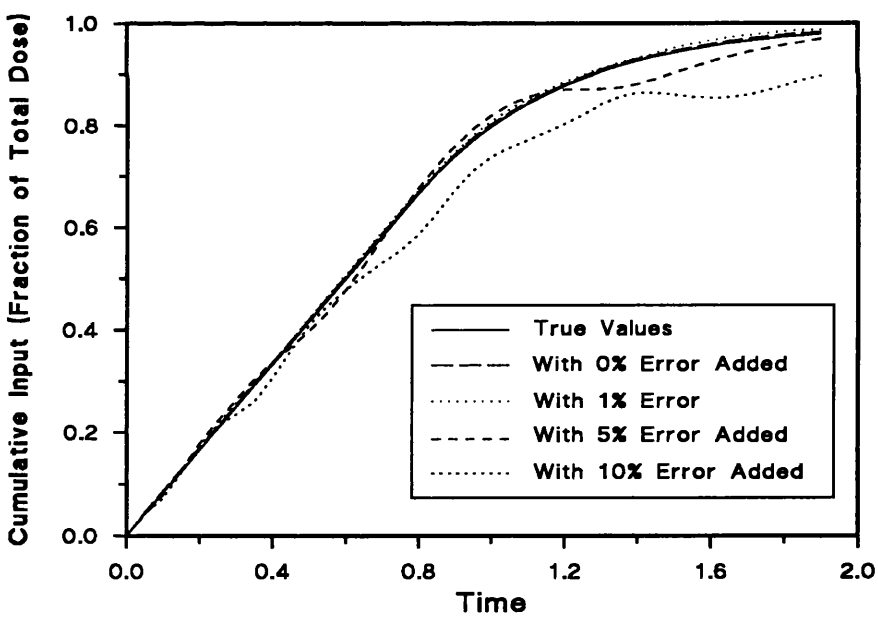


**Figure 14** : Cumulative Input produced by Numerical Deconvolution for the Zero Order Input Function with Increasing Levels of Error added to both Weighting and Response Functions.

the time course.

**(b) Semi-Numerical Deconvolution**

The input rate and cumulative fraction input (CFI) profiles produced by semi-numerical deconvolution are shown in Figures 15 and 16 respectively. The results produced are very similar to those seen with the numerical deconvolution.

When the data contains no noise the input rate produced is very close to the true value, even at the point of abrupt change from zero to first order. When noise is added to the data, the input rate produced begins to oscillate. These oscillations are very small at the 1% noise level, which still gives a good approximation to the true input rate, but get larger at the 5 and 10% noise levels, which show a marked degree of oscillation. The oscillations produced at the 10% noise level, however, are not as severe as those seen for numerical deconvolution at an equivalent level of noise.

The CFI profiles produced by semi-numerical deconvolution are also very similar to those produced by numerical deconvolution. In data with no noise or with a 1% noise level, the predicted CFI's are very close to the true values. In the case of the noise free data the CFI produced is almost identical to the true profile.

In data with 5% noise the early part of the profile follows the true profile very well but divergence from the true profile is seen at the later time points. The CFI produced from data with 10% noise added to it shows a divergence away from the true profiles much earlier than at the 5% level and that divergence becomes greater at the late time points.

**(c) Polynomial Deconvolution**

The input rates and CFI's produced by polynomial deconvolution are shown in Figures 17 and 18.

The input rates produced at all noise levels, including those produced from error free data, have difficulty in representing both the straight portion of the profile and the abrupt change from zero to first order processes at t=0.8. All the profiles produced diverge at either end of the time course over which the deconvolution was performed, but there is no clear increase in divergence away from the true input rate

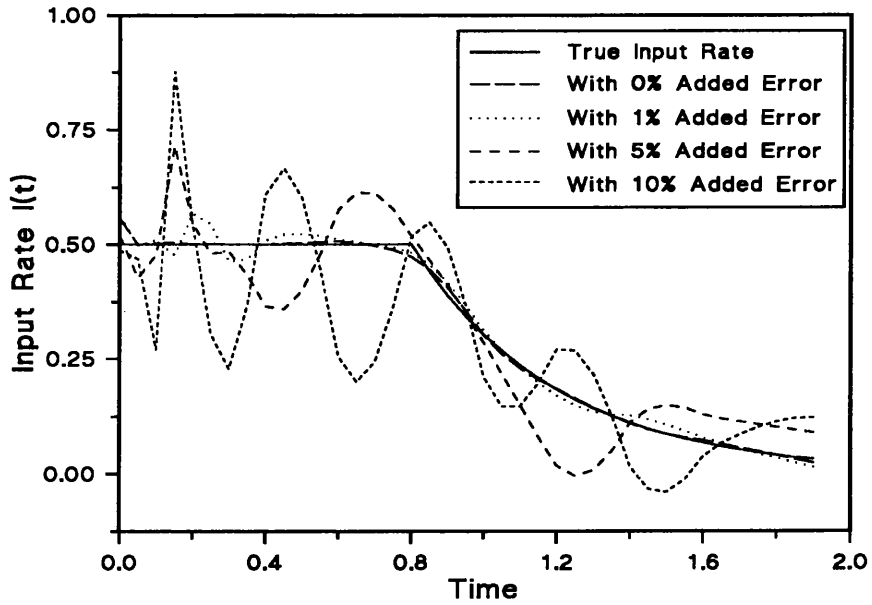


**Figure 15** : Input Rate produced by Semi-Numerical Deconvolution for the Zero Order Input Function with Increasing Levels of Error added to both the Weighting and Response Functions.

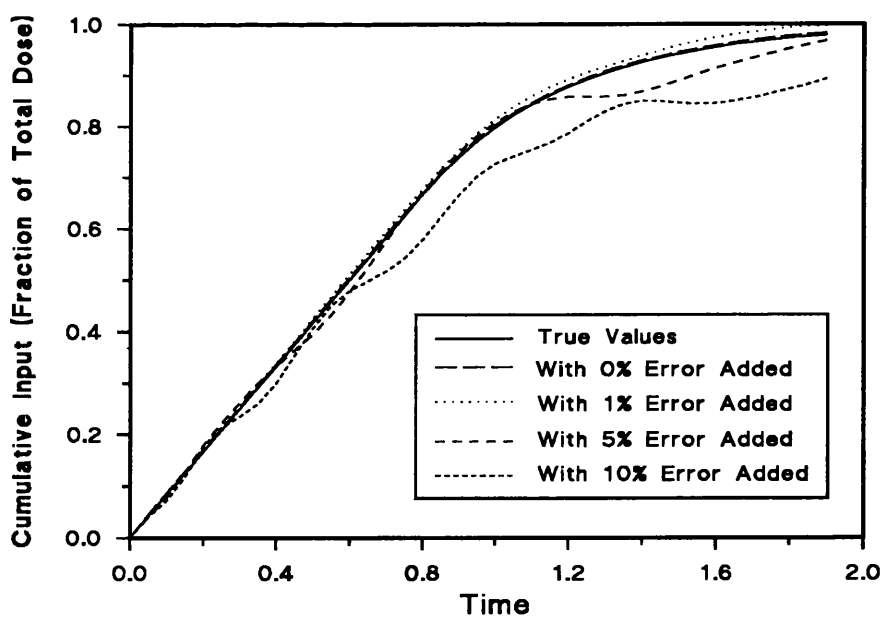


**Figure 16** : Cumulative Input produced by Semi-numerical Deconvolution for the Zero Order Input Function with Increasing Levels of Error added to both Weighting and Response Functions.

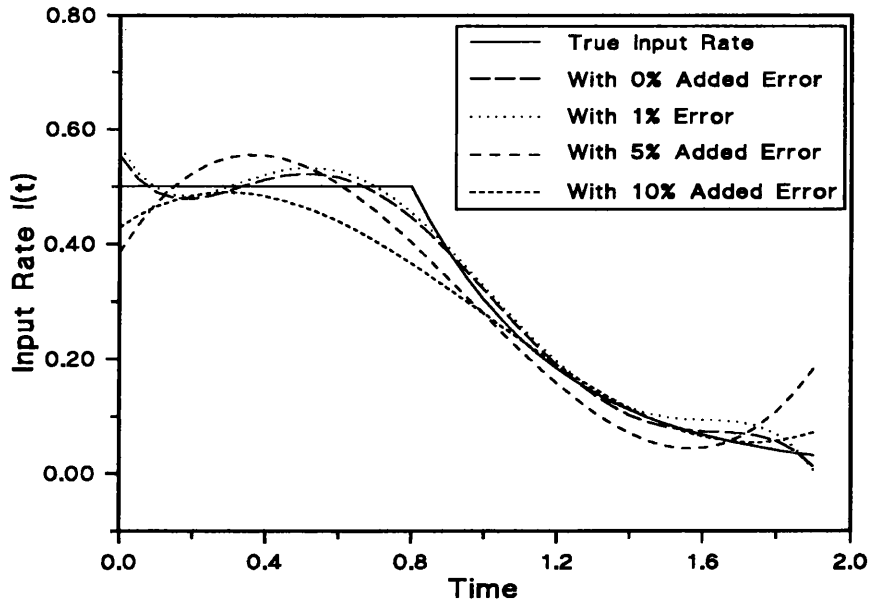


**Figure 17** : Input Rates produced by Polynomial Deconvolution for the Zero Order Input Function with Increasing Levels of Error added to both the Weighting and Response Functions.

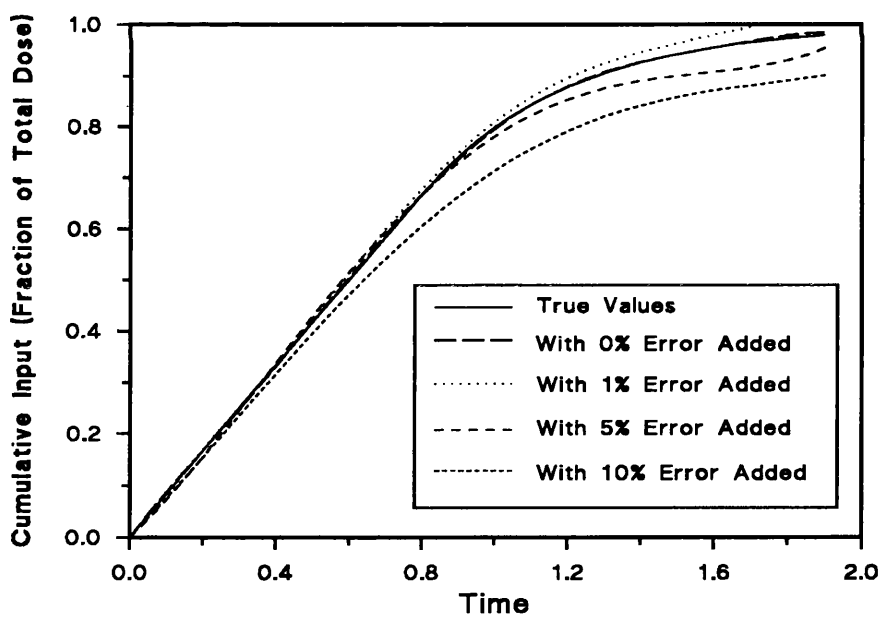


**Figure 18** : Cumulative Input produced by Polynomial Deconvolution for the Zero Order Input Function with Increasing Levels of Error added to both the Weighting and Response Functions.

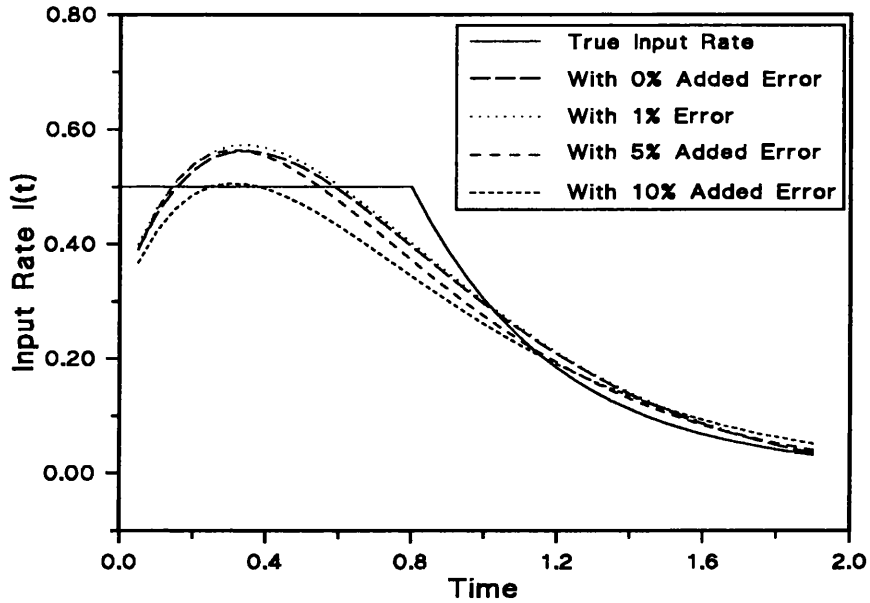


**Figure 19** : Input Rates produced by Polyexponential Deconvolution for the Zero Order Input Function with Increasing Levels of Error added to both Weighting and Response Functions.

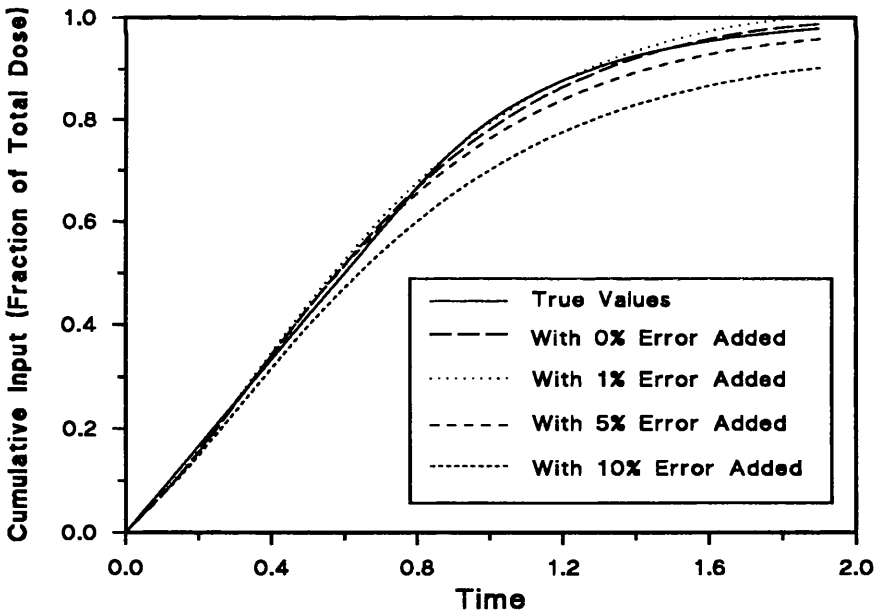


**Figure 20** : Cumulative Input produced by Polyexponential Deconvolution for the Zero Oreder Input Function with Increasing Levels of error added to both Weighting and Response Functions.

in the profiles produced from data with an increasing level of added noise.

The CFI's produced from noise free data are almost identical to the true profile and the CFI produced from data with 1% noise is a very close to the true profile. When data with 5% noise is used the CFI shows good agreement with the true values over the earlier part of the profile but diverges from the true values at the later time points. This picture is repeated with the profile produced from data with 10% noise, but the divergence from the true value is greater and begins at an earlier point.

**(d) Polyexponential Deconvolution**

The input rates and CFI's produced by polyexponential deconvolution are shown in Figures 19 and 20.

The input rates produced are very similar in both shape and values for the noise free data and all the different levels of added noise, except at the 10% noise level when the values differ although the shape of the profile remains the same. In all cases the input rates produced fail to cope with the abrupt change from zero to first order processes, and approximate the linear portion of the profile poorly.

The CFI profiles produced from noise free data and data containing a either a noise level of 1 or 5% are very close to the true values. However, the CFI profile produced from data containing 10% noise shows a marked divergence from the true profile at the later time points.

### 3.2.1.3 Percentage Difference between Predicted and True Values

For each of the data sets shown in Figures 13-20 the percentage difference between the true value and the predicted value for each point was calculated in the following way. The percentage difference for the input rate was calculated as the absolute value of the difference between the calculated input and the true input, divided by the true input at t=0 and multiplied by 100, i.e.

$$\%\text{diff } I(t) = \left| \text{Calc. } I(t) - \text{True } I(t) \right| * 100 / 0.5$$

where 0.5 is the exact value of the input rate at t=0

The percentage difference for the cumulative fraction input was calculated as the calculated fraction minus the true fraction multiplied by 100.

$$\%\text{diff fraction input} = \left| \text{calc. value} - \text{true value} \right| * 100$$

Each data set comprised 39 values over a time range of 0 to 1.9 at intervals of 0.05, which was the output from the deconvolution algorithms. The percentage differences, once calculated, were averaged for each data set and the mean and standard error of the means for these values are shown in Table 14 for the estimated input rate values and Table 15 for the estimated fraction input values.

| | Noise Level in original Data | | | |
|---|---|---|---|---|
| Type of Deconvolution | 0% | 1% | 5% | 10% |
| Numerical | 1.14 (0.327) | 3.30 (0.463) | 13.79 (1.599) | 27.91 (4.13) |
| Semi-Numerical | 1.13 (0.317) | 3.36 (0.484) | 14.08 (1.601) | 22.14 (2.814) |
| Polynomial | 2.94 (0.376) | 3.87 (0.446) | 8.74 (0.993) | 6.20 (1.107) |
| Polyexponential | 6.38 (0.855) | 6.70 (0.834) | 7.01 (1.039) | 8.32 (1.331) |

**Table 14 :** Mean Percentage Difference for Input Rate Values shown in Figures 13,15,17 and 19 for Increasing Levels of Added Noise. The S.E.M. values are shown in Parentheses (n=39).

When the mean percentage difference for the input rates are examined (Table 14) the following can be seen. With error free data, or at the 1% noise level, the numerical and semi-numerical methods have a smaller mean percentage difference than the polynomial method and a considerably smaller value than the polyexponential method. This situation becomes reversed at the higher noise levels where the mean percentage differences for the numerical and semi-numerical methods become much greater than those for the polynomial and polyexponential methods, and a great deal larger than the level of noise added to the original data.

The mean percentage difference's for the polynomial and polyexponential methods at the higher noise levels are slightly higher than those at the low noise levels but are still of the same order as the amount of noise added to the original data. There is a slight anomaly in the fact that the mean percentage difference for the polynomial deconvolution method at the 5% noise level is greater than that for the 10% noise level. This can be explained by the rapid divergence of the estimated rate from the true value at the later

time points (Figure 17) and the poor approximation of the first order portion of the input rate profile, for the 5% noise level. These deviations, which are not seen at the 10% level make the mean percentage difference higher than expected.

| | Noise Level in original Data | | | |
|---|---|---|---|---|
| Type of Deconvolution | 0% | 1% | 5% | 10% |
| Numerical | 0.318 (0.014) | 0.71 (0.046) | 1.84 (0.198) | 5.61 (0.543) |
| Semi-Numerical | 0.314 (0.014) | 1.21 (0.088) | 1.99 (0.282) | 6.19 (0.599) |
| Polynomial | 0.222 (0.026) | 1.48 (0.165) | 2.15 (0.249) | 5.69 (0.522) |
| Polyexponential | 0.892 (0.084) | 1.21 (0.140) | 2.052 (0.191) | 6.17 (0.578) |

**Table 15 :** Mean Percentage Difference for Cumulative Fraction Input Values shown in Figures 14,16,18 and 20 for Increasing Levels of Added Noise. The S.E.M. values are shown in Parentheses (n=39).

The figures in Table 15 show the mean percentage difference (SEM) for the CFI's. There is very little difference seen between any of the four deconvolution methods and all the methods show mean percentage differences which are less than, but of the same order, as the level of noise added to the original data. No one method shows any clear superiority at any noise level.

### 3.2.2 Constant Level of Noise Added to Ten Data Sets

#### 3.2.2.1 Method

In this second part the level of added noise was set at 10% and ten different random data sets were generated by using the addition of noise to the true weighting and response values shown in Table 11 using the NAG subroutine G05DDF (section 2.3.3). The ten data sets produced from this are shown in Tables C(5) and C(6) in Appendix C.

Each of the data sets was fitted to an equation of the form given in equation (3.3) using the non-linear least-squares fitting routine (section 2.1.1). The number of terms in the polyexponential was sequentially increased until there was no significant improvement in the residual sum of squares as judged by the F test at P=0.05 and n=13 (n is the number of data points). The parameters produced from this fitting are shown in Tables 16

(Weighting Function) and 17 (Response Function).

| Parameters / Subject | $A_1$ | $A_2$ | $A_3$ | $\alpha_1$ | $\alpha_2$ | $\alpha_3$ |
|---|---|---|---|---|---|---|
| 1 | -1.0583 | 1.0583 | | 14.7831 | 1.0103 | |
| 2 | -1.2167 | 1.2167 | | 13.1451 | 1.1509 | |
| 3 | -1.4511 | 1.4511 | | 9.7698 | 1.3730 | |
| 4 | -1.2241 | 1.2241 | | 14.8374 | 1.1877 | |
| 5 | -1.2916 | 1.2916 | | 12.6102 | 1.1787 | |
| 6 | -1.2704 | 1.2704 | | 12.5863 | 1.1836 | |
| 7 | -1.4036 | 1.4036 | | 13.6901 | 1.2980 | |
| 8 | -2.2218 | 0.7759 | 1.4459 | 10.2161 | 0.7469 | 5.3961 |
| 9 | -1.2670 | 1.2670 | | 14.2703 | 1.2403 | |
| 10 | -1.1304 | 1.1304 | | 16.2309 | 1.1238 | |

**Table 16 :** Parameters Obtained following Curve-fitting of the Weighting Data, shown in Table C(5), to a Polyexponential with Constants $A_i$ and Exponents $\alpha_i$.

The ten data sets produced were then processed through each of the four deconvolution algorithms (section 2.2) according to the details given below.

**(a) Numerical Deconvolution**

The interpolation time used was again 0.05, and both weighting and response data was interpolated prior to deconvolution.

**(b) Semi-Numerical Deconvolution**

The parameters from Table 16 were used to generate values for the weighting function at intervals of 0.05 and these, together with the response function data (interpolated at t=0.05), were used as input into the semi-numerical deconvolution algorithm.

**(c) Polynomial Deconvolution**

The parameters from Table 16 were used to represent the weighting function, the dose administered for the response function was 0.6 (see equation 3.4) and the

| Parameters / Subject | $A_1$ | $A_2$ | $A_3$ | $\alpha_1$ | $\alpha_2$ | $\alpha_3$ |
|---|---|---|---|---|---|---|
| 1 | -29.996 | 15.008 | 14.988 | 1.963 | 2.325 | 1.598 |
| 2 | -49.985 | 25.059 | 24.926 | 1.850 | 2.106 | 1.587 |
| 3 | -4.841 | 4.266 | 0.575 | 3.552 | 3.959 | 0.604 |
| 4 | -39.896 | 19.960 | 19.936 | 1.779 | 2.041 | 1.506 |
| 5 | -49.962 | 25.097 | 24.865 | 1.963 | 2.242 | 1.677 |
| 6 | -49.950 | 24.801 | 25.149 | 1.821 | 1.572 | 2.055 |
| 7 | -13.203 | 6.345 | 6.858 | 1.692 | 2.145 | 1.244 |
| 8 | -13.257 | 6.770 | 6.487 | 1.814 | 2.247 | 1.329 |
| 9 | -7.336 | 3.383 | 3.953 | 1.781 | 2.410 | 1.190 |
| 10 | -19.990 | 9.864 | 10.036 | 1.872 | 2.287 | 1.450 |

**Table 17 :** Parameters obtained following Curve-fitting of Response Data, shown in Table C(6), to a Polyexponential with Constants $A_i$ and Exponents $\alpha_i$.

| Subject | Selected Polynomial for the Input Rate |
|---|---|
| 1 | $I(t) = 0.3182 + 1.6288t - 2.4118t^2 + 0.7808t^3$ |
| 2 | $I(t) = 0.5931 -2.0587t +9.9043t^2 -16.6218t^3 +10.8846t^4 -2.4459t^5$ |
| 3 | $I(t) = 0.3857 - 1.1217t - 2.0002t^2 + 0.7325t^3$ |
| 4 | $I(t) = 0.5018 - 0.0203t - 0.1436t^2$ |
| 5 | $I(t) = 0.3728 + 1.3254t - 2.2464t^2 + 0.8001t^3$ |
| 6 | $I(t) = 0.5189 + 0.2486t - 0.7193t^2 + 0.2424t^3$ |
| 7 | $I(t) = 0.3700 + 0.3118t - 0.2909t^2$ |
| 8 | $I(t) = 0.4892 + 0.1712t - 0.2862t^2$ |
| 9 | $I(t) = 0.4423 + 0.1277t - 0.2121t^2$ |
| 10 | $I(t) = 0.4231 + 0.8158t - 1.3189t^2 + 0.4177t^3$ |

**Table 18 :** Selected Polynomials produced by Polynomial Deconvolution on Data from Tables C(5) and C(6).

values in Table C(6) were used for the response function. The data were then processed according to the polynomial deconvolution method (section 2.2.3) and the optimal polynomial to represent the input function was selected using the F Test

(section 2.4.1) at P=0.05 and n=13. The selected polynomials are shown in Table 18 and these were used to calculate the input rate, I(t), and their integrals used to calculate the cumulative fraction input.

**(d) Polyexponential Deconvolution**

The parameters from Table 16 were used to represent the weighting function and those from Table 17 used to represent the response function and together these formed the input into the polyexponential deconvolution algorithm.

Following deconvolution the mean and standard error of the mean over the ten data sets were calculated for the input rate and the cumulative fraction input (CFI) for each deconvolution method. The estimated fraction of dose released ($F_R$) produced for each data set was calculated by taking the maximum value reached in the cumulative fraction input profile. For each input rate produced the Mean Dissolution Time (MDT) was calculated according to the method described in section (2.5.1).

### 3.2.2.2 Results

For each deconvolution method the mean input rate and mean CFI for the ten data sets were plotted together with the standard error of the mean values (S.E.M.) and these are shown in Figures 21-24.

**(a) Numerical Deconvolution**

The mean input rate (n=10) and mean cumulative fraction input produced by numerical deconvolution are shown in Figure 21. The mean input rate shows two distinct features, firstly it has great difficulty in approximating the zero order portion of the profile, the consequence of this appears as oscillations in the predicted input rate over this portion of the profile. The second feature is the good approximation shown by the method of the first order portion of the curve, however the SEM values associated with the whole profile are very high. At some points the input profiles associated with individual subjects become negative, although this does not appear in the mean input rate.

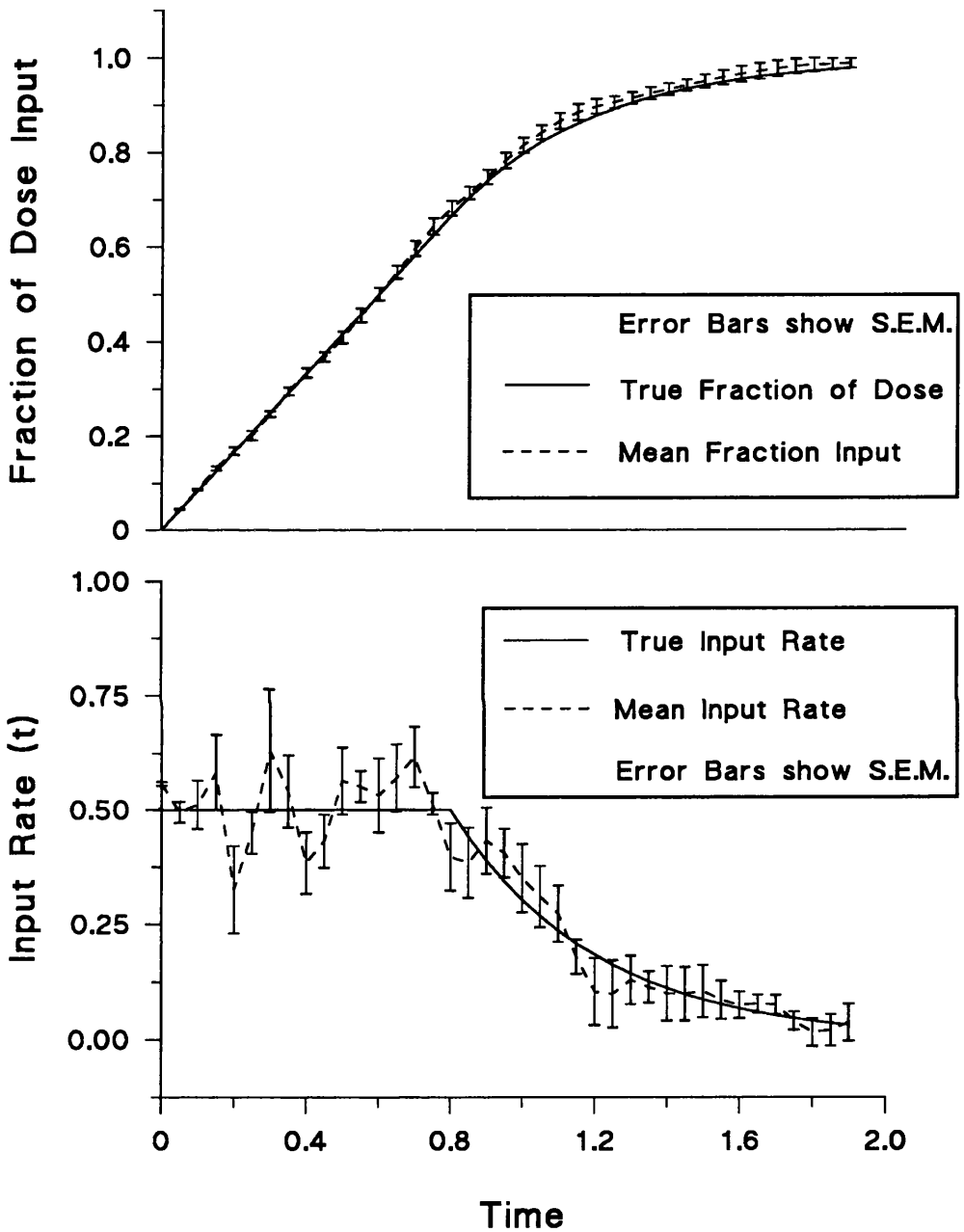


**Figure 21** : Mean results produced by Numerical Deconvolution for the Zero Order Input Function on 10 Data Sets with 10% Noise added to the Weighting and Response Functions

In contrast the mean CFI is very close to the true profile and the SEM values are much lower than those for the corresponding input rate.

**(b) Semi-Numerical Deconvolution**

The mean input rate (n=10) and the mean CFI produced by semi-numerical deconvolution are shown in Figure 22. Like the numerical method the semi-numerical method shows two features. The first is the difficulty shown in approximating the true input over the zero order portion of the profile and the second is the generally good approximation to the first order portion of the curve. The SEM values over the whole of the predicted input rate are large, and like the numerical method some of the individual input rates contain negative values.

The mean CFI predicted by semi-numerical deconvolution is very close to the true profile, despite the deviations apparent in the input rate and has much smaller SEM values than those for the corresponding input rate.

**(c) Polynomial Deconvolution**

The mean input rate (n=10) and the mean CFI produced by polynomial deconvolution are shown in Figure 23. The mean predicted input rate shows a very smooth profile, which fails to cope with the abrupt change from zero to first order in the true input rate. However, the input rate does show a generally constant rate over the first portion of the profile and a smoothly declining later portion which follows the true input rate very closely. The predicted input rate begins to diverge during the last few points and the SEM values which had been consistently small begin to rise.

The mean CFI profile agrees very closely with the true CFI, the SEM values are extremely small and the only slight deviation from the true profile occurs immediately following the point of change from zero to first order release.

**(d) Polyexponential Deconvolution**

The mean input rate (n=10) and the mean CFI produced by polyexponential deconvolution are shown in Figure 24. The mean input produced has a very smooth

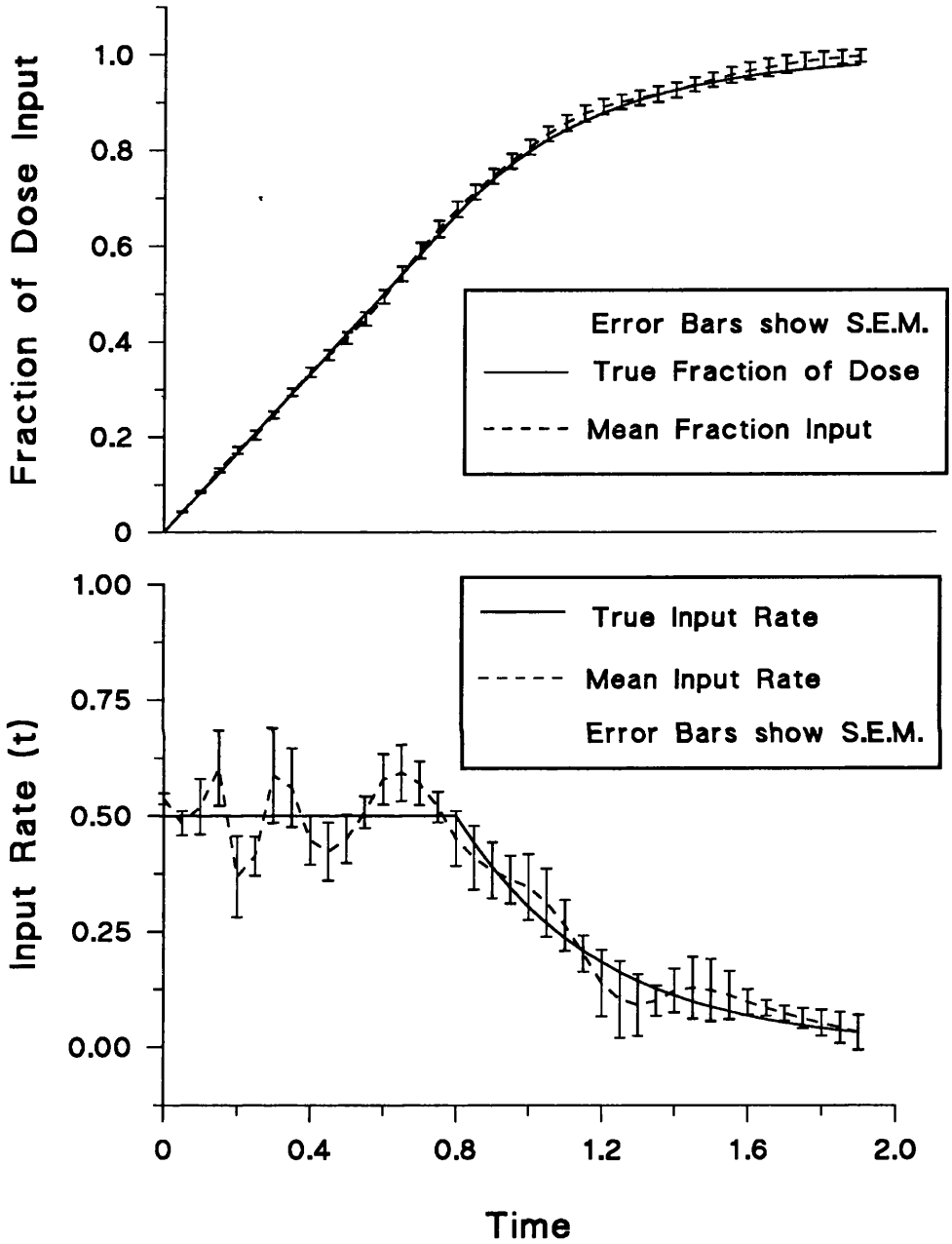


**Figure 22** : Mean results produced by Semi-Numerical Deconvolution for the Zero Order Input Function on 10 Data Sets with 10% Noise added to both the Weighting and Response Functions

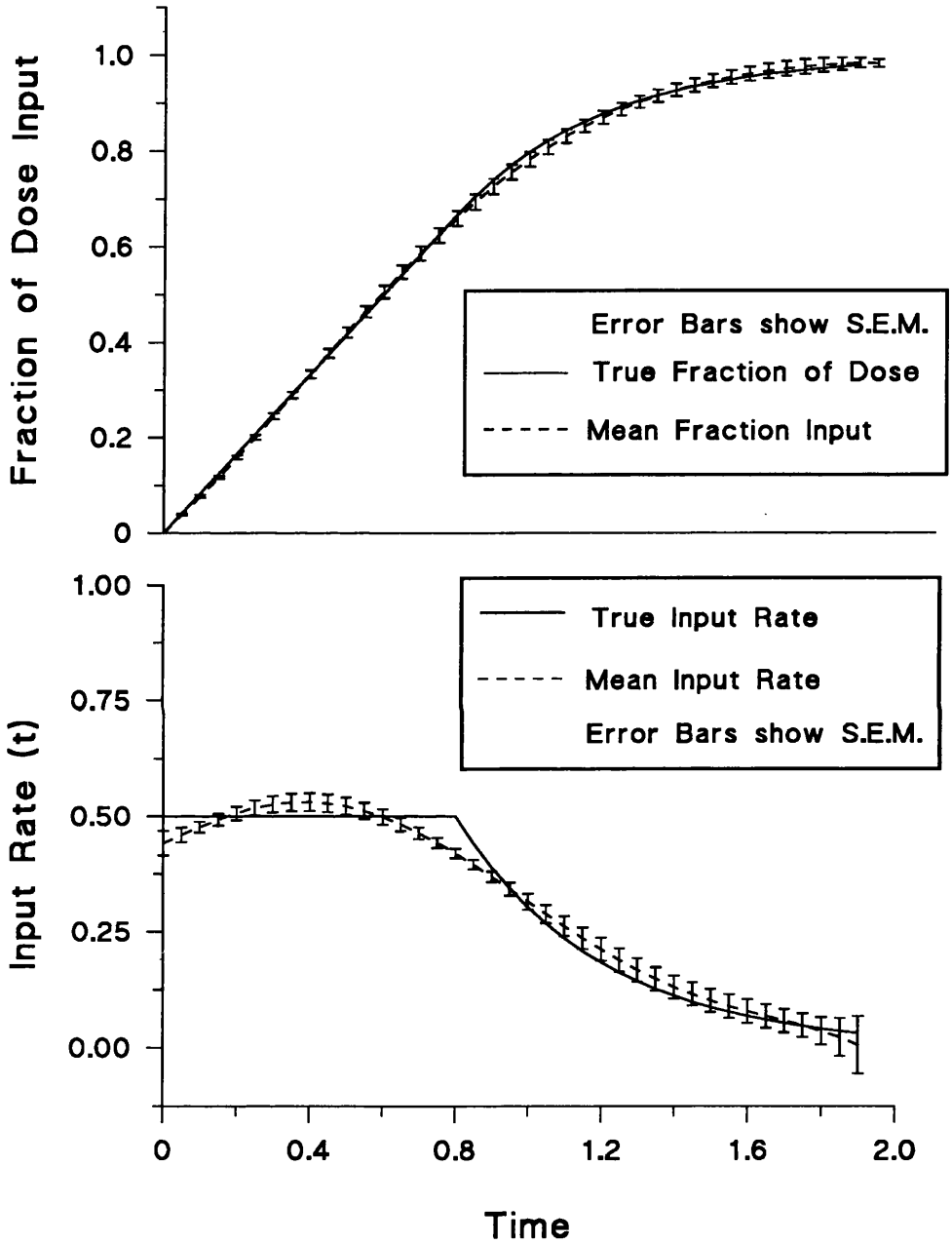


**Figure 23** : Mean results produced by Polynomial Deconvolution for the Zero Order Input Function on 10 Data Sets with 10% Error added to both the Weighting and Response Functions

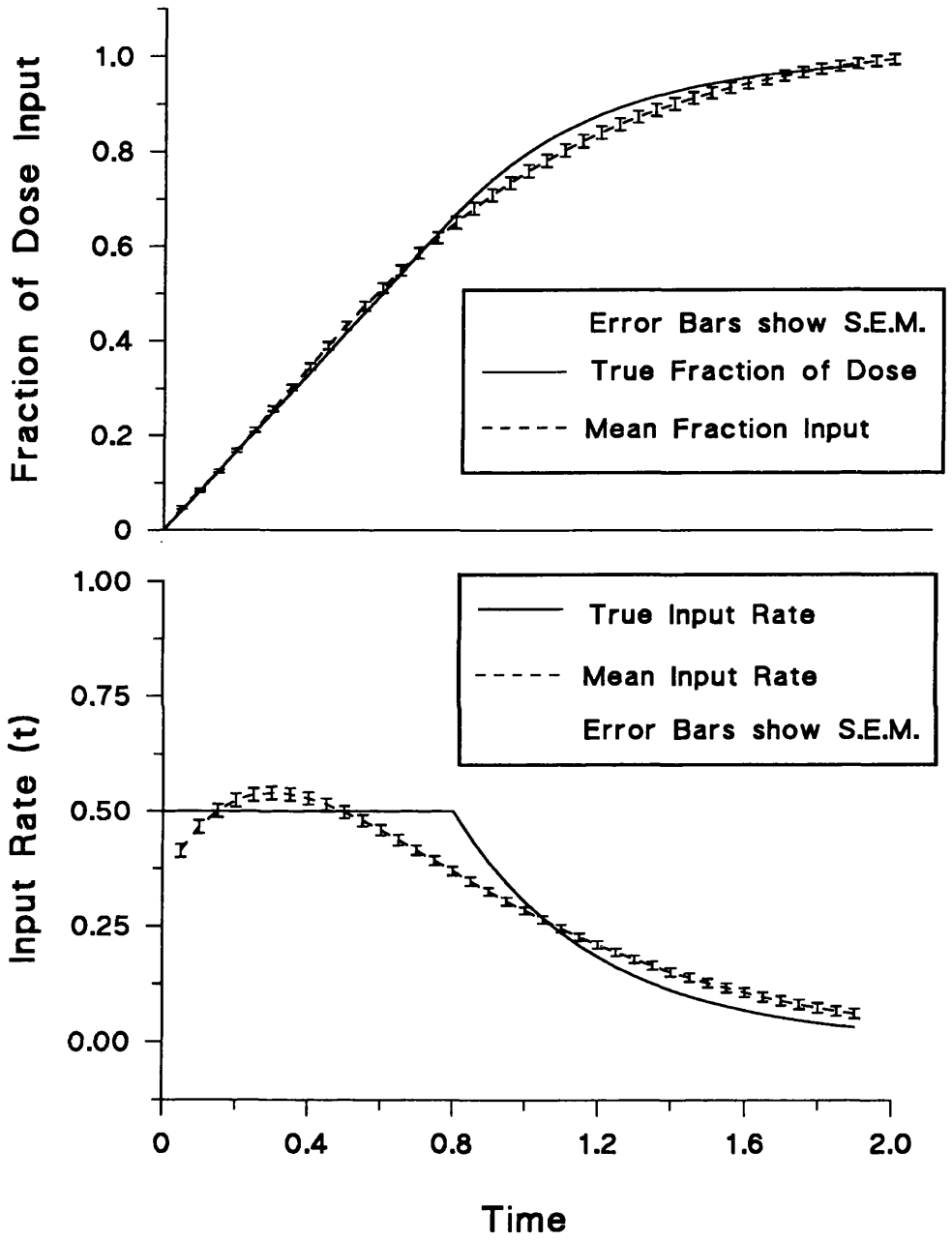


**Table 24** : Mean results produced by Polyexponential Deconvolution for the Zero Order Input Function on 10 Data Sets with 10% Error added to both the Weighting and Response Functions

profile and has very small SEM values associated with it, however, the method fails to cope with the abrupt change from zero to first order seen in the true profile. The predicted profile shows a somewhat constant portion at the start of the profile, this is then followed by a smoothly declining phase which follows the shape of the true profile well over the later time points.

The mean CFI follows the true profile very well, except over the period which is associated with the change in the input rate from zero to first order. In this area the predicted values underestimate the true values, however, by the later time points the two profiles are again in good agreement. The SEM values over the whole profile are very low.

### 3.2.2.3 Estimated Fraction Released $F_R$

The estimated fraction of dose released for each subject and each deconvolution method are shown in Table 19, together with the mean fraction released ($\bar{F}_R$), the standard deviation (SD) and the standard error of the mean (SEM) for each deconvolution method.

The mean fraction released produced for each of the deconvolution methods was compared with the true value of 0.979 using the t-test (section 2.4.2) at a probability level of P=0.05 and 9 degrees of freedom. The value of 0.979 is the fraction of dose released at t=1.9 calculated form the integral of $I(t) = 0.5$ for $t \leq 0.8$ and $I(t) = 0.5e^{-2.5(t-0.8)}$ for $t > 0.8$. The $t_s$ values were calculated according to the equation given below, the mean and SEM values were taken from Table 19 :

$$t_s = \bar{F}_R - 0.979 / SEM$$

where $\bar{F}_R$ is the mean fraction released.

The values of $t_s$ calculated for each of the four deconvolution methods were as follows

| | |
|---|---|
| Numerical Deconvolution | $t_s = 2.000$ |
| Semi-Numerical Deconvolution | $t_s = 1.655$ |
| Polynomial Deconvolution | $t_s = 2.206$ |
| Polyexponential Deconvolution | $t_s = 0.952$ |

| Subject | Numerical | Semi-Numerical | Polynomial | Poly-exponential |
|---|---|---|---|---|
| 1 | 0.983 | 0.983 | 0.975 | 0.980 |
| 2 | 1.005 | 1.002 | 1.057 | 0.998 |
| 3 | 0.977 | 0.973 | 0.982 | 0.938 |
| 4 | 0.983 | 0.987 | 0.985 | 0.997 |
| 5 | 0.972 | 0.962 | 0.978 | 0.955 |
| 6 | 0.965 | 0.967 | 0.972 | 0.978 |
| 7 | 1.032 | 1.085 | 1.008 | 1.017 |
| 8 | 0.977 | 0.967 | 1.018 | 0.973 |
| 9 | 1.043 | 1.025 | 0.985 | 0.993 |
| 10 | 1.050 | 1.057 | 1.043 | 1.058 |
| Mean | 0.999 | 1.001 | 1.000 | 0.989 |
| SD | 0.032 | 0.042 | 0.030 | 0.033 |
| SEM | 0.010 | 0.033 | 0.010 | 0.011 |

**Table 19 :** Fraction of Dose Released predicted by Four Deconvolution Algorithms for a Release Rate of $I(t) = 0.5$ for $t \leq 0.8$ and $I(t) = 0.5e^{-2.5(t-0.8)}$ with 10% Noise added to both Weighting and Response Functions

The value of $t_s$ taken from the tables at P=0.05 and 9 degrees of freedom ($t_{0.05(9)}$) is 2.26. All the values calculated for the deconvolution methods are less than this critical value, therefore there is no significant difference between the mean fraction released predicted by any of the deconvolution and the true value.

### 3.2.2.4 Mean Dissolution Times

The Mean Dissolution Times (MDT) calculated from the input rates predicted by the deconvolution methods, according to the method described in section 2.5.1, were calculated for each subject and each method. These MDT values, together with the mean, standard deviation (SD), and standard error of the mean (SEM), for each method, are shown in Table 20.

The mean MDT produced for each of the deconvolution methods was compared with the true value using the t-test (section 2.4.2) at a probability level of P=0.05 and 9 degrees

| Subject | Numerical | Semi-Numerical | Polynomial | Poly-Exponential |
|---|---|---|---|---|
| 1 | 0.560 | 0.543 | 0.545 | 0.601 |
| 2 | 0.629 | 0.639 | 0.587 | 0.662 |
| 3 | 0.661 | 0.682 | 0.707 | 0.709 |
| 4 | 0.643 | 0.656 | 0.648 | 0.692 |
| 5 | 0.633 | 0.638 | 0.657 | 0.623 |
| 6 | 0.605 | 0.629 | 0.634 | 0.642 |
| 7 | 0.691 | 0.730 | 0.693 | 0.769 |
| 8 | 0.570 | 0.586 | 0.510 | 0.630 |
| 9 | 0.634 | 0.671 | 0.655 | 0.727 |
| 10 | 0.626 | 0.654 | 0.657 | 0.669 |
| Mean | 0.625 | 0.643 | 0.629 | 0.672 |
| SD | 0.039 | 0.051 | 0.063 | 0.052 |
| SEM | 0.012 | 0.014 | 0.020 | 0.016 |

**Table 20 :** Mean Dissolution Times Estimated for the Input Rates produced by Four Deconvolution Algorithms for a Release Rate of $I(t) = 0.5$ for $t \leq 0.8$ and $I(t) = 0.5e^{-2.5(t-0.8)}$ for $t > 0.8$ with 10% Noise added to both Weighting and Response Functions.

of freedom. The MDT value was calculated up to t=1.9 using the method described by equation (2.49) in section 2.5.1, giving a $MDT_{t=1.9}$ of 0.6320. The $t_s$ values were calculated according to the equation given below, the mean and SEM values were taken from Table 20 :

$$t_s = \bar{M}DT - 0.6320 / SEM$$

where $\bar{M}DT$ is the mean MDT.

The values of $t_s$ calculated for each of the four deconvolution methods were as follows

| | |
|---|---|
| Numerical Deconvolution | $t_s = -0.583$ |
| Semi-Numerical Deconvolution | $t_s = 0.786$ |
| Polynomial Deconvolution | $t_s = -0.150$ |
| Polyexponential Deconvolution | $t_s = 2.500$ |

The value of $t_s$ taken from the table $t_{0.05(9)}$ for P=0.05 and 9 degrees of freedom was 2.26. All the $t_s$ values calculated, except that for the polyexponential method, for the mean MDT values of the four deconvolution methods were less than the critical value of 2.26. Therefore there is no significant difference between the estimates of MDT calculated from the input rates produced from the numerical, semi-numerical or polynomial deconvolution methods and the true value at the 0.95 probability level, but the mean MDT produced following polyexponential deconvolution is significantly different ($0.05 > P > 0.01$) from the true value.

### 3.2.3 Discussion

The simpler numerical and semi-numerical deconvolution algorithms, which do not approximate the input rate with an empirical function, produced good reflections of the true input rate when the original data contained little or no additional noise. They succeed in showing both the zero order and first order portions of the release profiles and cope very well with the abrupt change from one to the other. However at the higher noise levels both these deconvolution algorithms become unable to show, with any clarity, the true shape of the input rate. The oscillations they produce at these higher noise levels makes interpretation of any underlying form difficult.

The polynomial and polyexponential deconvolution algorithms show consistent results despite the increasing noise levels in the initial data. However, because their implementation requires that the unknown input rate be represented by an empirical function (a polynomial and polyexponential respectively) they are unable, as might be expected, to reflect the abrupt change from zero to first order characteristics of the true input rate. Because both of these empirical formulae produce smooth profiles they have some difficulty mimicking the zero order constant release which both methods portray as a broad curve which declines rapidly when the first order portion of the input rate is reached.

As expected, the cumulative fraction released (CFI) profiles for all the deconvolution methods at all noise levels are much closer to the true values than their corresponding rate profiles. The only divergence is seen at the highest level of noise, but this divergence is seen for all the methods, however the numerical and semi-numerical CFI profiles do not

follow the true shape of the CFI as closely as those produced by polynomial or polyexponential deconvolution.

When the ability of the different algorithms to predict the input rate at a constant noise level of 10%, over 10 data sets, is examined the following is seen. The polynomial and polyexponential methods are much more stable to data noise and produce smooth input rate profiles, unlike the numerical and semi-numerical methods where sharp changes in the input rate can still be seen in the mean data.

The polynomial and polyexponential methods fail to show the point of change from zero to first order with accuracy. For the polynomial methods, the predicted input rate agrees well with the true rate on either side of this point, and reflects the declining portion of the curve very well, and the underestimation of the input rate around the point of change is not large.

The polyexponential method, however, underestimates the input rate near the point of change by a marked degree, so that a reflection of this underestimation appears in the CFI profile. The polyexponential method does not show the presence of a constant rate in the early time points of the input rate as well as the polynomial method, nor does it agree as well with the declining input rate in the first order portion.

The numerical and semi-numerical methods show too much oscillation to enable either of them to show clearly the true shape of the input rate profile. There is little difference between the two methods themselves, despite the prior smoothing, by curve fitting, involved in the semi-numerical approach.

The mean CFI profiles produced by all the methods are similar despite the differences seen in the mean input rate profiles. The only real difference is seen in the polyexponential method, which underestimates the CFI in the region following the abrupt change in the input rate.

The fraction released ($F_R$) and Mean Dissolution Time (MDT) estimated for the numerical, semi-numerical, polynomial and polyexponential methods showed no significant difference to the true values, as judged by the t test at P=0.05 with 9 degrees of freedom, except for the MDT calculated for the polyexponential method which was significantly different ($0.05 > P > 0.01$) from the true value. That there is no significant difference in the fraction released is not surprising since it is estimated from the CFI

profiles which were shown to be very similar. The lack of difference between the calculated MDT values and the true values is perhaps more surprising since it is calculated from the estimated input rate values themselves.

## 3.3 CONTROLLED RELEASE INPUT FUNCTION

The input function (I(t)) was represented by a set of data, unlike the previous two input forms which have been represented by equations, because of this the response function could not be calculated algebraically and was calculated numerically according to equation (2.43) given in section 2.3.2.3. The total dose administered was found by calculating the area under the input function time curve between zero and t=2.3, which was the last time point. The dose $D_O$, calculated in this manner was 0.7344 and this was used as the dose administered to produce the response function.

The weighting function used was that shown previously in equation (3.1), this equation was used to generate values for the weighting function which were used as input to the algorithm shown in equation (2.43) to produce values for the response function. The true values for the weighting, input and response function are shown in Table 21.

| Time | True Input Function I(t) | True Weighting Function W(t) | True Response Function R(t) |
|---|---|---|---|
| 0.05 | 0.2000 | 0.5170 | 0.0000 |
| 0.10 | 0.3000 | 0.7756 | 0.0052 |
| 0.15 | 0.3800 | 0.8868 | 0.0155 |
| 0.20 | 0.4500 | 0.9159 | 0.0303 |
| 0.30 | 0.4950 | 0.8644 | 0.0696 |
| 0.40 | 0.5000 | 0.7690 | 0.1125 |
| 0.60 | 0.5000 | 0.5936 | 0.1886 |
| 0.80 | 0.5000 | 0.4670 | 0.2480 |
| 1.00 | 0.5000 | 0.3745 | 0.2948 |
| 1.20 | 0.4500 | 0.3037 | 0.3307 |
| 1.40 | 0.3030 | 0.2475 | 0.3462 |
| 1.60 | 0.1840 | 0.2022 | 0.3314 |
| 2.00 | 0.0680 | 0.1354 | 0.2591 |

**Table 21 :** Weighting Function data produced by $W(t) = -2e^{-10t} + e^{-5t} + e^{-t}$ , Input Function Data represented by the controlled release input function and Response Data produced from Convolution of the Weighting and Input Functions

### 3.3.1 Increasing Levels of Added Noise

#### 3.3.1.1 Method

Noise levels of 1, 5 and 10% were added to the values of the weighting and response functions shown in Table 21 using the NAG subroutine G05DDF (see section 2.3.3). The data sets produced following the addition of noise are shown in Tables C(7a) and C(7b) in appendix C.

The true data and the data sets containing the added noise were then processed through each of the four deconvolution algorithms (section 2.2) according to the details for each given in the sections below. The weighting and response data were fitted to polyexponentials of the form shown in equation (3.3) using the non-linear curve-fitting routine described in section 2.1.1. The number of terms in the exponential was increased sequentially and the data re-fitted until there was no significant reduction in the residual sum of squares as judged by the F test (section 2.4.1) at P=0.05 and n=13. The parameters obtained from the curve fitting of the weighting and response data are shown in Tables 22(a) and 22(b).

| Parameters | True Values | 0% Noise Added | 1% Noise Added | 5% Noise Added | 10% Noise Added |
|---|---|---|---|---|---|
| $A_1$ | -2.0000 | -2.0000 | -1.7981 | -1.2744 | -1.4263 |
| $A_2$ | 1.0000 | 1.0000 | 0.7681 | 1.2744 | 1.4263 |
| $A_3$ | 1.0000 | 1.0000 | 1.0300 | | |
| $\alpha_1$ | 10.0000 | 10.0000 | 10.5985 | 12.5635 | 9.7969 |
| $\alpha_2$ | 5.0000 | 5.00002 | 4.9262 | 1.1641 | 1.2741 |
| $\alpha_3$ | 1.0000 | 1.0000 | 1.0193 | | |

**Table 22(a) :** Parameters obtained following Curve-fitting of Weighting Data, shown in Table C(7a), to a Polyexponential with Constants $A_i$ and Exponents $\alpha_i$.

#### (a) Numerical Deconvolution

An interpolation interval of 0.05 was used for the spline interpolation of both weighting and response data prior to deconvolution.

| Parameters | 0% Noise Added | 1% Noise Added | 5% Noise Added | 10% Noise Added |
|---|---|---|---|---|
| $A_1$ | -9.8055 | -36.8026 | -49.8613 | -49.5733 |
| $A_2$ | 4.8383 | 17.9685 | 25.2009 | 25.0369 |
| $A_3$ | 4.9372 | 18.8341 | 24.6604 | 24.5364 |
| $\alpha_1$ | 1.6009 | 1.5461 | 1.5279 | 1.6145 |
| $\alpha_2$ | 1.0395 | 1.8442 | 1.7686 | 1.8782 |
| $\alpha_3$ | 2.1653 | 1.2673 | 1.2844 | 1.3520 |

**Table 22(b) :** Parameters obtained following Curve-fitting of Response Data, shown in Table C(7b), to a Polyexponential with Constants $A_i$ and Exponents $\alpha_i$.

### (b) Semi-Numerical Deconvolution

The response data was interpolated as for the numerical deconvolution. The parameters in Table 22(a) were used to generate the data for the weighting function at a time interval of 0.05 and these were used together with the interpolated response function for input into the semi-numerical deconvolution algorithm.

### (c) Polynomial Deconvolution

The parameters from Table 22(a) were used to represent the weighting function data, the dose administered was 0.7344 (see equation (3.2)), and together with the response data, these formed the input for the polynomial deconvolution method (see section 2.2.3).

The optimal polynomial to represent the input function was selected using the F test (section 2.4.1) on the residual sum of squares associated with that polynomial at P= 0.05 and n=13. The selected polynomials for each data set are shown in Table 23. These were then used to generate the values of the input function, and the integrals of these polynomials were used to generate the values of the cumulative fraction input (CFI).

| % Noise Added to Data | Selected Polynomial for the Input Rate I(t) |
|---|---|
| 0% | $I(t) = -0.0354 + 4.631t - 15.1332t^2 + 23.7452t^3 - 18.8496t^4 + 7.1923t^5 - 1.0489t^6$ |
| 1% | $I(t) = 0.0240 + 3.3106t - 8.246t^2 + 9.5137t^3 - 5.1436t^4 + 1.0224t^5$ |
| 5% | $I(t) = 0.1694 + 1.2665t - 1.2951t^2 + 0.3223t^3$ |
| 10% | $I(t) = 0.1284 + 1.5259t - 1.5768t^2 + 0.3971t^3$ |

**Table 23 :** Selected Polynomials produced by Polynomial Deconvolution on Data (from Table C(7)) with Increasing Levels of Added Noise

**(d) Polyexponential Deconvolution**

The parameters from Table 22(a) were used to represent the weighting function and those from Table 22(b) used to represent the response function and these two sets of parameters were used as input into the polyexponential deconvolution algorithm (section 2.2.4).

### 3.3.1.2 Results

The input rates and the cumulative fraction input's (CFI) produced for each level of added noise and each deconvolution method are shown in Figures 25-32.

**(a) Numerical Deconvolution**

The input rates produced by numerical deconvolution are shown in Figure 25 and the cumulative fraction released shown in Figure 26. The input rate produced from deconvolution of noise free data is indistinguishable from the true input rate, however when noise is added to the initial data oscillations begin to be produced in the predicted input rate. These oscillations are small for data containing 1% added noise, where the predicted input rate is still close to the true values, but at the higher noise levels, and towards the later time points they become too large to enable the form of the input function to be reliably defined.

The CFI's produced for all levels of noise are very close to the true values at the earlier time points, however deviations from the true values are seen at the 5 and

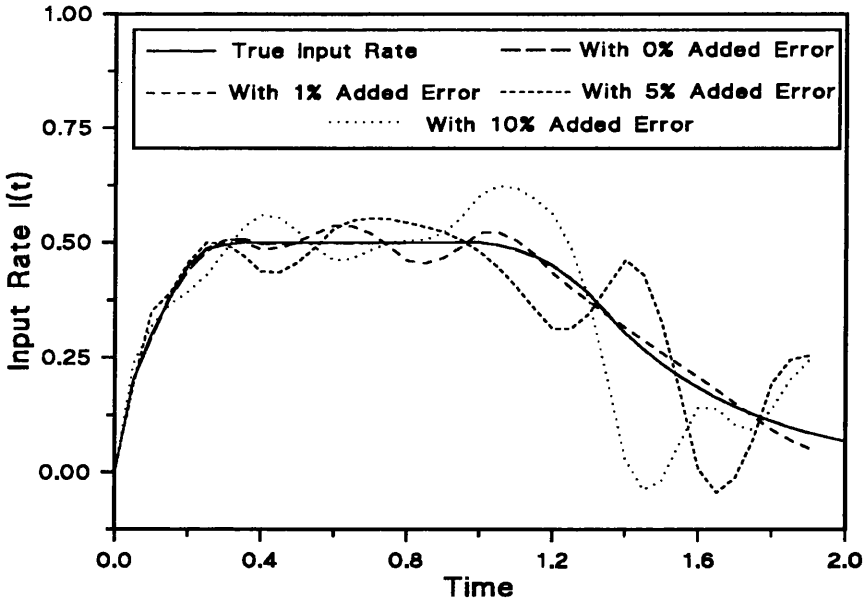


**Figure 25** : Input Rates produced by Numerical Deconvolution for the Controlled Release Input Function with Increasing Levels of Error added to both the Weighting and Response Functions

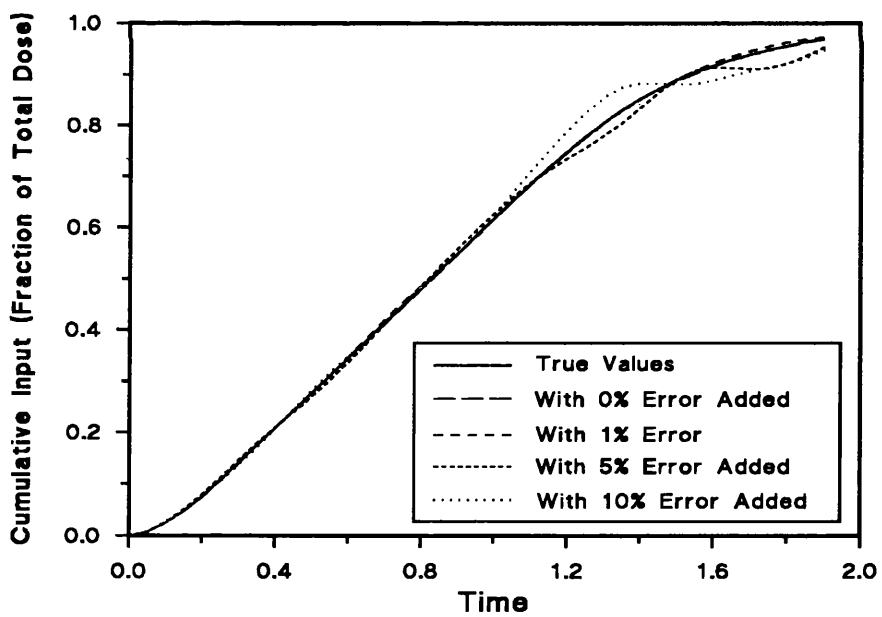


**Figure 26** : Cumulative Input produced by Numerical Deconvolution for the Controlled Release Input Function with Increasing Levels of Error added to both Weighting and Response Functions.

10% noise levels at the later time points.

**(b) Semi-Numerical Deconvolution**

The input rate and CFI's profiles produced by semi-numerical deconvolution are shown in Figures 27 and 28 respectively. The input rate produced by semi-numerical deconvolution on noise free data is indistinguishable from the true input, however when noise is added to the original data oscillations begin to appear in the predicted input rate. These oscillations are small for the 1% noise level but become much larger at the higher noise levels, making interpretation of the form of the input rate very difficult.

The CFI's produced by semi-numerical deconvolution are very close to the true values at the earlier time points, however deviations from the true values are seen at the later time points for data containing 5 and 10% noise.

**(c) Polynomial Deconvolution**

The input rates and CFI profiles produced by polynomial deconvolution are shown in Figures 29 and 30. The input rate predicted from noise free data agrees very well with the true input rate, as does that produced from data containing 1% noise, both of which correctly show the initial input rate to be zero and the existence of the linear portion in the input rate. At the 5 and 10% noise levels the predicted profiles show the same general shape as the true profile but fail to estimate correctly the initial input rate or to show the full extent of the linear portion of the input rate.

The CFI profiles produced at all levels of noise agree well with the true profile at the earlier points. At later time points the profiles for the 5 and 10% noise levels diverge from the true profiles.

**(d) Polyexponential Deconvolution**

The input rates and CFI profiles produced by polyexponential deconvolution are shown in Figures 31 and 32. The input rates produced by polyexponential deconvolution approximate the true profile badly at all noise levels and even with noise free data. The estimated input rates agree very well with the initial time points

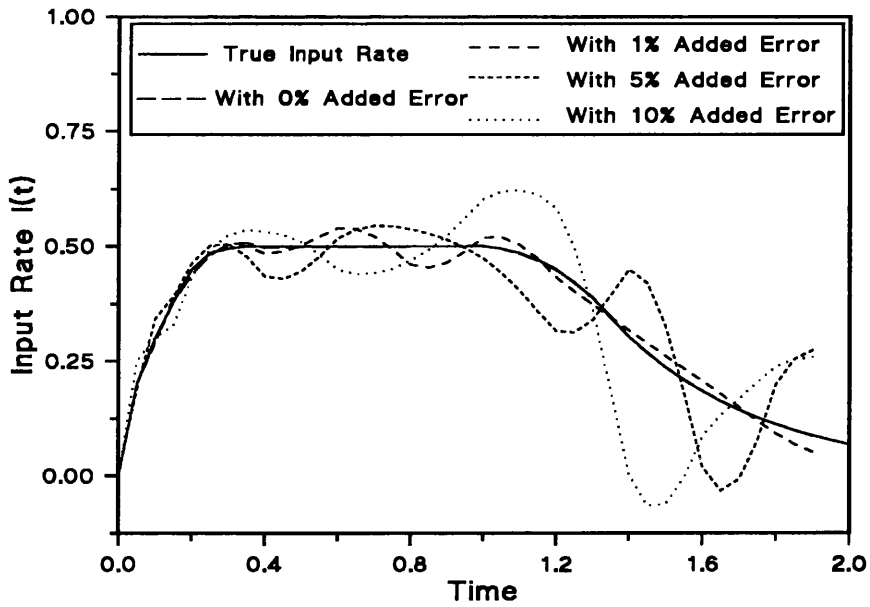


**Figure 27** : Input Rate produced by Semi-Numerical Deconvolution for the Controlled Release Input Function with Increasing Levels of Error added to both the Weighting and Response Functions.

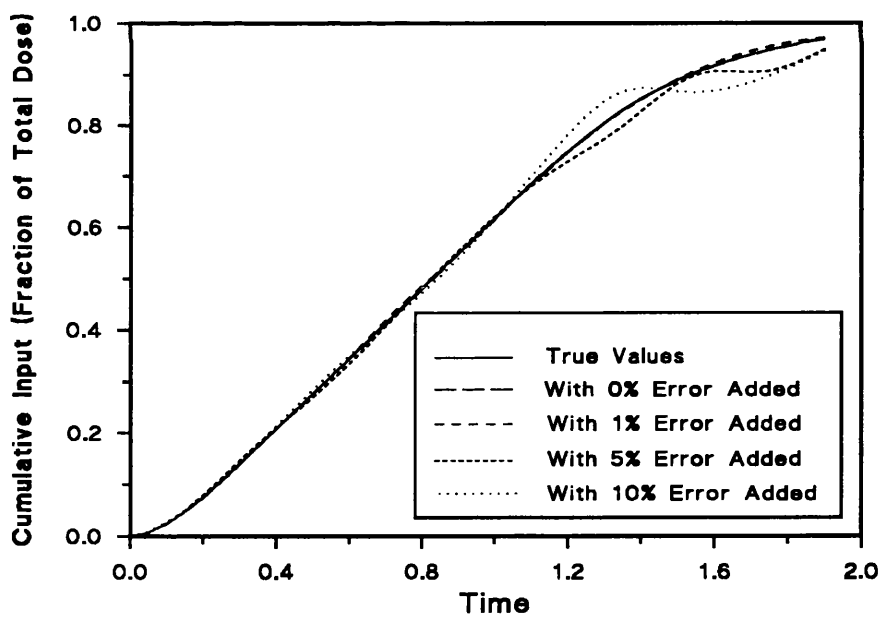


**Figure 28** : Cumulative Input produced by Semi-numerical Deconvolution for the Controlled Release Input Function with Increasing Levels of Error added to both Weighting and Response Functions.

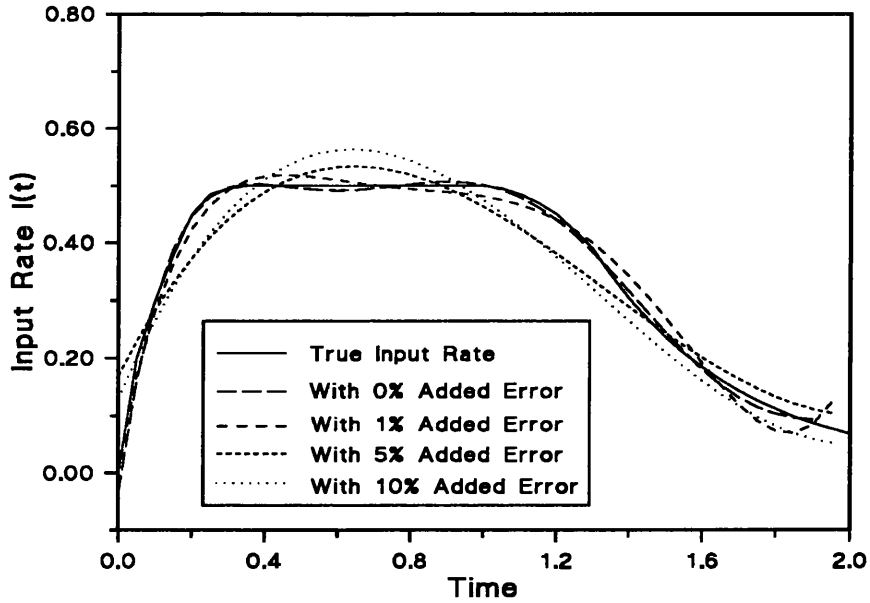


**Figure 29** : Input Rates produced by Polynomial Deconvolution for the Controlled Release Input Function with Increasing Levels of Error added to both the Weighting and Response Functions.

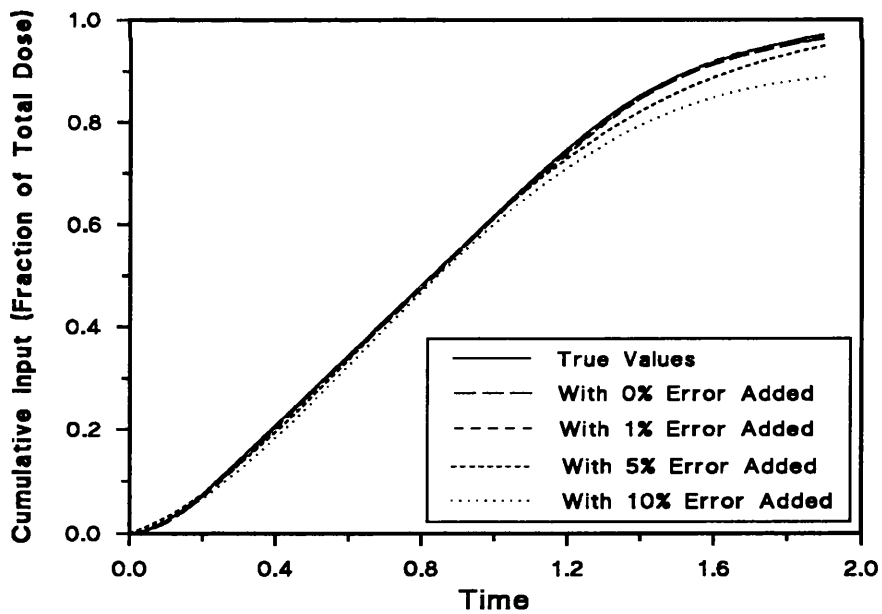


**Figure 30** : Cumulative Input produced by Polynomial Deconvolution for the Controlled Release Input Function with Increasing Levels of Error added to both the Weighting and Response Functions.

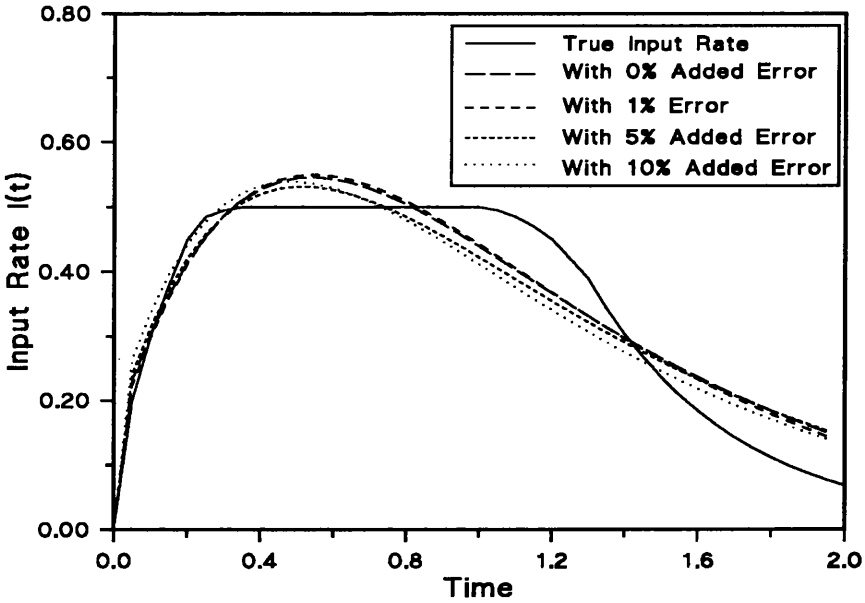


**Figure 31** : Input Rates produced by Polyexponential Deconvolution for the Controlled Release Input Function with Increasing Levels of Error added to both Weighting and Response Functions.

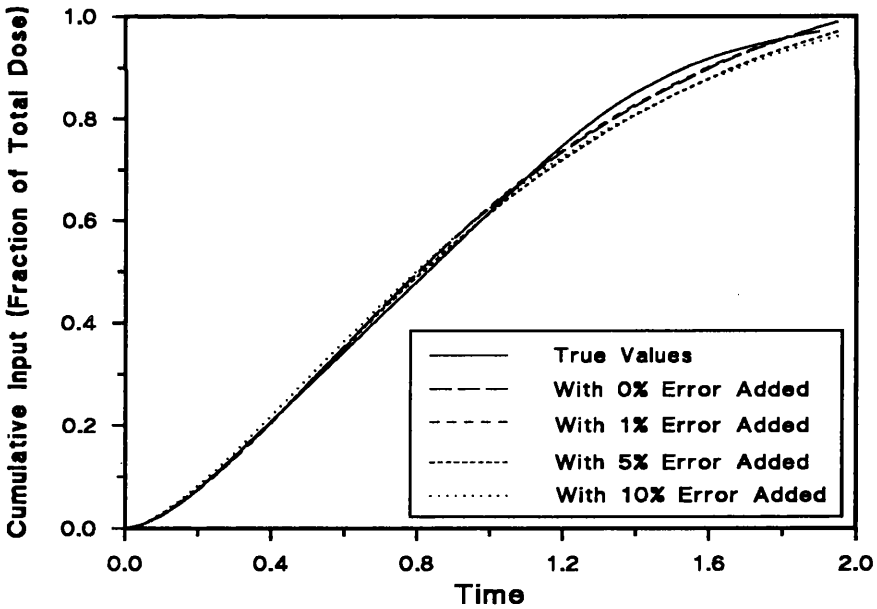


**Figure 32** : Cumulative Input produced by Polyexponential Deconvolution for the Controlled Release Input Function with Increasing Levels of error added to both Weighting and Response Functions.

but all profiles fail to show the length of the linear portion of the true input rate and they approximate the declining phase of the profile equally badly. However all the profiles show the initial input rate to be zero and there is little change of the predicted input rates with increasing levels of noise.

The CFI profiles' show good agreement with the true profile at all noise levels during the early time points, however at the later time points all the profiles show divergence away from the true values.

### 3.3.1.3 Percentage Difference between Predicted and True Values

For each of the data sets shown in Figures 25-32 the percentage difference between the true value and the predicted value for each point was calculated in the following way. The percentage difference for the input rate was calculated as the absolute value of the difference between the calculated input and the true input, and multiplied by 100, i.e.

$$\%\text{diff } I(t) = \left| \text{Calc. } I(t) - \text{True } I(t) \right| * 100$$

The percentage difference for the cumulative fraction input was calculated as the calculated fraction minus the true fraction multiplied by 100.

$$\%\text{diff fraction input} = \left| \text{calc. value - true value} \right| * 100$$

Each data set comprised 39 values over a time range of 0 to 1.9 at intervals of 0.05, which was the output from the deconvolution algorithms. The percentage differences, once calculated, were averaged for each data set and the mean and standard error of the means for these values are shown in Table 24 for the estimated input rate values and Table 25 for the estimated fraction input values.

| | Noise Level in original Data | | | |
|---|---|---|---|---|
| Type of Deconvolution | 0% | 1% | 5% | 10% |
| Numerical | 0.18 (0.040) | 1.64 (0.195) | 6.74 (0.915) | 7.114 (1.207) |
| Semi-Numerical | 0.18 (0.041) | 1.68 (0.201) | 6.60 (0.900) | 8.58 (1.365) |
| Polynomial | 0.74 (0.124) | 1.65 (0.180) | 3.47 (0.483) | 4.28 (0.396) |
| Polyexponential | 4.31 (0.401) | 4.22 (0.378) | 4.41 (0.472) | 4.62 (0.506) |

**Table 24 :** Mean Percentage Difference for Input Rate Values shown in Figures 25,27,29 and 31 for Increasing Levels of Added Noise. The S.E.M. values are shown in Parentheses (n=39).

When the mean percentage difference for the input rates are examined (Table 24) the following can be seen. With error free data, or at the 1% noise level, the numerical, semi-numerical and polynomial methods have a considerably smaller mean percentage difference than the polyexponential method which has a large percentage difference at the low noise levels. At the higher noise levels of 5 and 10% the mean percentage difference values for the numerical and semi-numerical deconvolution methods increase sharply while that of the polynomial method increases only slightly at the higher levels showing that the method is less susceptible to data noise. The percentage difference for the polyexponential method varies little, if at all, with the increase in error levels and the percentage difference associated with the higher noise levels is small.

| | Noise Level in original Data | | | |
|---|---|---|---|---|
| Type of Deconvolution | 0% | 1% | 5% | 10% |
| Numerical | 0.11 (0.006) | 0.22 (0.035) | 1.03 (0.161) | 1.58 (0.257) |
| Semi-Numerical | 0.11 (0.005) | 0.21 (0.033) | 1.20 (0.201) | 1.77 (0.293) |
| Polynomial | 0.46 (0.022) | 0.42 (0.045) | 1.41 (0.177) | 3.44 (0.418) |
| Polyexponential | 1.02 (0.131) | 0.98 (0.119) | 1.60 (0.245) | 2.04 (0.209) |

**Table 25 :** Mean Percentage Difference for Cumulative Fraction Input Values shown in Figures 26,28,30 and 32 for Increasing Levels of Added Noise. The S.E.M. values are shown in Parentheses (n=39).

The figures in Table 25 show the mean percentage difference (SEM) for the CFI's. There is very little difference seen between any of the four deconvolution methods and all the methods show mean percentage differences which are less than, but of the same order, as the level of noise added to the original data. The exception is the polyexponential method (on error free data) which shows a mean percentage difference larger than the other methods whose value is very low for the error free data. No one method shows any clear superiority at any noise level.

### 3.3.2 Constant Level of Noise Added to Ten Data Sets

#### 3.3.2.1 Method

In this second part the level of added noise was set at 10% and ten different random data sets were generated by using the addition of noise to the true weighting and response values shown in Table 21 using the NAG subroutine G05DDF (section 2.3.3). The ten data sets produced from this are shown in Tables C(8) and C(9) in Appendix C.

Each of the data sets was fitted to an equation of the form given in equation (3.3) using the non-linear least-squares fitting routine (section 2.1.1). The number of terms in the polyexponential was sequentially increased until there was no significant improvement in the residual sum of squares as judged by the F test at P=0.05 and n=13 (n is the number of data points). The parameters produced from this fitting are shown in Tables 26 (Weighting Function) and 27 (Response Function).

| Parameters / Subject | $A_1$ | $A_2$ | $A_3$ | $\alpha_1$ | $\alpha_2$ | $\alpha_3$ |
|---|---|---|---|---|---|---|
| 1 | -1.1810 | 1.1810 | | 13.9631 | 1.0969 | |
| 2 | -1.2915 | 1.2915 | | 11.9909 | 1.1412 | |
| 3 | -1.1643 | 1.1643 | | 16.7531 | 1.0861 | |
| 4 | -1.0419 | 1.0419 | | 15.2997 | 1.0001 | |
| 5 | -1.1828 | 1.1928 | | 14.8537 | 1.1056 | |
| 6 | -1.2897 | 1.2897 | | 11.5267 | 1.1937 | |
| 7 | -1.3277 | 1.3277 | | 12.8574 | 1.2384 | |
| 8 | -1.2456 | 1.2456 | | 12.4204 | 1.1559 | |
| 9 | -1.1930 | 1.1930 | | 14.2910 | 1.1551 | |
| 10 | -1.4263 | 1.4263 | | 9.7969 | 1.2741 | |

**Table 26 :** Parameters Obtained following Curve-fitting of the Weighting Data, shown in Table C(8), to a Polyexponential with Constants $A_i$ and Exponents $\alpha_i$.

The ten data sets produced were then processed through each of the four deconvolution algorithms (section 2.2) according to the details given below.

#### (a) Numerical Deconvolution

The interpolation time used was again 0.05, and both weighting and response

data was interpolated prior to deconvolution.

| Parameters / Subject | $A_1$ | $A_2$ | $A_3$ | $\alpha_1$ | $\alpha_2$ | $\alpha_3$ |
|---|---|---|---|---|---|---|
| 1 | -50.1675 | 25.4009 | 24.7666 | 1.5894 | 1.8548 | 1.3270 |
| 2 | -50.1583 | 25.0958 | 25.0625 | 1.4894 | 1.7247 | 1.2555 |
| 3 | -54.2925 | 25.6869 | 28.6056 | 1.5222 | 1.7838 | 1.2937 |
| 4 | -41.6910 | 19.7336 | 21.9574 | 1.4705 | 1.7602 | 1.2167 |
| 5 | -54.1195 | 26.5609 | 27.5586 | 1.6303 | 1.9086 | 1.3700 |
| 6 | -43.3911 | 25.8120 | 17.5791 | 1.5502 | 1.7667 | 1.2394 |
| 7 | -41.7453 | 23.2964 | 18.4489 | 1.5778 | 1.8156 | 1.2812 |
| 8 | -41.8064 | 23.0972 | 18.7092 | 1.4445 | 1.6653 | 1.1720 |
| 9 | -50.7336 | 25.5932 | 25.1404 | 1.4812 | 1.7242 | 1.2391 |
| 10 | -47.9828 | 33.6078 | 14.3750 | 1.4437 | 1.5889 | 1.1045 |

**Table 27 :** Parameters obtained following Curve-fitting of Response Data, shown in Table C(9), to a Polyexponential with Constants $A_i$ and Exponents $\alpha_i$.

### (b) Semi-Numerical Deconvolution

The parameters from Table 26 were used to generate values for the weighting function at intervals of 0.05 and these, together with the response function data (interpolated at t=0.05), were used as input into the semi-numerical deconvolution algorithm.

### (c) Polynomial Deconvolution

The parameters from Table 26 were used to represent the weighting function, and the values in Table C(9) were used for the response function. The data were then processed according to the polynomial deconvolution method (section 2.2.3) and the optimal polynomial to represent the input function was selected using the F Test (section 2.4.1) at P=0.05 and n=13. The selected polynomials are shown in Table 28 and these were used to calculate the input rate, I(t), and their integrals used to calculate the cumulative fraction input.

| Subject | Selected Polynomial for the Input Rate |
|---|---|
| 1 | $I(t) = 0.2012 + 0.8042t - 0.4912t^2$ |
| 2 | $I(t) = -0.1718 + 7.5070t - 25.3365t^2 + 34.3906t^3 - 20.0947t^4 + 4.1876t^5$ |
| 3 | $I(t) = 0.1657 - 0.9778t - 0.5894t^2$ |
| 4 | $I(t) = 0.0606 + 1.9906t - 2.0362t^2 + 0.5361t^3$ |
| 5 | $I(t) = 0.0341 + 2.3848t - 2.7299t^2 + 0.8088t^3$ |
| 6 | $I(t) = 0.1342 + 1.3533t - 1.4133t^2 + 0.3767t^3$ |
| 7 | $I(t) = 0.1061 + 1.8142t - 2.2686t^2 + 0.7374t^3$ |
| 8 | $I(t) = 0.2291 + 1.1696t - 1.3546t^2 + 0.4010t^3$ |
| 9 | $I(t) = 0.1279 + 1.4156t - 1.3509t^2 + 0.3239t^3$ |
| 10 | $I(t) = 0.2903 + 0.5770t - 0.4933t^2 + 0.0816t^3$ |

**Table 28 :** Selected Polynomials produced by Polynomial Deconvolution on Data from Tables C(8) and C(9).

**(d) Polyexponential Deconvolution**

The parameters from Table 26 were used to represent the weighting function and those from Table 27 used to represent the response function and together these formed the input into the polyexponential deconvolution algorithm.

Following deconvolution the mean and standard error of the mean over the ten data sets were calculated for the input rate and the cumulative fraction input (CFI) for each deconvolution method. The estimated fraction of dose released ($F_R$) produced for each data set was calculated by taking the maximum value reached in the CFI profile. For each input rate produced the Mean Dissolution Time (MDT) was calculated according to the method described in section (2.5.1).

### 3.3.2.2 Results

For each deconvolution method the mean input rate and mean cumulative fraction input for the ten data sets were plotted together with the standard error of the mean values (S.E.M.) and these are shown in Figures 33-36.

**(a) Numerical Deconvolution**

The mean input rate (n=10) and mean CFI profile produced by numerical deconvolution are shown in Figure 33. The mean input rate predicted by numerical deconvolution shows the form of the true input rate well over the initial increase in input rate, as well as over the linear portion of the profile. The predicted profile fails show the smooth decline in the true input rate over the later time points and instead begins to show a degree of oscillation. The SEM values associated with the predicted input rate are large, showing the degree of variability in results produced by the additional error in the data.

The mean CFI produced by the numerical deconvolution is very close to the true profile and the SEM values associated with it are very small. The only slight deviation from the true profile occurs during the declining phase of the input rate when the true rate is approximated least well.

**(b) Semi-Numerical Deconvolution**

The mean input rate (n=10) and the mean CFI profile produced by semi-numerical deconvolution are shown in Figure 34. The mean input rate predicted by semi-numerical deconvolution shows the general form of the input rate up to the end of the linear portion fairly well, however the method fails to approximate the declining phase of the input rate with any degree of accuracy. The SEM values associated with the predicted input rate profile are large showing the influence of the additional error on the performance of the deconvolution algorithm.

The mean CFI however, is a very good approximation of the true profile and has very small SEM values associated with it. Like the numerical deconvolution, the only slight deviations from the true profile are seen during the declining phase, when the input rate is poorly approximated.

**(c) Polynomial Deconvolution**

The mean input rate (n=10) and the mean CFI profile produced by polynomial deconvolution are shown in Figure 35. The mean input rate predicted by polynomial deconvolution gives a reasonably good approximation to the true input rate but

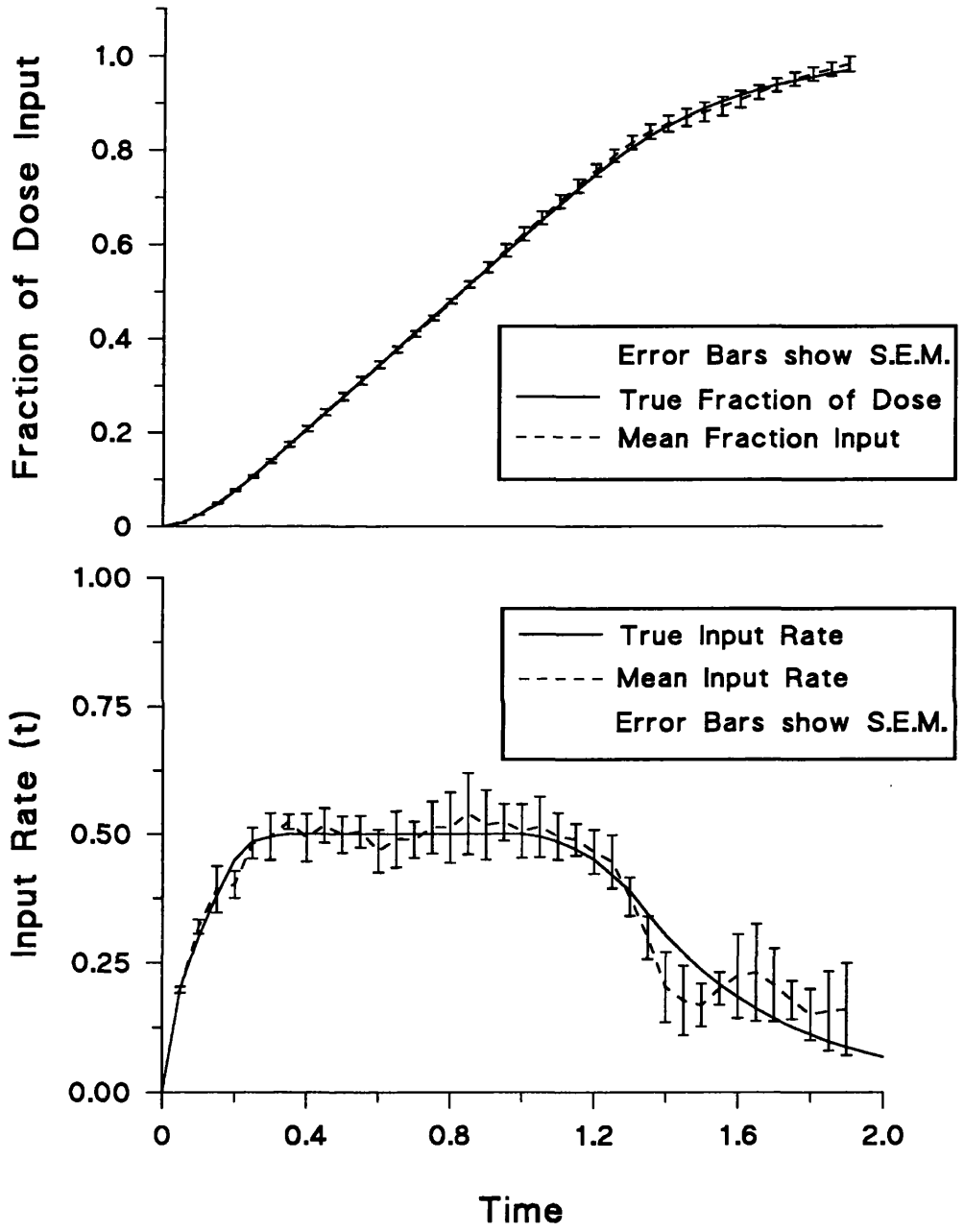


**Figure 33** : Mean results produced by Numerical Deconvolution for the Controlled Release Input Function on 10 Data Sets with 10% Noise added to the Weighting and Response Functions

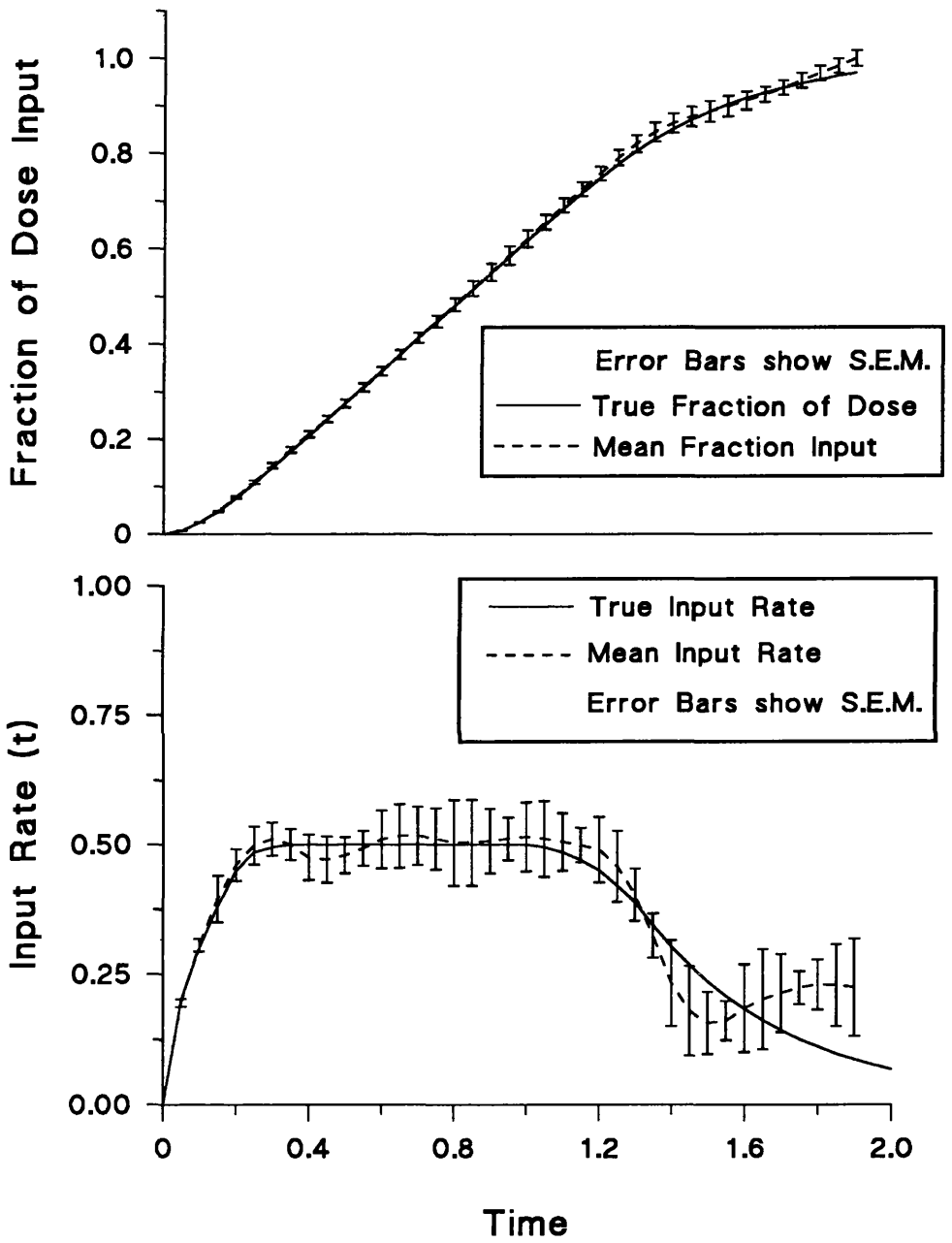


**Figure 34** : Mean results produced by Semi-Numerical Deconvolution for the Controlled release Input Function on 10 Data Sets with 10% Noise added to both the Weighting and Response Functions

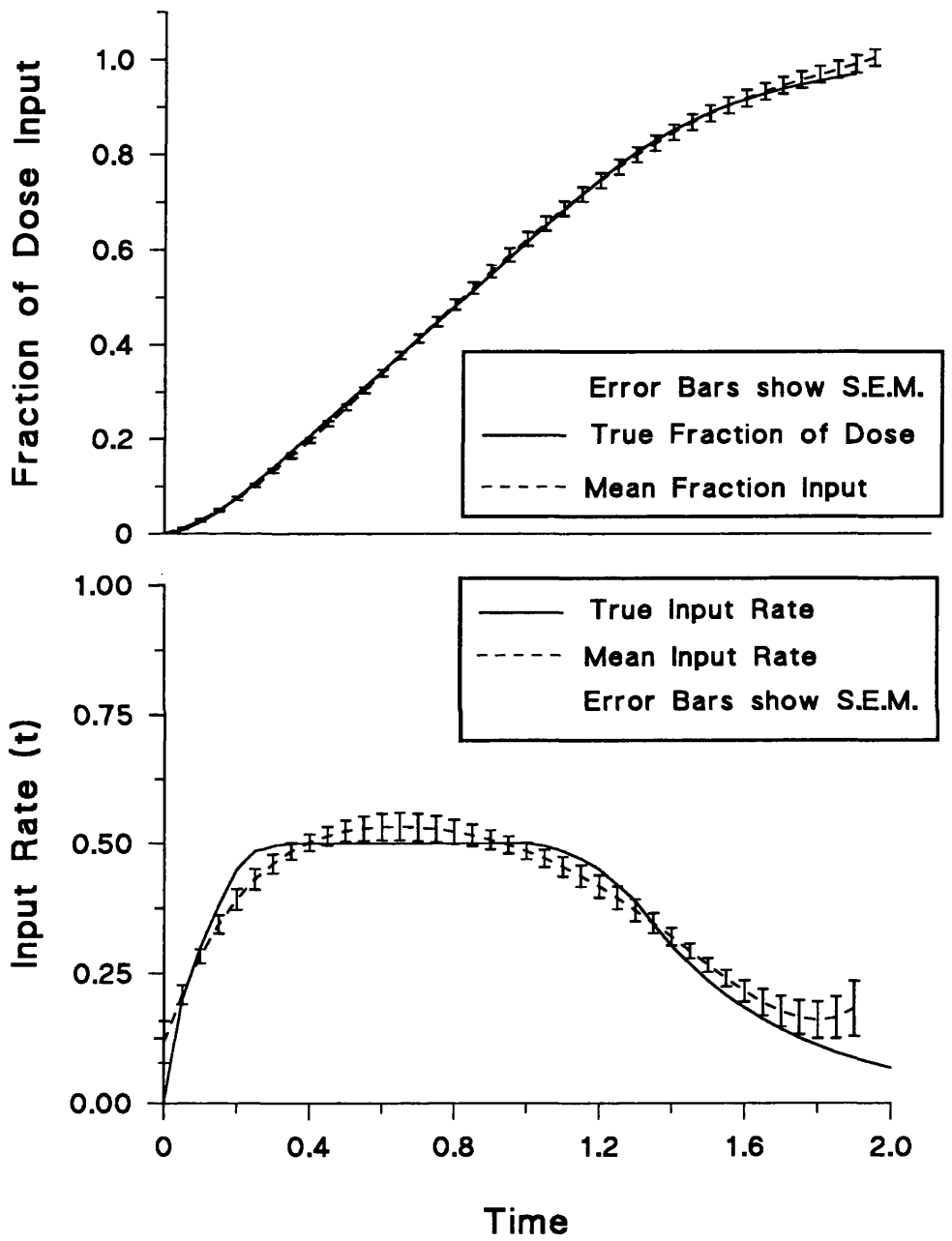


**Figure 35** : Mean results produced by Polynomial Deconvolution for the Controlled Release Input Function on 10 Data Sets with 10% Error added to both the Weighting and Response Functions

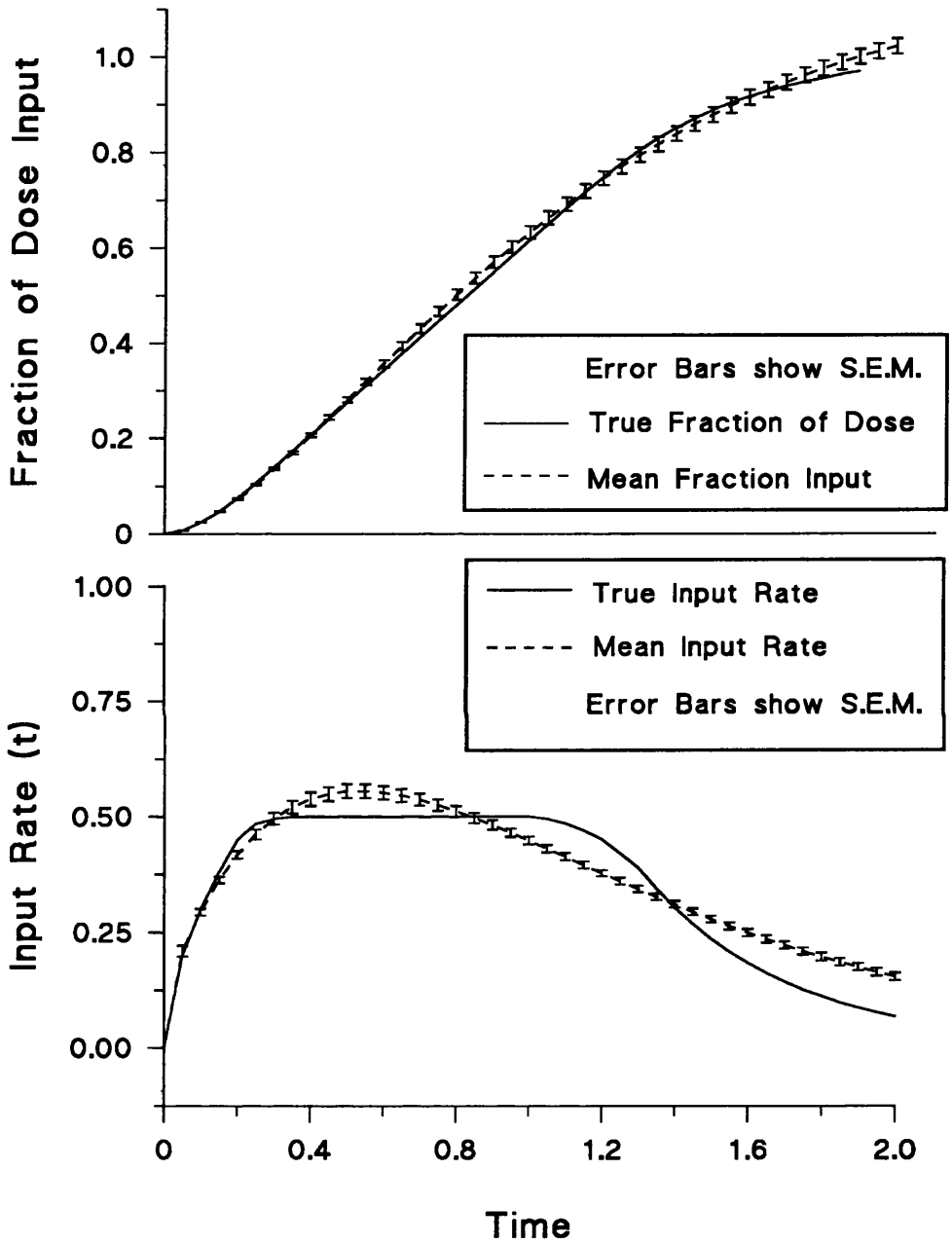


**Figure 36** : Mean results produced by Polyexponential Deconvolution for the Controlled Release Input Function on 10 Data Sets with 10% Error added to both the Weighting and Response Functions

marked deviations to the true input rate are seen at either end of the time course over which deconvolution was performed. The method fails to show that the initial value of the input rate is zero and the predicted input rate begins to deviate markedly towards the end of the time period considered. The linear portion of the true input rate appears more as a broad, gentle curve in the mean predicted rate and because of this the predicted rate underestimates the true rate at either end of the linear portion. The SEM values associated with the predicted rate are very small except at the late time points (where the predicted input rate begins to diverge from the true rate) when they begin to increase.

The mean CFI is a very good prediction of the true values and there is little deviation seen from the true profile. The SEM values associated with the predicted CFI are very small.

**(d) Polyexponential Deconvolution**

The mean input rate (n=10) and the mean CFI profile produced by polyexponential deconvolution are shown in Figure 36. The mean input rate predicted by polyexponential deconvolution does not approximate the true rate with any degree of accuracy. The initial rising rate is shown very well, however the linear portion of the true input rate cannot be seen in the predicted rate, where the input rate is first overestimated then underestimated. The method fails also to show correctly the declining phase of the true input rate and during the late time points the input rate is overestimated. The SEM values associated with the predicted input rate are very small.

The mean CFI is a fair approximation to the true profile but it alternately overestimates and underestimates the true profile and the final estimation of the CFI is overestimated. Like the input rate the SEM values associated with the profile are small.

### 3.3.2.3 Estimated Fraction Released $F_R$

The estimated fraction of dose released for each subject and each deconvolution method are shown in Table 29, together with the mean fraction released ($\overline{F}_R$), the standard

deviation (SD) and the standard error of the mean (SEM) for each deconvolution method.

| Subject | Numerical | Semi-Numerical | Polynomial | Poly-exponential |
|---|---|---|---|---|
| 1 | 0.972 | 0.979 | 0.963 | 0.991 |
| 2 | 0.931 | 0.929 | 0.936 | 0.942 |
| 3 | 0.987 | 0.981 | 0.957 | 1.010 |
| 4 | 1.077 | 1.089 | 1.100 | 1.076 |
| 5 | 0.953 | 1.046 | 1.057 | 1.051 |
| 6 | 0.943 | 0.954 | 0.957 | 0.958 |
| 7 | 0.944 | 0.953 | 0.973 | 0.925 |
| 8 | 1.040 | 1.037 | 1.051 | 1.005 |
| 9 | 1.039 | 1.047 | 1.052 | 1.058 |
| 10 | 0.947 | 0.993 | 1.006 | 0.991 |
| Mean | 0.983 | 1.001 | 1.005 | 1.001 |
| SD | 0.051 | 0.051 | 0.056 | 0.050 |
| SEM | 0.016 | 0.016 | 0.018 | 0.016 |

**Table 29 :** Fraction of Dose Released predicted by Four Deconvolution Algorithms for the Controlled Release Input Rate with 10% Noise added to both Weighting and Response Functions

The mean fraction released produced for each of the deconvolution methods was compared with the true value of 0.970 using the t-test (section 2.4.2) at a probability level of P=0.05 and 9 degrees of freedom. The value of 0.970 is the fraction of dose released at t=1.9 calculated form the integral of the controlled release input rate. The $t_s$ values were calculated according to the equation given below, the mean and SEM values were taken from Table 29 :

$$t_s = \bar{F}_R - 0.970 / SEM$$

where $\bar{F}_R$ is the mean fraction released.

The values of $t_s$ calculated for each of the four deconvolution methods were as follows

Numerical Deconvolution $t_s = 0.813$

Semi-Numerical Deconvolution $t_s = 1.938$

Polynomial Deconvolution $t_s = 1.944$

Polyexponential Deconvolution $t_s = 1.938$

The value of $t_s$ taken from the tables at P=0.05 and 9 degrees of freedom ($t_{0.05(9)}$) is 2.26. All the values calculated for the deconvolution methods are less than this critical value, therefore there is no significant difference between the mean fraction released predicted by any of the deconvolution methods and the true value.

### 3.3.2.4 Mean Dissolution Times

The Mean Dissolution Times (MDT) calculated from the input rates predicted by the deconvolution methods, according to the method described in section 2.5.1, were calculated for each subject and each method. These MDT values, together with the mean, standard deviation (SD), and standard error of the mean (SEM), for each method, are shown in Table 30.

| Subject | Numerical | Semi-Numerical | Polynomial | Poly-Exponential |
|---|---|---|---|---|
| 1 | 0.829 | 0.860 | 0.832 | 0.863 |
| 2 | 0.824 | 0.834 | 0.861 | 0.877 |
| 3 | 0.808 | 0.786 | 0.784 | 0.889 |
| 4 | 0.864 | 0.886 | 0.870 | 0.864 |
| 5 | 0.831 | 0.841 | 0.849 | 0.838 |
| 6 | 0.779 | 0.850 | 0.882 | 0.888 |
| 7 | 0.884 | 0.896 | 0.918 | 0.874 |
| 8 | 0.888 | 0.888 | 0.906 | 0.905 |
| 9 | 0.872 | 0.884 | 0.892 | 0.911 |
| 10 | 0.808 | 0.915 | 0.891 | 0.935 |
| Mean | 0.839 | 0.864 | 0.869 | 0.884 |
| SD | 0.037 | 0.038 | 0.039 | 0.028 |
| SEM | 0.012 | 0.012 | 0.012 | 0.009 |

**Table 30 :** Mean Dissolution Times Estimated for the Input Rates produced by Four Deconvolution Algorithms for the Controlled Release Input Rate with 10% Noise added to both Weighting and Response Functions.

The mean MDT produced for each of the deconvolution methods was compared with the true value using the t-test (section 2.4.2) at a probability level of P=0.05 and 9 degrees of freedom. The MDT value was calculated up to t=1.9 using the method described by equation (2.49) in section 2.5.1, giving a $MDT_{t=1.9}$ of 0.827. The $t_s$ values were calculated according to the equation given below, the mean and SEM values were taken from Table 30 :

$$t_s = \bar{MDT} - 0.827 / SEM$$

where $\bar{MDT}$ is the mean MDT.

The values of $t_s$ calculated for each of the four deconvolution methods were as follows

| | |
|---|---|
| Numerical Deconvolution | $t_s = 0.167$ |
| Semi-Numerical Deconvolution | $t_s = 3.083$ |
| Polynomial Deconvolution | $t_s = 3.500$ |
| Polyexponential Deconvolution | $t_s = 6.333$ |

The value of $t_s$ taken from the table $t_{0.05(9)}$ for P=0.05 and 9 degrees of freedom was 2.26. The $t_s$ value calculated for the MDT value for the numerical deconvolution method was less than the critical value of 2.26. Therefore there is no significant difference between the estimates of MDT calculated from the input rate produced from the numerical deconvolution method and the true value at the 0.95 probability level. The $t_s$ values produced for the other three methods are all greater than 2.26 showing the differences are significant at the 95% probability level. The deviation from the true values is significant at the 95% probability level ($0.05 > P > 0.01$) for the semi-numerical method, at the 99% level ($0.01 > P > 0.001$) for the semi-numerical method and at the 99.9% level ($P < 0.001$) for the polyexponential method.

### 3.3.3 Discussion

The simpler numerical and semi-numerical algorithms (which do not approximate the input rate with an empirical function) and the polynomial algorithm (which approximates the input function with a polynomial) all provide good predictions of the true input rate

when the initial data is error free or contains very low levels of added noise. When more noise is added to the data the numerical and semi-numerical methods become unstable, and very little can be interpreted from the input profiles seen. The profile is more stable when the mean input rate is considered, but both algorithms are very susceptible to data noise.

The change seen in the predicted input rate profile for the polynomial algorithm at the higher noise levels is less drastic. The predicted profile is still close enough to the true values that its general form can be seen, and the algorithm itself is very stable to data error (as shown by the small SEM values shown in Figure 35).

The polyexponential algorithm shows little change in the predicted input rate with increasing levels of noise (as shown by Figure 32), however at no point does it succeed in showing the correct form of the input rate.

The cumulative fraction input profiles for all algorithms and at all noise levels show profiles which are very close to the true values. The cumulative profiles produced by the deconvolution algorithms are much more stable to data error than their corresponding input rate profiles and give very good predictions of the true values.

There was no significant difference seen between the estimated fraction released (at t=1.9) for any of the methods and the true value, however when the predicted $MDT_{1.9}$ were examined only the numerical algorithm showed no significant difference to the true value at t=1.9. The semi-numerical, polynomial and polyexponential algorithms all gave significantly different mean values.

In all these three cases the MDT overestimated the true value, and a consideration of the mean input rate profiles would suggest that this is due to the overestimation of the input rate for the late time points, especially for the polyexponential method.

## 3.4 CONCLUSIONS

The work in this chapter was designed to address the first three of the objectives given at the end of the introduction, and from the work presented in this chapter the following conclusions can be drawn with regard to those objectives.

- Throughout the chapter the deconvolution algorithms which used empirical formula

to represent the unknown input rate (the polynomial and polyexponential algorithms) are much more stable to data noise than the numerical and semi-numerical methods which place no restriction on the form of the input rate.

- There is no advantage in smoothing the weighting function prior to numerical deconvolution i.e. throughout the chapter there was no difference seen, in any aspect, between the numerical and semi-numerical algorithms.

- The choice of algorithm is dependant on what information is desired from the deconvolution process. If the aim of the deconvolution is to calculate point values (MDT and $F_R$) or to look at the cumulative profiles then there is no advantage to using any of the more complex algorithms. In fact, the numerical algorithm provide results which are as good as (and in some cases, better than) those of the more complex algorithms.

- Only when the aim of the deconvolution is to obtain information about the mechanism of drug release does the choice of algorithm become important. In this case one of the more complex algorithms should be used. The polynomial algorithm is more flexible in approximating an unknown input function than the polyexponential algorithm and is the method of choice for those input functions examined in this chapter.

- None of the deconvolution algorithms which involve approximation of the input function by an empirical function can show abrupt changes in the input rate, however if the input rate is expected to vary smoothly then the these methods will give a good reflection of the unknown input rate.

- The fact that little difference is seen between the methods, except when the input rate itself is considered, is due mainly to the fact that the integration of the input rate acts like a smoothing process and much detail apparent in the input rate is automatically lost on conversion to the CFI.

# 4 *IN VIVO* RELEASE CHARACTERISTICS OF CONTROLLED RELEASE METOPROLOL

In the previous chapter the ability of the four deconvolution algorithms at predicting the form and values of different input rates was examined using pseudo-experimental data, together with their ability to cope with varying levels of additional noise in the source data. The aim of the work presented in that chapter was to meet the first three of the objectives stated at the end of the introduction, and the discussion presented at the end of chapter three covers the degree to which these objectives were achieved.

This next chapter is concerned with objective four, that is to use the four different deconvolution algorithms to analyze actual clinical data with the aim of highlighting any problems which may arise when deconvolution is used in a practical situation. In this next chapter the four deconvolution algorithms will be used to analyze the *in vivo* drug release characteristics of metoprolol from three different controlled release tablets, using the plasma concentrations following administration of a bolus solution of 95mg metoprolol succinate as the weighting function for the deconvolution process.

After the deconvolution has been performed the resulting release rate profiles and cumulative fraction released profiles will be used to characterise the release process through consideration of the following parameters :

(a) The shape and characteristics of the dissolution rate and the cumulative fraction released profiles themselves

(b) The Fraction of Dose Released, $F_R$

(c) The estimated MDT *in vivo* for all subjects

(c) *In vitro - in vivo* correlation using $MDT_{in\ vivo}$ vs $MDT_{in\ vitro}$ Plots

The examination of the differences in these characteristics produced by the different algorithms will show any differences in the values which arise due to the instability of the deconvolution algorithms themselves.

The clinical data used in this chapter has been supplied by AB Hässle, Mölndal, Sweden and further details of the study particulars are given by Sandberg et al (1991).

## 4.1 DETAILS OF THE CLINICAL DATA

The clinical data obtained are the results of a single dose study of controlled release metoprolol. The study was an open label, five way, cross-over design, with the study drugs given in randomised order to ten healthy male volunteers aged between 20 and 29 (mean 24) and weight 70-86kg (mean 78). Each subject received a single dose of each of the five treatments shown below :

(1) IV solution of Metoprolol Tartrate 10mg

(2) Oral solution of Metoprolol Succinate 95mg/100mls

(3) CR Tablet A of Metoprolol Succinate 95mg

(4) CR Tablet B of Metoprolol Succinate 95mg

(5) CR Tablet C of Metoprolol Succinate 95mg

The treatment days were separated by wash out periods of at least five days and each CR tablet was administered with 200mls of water and the oral solution was administered with 100mls water. The plasma concentrations arising from the solution and the three controlled release tablets are shown in tables D(1)-D(4) in Appendix D.

## 4.2 DETAILS OF THE CONTROLLED RELEASE TABLETS

The three controlled release tablets are all multiple-unit controlled release systems (Sandberg et al 1988) which consist of several hundred small pellets of metoprolol succinate coated with a non-disintegrating polymeric membrane. The pellets are compressed with inert excipient granules to form tablets. These tablets disintegrate rapidly releasing the pellets, which act as individual dosage forms, releasing their drug at a constant rate.

The rate of release of the multiple-unit dosage form is controlled by the thickness of the membrane coating each pellet. The three metoprolol CR tablets have *in vitro* release rates of ~7%/hr, ~5.7%/hr and ~3.3%/hr for CR A, CR B and CR C respectively.

## 4.3 *IN VITRO* DISSOLUTION STUDIES

The *in vitro* dissolution testing was performed using a USP apparatus 2 (rotating

paddle) at 37°C with paddle speeds of 50, 100 and 150rpm and at pH's of 1.2, 4.0 and 6.8. The mean results (n=6) are shown in Tables D(5)-D(7) in Appendix D. The rate of drug release for all three formulations was shown to be insensitive to changes in either agitation or pH.

## 4.4 JUSTIFICATION OF LINEARITY

In order to justify the use of deconvolution in a practical situation the system under study must be shown to be linear, i.e. the disposition kinetics of metoprolol must be shown to be linear. Metoprolol is eliminated largely by the mono-oxygenase system of the liver (Regårdh and Johnsson 1980) and therefore there is a possibility of Michaelis-Menton kinetics, if the metabolism is saturable, and hence non-linearity. However Kendall et al (1977) showed that the half-life of metoprolol is not influenced by the dose within the usual therapeutic dosage range and that the bioavailability of single oral doses is constant over the normal dose range (but may increase with higher doses above that).

On this evidence the system can be assumed to be linear in the dose region being used. However, if the nature of the dosage forms (i.e. that they are controlled release) affects the rate of metabolism or the bioavailability then the linearity of the system will be violated.

## 4.5 METHOD

Each of the three metoprolol CR tablets was analyzed by each of the four deconvolution algorithms described in detail in section 2.2. Prior to deconvolution the plasma concentrations for each subject following administration of the oral solution were fitted to a polyexponential equation, of the form shown in equation (4.1), using the non-linear least squares curve-fitting routine described in section 2.1.1. C(t) is the plasma concentration at time t.

$$\begin{aligned} C(t) &= 0 && \text{for } t < tlag \\ &= \sum_{i=1}^{n} A_i e^{-\alpha_i (t - tlag)} && \text{for } t \geq tlag \\ \text{where} \quad A_n &= \sum_{i=1}^{n-1} A_i \end{aligned} \tag{4.1}$$

The parameters obtained following this curve fitting are shown in Table 31. These parameters (or the plasma concentrations themselves) were used as the weighting function in the deconvolution process. In this manner the input rate produced by the deconvolution will represent the *in vivo* drug release rate of metoprolol from the three controlled release tablets.

As can be seen from Table 31, in all subjects except subjects 6 and 9 there is a small but distinct delay before metoprolol appears in the plasma. The parameters from Table 31

| Subject | tlag $hrs^{-1}$ | $\alpha_1$ $h^{-1}$ | $A_2$ $\mu mol\ l^{-1}$ | $\alpha_2$ $h^{-1}$ | $A_3$ $\mu mol\ l^{-1}$ | $\alpha_3$ $h^{-1}$ |
|---|---|---|---|---|---|---|
| 1 | 0.407 | 1.1832 | 0.4450 | 0.3444 | | |
| 2 | 0.222 | 4.9451 | 0.9558 | 0.0881 | | |
| 3 | 0.215 | 6.4748 | 0.2718 | 0.3036 | 0.8508 | 7.4107 |
| 4 | 0.235 | 4.6577 | 1.0948 | 6.1370 | 0.7150 | 0.2856 |
| 5 | 0.262 | 2.5349 | 1.5854 | 3.1252 | 0.5826 | 0.2273 |
| 6 | 0.000 | 1.1441 | 1.0759 | 0.0738 | | |
| 7 | 0.226 | 6.7113 | 0.4740 | 9.2367 | 0.4740 | 0.2224 |
| 8 | 0.316 | 1.5042 | 2.8105 | 1.8170 | 0.9304 | 0.2754 |
| 9 | 0.000 | 2.7057 | 0.6191 | 0.2628 | | |
| 10 | 0.055 | 2.5293 | 7.3607 | 2.8072 | 0.9276 | 0.1316 |

**Table 31 :** Parameters obtained by Curve Fitting Plasma Concentrations following administration of Metoprolol Solution 95mg(shown in Table D(1)) to a polyexponential equation (shown in equation (4.1)).

were be used to represent the solution data (as the weighting function) in the semi-numerical, polynomial and polyexponential algorithms. However,the polyexponential algorithm does not allow for the existence of any time delay in the weighting function and therefore, for the polyexponential algorithm, the parameters in Table 31 were used without the time lag, since in most cases this value was very small.

### 4.5.1 Deconvolution Details

The thirty separate data sets shown in Tables D(2)-D(4) were each deconvolved using each of the four deconvolution algorithms described in section 2.2, according to the

specific details for each method given in the sections below. The doses for the oral solution and the CR tablets were converted to μmoles prior to their incorporation (if required) into any deconvolution algorithm.

Following deconvolution, the release rate profiles were examined. Any subject whose profile showed consistently negative values after a certain time point was assumed to have had complete release from the controlled release tablet administered at that time point. In any subject where release was considered complete before the 30hr time span then the release rates following the time point at which release was complete were set to zero and the cumulative fraction released profile stopped at that point.

#### 4.5.1.1 Numerical Deconvolution

The plasma concentration values following administration of the oral solution and each of the three metoprolol CR tablets (CR A, CR B and CR C) for each subject were interpolated by cubic spline interpolation at time intervals of 0.5 hrs. The interpolated data was used as input to the numerical deconvolution algorithm to produce an estimated profile of the release rate of metoprolol with time for each subject and each of the CR tablets. Following deconvolution, the cumulative fraction released as a function of time was calculated according to the details given in section 2.2.1.

#### 4.5.1.2 Semi-Numerical Deconvolution

The parameters shown in Table 31 were used to represent the solution data and were used to generate plasma concentration values at 0.5hr intervals. These concentrations were used as the weighting function for the deconvolution of the CR tablets. The plasma concentrations for each subject, following administration of the CR tablets, were interpolated at 0.5hr intervals and the interpolated data, together with the weighting data, were used as input into the deconvolution algorithm. Following deconvolution, the cumulative fraction released as a function of time was calculated according to the details given in section 2.2.2.

#### 4.5.1.3 Polynomial Deconvolution

The parameters in Table 31 were used to represent the oral solution data and were used as the weighting function for the polynomial deconvolution algorithm. These parameters, together with the data shown in Tables D(2)-D(4), were used as input into the polynomial deconvolution algorithm. The unknown release rate (μmol/hr) was represented by a polynomial, the number of terms in the polynomial was increased sequentially until the inclusion of additional terms gave no significant improvement as judged by the F test (section 2.4.1) with n=15 at P=0.05. The release rate of the CR tablets is then represented by this selected polynomial and the cumulative amount released was represented by its integral. Following deconvolution the cumulative fraction released as a function of time was calculated according to the details given in section 2.2.3.

| Subject | $A_1$ μmol $l^{-1}$ | $\alpha_1$ $h^{-1}$ | $A_2$ μmol $l^{-1}$ | $\alpha_2$ $h^{-1}$ |
|---|---|---|---|---|
| 1 | -0.4820 | 0.1892 | 0.4820 | 0.1361 |
| 2 | -5.9183 | 0.1411 | 5.9183 | 0.1178 |
| 3 | -0.1300 | 0.3981 | 0.1300 | 0.1653 |
| 4 | -0.1140 | 0.5292 | 0.1140 | 0.0508 |
| 5 | -3.6155 | 0.2555 | 3.6155 | 0.2311 |
| 6 | -0.7210 | 0.2891 | 0.7210 | 0.0398 |
| 7 | -0.1225 | 0.5409 | 0.1225 | 0.0606 |
| 8 | -4.9854 | 0.2039 | 4.9854 | 0.1855 |
| 9 | -0.1606 | 0.4939 | 0.1606 | 0.0787 |
| 10 | -0.7990 | 0.2440 | 0.7990 | 0.0778 |

**Table 32 :** Parameters obtained following Curve Fitting of Plasma Concentrations from Metoprolol CR A (Table D(2)) to a polyexponential (equation 4.1)

#### 4.5.1.4 Polyexponential Deconvolution

The parameters in Table 31 were used to represent the solution data for each subject, with the exception of the time lag value. The plasma concentrations for each of the metoprolol CR tablets (Tables D(2)-D(4)) were fitted to a polyexponential equation of the form of that shown in equation (4.1) using the non-linear curve-fitting

techniques described in section 2.1.1. The number of terms in the equation was increased until there is no significant improvement seen as judged by the F test with n=15 and P=0.05.

| Subject | $A_1$ µmol $l^{-1}$ | $\alpha_1$ $h^{-1}$ | $A_2$ µmol $l^{-1}$ | $\alpha_2$ $h^{-1}$ | $A_3$ µmol $l^{-1}$ | $\alpha_3$ $h^{-1}$ |
|---|---|---|---|---|---|---|
| 1 | -1.3156 | 0.1217 | 0.5896 | 0.0940 | 0.7260 | 0.1273 |
| 2 | -10.1208 | 0.1286 | 10.1208 | 0.1197 | | |
| 3 | -0.1565 | 0.1297 | 0.1565 | 0.0832 | | |
| 4 | -10.0324 | 0.1109 | 10.0324 | 0.1096 | | |
| 5 | -0.4040 | 0.1865 | 0.4040 | 0.1036 | | |
| 6 | -0.5420 | 0.1899 | 0.5420 | 0.0287 | | |
| 7 | -0.0579 | 0.6011 | 0.0579 | 0.0172 | | |
| 8 | -0.2660 | 0.2347 | 0.2660 | 0.0762 | | |
| 9 | -0.0710 | 0.6332 | 0.0710 | 0.0242 | | |
| 10 | -0.9667 | 0.1363 | 0.9667 | 0.0737 | | |

**Table 33 :** Parameters obtained following Curve Fitting of Plasma Concentrations from Metoprolol CR B (Table D(3)) to a polyexponential (equation 4.1)

| Subject | tlag h | $A_1$ µmol $l^{-1}$ | $\alpha_1$ $h^{-1}$ | $A_2$ µmol $l^{-1}$ | $\alpha_2$ $h^{-1}$ |
|---|---|---|---|---|---|
| 1 | 1.0 | -0.8580 | 0.0583 | 0.8580 | 0.0540 |
| 2 | 1.0 | -4.9978 | 0.0270 | 4.9978 | 0.0236 |
| 3 | 1.0 | -0.9413 | 0.0671 | 0.9413 | 0.0637 |
| 4 | 0.0 | -4.9978 | 0.0589 | 54.9978 | 0.0577 |
| 5 | 1.0 | -1.0620 | 0.0525 | 1.0620 | 0.0465 |
| 6 | 0.0 | -10.0000 | 0.0310 | 10.0000 | 0.0289 |
| 7 | 1.0 | -0.4705 | 0.0342 | 0.4705 | 0.0252 |
| 8 | 0.0 | -0.0825 | 0.1128 | 0.0825 | 0.0113 |
| 9 | 1.0 | -1.9960 | 0.0200 | 1.9960 | 0.0183 |
| 10 | 1.0 | -4.8090 | 0.0495 | 4.8090 | 0.0456 |

**Table 34 :** Parameters obtained following Curve Fitting of Plasma Concentrations from Metoprolol CR C (Table D(4)) to a polyexponential (equation 4.1)

The parameters obtained following the curve fitting of the data for CR A, CR B and CR C are shown in Tables 32, 33 and 34 respectively.

These parameters were used to represent the response function for CR A,CR B and CR C respectively in the polyexponential deconvolution algorithm. Following deconvolution the cumulative fraction released as a function of time was calculated according to the details given in section 2.2.4.

### 4.5.2 Calculation of the Fraction of Dose Released, $F_R$

The fraction of dose released at 30hrs was calculated by taking the maximum value reached in the cumulative fraction released profile, produced by each of the deconvolution algorithms. This value was calculated for each subject and for each of the three different tablets.

### 4.5.3 Calculation of Mean Dissolution Time *in vivo* , MDT

The MDT was calculated according to the method described in section 2.5.1 and was calculated up to the last data point at 30hrs. The mean dissolution time ($MDT_{30}$) was calculated and not the true value, ($MDT_{\infty}$), since the aim of the calculation was to compare deconvolution methods, therefore no extrapolation was required. When the release was completed before the 30hr time interval the true MDT and $MDT_{30}$ are the same, only in the case of incomplete release will the two values differ.

## 4.6 RESULTS

The mean (n=10) release rate (μmol/hr) and mean fraction of dose released for each CR tablet together with the SEM values are shown in Figures 37-40 and are described in detail below. The emphasis has been placed on the similarities and differences produced in the profiles due to the different deconvolution algorithms.

### 4.6.1 Mean *in vivo* Release Rates

#### 4.6.1.1 Similarities

All the deconvolution methods show the same general features in the mean *in*

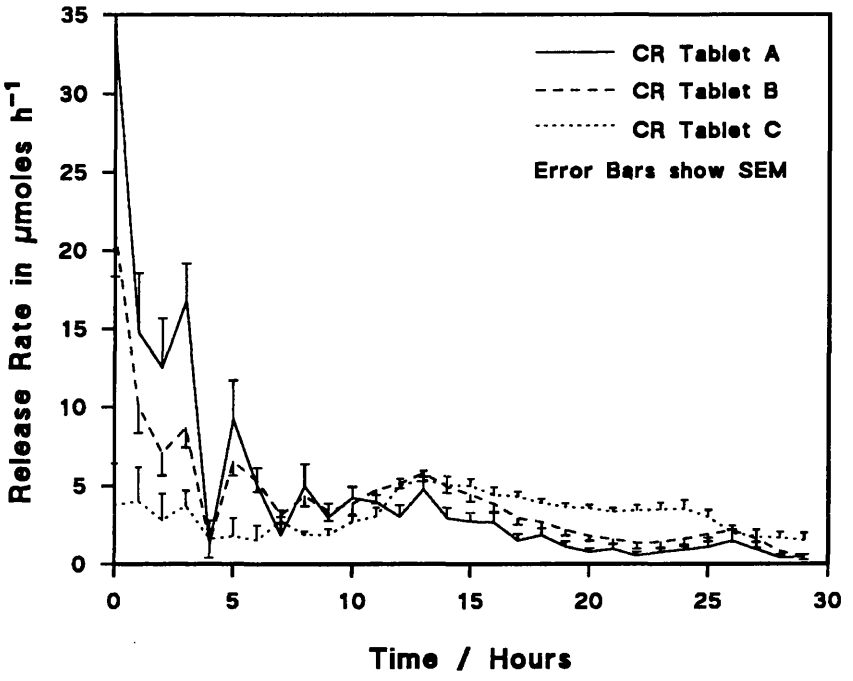


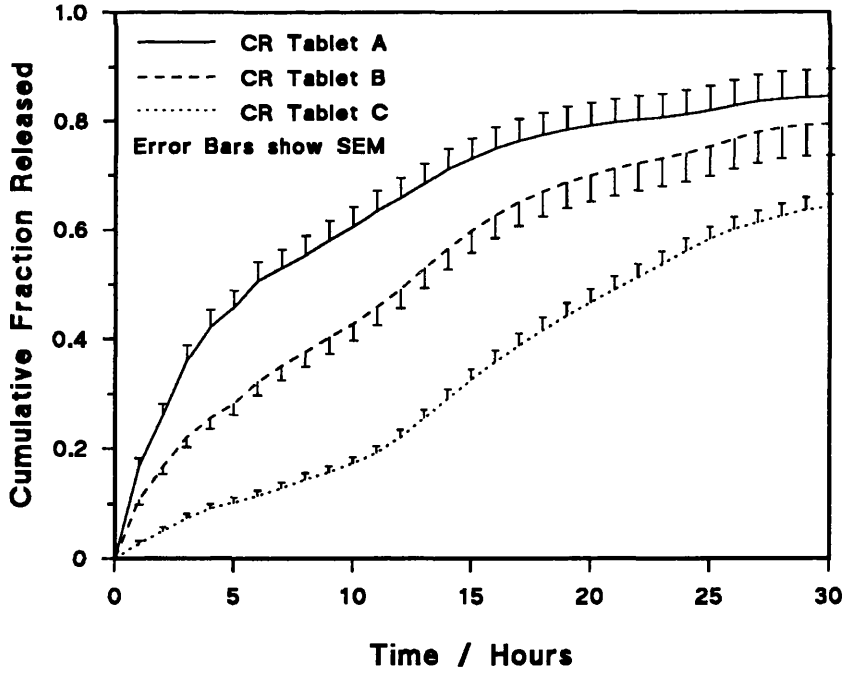


**Figure 37** : Mean Results (n=10) produced by Numerical Deconvolution of Three Controlled Release Metoprolol 95mg Tablets

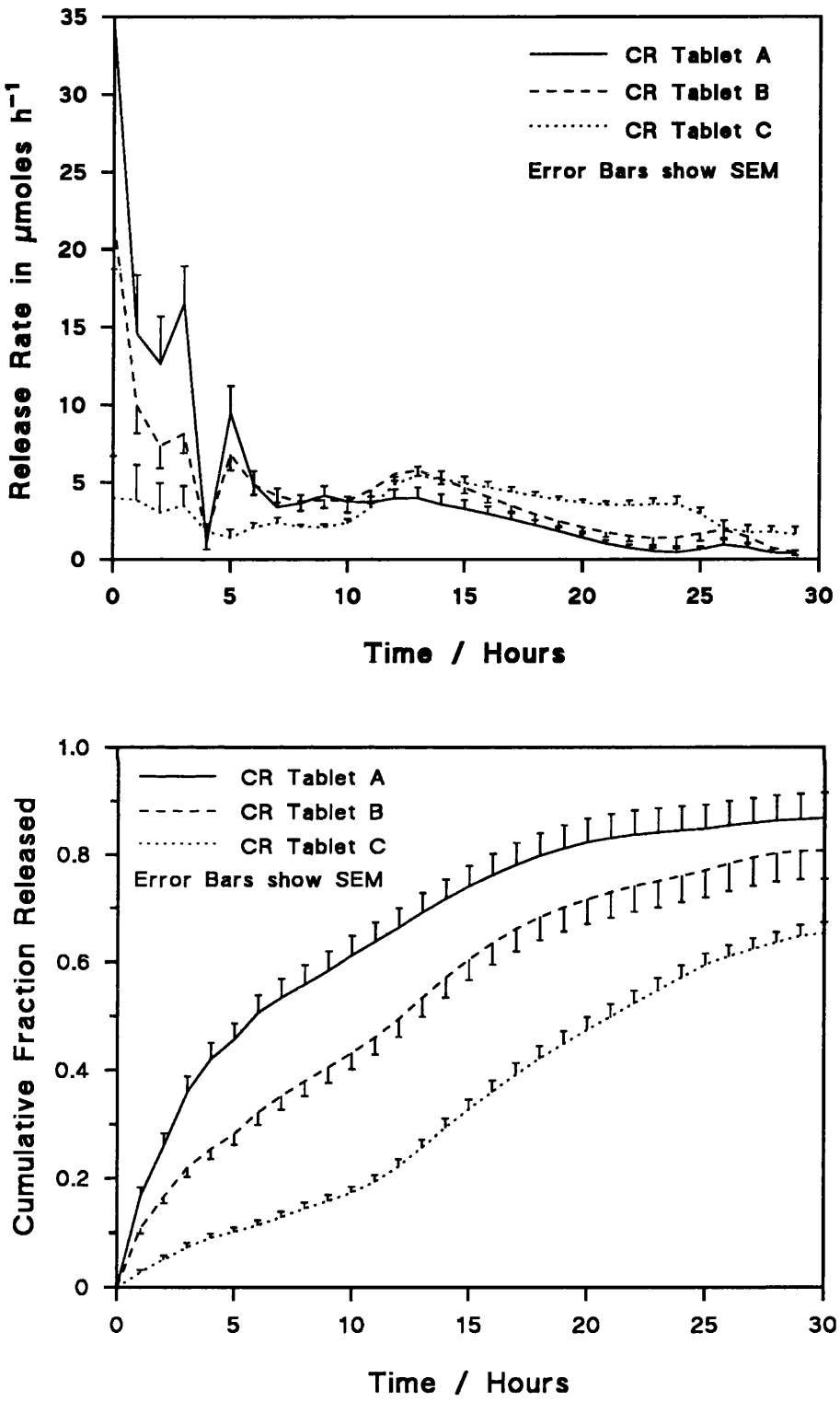


**Figure 38** : Mean Results (n=10) produced by Semi-Numerical Deconvolution of Three Controlled Release Metoprolol 95mg Tablets

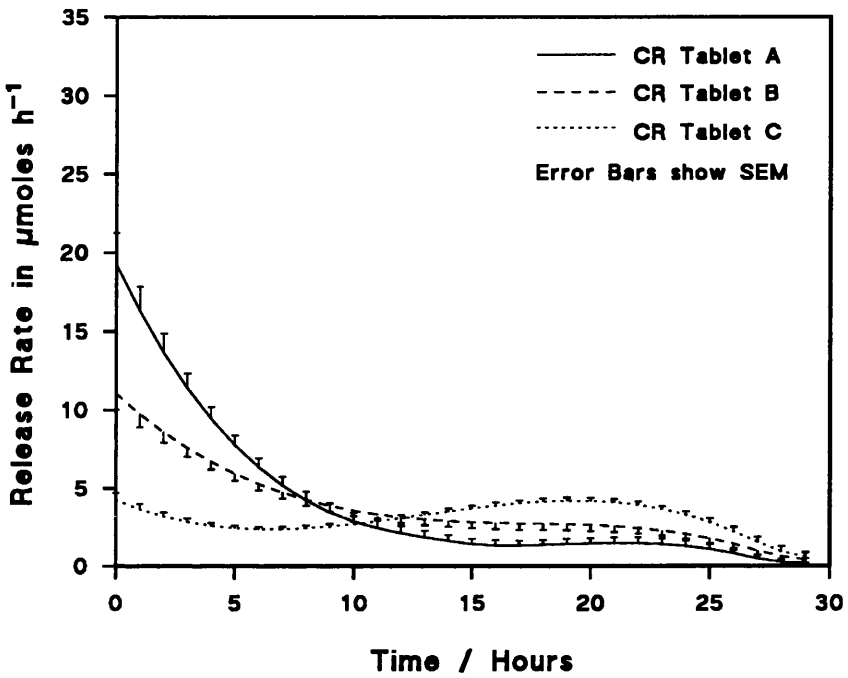


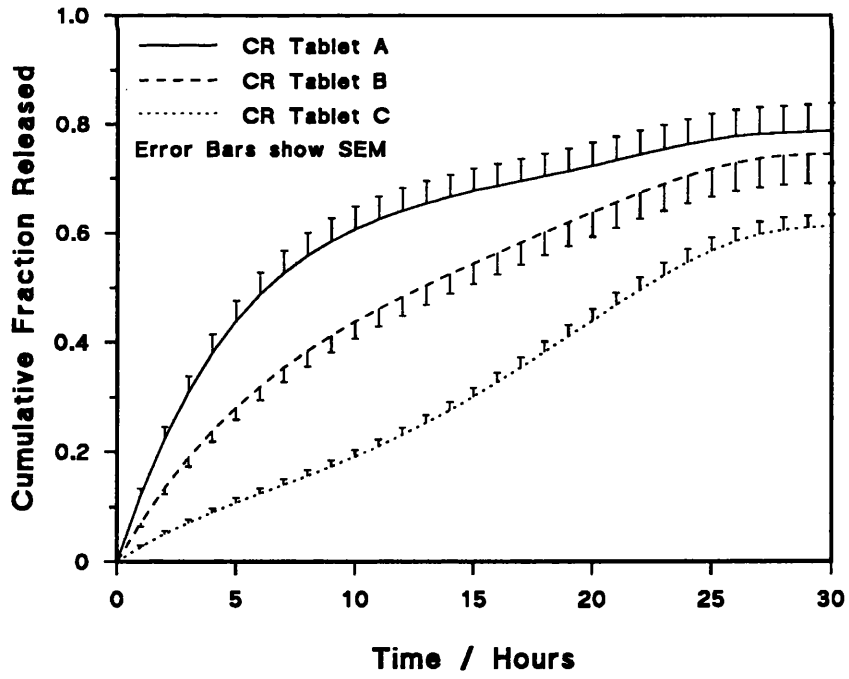


**Figure 39** : Mean Results (n=10) produced by Polynomial Deconvolution of Three Controlled Release Metoprolol 95mg Tablets

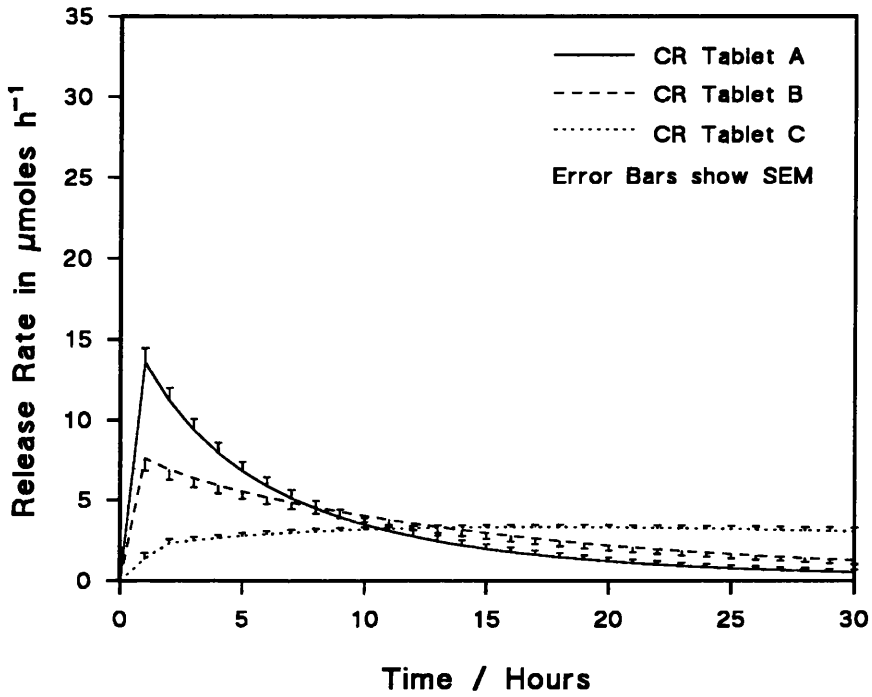


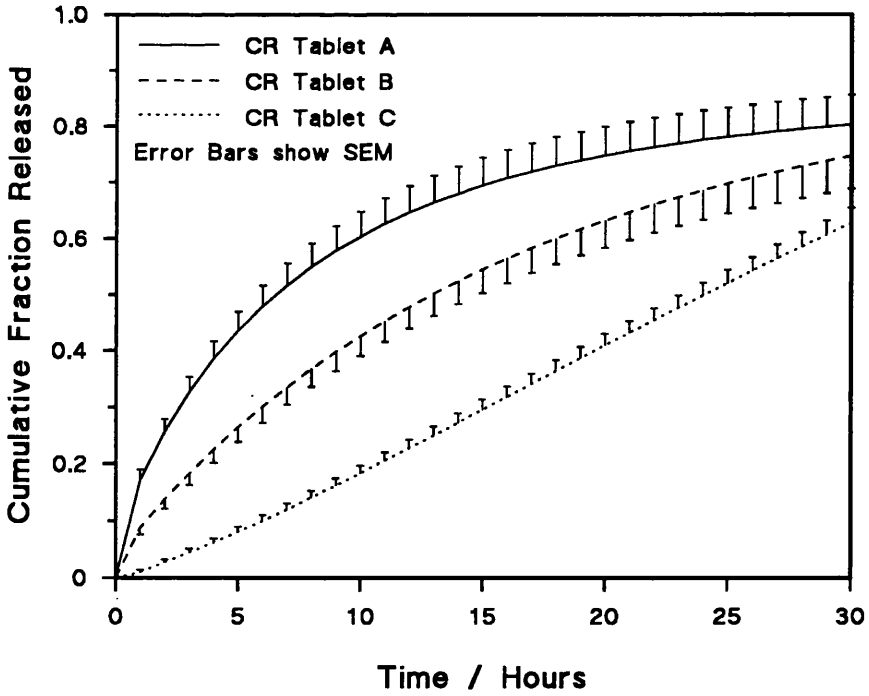


**Figure 40** : Release Rate and Cumulative Fraction Released for Three Metoprolol CR Tablets predicted by Polyexponential Deconvolution

*vivo* release rates predicted for each tablet. All the tablets have an initial period of rapid release over the first few hours, with the initial release rate of CR A being higher than that of CR B , which is in turn higher than that of CR C. This ranking would be expected since CR A has the highest *in vitro* release rate and CR C the lowest.

Also, all the methods show that at later time periods the release rates become reversed with the release rate of CR C being much greater than that of CR A and CR B while the release rates of CR A and CR B are very close but that of CR B is slightly greater than that of CR A.

Apart from the initial rapid release, all the methods show that the release rate of metoprolol from CR B and CR C is fairly constant over a large portion of the time scale.

#### 4.6.1.2 Differences

The only real difference in the general features of the release rate shown by the four deconvolution methods is shown by the polynomial deconvolution method, where the release rate towards 30hrs becomes minimal. The other three methods all show that the release rate for CR C is still about 3-4μmol/hr at the end of the time span, suggesting release is still occurring at this late time period.

The other striking differences between the profiles are the smoothness of their predicted release rates and the size of the SEM values. The profiles predicted by the numerical and semi-numerical methods are very variable especially over the initial time periods where the rate of change of the release rate is most rapid, also the form of the release rate, seen clearly in the polynomial and polyexponential methods, is much more difficult to discern. The SEM values of the four methods at the later time periods, where the rate of change of release rate is small, are very similar.

### 4.6.2 Mean Cumulative Fraction Released Profiles

The CFI profiles produced by the different methods were so similar they have been plotted on a separate graph (Figure 41) to enable a better comparison to be made.

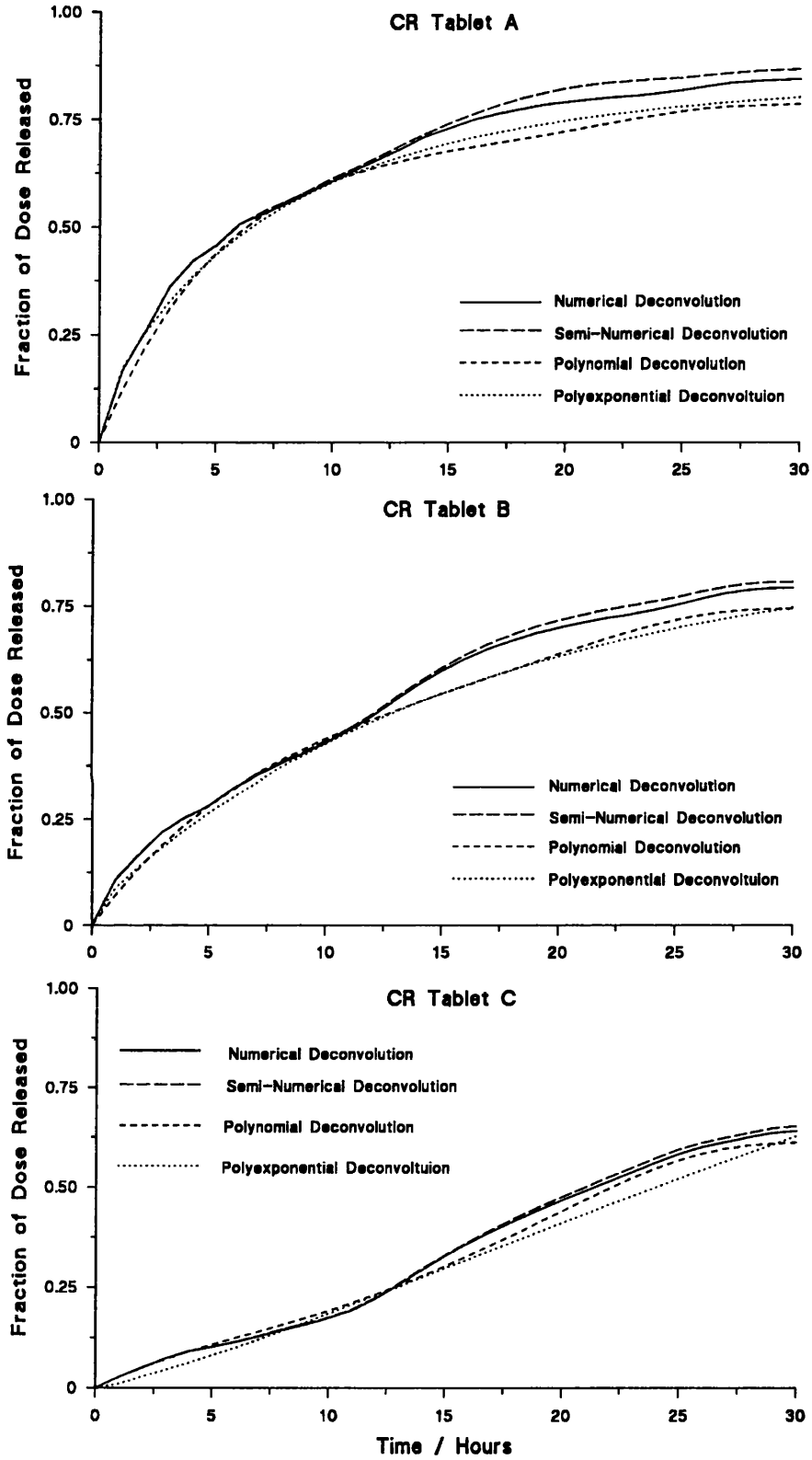


**Figure 41** : Fraction of Dose Released predicted by Four Deconvolution Methods for Three Metoprolol CR Tablets

#### 4.6.2.1 Similarities

All the methods show the same general form for the profiles for the three CR tablets and that the SEM values are similar for each tablet and for each algorithm. All the algorithms show that at all times the fraction of dose released from CR A is greater than that from CR B which is in turn greater than that from CR C. All the methods also show that the release from CR A is completed well before 30hrs, that from CR B at nearly 30hrs and that the release from CR C is still continuing at 30hrs.

#### 4.6.2.2 Differences

The only difference apparent is that only three of the deconvolution algorithms show an inflexion in the profile for CR C between 10 and 15hrs. At this point the release from CR C becomes more rapid and the gradient of the cumulative profile increases. This feature is not shown by the polyexponential deconvolution algorithm because the release rate predicted by this method does not show the decrease (around 5hrs) in release rate prior to its subsequent increase which is shown by other methods.

### 4.6.3 Estimated Fraction of Dose Released, $F_R$

The estimated fraction of dose released, calculated at 30hrs, for all subjects, all CR tablets and all methods is shown in Table 35, together with the mean and SEM values for each CR tablet and each deconvolution method.

The values in Table 35 were analyzed by a model I, two way ANOVA (Sokal and Rohlf 1981b). However, prior to this, analysis of the homogeneity of the variances for the twelve different groups of data was performed using Hartleys $F_{max}$ test for homogeneity of variances (Sokal and Rohlf 1981c), since the assumption of the homogeneity of variances is implicit in the analysis of variance.

Hartley's $F_{max}$ test uses a statistic that is the ratio of the largest to the smallest of the sample variances. The statistic calculated should be less than the value obtained from an $F_{max}$ table of critical values for a samples and n-1 degrees of freedom, where a is the number of separate samples (in this case 12) and n is the number of values in each

| Deconvolution | | Numerical | Semi-Numerical | Polynomial | Poly-exponential |
|---|---|---|---|---|---|
| Tablet | Subject | | | | |
| CR A | 1 | 1.06 | 1.07 | 1.02 | 1.05 |
| | 2 | 0.82 | 0.90 | 0.81 | 0.79 |
| | 3 | 0.62 | 0.62 | 0.51 | 0.55 |
| | 4 | 0.73 | 0.82 | 0.75 | 0.71 |
| | 5 | 0.62 | 0.67 | 0.60 | 0.67 |
| | 6 | 1.01 | 0.95 | 0.91 | 0.72 |
| | 7 | 0.81 | 0.80 | 0.72 | 0.76 |
| | 8 | 0.93 | 1.00 | 0.89 | 0.99 |
| | 9 | 0.83 | 0.83 | 0.72 | 0.75 |
| | 10 | 1.01 | 1.03 | 0.96 | 1.03 |
| Mean | | 0.84 | 0.87 | 0.79 | 0.80 |
| SD | | 0.158 | 0.150 | 0.161 | 0.167 |
| SEM | | 0.050 | 0.047 | 0.051 | 0.053 |
| CR B | 1 | 1.01 | 1.12 | 1.08 | 1.10 |
| | 2 | 0.58 | 0.61 | 0.55 | 0.56 |
| | 3 | 0.94 | 0.91 | 0.83 | 0.69 |
| | 4 | 0.47 | 0.52 | 0.47 | 0.42 |
| | 5 | 0.71 | 0.76 | 0.72 | 0.74 |
| | 6 | 0.86 | 0.83 | 0.78 | 0.83 |
| | 7 | 0.73 | 0.72 | 0.67 | 0.70 |
| | 8 | 0.85 | 0.91 | 0.81 | 0.87 |
| | 9 | 0.79 | 0.79 | 0.70 | 0.73 |
| | 10 | 0.88 | 0.90 | 0.85 | 0.85 |
| Mean | | 0.78 | 0.81 | 0.75 | 0.75 |
| SD | | 0.164 | 0.170 | 0.169 | 0.184 |
| SEM | | 0.052 | 0.054 | 0.053 | 0.058 |
| CR C | 1 | 0.71 | 0.71 | 0.69 | 0.70 |
| | 2 | 0.66 | 0.68 | 0.66 | 0.73 |
| | 3 | 0.64 | 0.63 | 0.57 | 0.56 |
| | 4 | 0.49 | 0.54 | 0.46 | 0.45 |
| | 5 | 0.57 | 0.59 | 0.60 | 0.59 |
| | 6 | 0.62 | 0.62 | 0.61 | 0.66 |
| | 7 | 0.69 | 0.69 | 0.63 | 0.62 |
| | 8 | 0.62 | 0.66 | 0.64 | 0.68 |
| | 9 | 0.65 | 0.65 | 0.59 | 0.58 |
| | 10 | 0.74 | 0.77 | 0.67 | 0.70 |
| Mean | | 0.64 | 0.65 | 0.61 | 0.63 |
| SD | | 0.072 | 0.064 | 0.065 | 0.085 |
| SEM | | 0.023 | 0.020 | 0.021 | 0.027 |

**Table 35 :** Estimated Fraction of Dose Released, $F_R$, in ten subjects, predicted for Three CR Metoprolol Tablets (CR A,CR B and CR C) by Four Deconvolution Methods.

sample. When the data in Table 35 was tested using Hartley's test an $F_{max}$ value of 82.68 was obtained, the critical $F_{max}$ value for 12 samples and 9 degrees of freedom was 10.7 (P=0.05) showing the value of $F_{max}$ is clearly significant and the variances of the samples are not homogeneous.

The data in Table 35 where therefore transformed by conversion to their log values. Hartley's test for uniformity of variance was then repeated using the log values. The $F_{max}$ value obtained in this case was 6.5 which, when compared to the critical $F_{max}$ value for P=0.05, a=12 and n=10 (10.7) was not significant showing that the sample variances are now homogeneous and ANOVA can now be applied.

The logs of the values in Table 35 were analyzed by a model I, two way ANOVA and the results from this analysis are shown in Table 36, where SS is the sum of squares, MS is the Mean Sum of Squares (SS/df) and df are the degrees of freedom associated with each SS value.

| Source of Variation | df | SS | MS | F |
|---|---|---|---|---|
| Deconvolution Methods | 3 | 0.0253 | 0.00844 | 1.2114 ns |
| CR Tablets | 2 | 0.2577 | 0.1289 | 18.50 *** |
| Interaction | 6 | 0.0014 | 0.00023 | 0.0330 ns |
| Error | 108 | 0.7522 | 0.00697 | |
| Total | 119 | 1.0366 | | |
| $F_{0.05(6,108)} = 2.23$ $F_{0.05(2,108)} = 3.13$ $F_{0.01(2,108)} = 4.94$ $F_{0.001(2,108)} = 7.67$ $F_{0.05(3,108)} = 2.74$ | | | | |

**Table 36 :** ANOVA table for log Transforms of the Estimated Fraction Released data (shown in Table 35) for different Metoprolol CR tablets and Deconvolution methods. (Model I - two way)

Although the results of the ANOVA show a significant difference between the estimated fraction released for each tablet ($P < 0.001$), there is no significant difference seen between the values estimated by different deconvolution methods. This result confirms the results presented in chapter three.

### 4.6.4 Mean Dissolution Time, $MDT_{30}$

The $MDT_{30}$ at 30hrs calculated for each subject, each method and each tablet are shown in Table 37 together with mean (n=10), standard deviation (SD) and standard error of the mean (SEM) for each tablet and deconvolution method.

| Deconvolution | | Numerical | Semi-Numerical | Polynomial | Poly-exponential |
|---|---|---|---|---|---|
| Tablet | Subject | | | | |
| CR A | 1 | 7.33 | 7.33 | 7.66 | 7.90 |
| | 2 | 5.40 | 6.41 | 4.69 | 4.60 |
| | 3 | 4.08 | 4.03 | 4.69 | 4.84 |
| | 4 | 8.68 | 9.35 | 9.46 | 9.66 |
| | 5 | 3.03 | 3.97 | 3.31 | 3.22 |
| | 6 | 8.35 | 6.77 | 6.98 | 6.34 |
| | 7 | 8.92 | 8.61 | 8.58 | 8.40 |
| | 8 | 5.81 | 6.25 | 5.67 | 5.37 |
| | 9 | 7.97 | 8.08 | 7.91 | 7.04 |
| | 10 | 6.95 | 6.91 | 6.87 | 6.50 |
| Mean | | 6.65 | 6.77 | 6.58 | 6.39 |
| SD | | 2.01 | 1.76 | 1.95 | 1.95 |
| SEM | | 0.636 | 0.556 | 0.616 | 0.616 |
| CR B | 1 | 10.74 | 11.06 | 11.18 | 11.42 |
| | 2 | 5.30 | 5.81 | 4.84 | 5.05 |
| | 3 | 11.16 | 10.77 | 11.14 | 11.39 |
| | 4 | 9.82 | 10.44 | 10.31 | 10.79 |
| | 5 | 7.94 | 8.46 | 8.35 | 8.25 |
| | 6 | 10.05 | 9.01 | 9.10 | 8.76 |
| | 7 | 11.70 | 11.49 | 11.67 | 11.53 |
| | 8 | 8.92 | 9.28 | 8.92 | 9.04 |
| | 9 | 11.25 | 11.34 | 11.46 | 11.16 |
| | 10 | 8.43 | 8.53 | 8.71 | 8.89 |
| Mean | | 9.53 | 9.62 | 9.57 | 9.63 |
| SD | | 1.95 | 1.77 | 2.08 | 2.06 |
| SEM | | 0.616 | 0.558 | 0.657 | 0.651 |
| CR C | 1 | 14.28 | 14.48 | 13.87 | 14.70 |
| | 2 | 14.33 | 14.44 | 13.73 | 14.95 |
| | 3 | 14.12 | 13.89 | 13.40 | 13.34 |
| | 4 | 13.73 | 14.17 | 14.52 | 14.09 |
| | 5 | 14.30 | 14.40 | 13.74 | 14.64 |
| | 6 | 13.20 | 12.97 | 13.29 | 13.47 |
| | 7 | 16.01 | 15.89 | 16.02 | 15.95 |
| | 8 | 13.98 | 14.14 | 14.56 | 14.30 |
| | 9 | 16.49 | 16.54 | 16.93 | 16.58 |
| | 10 | 12.74 | 12.91 | 13.48 | 13.76 |
| Mean | | 14.32 | 14.38 | 14.35 | 14.68 |
| SD | | 1.15 | 1.13 | 1.22 | 0.96 |
| SEM | | 0.362 | 0.357 | 0.384 | 0.302 |

**Table 37 :** Estimated Mean Dissolution Time $MDT_{30}$ (hrs), in ten subjects, predicted for Three CR Metoprolol Tablets (CR A,CR B and CR C) by Four Deconvolution Methods.

The values in Table 37 were to be analyzed by a model I, two way ANOVA. However, prior to this, analysis of the homogeneity of the variances for the twelve different groups of data was performed using Hartley's $F_{max}$ test for homogeneity of variances (Sokal and Rohlf 1981c). When the data in Table 37 was tested using Hartley's Hartley's test an $F_{max}$ value of 4.69 was obtained, the critical $F_{max}$ value for 12 samples and 9 degrees of freedom was 10.7 (P=0.05) showing the value of $F_{max}$ is not significant and the variances of the samples are homogeneous.

The values in Table 37 were then analyzed by a model I, two way ANOVA and the results from this analysis are shown in Table 38, where SS is the sum of squares, MS is the Mean Sum of Squares (SS/df) and df are the degrees of freedom associated with each SS value.

| Source of Variation | df | SS | MS | F |
|---|---|---|---|---|
| Deconvolution Methods | 3 | 0.188 | 0.063 | 0.021 ns |
| CR Tablets | 2 | 1250.8 | 625.4 | 213.4 *** |
| Interaction | 6 | 1.470 | 0.245 | 0.084 ns |
| Error | 108 | 316.5 | 2.931 | |
| Total | 119 | 1568.958 | | |
| $F_{0.05(6,108)} = 2.23$ $F_{0.05(2,108)} = 3.13$ $F_{0.01(2,108)} = 4.94$ $F_{0.001(2,108)} = 7.67$ $F_{0.05(3,108)} = 2.74$ | | | | |

**Table 38 :** ANOVA table for the Mean Dissolution Time data (shown in Table 37) for different Metoprolol CR tablets and Deconvolution methods. (Model I - two way)

Although the results of the ANOVA show a significant difference between the estimated $MDT_{30}$ for each CR tablet ($P < 0.001$), there is no significant difference seen between the values of the $MDT_{30}$ estimated by different deconvolution methods.

### 4.6.5 *In vivo - in vitro* Correlation using MDT values

The mean $MDT_{30}$ values calculated for the different deconvolution algorithms (shown in Table 37) were plotted against the $MDT_{in\ vitro}$ values, for different dissolution conditions, calculated from the dissolution data shown in Tables D(5)-D(7) in Appendix D and presented previously by Sandberg et al (1991). These *in vitro* MDT values are shown in Table 39.

For each set of values plotted the following parameters were calculated : the gradient, the Y intercept and the correlation coefficient (r). These values are shown in Table 40 for each deconvolution method and each set of different dissolution conditions.

| Dissolution Conditions | Formulation | | |
|---|---|---|---|
| | CR A | CR B | CR C |
| pH 1.2 / 100 rpm | 4.8 | 8.4 | 13.6 |
| pH 4.0 / 100 rpm | 5.7 | 8.8 | 13.7 |
| pH 6.8 / 100 rpm | 5.3 | 8.6 | 13.8 |
| pH 6.8 / 50 rpm | 5.7 | 8.6 | 14.1 |

**Table 39 :** ***In vitro*** MDT (hrs) calculated for three Metoprolol CR Tablets from data shown in Tables D(5)-D(7)

| Dissolution Conditions | | Deconvolution Algorithm | | | |
|---|---|---|---|---|---|
| | | Numerical | Semi-Numerical | Polynomial | Poly-exponential |
| pH 1.2 100 rpm | Gradient | 0.8751 | 0.8684 | 0.8855 | 0.9441 |
| | Y Intercept | 2.3491 | 2.4993 | 2.2560 | 1.7993 |
| | r | 0.9992 | 0.9992 | 0.9996 | 0.9998 |
| pH 4.0 100 rpm | Gradient | 0.9604 | 0.9531 | 0.9716 | 1.0357 |
| | Y Intercept | 1.1384 | 1.2978 | 1.0333 | 0.4974 |
| | r | 0.9999 | 0.9999 | 0.9999 | 0.9999 |
| pH 6.8 100 rpm | Gradient | 0.9040 | 0.8971 | 0.9146 | 0.9749 |
| | Y Intercept | 1.8194 | 1.9735 | 1.7221 | 1.2315 |
| | r | 0.9998 | 0.9999 | 0.9999 | 0.9999 |
| pH 6.8 50 rpm | Gradient | 0.9076 | 0.9007 | 0.9177 | 0.7997 |
| | Y Intercept | 1.5750 | 1.7305 | 1.4793 | 0.9758 |
| | r | 0.9994 | 0.9995 | 0.9990 | 0.9988 |
| r = the XY correlation coefficient | | | | | |

**Table 40 :** Parameters obtained following Linear Regression of $MDT_{in\ vivo}$ against the $MDT_{in\ vitro}$ for Three Metoprolol CR Tablets.

The values presented in Table 40 show that all the deconvolution methods give very good *in vivo - in vitro* correlations for all the dissolution data. The critical values of the correlation coefficient, r, for n=3 (1 degree of freedom) are 0.997 for P=0.05 and 1.00 for P=0.01. All the correlation coefficients shown in Table 40 are greater than 0.997, therefore there is a significant correlation between the $MDT_{in\ vitro}$ and the $MDT_{in\ vivo}$ , $P < 0.05$.

Although the correlations obtained for different deconvolution methods (for the same dissolution conditions) are all good, the values of the gradient and the Y intercept differ between the different methods. The greatest difference between these values is seen, for all dissolution conditions, to lie between the polyexponential and the other three methods.

## 4.7 DISCUSSION

All the deconvolution methods predicted that the release of metoprolol was still occurring from all the CR tablets after 20 hours and still occurring from the CR tablet C after 30 hours. Since metoprolol is similarly absorbed between the pylorus and the rectum and will be absorbed wherever it is released (Godbillon et al 1985) then it is possible that both release and absorption are still occurring in the colon even at these late time points.

The initial rapid release seen in CR tablets A and B may be due to the presence of crushed pellets within the tablet, following compression during the tableting process. These crushed pellets possess no controlled release properties since the polymeric membrane is no longer intact, therefore they will release their content rapidly. This period of rapid release may well be overestimated by the polynomial and polyexponential methods (which estimate it to be about 5 hours) because of their inability to cope with sudden changes in the release rate, which was demonstrated with the simulated data in chapter 3.

The different release rate predicted by the polyexponential algorithm for CR C is probably due to the poor approximation of the plasma concentrations by the selected polyexponential. The plasma values for CR C appeared to indicate that the peak plasma concentrations lay between 14 and 24 hours when no samples were taken, as a consequence of this the parameters obtained by curve fitting approximated poorly to the plasma curves (unlike those for CR A and CR B which reflected their plasma curves very

well). This poor approximation of the plasma concentrations for CR tablet C is only important for the polyexponential method, as this is the only method which uses function approximation of the response function, therefore the discrepancy in the predicted release rate for this method is probably due to poor parameter estimates.

The additional complication for the polyexponential method was the existence of a time lag in the solution data. For the metoprolol CR tablets, ignoring this time lag made no discernable difference in the release rate values produced, perhaps because the time lag in most subjects, was very small.

There was no significant difference found between the values predicted for either the $MDT_{30}$ or the total fraction of dose released, $F_R$ using the different deconvolution algorithms. All the methods gave $F_R$ values of less than one, suggesting incomplete release from the CR tablets. However, since the weighting function is from administration of a solution and a major portion of the release (and absorption) is occurring in the colon where the drug, contained in the solution, may never have reached, there is another possible explanation. This is that the assumption of linearity has been violated.

This could occur in two ways, firstly if there was no absorption from the colon, this would appear in the deconvolution as a predicted lack of release. This cannot be valid in the case of metoprolol as it has been shown (Godbillon et al 1985) to be well absorbed from the colon. The other possibility is that the rate of release of metoprolol affects the rate of its metabolism, this would be an example of the input function affecting the weighting function. This is possible for metoprolol since it has a high first pass metabolism and it has been suggested (Sandberg et al 1991) as the reason for the apparent lack of release, especially from CR C.

The third possibility is that the release was actually incomplete, however deconvolution itself will give no way of distinguishing between these various possibilities.

It is apparent from Table 40 that any of the deconvolution methods could be used to provide a good *in vivo - in vitro* correlation, but that the exact correlation will vary with the deconvolution method used and the *in vivo* MDT predicted from an *in vitro* dissolution test will be slightly different depending on which method was used for the original correlation.

## 4.8 CONCLUSIONS

The aim of this chapter was to highlight any problems to the use of deconvolution in a practical situation, and although in no case was deconvolution by any of the algorithms impossible, some problems were encountered.

The existence of a time lag in the data used for the weighting function may prohibit the use of the polyexponential algorithm, although this was not the case for the metoprolol data since the time lags were so small.

The quality of the data is important for the accuracy of the deconvolution methods. When the data is less than perfect, as for CR C where the peak of the plasma profile was poorly described, then the parameters obtained following curve fitting do not give good approximations of the true profiles, and this inaccuracy is carried forward into the deconvolution process.

The final point is that care should be taken in the interpretation of the results produced by deconvolution, especially when solution data is being used as the weighting function for a controlled release product. There is a possibility in such cases that the linearity of the system may be violated either by lack of absorption from the distal regions of the gastrointestinal tract or by a change in metabolism due to the rate of drug release.

# 5 MAXIMUM ENTROPY IN THE ESTIMATION OF *IN VIVO* DRUG RELEASE / ABSORPTION RATES

The application of Maximum Entropy is the most recent and perhaps the most sophisticated of all the techniques used to evaluate the rates of release / absorption of drugs. This chapter aims to provide an introduction to the method and to elaborate on the principle upon which the technique is based, together with details of the calculations involved. The subsequent two chapters aim to evaluate the technique using pseudo-experimental data then use it in a practical situation to analyze the clinical Metoprolol data used in chapter 4.

Using Maximum Entropy to evaluate the *in vivo* release/absorption rates of drugs theoretically has advantages over the deconvolution techniques. Firstly, like the simpler deconvolution algorithms, it makes no assumptions about the form of the input function it aims to approximate. Therefore, any structure present in the predicted input function must be due to evidence present in the data itself.

Secondly, like the more complex deconvolution algorithms which involve approximation of the unknown input rate by empirical functions, the predicted input rate is a smooth function enabling a clear picture of the unknown release/absorption rates to be seen. Therefore, potentially Maximum Entropy combines the best features of all the deconvolution methods.

To be able to understand the application of the Principle of Maximum Entropy to the evaluation of rates of release or absorption, it is first necessary to understand something about Bayesian inference. For this reason the first few sections in this chapter aim to cover the basic principles of Bayesian inference, these are followed by sections which cover the background of the development of the equations used to represent entropy. In the latter sections of the chapter the Bayesian techniques are combined with those of Maximum Entropy to show the evaluation of drug release rates through the employment of both techniques.

## 5.1 THE APPLICATION OF BAYESIAN METHODS

### 5.1.1 Basis of Probability Theory

Cox (1946) derived the basic product and sum rules for probability theory based on the requirements of consistency. These are as follows :

$$\mathbf{P(A,B) = P(A).\ P(B|A)}$$

$$\mathbf{= P(B).\ P(A|B)}$$

**and**

$$\mathbf{P(A + B) = P(A) + P(B) - P(A,B)}$$

where P(A,B) is the join probability of both A and B being true.

P(A) is the probability of A being true.

P(B|A) is the probability that B is true given that A is true.

P(B) is the probability that B is true.

P(A|B) is the probability that A is true given that B is true.

P(A + B) is the probability that either A or B is true (if A and B are mutually exclusive the third term vanishes).

These two rules form the basis of Bayesian reasoning and probability theory which are concerned with the process of inference, which is discussed in section 5.1.2.

### 5.1.2 Inference and Inverse Probability

The process of inference is the opposite to that of deductive reasoning. Suppose there is an hypothesis h, some new data **D** and any previous information, $I_f$, then the process of inference would reason along the lines of - given the new data **D** and any previous information, $I_f$, what can be inferred about the hypothesis h? The concept of inference is sound but it must be amenable to transplantation into a practical situation, i.e. how can inferences be made quantitatively.

This is where the rules of probability theory become useful, and inference must be examined in terms of the conditional probabilities of our hypothesis together with the new data. In other words, the value $P(h|\mathbf{D},I_f)$, which is the probability of the hypothesis given

the new data **D**, and any previous information possessed, ($I_f$), must be examined. This is known as the **inverse probability** because the reasoning process goes from the observed data to the hypothesis.

If the first of Cox's rules is restated in terms of the hypothesis h and the data **D** then the equation becomes

$$\begin{aligned} P(h,\mathbf{D} \mid I_f) &= P(h \mid I_f).\ P(\mathbf{D} \mid h,I_f) \\ &= P(\mathbf{D} \mid I_f).\ P(h \mid \mathbf{D},I_f) \end{aligned}$$

Rearrangement of this gives us Bayes' Theorem :

$$P(h \mid \mathbf{D},I_f) = P(h \mid I_f).\ P(\mathbf{D} \mid h,I_f) \ /\ P(\mathbf{D} \mid I_f) \qquad (5.1)$$

The equation used for Bayes Theorem deserves some elaboration. The term $P(h \mid I_f)$ is known as the **prior probability**, it represents the existing state of knowledge before the new data is taken into account. $P(\mathbf{D} \mid h,I_f)$ is the likelihood and can be calculated from the data itself, it is a measure of how close the data, D, fits the hypothesis. The expression $P(\mathbf{D} \mid I_f)$ is known at the evidence and can also be calculated from the data. $P(h \mid \mathbf{D},I_f)$, the quantity of interest, is known as the **posterior probability** and is the probability of the hypothesis h after consideration of the new data **D**. Having defined the various terms of Bayes equation it can seen that the essence of Bayesian inference is the revision of the hypothesis h in light of the new data **D**. Bayesian analysis on its own is already used in biopharmaceutical research (Louis 1991) to analyze data from multi-centre clinical trials.

Equation (5.1), as can be seen, goes some way to quantifying the process of inference but if this equation is to be used in practical situations then a way must be found to represent the initial state of knowledge about the hypothesis h, i.e. we must find a way to assign a prior probability distribution to the hypothesis h.

To do this the technique of Bayesian inference must be combined with that of Maximum Entropy.

## 5.2 MAXIMUM ENTROPY

The Principle of Maximum Entropy is a method of assigning values to a distribution. The entropy of a distribution represents of a measure of ignorance and, by selecting the distribution which maximises this value, a distribution is obtained which contains only structure for which there is evidence.

### 5.2.1 The Origins of the Maximum Entropy Equation

It should be stated initially that the entropy which forms the basis of this technique is not thermodynamic entropy with which most people are at least partially familiar. It is instead what is called **information theory** entropy which is an entirely different concept. The confusion arises because the equation used to represent the information entropy is very similar to that used to calculate the thermodynamic entropy in certain physical situations.

The original equation was proposed by Shannon (1948) whilst he was working on the theory of communication processes. In his article Shannon proposed that : **if in a communication process the message $M_i$ is assigned a probability $P_i$ then the entropy $S(P_i)$ represented by equation (5.2) gives a measure of "information."**

$$S(P_i) = -\Sigma(P_i)\log(P_i) \tag{5.2}$$

Although not stated by Shannon, Jaynes (1983) surmised that the quantity $S(P_i)$ must represent, not a measure of information, but the degree of ignorance possessed by the communications engineer when designing the equipment through which the message was to be sent. If this is so then, the probabilities assigned to individual messages $M_i$ cannot be measurable frequencies (which is the more normal interpretation of the term probability), instead they are a means of describing a state of knowledge about the system. The distribution of $P_i$ which maximises the entropy $S(P_i)$ (subject to any constraints imposed by the prior knowledge) will provide the least informative probability distribution subject to that previous knowledge. This is **the Principle of Maximum Entropy.**

### 5.2.2 Assigning Probability Distributions with Maximum Entropy

Suppose the hypothesis, h, is the value of a parameter and the estimate of this parameter is to be updated in the light of new data, **D**, using Bayes Theorem. To do this the probability distribution of the possible parameter values is needed. If the parameter h can have any value $h_i$ between $h_1$ and $h_n$ then the entropy of the distribution can be represented as shown in equation (5.3), where $P(h_i|I_f)$ is the probability of the parameter value being equal to $h_i$.

$$S(h) = -\sum_{i=1}^{n} P(h_i \mid I_f) \log P(h_i \mid I_f) \tag{5.3}$$

Suppose that the only prior knowledge is that the sum of the individual probabilities must total one, as shown in equation (5.4).

$$1 - \sum_{i=1}^{n} P(h_i \mid I_f) = 0 \tag{5.4}$$

If this equation is incorporated into the basic entropy equation, equation (5.5) is obtained (Bretthorst 1990).

$$S(h) = -\sum_{i=1}^{n} P(h_i \mid I_f) \log P(h_i \mid I_f) + \beta_L \left[ 1 - \sum_{i=1}^{n} P(h_i \mid I_f) \right] \tag{5.5}$$

where $\beta_L$ is a Lagrange multiplier

When the value of S(h) is a maximum the partial derivatives $\delta S(h)/\delta P(h_i|I_f)$ and $\delta S(h)/\delta \beta_L$ are equal to zero. The values of the unknown probabilities can be determined by solving the n+1 equations for $P(h_i|I_f)$ and $\beta_L$.

When nothing is known about the possible value of the parameter except that the probability distribution is normalised, the Maximum Entropy approach yields a uniform distribution. However, if there is some reason to suspect that the parameter has a particular value, then this knowledge can be incorporated into the constraints on the entropy term and will therefore be taken into account when assigning the distribution.

### 5.2.3 Application of Maximum Entropy to other Distributions

We have shown in the last section how the principle of Maximum Entropy can be used to assign a probability distribution. However, using the Principle of Maximum Entropy to assign values to a distribution, can be used on distributions other than those of probability.

The probability distribution can, by definition, be described as a **normalised positive additive** distribution. It is positive in the sense that $P_i > 0$ , additive in the sense that the overall probability is equal to the sum of the probabilities of its constituent parts and normalised because the sum of these probabilities is 1. The probability distribution is only one member of a family to which the Principle of Maximum Entropy can be applied, in fact, the principle can be applied to **any** positive additive distribution even when non-normalised, and Shannon's equation can be adapted for this generalisation. One example of a positive additive distribution (PAD) would be the intensity of light as a function of position.

Suppose there is a PAD h which is a function of x then the Principle of Maximum Entropy can be used to find the most probable distribution h(x), subject to any constraints imposed by previous knowledge about the PAD h(x). Skilling (1989) showed that a generalisation of Shannon's equation to any PAD led to the following equation (5.6), where $d_i$ is the measure assigned to cell i, and h(x) is represented by a vector **h**.

$$S(h,d) = \Sigma(h_i - d_i - h_i \log(h_i/d_i)) \tag{5.6}$$

In practice the vector **d** is used to hold the default values for the distribution **h** to which **h** will tend in the absence of any knowledge about the distribution. Skilling (1989) showed that the most probable value for the vector **h** could be found by maximising its entropy S(h,d) as given by equation (5.6). Equation (5.6) can be extended to represent the continuous function h(x) as follows.

$$S(h,d) = \Sigma(h(x) - d(x) - h(x)\log\frac{h(x)}{d(x)}) \tag{5.7}$$

By using the Principle of Maximum Entropy in the form of equation (5.6) the most probable value of any PAD can be assigned.

### 5.2.4 Positive Additive Distributions in Pharmacokinetics

In the previous sections, the use of the Principle of Maximum Entropy to assign the most probable values to a distribution has been discussed. There appears to be little application, so far, to pharmacokinetics in general, or prediction of drug release rates in particular. However, if the process of drug absorption is examined it can be seen that the rate of drug absorption is, in fact, a positive additive distribution since it can be regarded as the distribution of the times each individual molecule takes to be absorbed.

This is not a new concept and has been used extensively to justify the use of statistical moments in pharmacokinetic analysis (Riegelman and Collier 1980). In the same way the rate of drug release from a dosage form can be regarded as a distribution of the time which each individual molecule takes to leave the dosage form and reach the site of absorption, and is therefore also a PAD.

Although the use of Maximum Entropy in pharmacokinetics is still not obvious, the potential for application is now apparent since the Principle of Maximum Entropy can be applied to PAD's and the absorption and release rates of drugs can both be regarded as PAD's.

## 5.3 COMBINING MAXIMUM ENTROPY AND BAYESIAN INFERENCE

Perhaps at this point, the end objective of the inference should be restated, this is to calculate the posterior probability distribution for our vector h. To do this the prior probability distribution and the likelihood must be calculated and the product of these used to find our posterior probability distribution, according to equation (5.1).

### 5.3.1 Representing the Prior Probability Distribution

At first glance the two previous sections seem to be totally divorced from each other, however they are drawn together when the problem remaining at the end of the first section is considered. How is the prior probability distribution of the hypothesis h to be represented?

Suppose the hypothesis was not a single value or even a theory, but was in fact a distribution represented by a vector **h**, then the hypothesis is now, in effect, the values held by the elements of the vector **h**.

In section 5.2 a method of representing the most probable values for a positive additive distribution by maximising its entropy according to equation (5.6) was shown. If the hypothesis **h** is not just a vector but a vector which is both positive and additive, then in effect the hypothesis **h** is a PAD and the Principle of Maximum Entropy can be used to assign the most probable values to the vector **h**, subject to any constraints imposed by our prior knowledge of **h**.

This will give the most probable vector of **h** but will still not give the **prior probability distribution** ($P(\mathbf{h}|I_f)$) for the vector **h**. However, Skilling (1989) states that the prior probability distribution $P(\mathbf{h}|I_f)$ must be some unknown but monotonically increasing function of the entropy $S(\mathbf{h},d)$ of the vector **h** (equation (5.8)).

$$P(\mathbf{h}) = \Phi(S(\mathbf{h},d)) \tag{5.8}$$

where $\Phi$ is an unknown monotonically increasing function

He went on to show that $\Phi(S(\mathbf{h},d)) \propto \exp(\alpha_R S)$ where $\alpha_R$ is some constant, and the full expression for the prior probability distribution of **h**, $P(\mathbf{h}|d)$ is of the form shown in equation (5.9) (Skilling 1989).

$$P(h|d) = \frac{\exp(\alpha_R S(h,d))}{Z_s(\alpha_R)} \tag{5.9}$$

where $$Z_s(\alpha_R) = \int d\mu \, \exp(-\alpha_R S(h,d))$$

The prior probability distribution is now determined almost completely and the only unknown parameter remaining in the expression is $\alpha_R$. This cannot be evaluated a priori and must be determined during the analysis. $\alpha_R$ is known as the regularising parameter, the reason for which will become apparent later.

### 5.3.2 Representing the Likelihood

The likelihood can be expressed as follows (Gull 1989)

$$P(D|h) = \frac{\exp(-L(h))}{Z_L}$$

$$\text{where} \quad Z_L = \int d^N D \exp(-L(h)) \tag{5.10}$$

$$\text{and} \quad N = \text{number of cells in vector } h$$

If the errors are Gaussian and independent then L is related to the $\chi^2$ value but in many cases the noise may not be well determined, and it is better to leave equation (5.10) in its more general form.

### 5.3.3 Combining The Prior and Likelihood

The combined probability of the vector **h** and the data **D** can be expressed by Cox's product rule as shown previously in equation (5.1). Because the values of d and $\alpha_R$ are needed to be known then they must be included in equation (5.1) to give equation (5.11).

$$P(\mathbf{h},\mathbf{D}|\alpha_R,d) = P(\mathbf{h}|\alpha_R,d).P(\mathbf{D}|\mathbf{h}) \tag{5.11}$$

$$= P(\mathbf{D}).\ P(\mathbf{h}|\mathbf{D},\alpha_R,d)$$

therefore

$$P(\mathbf{h}|\mathbf{D},\alpha_R,d) \propto P(\mathbf{h}|\alpha_R,d).P(\mathbf{D}|\mathbf{h}) \tag{5.12}$$

$$P(\mathbf{h}|\mathbf{D},\alpha_R,d) \propto Z_L^{-1}\, Z_S^{-1} \exp\,(\alpha_R S(\mathbf{h},d) - L(\mathbf{h}))$$

From equation (5.12) it can be seen that the posterior probability distribution is proportional to $Z_L^{-1}\, Z_S^{-1} \exp\,(\alpha_R S(\mathbf{h},d) - L(\mathbf{h}))$ and the best estimate of **h** is one which will maximise the entropy of the <u>posterior</u> probability distribution ($P(\mathbf{h}|\mathbf{D},\alpha_R,d)$), which also happens to be one which maximises the value Q in equation (5.13) (Gull 1989).

$$Q = \alpha_R S(\mathbf{h},d) - L(\mathbf{h}) \tag{5.13}$$

Therefore, the vector **h** found by maximising the value of Q, represents the revision of the hypothesis **h** in light of the new data.

### 5.3.4 The Regularising Parameter $\alpha_R$

If equation (5.13) is examined then it can be seen why $\alpha_R$ is called the regularising parameter since it controls the emphasis given to the entropy and the likelihood. When $\alpha_R$ is large then the entropy term predominates and the vector **h** will be close to its model. If $\alpha_R$ is small then the vector **h** will tend to fit to the errors in the experimental data and the likelihood predominates.

### 5.3.5 Historic vs Classic Maximum Entropy

In the **historic** Maximum Entropy approach (Gull and Skilling 1984) the practice was to set $\alpha_R$ so that the $\chi^2$ value was set to the number of independent data points in the data **D**. In this event, the vector **h** could be found by maximising the entropy S(**h**,m), subject to the constraint $\chi^2(h) = N$ (where N was the number of independent data points).

Using Bayesian analysis, Gull (1989) showed that the value of $\alpha_R$ should be selected so that a measure $-2\alpha_R S$ should be equal to the number of good singular values contained in the data or the number of degrees of freedom associated with the entropy. The term $-2\alpha_R S$ is an expression of the amount of structure produced in the reconstruction. This approach is called the **classic** Maximum Entropy approach and is regarded as the superior approach since the optimal value for $\alpha_R$ has been found through Bayesian analysis and is not an ad hoc value.

**In summary, the essence of the approach is that the values given to the vector h are those which maximise the entropy of the posterior probability distribution (found by finding the maximum value of Q), which itself is found through the calculation of the likelihood and the prior probability distribution.**

## 5.4 MAXIMUM ENTROPY TECHNIQUES IN PHARMACOKINETICS

### 5.4.1 A Statement of the Problem

In the previous three sections the use of Maximum Entropy techniques for the reconstruction of a vector representing a positive additive distribution has been described.

In the section on the occurrence of PAD's in pharmacokinetics, it was stated that both the absorption and release rate of drugs can be regarded as PAD's. Perhaps the best approach to this section is a restatement of the information covered in previous sections from the viewpoint of pharmacokinetics.

The objective is to find the release rate of a drug from a dosage form following administration of that dosage form to a patient. If, after administration of the dosage form, blood levels are taken, then a set of data can be obtained which is directly related to the release rate of the drug from the dosage form.

Given this set of data, it is possible to make some inference about the release rate of the drug. To do this it is necessary to return to Bayes Theorem (equation (5.1)) and redefine its variables in terms of the current problem.

If the rate at which the drug is released from the dosage form is I(t), a continuous function, which is represented by a vector **I** (where $I_i$ is the proportion of the dose released in the period $(i-1)\Delta t$ to $i.\Delta t$, and $\Delta t$ is the time interval of the elements of the vector **I**), and the set of data resulting from administration of the dosage form is represented by the vector **D**, then the objective is to find the most probable values of the vector **I** to represent the release rate of the drug, using information obtained from the data **D**.

Charter and Gull (1987) proposed a method based on the Historic Maximum Entropy approach to calculate the absorption rate of a drug. This has since been superseded by the Classic Maximum Entropy approach whose application to drug absorption rates has been described in more recent papers by Charter (1990 and 1991).

In section 5.3.3 it was shown that the optimum value for a PAD could be found by maximising the value of Q in equation (5.13). In order to do this, the entropy and the likelihood terms must first be calculated.

### 5.4.2 Calculation of the Entropy

The entropy of a PAD represented by a vector **f** can be assigned using equation (5.6).

$$S(\mathbf{f},d) = \Sigma_i( f_i - d_i - f_i\log(f_i/d_i)) \qquad (5.14)$$

where d represents the estimate of the distribution **f** before the start of the analysis. Charter (1990) showed that the PAD **f** is not equivalent to the input rate **I** in which we are interested, but can be related to it (see section 5.4.4).

### 5.4.3 Calculation of the Likelihood

If the errors in the data **D** are Gaussian, then the likelihood is essentially the chi squared statistic (Charter 1990).

$$L(\mathbf{f}) = \chi^2 /2 = 1/2(R_e\text{-}\mathbf{D})^T V(R_e\text{-}\mathbf{D}) \tag{5.15}$$

where V is the covariance matrix known to within a scaling factor $\sigma^2$ and $R_e = R_e(t)$ are the predicted data. The predicted data must be calculated in two stages, firstly the distribution **f** must be transformed to the input rate **I**, which must then be used to calculated the predicted plasma concentration $R_e$.

### 5.4.4 Calculation of Predicted Data

#### 5.4.4.1 Prediction of the Input Rate from f

Charter (1990) showed that it was physically unrealistic to have an input rate **I** which contained discontinuities. He justified this through a consideration of the number of diffusive processes any one molecule being absorbed must undergo. The consequence of this is that the input rate is constructed by creating a "blurred" version of the underlying distribution **f** according to equation (5.16).

$$I(t) = \int_0^\infty C(x,t) f(x)\, dx \tag{5.16}$$

The operator C(x,t) which performs the "blurring" process is called the Intrinsic Correlation Function (ICF) (Charter 1991).

#### 5.4.4.2 Calculation of Predicted Data from Input Rate

If the kinetics of the drug in question are linear in the dose range being considered, then the blood concentration after administration of the dosage form can be calculated by convolution of the input rate **I** with the weighting function. The weighting function is the plasma concentration time profile obtained following administration of a unit bolus dose of the drug in solution given orally. Such profiles

can generally be represented in pharmacokinetics by an equation of the following form.

$$W(t) = \Sigma_{i=1}^{n} A_i e^{-\alpha_i t}$$

$$\text{where} \quad A_n = -\Sigma_{i=1}^{n-1} A_i \tag{5.17}$$

This equation is used in the convolution process to calculate $R_e(\mathbf{f})$.

### 5.4.5 The Intrinsic Correlation Function

Charter (1990) showed that the degree of pre-blur incorporated into the ICF is controlled by a single parameter, and the characteristics of the ICF are such that the width of the blur produced with any given value of this parameter increases with time. The incorporation of the ICF into the method gives one more parameter to be determined - the width of the ICF. In practice this width is chosen to maximise the value of the term **logprob** returned by **memsys5** at convergence. The value of the ICF width is not absolute and if a plot of **logprob** vs ICF width is broad then the choice of the ICF width is not obvious and many choices may be equally as good.

## 5.5 PRACTICAL IMPLEMENTATION

Only two sets of data are required for the practical implementation of the Maximum Entropy approach, these are the parameters obtained following curve fitting of the weighting data to a polyexponential and the plasma concentration values following administration of the dosage form for which the release rate is to be estimated. This data is used as input into the MAXENT program for use by the main module, **memsys5**.

Certain parameters can be varied by the user, these include the ICF width, the number and width of the vector elements and the initial default values for the vector I. Further details of the construction of the control files can be found in the MADAME users manual.

The default values for the vector are usually set to a constant which is the reciprocal of the number of vector elements, however, as long as the default values are reasonable

they have little effect on the final estimated release rate. Changing the width and number of vector elements changes the smoothness of the profile produced but does not greatly affect the shape of the predicted release rate, the choice of both number and width are a matter of personal preference. The ICF, as mentioned previously, performs a smoothing function, and this more than any other factor can influence the shape of the predicted release rate, runs should be performed at several ICF widths to provide some indication of how the change in ICF width may affect the shape of the predicted release rate.

# 6 EVALUATION OF MAXENT USING PSEUDO-EXPERIMENTAL DATA

The aim of the work presented in this chapter is to meet objectives (5) and (6) given at the end of chapter one. That is to (a) investigate the stability of the Maximum Entropy method to increasing levels of noise in the source data, and (b) investigate the ability of the Maximum Entropy method to predict the form of unknown input functions, both of these objectives to be obtained using pseudo-experimental data.

The application of Maximum Entropy to predict the input function will, in future, be termed MAXENT. As in chapter 3, three different forms of input function were used to examine the deconvolution methods and these three forms were the same as those used previously. These were the :

(a) Monoexponential Input Function

(b) Zero Order Release Function

(c) Controlled Release Input Function

The weighting function used in all cases was a triexponential equation with one negative coefficient (see equation (3.1)). In all cases the pseudo-experimental data used for the input, weighting and response functions was the same as that used in chapter 3 for the equivalent form of input function.

As in chapter 3, two examinations were made. Firstly the effect on the predicted input rate, from one data set, due to increasing levels of added noise and secondly, the effect on the mean predicted input rate produced by MAXENT from multiple data sets containing a constant level of added noise.

## 6.1 MONOEXPONENTIAL INPUT FUNCTION

The input function was represented by $I(t) = 1.2e^{-2t}$, the weighting function by equation (3.1) and the response function calculated by convolution of the input and weighting functions according to the procedure given in section 2.3.2. This gives the true data for the input, weighting and response functions shown in Table 1.

### 6.1.1 Increasing Levels of Added Noise

#### 6.1.1.1 Method

Noise levels of 1,5 and 10% were added to the values of the weighting and response functions shown in Table 1 using the NAG subroutine G05DDF (section 2.3.3) to give the data for the weighting and response functions shown in Tables C(1a) and C(1b) in Appendix C.

The weighting data (Table C(1a)) was fitted to a polyexponential of the form shown in equation (3.3) using the non-linear curve fitting routine described in section 2.1.1. The number of terms was increased sequentially and the data re-fitted until there was no significant reduction in the residual sum of squares as judged by the F test (section 2.4.1) at P=0.05 and n=13 (n is the number of data points). The parameters obtained following curve fitting are shown in Table 2(a).

The data in Table C(1b) was analyzed by MAXENT using the details shown. The parameters from Table 2(a) were used to represent the weighting function in the MAXENT program and the dose used for the response function was 0.6. The optimal value of the ICF was found to be 0.16, this optimal value was found by performing several runs over a range of ICF values and recording the values of **logprob** (see section 5.4.5) returned by the program. The optimal value of the ICF was that which corresponded to the maximum value of **logprob**.

The vector used to represent the input function contained 50 elements each with a time width of 0.05. The analysis was repeated using 80 elements with a width of 0.025 but no improvement in definition was seen.

#### 6.1.1.2 Results

Both the input rate and the cumulative fraction input (CFI) produced by MAXENT from data with 1% added noise were so close to those produced from error free data as to be indistinguishable and have therefore been omitted from the graphs. The input rates produced by MAXENT with increasing levels of added noise are shown in Figure 42 and the cumulative input as a fraction of the total dose shown in Figure 43.

As can be seen from Figure 42, the estimated input rates produced by MAXENT are all very similar, and all are very close to the true input rate. The only discrepancies occur

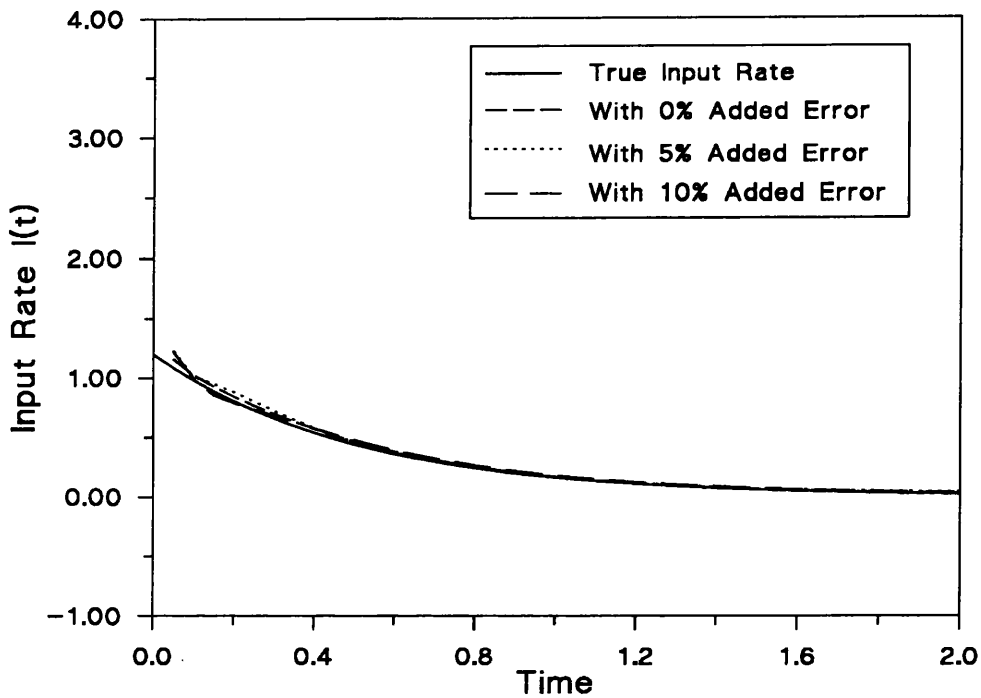


**Figure 42** : Input Rates produced by MAXENT for the Monoexponential Input Function with Increasing Levels of Error added to both the Weighting and Response Functions

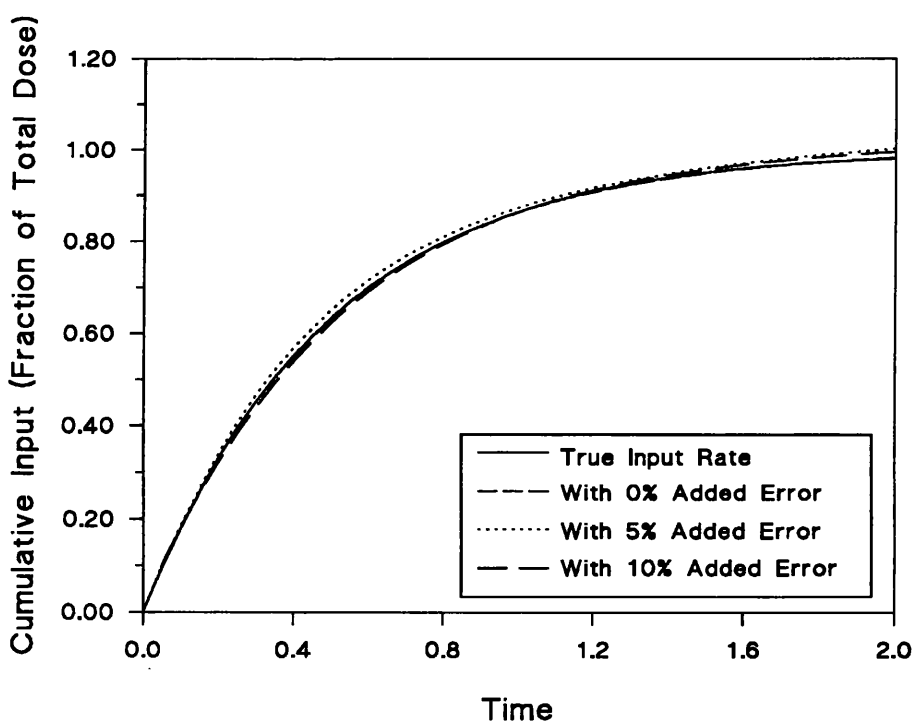


**Figure 43** : Cumulative Input produced by MAXENT for the Monoexponential Input Function with Increasing Levels of Error added to both Weighting and Response Functions.

at the very early time points, but even here the differences between the estimated and true values are very small.

The CFI profiles like the input rates are all very close to the true value and show very little change with increasing levels of noise. All the profiles show the correct shape of both profiles very well.

#### 6.1.1.3 Percentage Difference between Predicted and True Values

For each of the data sets shown in Figures 42 and 43 the percentage difference between the true value and the predicted value for each point was calculated in the following way.

The percentage difference for the input rate was calculated as the absolute value of the difference between the calculated input and the true input, divided by the true input at t=0 and multiplied by 100, i.e.

$$\%\text{diff } I(t) = \left| \text{Calc. } I(t) - \text{True } I(t) \right| * 100 / 1.2$$

where 1.2 is the exact value of the input rate at t=0

The percentage difference for the cumulative fraction input was calculated as the calculated fraction minus the true fraction multiplied by 100.

$$\%\text{diff fraction input} = \left| \text{calc. value - true value} \right| * 100$$

Each data set comprised 39 values over a time range of 0.05 to 1.95 at intervals of 0.05, which was the output from MAXENT. The percentage differences, once calculated, were averaged for each data set and the mean and standard error of the mean for these values are shown in Table 41 for the estimated input rate values and Table 42 for the estimated fraction input values.

| Noise Level % | 0% | 1% | 5% | 10% |
|---|---|---|---|---|
| Mean | 1.27 | 1.38 | 1.75 | 1.81 |
| SD | 1.35 | 1.39 | 2.44 | 1.71 |
| SEM | 0.217 | 0.224 | 0.390 | 0.273 |

**Table 41 :** Mean Percentage Difference for Input Rate Values shown in Figure 42 for Increasing Levels of Added Noise.

| Noise Level % | 0% | 1% | 5% | 10% |
|---|---|---|---|---|
| Mean | 0.083 | 0.242 | 1.172 | 0.629 |
| SD | 0.052 | 0.114 | 0.437 | 0.394 |
| SEM | 0.008 | 0.018 | 0.069 | 0.062 |

**Table 42 :** Mean Percentage Difference for Cumulative Fraction Input Values shown in Figure 43 for Increasing Levels of Added Noise.

All the percentage difference values are very small, both for the input rates and for the CFI's and at the higher noise levels the mean percentage differences are well below the level of noise added to the original data. When the mean values calculated for the input rate and CFI's produced by MAXENT are compared with those produced by the deconvolution algorithms for the equivalent input function (Tables 4 and 5) it can be seen that MAXENT produces lower mean percentage differences at the higher noise levels than all but the polyexponential algorithm, and the mean percentage differences are comparable with this method.

### 6.1.2 Constant Level of Noise Added to Ten Data Sets

#### 6.1.2.1 Method

The noise level for all the data sets was set to 10%, and ten data sets were generated by addition of noise to the weighting and response function data shown in Table 1 using the NAG subroutine G05DDF (section 2.3.3). The ten data sets produced are shown in Tables C(2) and C(3) in Appendix C.

The data sets shown in Table C(2) were fitted to a polyexponential equation of the form shown in equation (3.3) using the non-linear least-squares fitting routine (section 2.1.1). The number of terms in the polyexponential was sequentially increased until there was no significant improvement in the residual sum of squares as judged by the F test (section 2.4.1) at P=0.05 and n=13. The parameters obtained following curve-fitting are shown in Table 6.

The ten data sets were then processed using MAXENT according to the details given below. The parameters from Table 6 were used to represent the weighting function for the data sets, the dose administered for the response function was 0.6. The optimal ICF value

was found to be around 0.4, in practice a value of 0.4 was used and the vector used to represent the input function contained 50 elements with a width of 0.05.

Following the application of MAXENT the mean and standard error of the mean for the ten data sets were calculated for the predicted input rates and the predicted CFI's. The estimated fraction of dose released, $F_R$, was calculated for each data set by taking the maximum value reached on the CFI profile, up to and including t=1.9 to enable comparison with the results produced by the deconvolution algorithms.

For each input rate the $MDT_{1.9}$ was calculated according to the method given in section 2.5.1 using equation (2.49) since the output vector from MAXENT holds the fraction of dose released per vector element.

#### 6.1.2.2 Results

The mean input rate and mean cumulative fraction input for the ten data sets were plotted together with the standard error of the mean values (S.E.M.) and these are shown in Figure 44.

The mean input rate shown in Figure 44 is a good reflection of the true input rate, however it consistently overestimates the input rate at the later time points and the input rate for the first few time points is also poorly approximated. The SEM values associated with the mean input rate are very small, showing the consistency of the method in coping with the noise present in the data.

The mean CFI profile also gave a good approximation to the true profile with only slight deviations seen from the true profile at the later time points. Like the mean input rate the SEM values associated with the CFI profile are very small.

When the mean profiles shown in Figure 44 were compared with the corresponding profiles produced for each of the deconvolution algorithms (Figures 9-12) the following was observed. The mean input rate produced by MAXENT was a better reflection of the true input rate than either of those produced by numerical or semi-numerical deconvolution, was similar to that produced by polyexponential deconvolution (except at the later time points) but is poorer than that produced by the polynomial deconvolution algorithm, which gave a very good reflection of the true profile.

The CFI profiles are very similar for both MAXENT and all the deconvolution

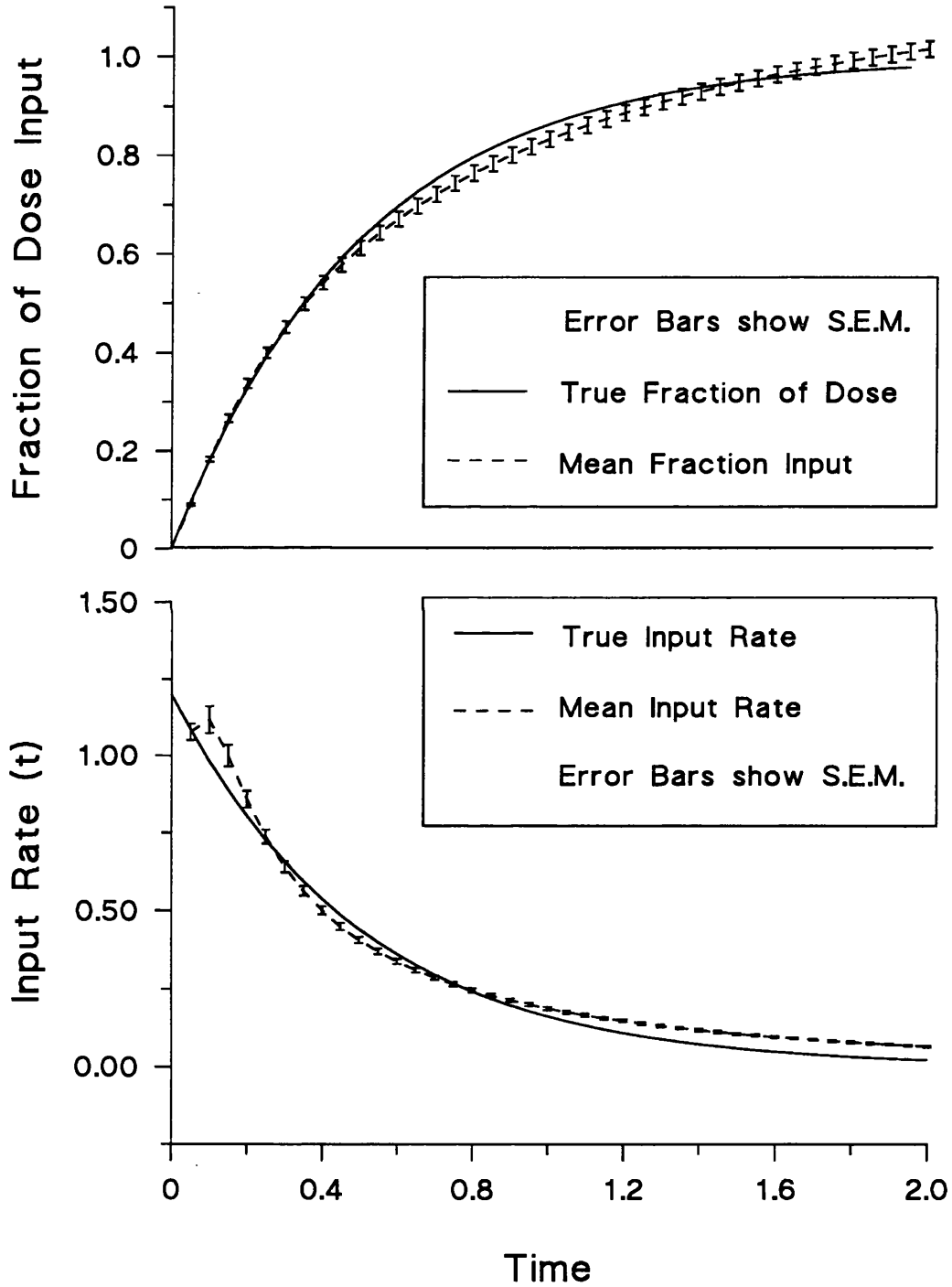


**Figure 44** : Mean results (n=10) produced by MAXENT for the Monoexponential Input Function with 10% Error added to both the Weighting and Response Functions

methods, however of all the profiles, that produced by polynomial deconvolution approximated the true CFI most closely.

### 6.1.2.3 Estimated Fraction Released $F_R$

The estimated fraction of dose released, $F_R$, at t=1.9, for each subject produced by MAXENT are shown in Table 43, together with the mean fraction released ($\bar{F}_R$), the standard deviation (SD) and the standard error of the mean (SEM).

| Subject | $F_R$ | Subject | $F_R$ |
|---|---|---|---|
| 1 | 1.062 | 6 | 0.900 |
| 2 | 0.944 | 7 | 1.032 |
| 3 | 1.002 | 8 | 1.045 |
| 4 | 1.049 | 9 | 1.035 |
| 5 | 1.005 | 10 | 0.982 |
| Mean 1.006 | SD 0.0513 | SEM 0.0162 | |

**Table 43 :** Fraction of Dose Released predicted by MAXENT for a Release Rate of $I(t) = 1.2e^{-2t}$ with 10% Noise Added to both Weighting and Response Functions

The mean fraction produced (1.006) was compared with the true value of 0.978 using the t-test (section 2.4.2) at a probability level of P=0.05 and 9 degrees of freedom. The value of 0.978 is the fraction of the dose released at t=1.9 calculated from the integral of $I(t) = 1.2e^{-2t}$. The $t_s$ value was calculated according to the formula given below, the mean and SEM values were taken from Table 43.

$$t_s = \bar{F}_R - 0.978 / SEM$$

where $\bar{F}_R$ is the mean fraction released.

The value of $t_s$ calculated for MAXENT was (1.006 - 0.978) / 0. 0162 = 1.728.

The value of $t_s$ taken from the tables at P=0.05 and 9 degrees of freedom ($t_{0.05(9)}$) was 2.26, since the calculated value of $t_s$ is less than the critical value taken from the tables there is no significant difference between the mean fraction released predicted by MAXENT and the true value at the 95% probability level.

#### 6.1.2.4 Mean Dissolution Times

The Mean Dissolution Time (MDT) was calculated for each subject, from the input vector produced by MAXENT, according to the method described in section 2.5.1 (using equation (2.49)). These MDT values, together with the mean, standard deviation (SD), and standard error of the mean (SEM) are shown in Table 44.

| Subject | $MDT_{1.9}$ | Subject | $MDT_{1.9}$ |
|---|---|---|---|
| 1 | 0.511 | 6 | 0.587 |
| 2 | 0.491 | 7 | 0.517 |
| 3 | 0.503 | 8 | 0.563 |
| 4 | 0.519 | 9 | 0.547 |
| 5 | 0.537 | 10 | 0.500 |
| Mean 0.5275 | SD 0.0306 | SEM 0.0097 | |

**Table 44** Mean Dissolution Times Estimated for the Input Rates predicted by MAXENT for a Release Rate of $I(t) = 1.2e^{-2t}$ with 10% Noise Added to both Weighting and Response Functions

The mean MDT produced by MAXENT was compared with the true value using the t-test (section 2.4.2) at a probability level of P=0.05 and 9 degrees of freedom. The true $MDT_{1.9}$ calculated up to t=1.9 was calculated according to equation (2.49) in section 2.5.1 and this gave the value of $MDT_{1.9}$ to be 0.4634. The $t_s$ value was calculated according to the formula given below.

$$t_s = \bar{M}DT - 0.4634 / SEM$$

where $\bar{M}DT$ is the mean MDT.

The value of $t_s$ calculated for MAXENT was (0.5275 - 0.4634) / 0.0097 = 6.608. The value of $t_s$ taken from the table $t_{0.05(9)}$ for P=0.05 and 9 degrees of freedom was 2.26. The calculated value of $t_s$ (6.608) is greater than the critical value obtained from the tables therefore there is a significant difference between the mean MDT and the true value, in fact the difference is highly significant, $P < 0.001$.

### 6.1.3 Discussion

From the little variation seen in the predicted input rate profiles produced from data

with increasing levels of added noise (Figure 42) and from the very small SEM values seen for the mean input rate produced from multiple data sets (Figure 44) it can be seen that the MAXENT method is very stable to the presence of noise in the source data.

The form of the predicted input rate was close to the true form in all cases, however the mean input rate deviated from the true value at the later time points (Figure 44). The mean input rate produced by MAXENT, when compared with those produced by the deconvolution methods, was not as accurate as that produced by the polynomial or polyexponential algorithms (Figures 11 and 12) but was far superior to either the numerical or semi-numerical methods (Figures 9 and 10).

The CFI profiles however, in all cases were very close to the true values and their was very little difference between the mean predicted fraction released and the true value. The CFI profiles compared very well with those produced by the polynomial and polyexponential algorithms and showed less variation and much smaller SEM values than those produced by the numerical and semi-numerical algorithms.

The difference between the true $MDT_{1.9}$ and the mean calculated $MDT_{1.9}$ was however significant ($P < 0.001$) this was due to the consistent overestimation of the input rate at the later time points, since the calculation of MDT is heavily dependant on the values of the later time points.

## 6.2 ZERO ORDER INPUT FUNCTION

The input function was represented by equation (3.4) shown at the beginning of section 3.2, the weighting function was again represented by equation (3.1) and the response function calculated by convolution of the input and weighting functions according to the procedure given in section 2.3.2 to give the values for the true input, weighting and response functions shown in Table 11.

### 6.2.1 Increasing Levels of Added Noise

#### 6.2.1.1 Method

Noise levels of 1,5 and 10% were added to the values of the weighting and response functions shown in Table 11 using the NAG subroutine G05DDF (section 2.3.3) to give the data for the weighting and response function shown in Tables C(4a) and C(4b) in

Appendix C.

The weighting data (Table C(4a)) was fitted to a polyexponential of the form shown in equation (3.3) using the non-linear curve fitting described in section 2.1.1. The number of terms was increased sequentially and the data re-fitted until there was no significant reduction in the residual sum of squares as judged by the F test (section 2.4.1) at P=0.05 and n=13 (n is the number of data points). The parameters obtained following curve fitting are shown in Table 12(a).

The data in Table C(4b) was analyzed by MAXENT using the details shown. The parameters from Table 12(a) were used to represent the weighting function in the MAXENT program and the dose used for the response function was 0.6. The optimal value of the ICF was found to be 0.1, this optimal value was found by doing several runs over a range of ICF values and recording the values of **logprob** returned by the program. The optimal value of ICF was that which corresponded to the maximum value of **logprob.**

The vector used to represent the input function contained 50 elements each with a time width of 0.05. The analysis was repeated using 80 elements with a width of 0.025 but no improvement in definition was seen.

#### 6.2.1.2 Results

The input rate and the cumulative fraction input (CFI) produced by MAXENT for the zero order release function with increasing levels of noise present in the source data are shown in Figures 45 and 46 respectively.

As can be seen from Figure 45, the profiles produced from data at all levels of error are very similar and there is no sudden deterioration in the quality of the predicted input rate with increasing levels of noise, although the profile produced from data containing 10% noise is most deviant from the true profile. None of the predicted input profiles show perfectly the constant input rate at the earlier time points, however they all show the presence of an almost linear release rate over this period. The abrupt point of change from zero to first order is missed at all levels of noise but is missed by only a small degree at the lower levels.

The CFI profiles, shown in Figure 46, are all very close to the true profile except for the CFI predicted from data with 10% added noise, which is much lower than the other

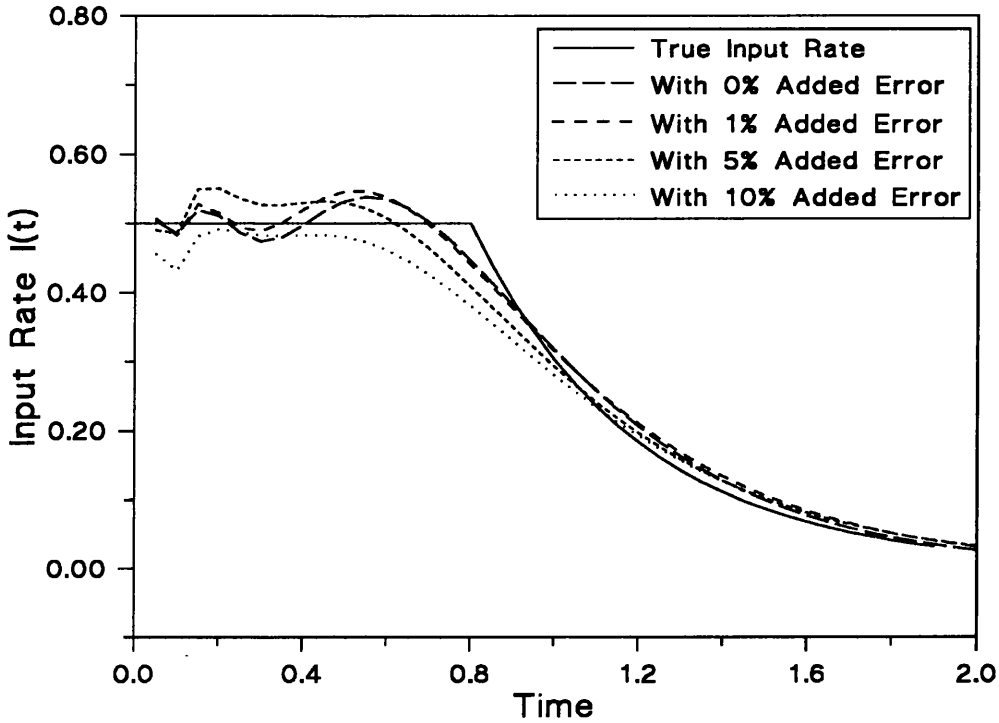


**Figure 45** : Input Rates produced by MAXENT for the Zero Order Input Function with Increasing Levels of Error added to both the Weighting and Response Functions

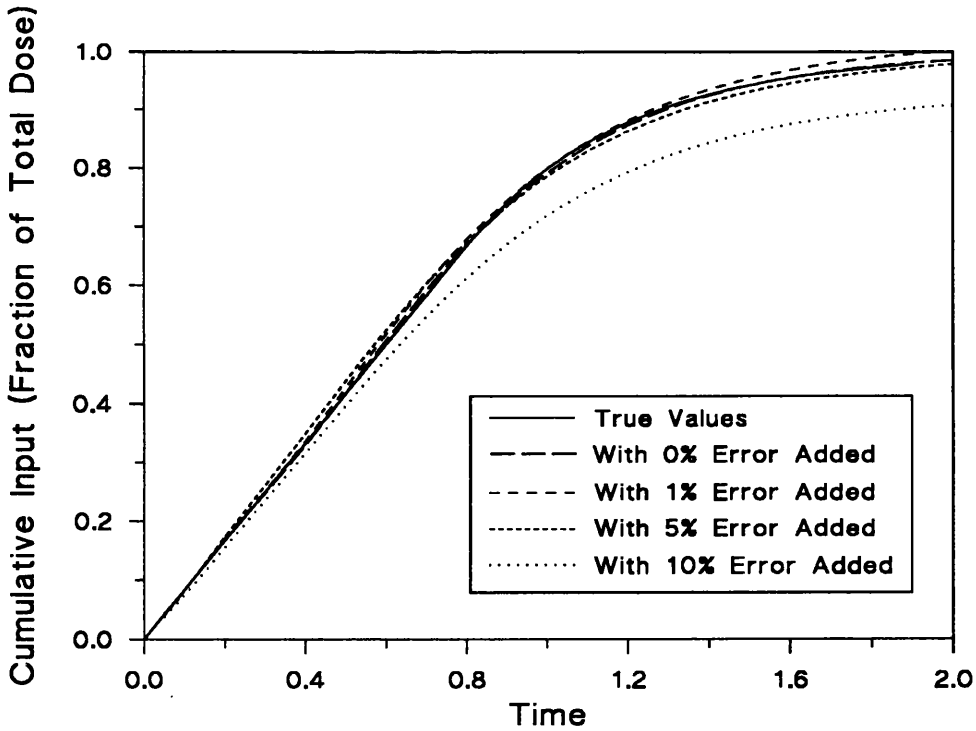


**Figure 46** : Cumulative Input produced by MAXENT for Zero Order Input Function with Increasing Levels of Error added to both Weighting and Response Functions.

profiles, this is probably due to the underestimation of the input rate over the region of change from zero to first order input. There is little variation (apart from that shown at the 10% noise level) of the CFI profiles with increasing levels of noise in the original data.

### 6.2.1.3 Percentage Difference between Predicted and True Values

For each of the data sets shown in Figures 45 and 46 the percentage difference between the true value and the predicted value for each point was calculated in the following way.

The percentage difference for the input rate was calculated as the absolute value of the difference between the calculated input and the true input, divided by the true input at t=0 and multiplied by 100, i.e.

$$\%\text{diff } I(t) = \left| \text{Calc. } I(t) - \text{True } I(t) \right| * 100 / 0.5$$

where 0.5 is the exact value of the input rate at t=0

The percentage difference for the cumulative fraction input was calculated as the calculated fraction minus the true fraction multiplied by 100.

$$\%\text{diff fraction input} = \left| \text{calc. value - true value} \right| * 100$$

Each data set comprised 39 values over a time range of 0.05 to 1.95 at intervals of 0.05, which was the output from MAXENT. The percentage differences, once calculated, were averaged for each data set and the mean and standard error of the mean (SEM) for these values are shown in Table 45 for the estimated input rate values and Table 46 for the estimated fraction input values.

| Noise Level % | 0% | 1% | 5% | 10% |
|---|---|---|---|---|
| Mean | 3.235 | 4.018 | 4.584 | 5.464 |
| SD | 2.243 | 2.557 | 3.774 | 5.540 |
| SEM | 0.359 | 0.409 | 0.604 | 0.887 |

**Table 45 :** Mean Percentage Difference for Input Rate Values shown in Figure 45 for Increasing Levels of Added Noise.

All the mean percentage difference values shown for the input rate are small, and are

all very similar to each other. At the higher noise levels the mean percentage differences are well below the level of noise added to the original data. The mean percentage

| Noise Level % | 0% | 1% | 5% | 10% |
|---|---|---|---|---|
| Mean | 0.312 | 0.830 | 1.174 | 5.518 |
| SD | 0.258 | 0.636 | 0.628 | 3.142 |
| SEM | 0.041 | 0.102 | 0.101 | 0.503 |

**Table 46 :** Mean Percentage Difference for Cumulative Fraction Input Values shown in Figure 46 for Increasing Levels of Added Noise.

differences shown for the CFI profiles are also all small, although the greatest difference is seen between the 5 and 10% noise levels, however the percentage difference for the CFI at 10% is still less than the level of noise in the original data. The SEM values associated with both the input rate and CFI's are very small emphasising the consistent stability of the MAXENT method to the presence of noise.

When the mean percentage differences shown in Tables 45 and 46 are compared with those produced by the different deconvolution methods for the equivalent data (Tables 14 and 15) it can be seen that, for the input rate, with error free data and at very low levels of error the numerical and semi numerical methods have lower mean percentage difference values than MAXENT, the polynomial algorithm has almost equivalent values and the polyexponential algorithm has higher values. This situation changes at the high noise levels where the MAXENT method has lower percentage differences than all the deconvolution methods, but this difference is small for the polynomial algorithm.

When the percentage difference values for the CFI profiles are also compared all the methods (both MAXENT and the deconvolution algorithms) produce very similar values.

### 6.2.2 Constant Level of Noise Added to Ten Data Sets

#### 6.2.2.1 Method

The noise level for all the data sets was set to 10%, and ten data sets were generated by addition of noise to the weighting and response functions shown in Table 11 using the NAG subroutine G05DDF (section 2.3.3). The ten data sets produced are shown in Tables

C(5) and C(6) in Appendix C.

The data sets shown in Table C(5) were fitted to a polyexponential equation of the form shown in equation (3.3) using the non-linear least-squares fitting routine (section 2.1.1). The number of terms in the polyexponential was sequentially increased until there was no significant improvement in the residual sum of squares as judged by the F test (section 2.4.1) at P=0.05 and n=13. The parameters obtained following curve-fitting are shown in Table 16.

The ten data sets were then processed using MAXENT according to the details given below. The parameters from Table 16 were used to represent the weighting function for the data sets, the dose administered for the response function was 0.6. The optimal ICF value was found to be 0.1, and the best vector found to represent the input function contained 35 elements with a width of 0.075.

Following the use of MAXENT the mean and standard error of the mean for the ten data sets were calculated for the predicted input rates and the predicted CFI's. The estimated fraction of dose released $F_R$ was calculated for each data set by taking the maximum value reached on the CFI profile, up to and including t=1.95 to enable comparison with the results produced by the deconvolution algorithms.

For each input rate the $MDT_{1.95}$ was calculated according to the method given in section 2.5.1 using equation (2.49) since the output vector from MAXENT holds the fraction of dose released per vector element.

#### 6.2.2.2 Results

The mean input rate and the mean CFI predicted by MAXENT for the zero order input function are shown in Figure 47 together with their SEM values. The mean input rate shown in Figure 47 is a very good reflection of the true input rate, the shape of the declining phase of the profile is approximated very well although the predicted values are slightly higher than the true values. The zero order portion of the true input rate is not predicted perfectly but the predicted mean rate does show a generally constant portion at the early time points, and the abrupt change from zero to first order is missed only by a small degree. The SEM values associated with the mean input rate are very small once again showing the stability of the method to the presence of noise in the data.

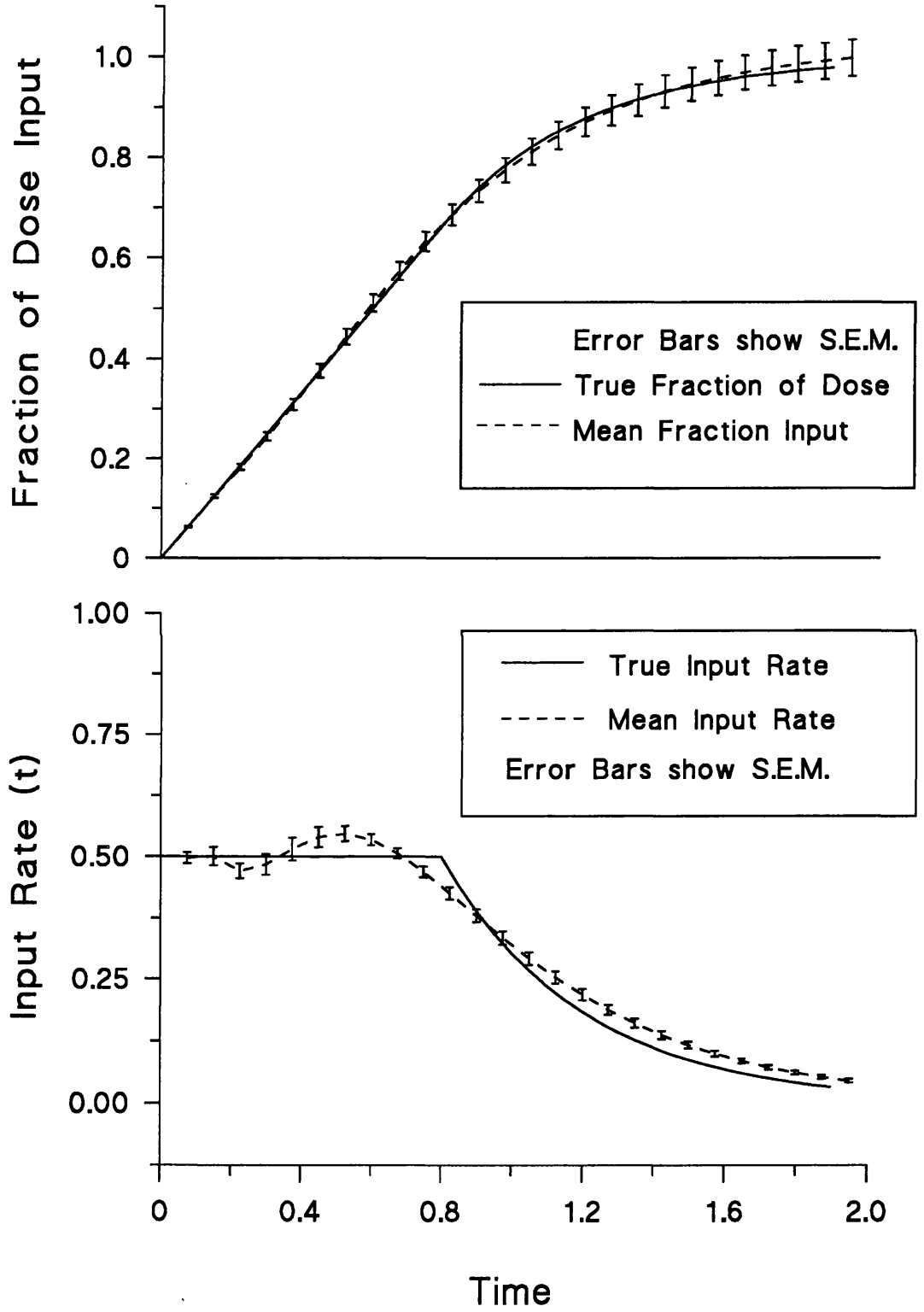


**Figure 47** : Mean results (n=10) produced by MAXENT for the Zero Order Input Function with 10% Error added to both the Weighting and Response Functions

The mean CFI profile is a very good approximation to the true CFI profile and shows no deviation from it, the SEM values associated with the mean profile are small.

When the mean input rate predicted by MAXENT is compared to the mean input rates predicted by the four deconvolution methods for the equivalent data (Figures 21-24) it can be seen that MAXENT gives the best possible approximation to the true input rate. Of the deconvolution methods only the polynomial method gives a good approximation to the true input rate, but it misses the abrupt change in the input rate from zero to first order by a greater degree than MAXENT and also deviates away from the true input rate at either end of the time period.

A similar comparison of the CFI profiles does not show the same discrepancies, as all the profiles are very similar and any deviations from the true profiles are small.

#### 6.2.2.3 Estimated Fraction Released $F_R$

The estimated fraction of dose released, $F_R$, at t=1.95, produced by MAXENT for each subject are shown in Table 47, together with the mean fraction released ($\bar{F}_R$), the standard deviation (SD) and the standard error of the mean (SEM).

The mean fraction released produced by MAXENT was compared with the true fraction released at t=1.95 (which was 0.982) using a t-test (section 2.4.2) at a probability level of 0.05 and with 9 degrees of freedom. The value 0.982 is the fraction of dose released at t=1.95 calculated from the integral of the true input rate ($I(t) = 0.5$ for $t \leq 0.8$ and $I(t) = 0.5e^{-2.5(t-0.8)}$ for $t > 0.8$).

| Subject | $F_R$ | Subject | $F_R$ |
|---|---|---|---|
| 1 | 0.948 | 6 | 0.820 |
| 2 | 1.037 | 7 | 1.108 |
| 3 | 0.913 | 8 | 1.008 |
| 4 | 0.983 | 9 | 1.073 |
| 5 | 0.882 | 10 | 1.212 |
| Mean 0.998 | SD 0.1156 | SEM 0.0365 | |

**Table 47 :** Fraction of Dose Released predicted by MAXENT for a Release Rate of $I(t) = 0.5$ for $t \leq 0.8$ and $I(t) = 0.5e^{-2.5(t-0.8)}$ for $t > 0.8$ with 10% Noise Added to both Weighting and Response Functions

The $t_s$ value was calculated according to the formula given below, the mean and SEM values were taken from Table 47.

$$t_s = (\bar{F}_R - 0.982) / SEM$$

where $\bar{F}_R$ is the mean fraction released

The value of $t_s$ calculated for MAXENT was (0.998 - 0.982) / 0.0365 = 0.438 The value of $t_s$ taken from the tables at P=0.05 and 9 degrees of freedom ($t_{0.05(9)}$) was 2.26, since the calculated value of $t_s$ is less than the critical value taken from the tables there is no significant difference between the mean fraction released predicted by MAXENT and the true value at the 95% probability level.

#### 6.2.2.4 Mean Dissolution Times

The Mean Dissolution Times (MDT) were calculated, from the input vector produced by MAXENT, according to the method described in section 2.5.1 (using equation (2.49)), for each subject. These MDT values, together with the mean, standard deviation (SD), and standard error of the mean (SEM) are shown in Table 48.

The mean MDT produced by MAXENT was compared with the true value using the t-test (section 2.4.2) at a probability level of P=0.05 and 9 degrees of freedom. The true

| Subject | $MDT_{1.95}$ | Subject | $MDT_{1.95}$ |
|---|---|---|---|
| 1 | 0.648 | 6 | 0.631 |
| 2 | 0.658 | 7 | 0.657 |
| 3 | 0.648 | 8 | 0.655 |
| 4 | 0.651 | 9 | 0.655 |
| 5 | 0.643 | 10 | 0.673 |
| Mean 0.6518 | SD 0.0109 | SEM 0.0035 | |

**Table 48** Mean Dissolution Times Estimated for the Input Rates predicted by MAXENT for a Release Rate of I(t) = 0.5 for t ≤ 0.8 and $I(t) = 0.5e^{-2.5(t-0.8)}$ with 10% Noise Added to both Weighting and Response Functions

$MDT_{1.95}$ calculated up to t=1.95 was calculated according to equation (2.49) in section 2.5.1 and this gave the value of $MDT_{1.95}$ to be 0.6348. The $t_s$ values were calculated according to the formula given below.

$$t_s = \bar{M}DT - 0.6348 / SEM$$

where $\bar{M}DT$ is the mean MDT.

The value of $t_s$ calculated for MAXENT was (0.6518 - 0.6348) / 0.0035 = 4.857. The value of $t_s$ taken from the tables $t_{0.05(9)}$ for P=0.05 and 9 degrees of freedom was 2.26. The calculated value of $t_s$ (4.857) is greater than the critical value obtained from the table therefore there is a significant difference between the mean predicted MDT and the true value, in fact the difference is highly significant, $P < 0.001$.

### 6.2.3 Discussion

The input rates and CFI profiles produced from data containing different levels of noise are all very similar to each other showing that the MAXENT method is very stable to the presence of noise in the original data.

Like the deconvolution algorithms, the MAXENT method has trouble approximating this unrealistic function, but it does produce a mean input rate profile which is closer to the true input rate than any of those produced by the four deconvolution algorithms. However, because the MAXENT method is constrained to produce a smooth input function the method does not show the abrupt change in the input rate from zero to first order and for the same reason the zero order portion of the profile appears as gentle curves. Despite these vagrancies the mean predicted input rate does give a good reflection of the true profile.

The mean CFI profile, as would be expected, gives a very good reflection of the true profile and the mean $F_R$ value predicted from these profiles is not significantly different to the true value at the 95% probability level.

The mean MDT value predicted from the estimated input rate is significantly different ($P < 0.001$) from the true value. This may be due in part to the slight overestimation of the input rate during the declining phase of the profile. It is strange however, that for the equivalent input rate,the only deconvolution method to show a significant difference in the estimated mean MDT was the polyexponential algorithm, despite the better approximation to the true input rate produced by the MAXENT method. This is doubly strange when the mean MDT arising from the MAXENT method only differs from the true value by ≈ 2.5% compared with 1.1, 1.7, 0.5 and 6.3% for the numerical, semi-

numerical, polynomial and polyexponential deconvolution methods respectively (of which only the polyexponential MDT was significantly different).

These findings can be explained when the standard deviation of the mean MDT values are examined. These values are so small for the MAXENT method that the 2.5% difference between the estimated and true values becomes significant, this would also suggest that because of the higher standard deviations associated with the MDT values produced by the deconvolution algorithms the number of data sets used to produce the mean MDT would need to be increased before the t-test would show any significant difference between the estimated and true MDT values.

## 6.3 CONTROLLED RELEASE INPUT FUNCTION

The input function was represented by the same data described in the corresponding section (3.3) in chapter 3, the weighting function was again represented by the equation shown in equation (3.1) and the response data was produced by convolution of the weighting and input data according to the method shown in section 2.3.2.3. The true values produced for the input, weighting and response functions are shown in Table 21.

### 6.3.1 Increasing Levels of Added Noise

#### 6.3.1.1 Method

Noise levels of 1, 5 and 10% were added to the values of the weighting and response functions shown in Table 21 using the NAG subroutine G05DDF (see section 2.3.3). The data sets produced following the addition of noise are shown in Tables C(7a) and C(7b) in appendix C.

The weighting data (Table C(7a)) was fitted to a polyexponential of the form shown in equation (3.3) using the non-linear curve fitting described in section 2.1.1. The number of terms was increased sequentially and the data re-fitted until there was no significant reduction in the residual sum of squares as judged by the F test (section 2.4.1) at P=0.05 and n=13 (n is the number of data points). The parameters obtained following curve fitting are shown in Table 22(a).

The data in Table C(7b) was analyzed by MAXENT using the details shown. The parameters from Table 22(a) were used to represent the weighting function in the

MAXENT program and the dose used for the response function was 0.7344 (see section 3.2). The optimal value of the ICF was found to be 0.06, this optimal value was found by performing several runs over a range of ICF values and recording the values of **logprob** returned by the program. The optimal value of ICF was that which corresponded to the maximum value of **logprob**.

The vector used to represent the input function contained 50 elements each with a time width of 0.05. The analysis was repeated using 100 elements with a width of 0.02 but no improvement in definition was seen.

#### 6.3.1.2 Results

The input rates and CFI profiles produced by MAXENT for the controlled release input function, using data with increasing levels of added noise, are shown in Figures 48 and 49 respectively.

The input rates produced (Figure 48) show very similar profiles at all levels of added noise although none of these profiles match the true input rate perfectly, all show a good similarity. The profiles produced from error free data and from data with 1% added noise are very similar and show a very good agreement with the true input rate, though they approximated the zero order portion of the profile by using very shallow curves. The profiles produced from data containing higher levels of noise show more deviation from the true input rate although they are still able to show the correct form of the input rate.

When the input rates predicted by MAXENT are compared with those produced for the equivalent input function using the deconvolution algorithms (Figures 25,27,29 and 31) then it can be seen that only the polynomial method approximates the true input function as well as the MAXENT method and this is only for data containing little or no noise. At the higher noise levels the polynomial method fails to show that the initial input rate rises rapidly from zero, and it approximates the two ends of the zero order portion of the profile badly. The MAXENT method shows both the initial rapidly rising release from zero and approximates the rapid changes in the input rate very well.

The CFI profiles produced by MAXENT (Figure 49) are very similar for all levels of noise and all the profiles produced are close to the true values. When the CFI profiles produced by MAXENT are compared with those produced for the equivalent input

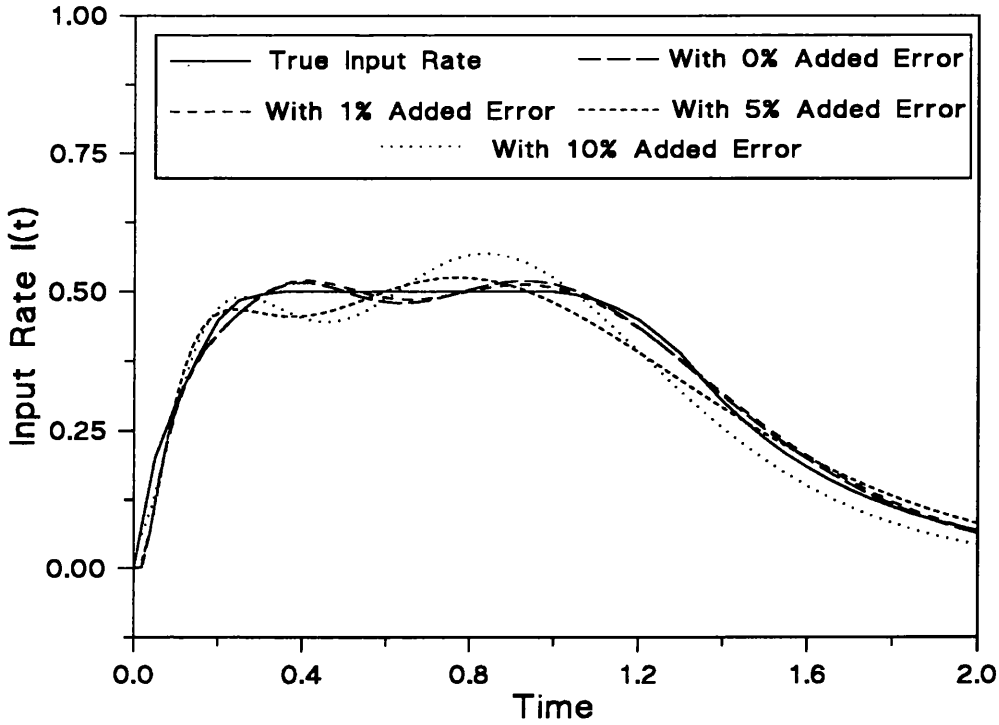


**Figure 48** : Input Rates produced by MAXENT for Controlled Release Input Function with Increasing Levels of Error added to both the Weighting and Response Functions

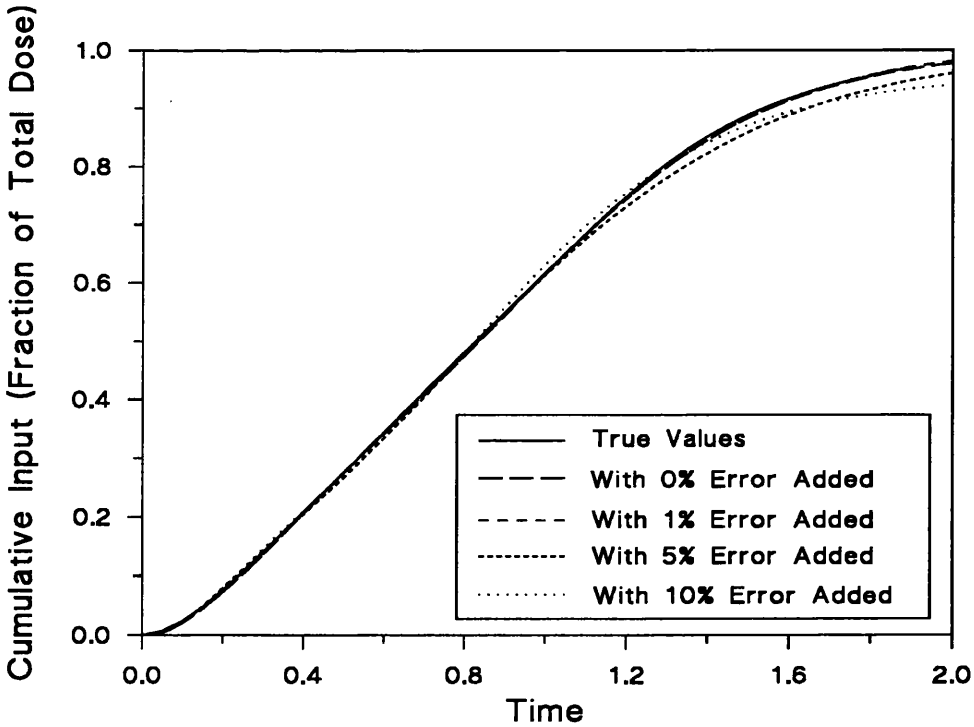


**Figure 49** : Cumulative Input produced by MAXENT the Controlled Release Input Function with Increasing Levels of Error added to both Weighting and Response Functions.

function using the four deconvolution algorithms (Figures 26,28,30 and 32) all the profiles are very similar but those produced by MAXENT at the higher noise levels give a slightly better approximation to the true CFI.

### 6.3.1.3 Percentage Difference between Predicted and True Values

For each of the data sets shown in Figures 48 and 49 the percentage difference between the true value and the predicted value for each point was calculated in the following way.

The percentage difference for the input rate was calculated as the absolute value of the difference between the calculated input and the true input, and multiplied by 100, i.e.

$$\%\text{diff } I(t) = \left| \text{Calc. } I(t) - \text{True } I(t) \right| * 100$$

The percentage difference for the cumulative fraction input was calculated as the calculated fraction minus the true fraction multiplied by 100.

$$\%\text{diff fraction input} = \left| \text{calc. value} - \text{true value} \right| * 100$$

Each data set comprised 39 values over a time range of 0.05 to 1.95 at intervals of 0.05, which was the output from MAXENT. The percentage differences, once calculated, were averaged for each data set and the mean and standard error of the mean (SEM) for these values are shown in Table 49 for the estimated input rate values and Table 50 for the estimated fraction input values.

All the mean percentage difference values are very small both for the input rate and for the CFI profiles and there is little change in their values with increased levels of noise.

| Noise Level % | 0% | 1% | 5% | 10% |
|---|---|---|---|---|
| Mean | 1.260 | 1.331 | 2.579 | 3.717 |
| SD | 1.312 | 1.321 | 1.813 | 1.841 |
| SEM | 0.210 | 0.212 | 0.290 | 0.295 |

**Table 49 :** Mean Percentage Difference for Input Rate Values shown in Figure 48 for Increasing Levels of Added Noise.

At the higher levels of noise the mean percentage difference values are substantially lower than the amount of noise added to the original data. The SEM values associated with both the input rates and the CFI profiles are low and change little at the higher noise levels.

| Noise Level % | 0% | 1% | 5% | 10% |
|---|---|---|---|---|
| Mean | 0.482 | 0.561 | 1.173 | 1.475 |
| SD | 0.349 | 0.321 | 0.850 | 1.065 |
| SEM | 0.056 | 0.051 | 0.136 | 0.170 |

**Table 50 :** Mean Percentage Difference for Cumulative Fraction Input Values shown in Figure 49 for Increasing Levels of Added Noise.

When the values in Tables 49 and 50 are compared with those produced by the four deconvolution methods for the equivalent input function (Tables 24 and 25) then the following is seen. For data containing little or no added noise the mean percentage difference for the input rate produced by MAXENT is greater than those seen with the numerical and semi-numerical algorithms, similar to that produced by the polynomial algorithm and lower than that produced by the polyexponential algorithm. However, at the higher noise levels the mean percentage difference produced by MAXENT is lower that all those produced by deconvolution but is of a similar size to that produced by polynomial deconvolution.

When the mean percentage differences for the CFI profiles produced by MAXENT are compared with those produced by deconvolution there is very little difference seen and all the methods produced very similar values.

### 6.3.2 Constant Level of Noise Added to Ten Data Sets

#### 6.3.2.1 Method

The noise level for all the data sets was set to 10%, and ten data sets were generated by addition of noise to the weighting and response functions shown in Table 21 using the NAG subroutine G05DDF (section 2.3.3). The ten data sets produced are shown in Tables C(8) and C(9) in Appendix C.

The data sets shown in Table C(8) were fitted to a polyexponential equation of the form shown in equation (3.3) using the non-linear least-squares fitting routine (section 2.1.1). The number of terms in the polyexponential was sequentially increased until there was no significant improvement in the residual sum of squares as judged by the F test (section 2.4.1) at P=0.05 and n=13. The parameters obtained following curve-fitting are

shown in Table 26.

The ten data sets were then processed using MAXENT according to the details given below. The parameters from Table 26 were used to represent the weighting function for the data sets, the dose administered for the response function was 0.7344 (see section 3.3). The optimal ICF value was found to be 0.06, and the vector used to represent the input function contained 40 elements with a width of 0.05. The runs were repeated using a vector containing 100 elements with a width of 0.02 and a slight improvement in definition was seen, therefore a vector of 100 elements was used for this section.

Following the use of MAXENT the mean and standard error of the mean for the ten data sets were calculated for the predicted input rates and the predicted CFI's. The estimated fraction of dose released, $F_R$, was calculated for each data set by taking the maximum value reached on the CFI profile, up to and including t=1.9 to enable comparison with the results produced by the deconvolution algorithms.

For each input rate the $MDT_{1.9}$ was calculated according to the method given in section 2.5.1 using equation (2.49) since the output vector from MAXENT holds the fraction of dose released per vector element.

#### 6.3.2.2 Results

The mean input rate and the mean CFI predicted by MAXENT for the controlled release input function are shown in Figure 50 together with their SEM values. The mean input rate shown in Figure 50 is a very good reflection of the true input rate, the initial rise and the change to zero order release is well approximated and the decay into first order release is shown fairly well. However the declining phase of the true input rate is overestimated towards the later time points. The SEM values associated with the mean profile are very small showing the stability of the MAXENT method to noisy data.

When the mean input rate produced by MAXENT is compared with the mean input rates produced by the deconvolution methods for the equivalent input function (Figures 33-36) it can be seen that the input rate produced by MAXENT provides a better approximation to the true rate than any of the deconvolution algorithms. The polynomial algorithm provides almost as good an approximation but it fails to show the initial rate well and begins to deviate wildly at the later time points.

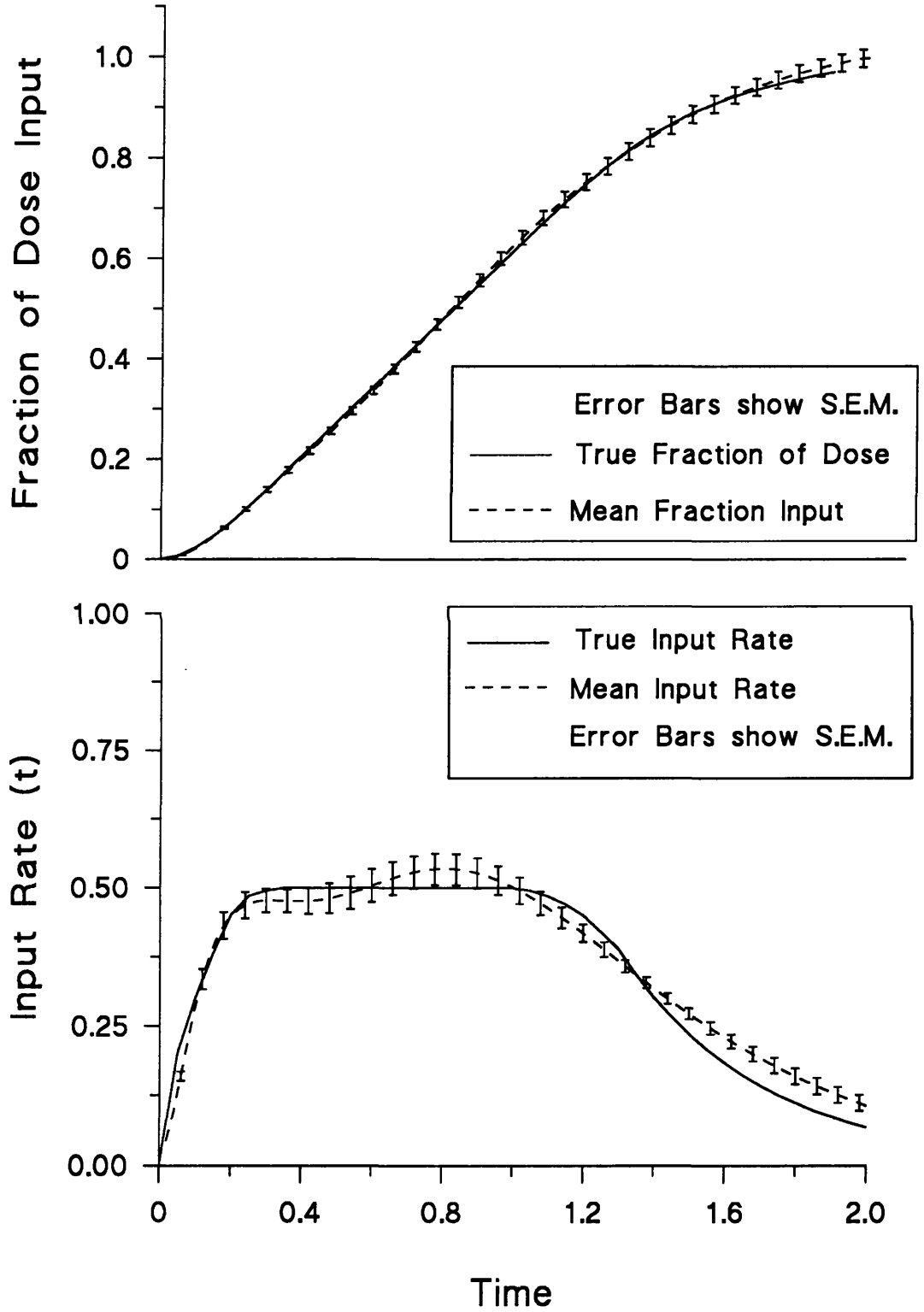


**Figure 50** : Mean results (n=10) produced by MAXENT for the Controlled Release Input Function with 10% Error added to both the Weighting and Response Functions

The mean CFI profile produced by MAXENT (Figure 50) provides a very good reflection of the true profile and has very low SEM values associated with this profile. When the mean CFI profile produced by MAXENT is compared with those produced by the different deconvolution algorithms (Figures 33-36), very little difference can be seen between the different profiles and all the profiles provide a good reflection of the true values with the exception of the polyexponential method whose profile deviates slightly.

### 6.3.2.3 Estimated Fraction Released $F_R$

The estimated fraction of dose released, $F_R$, at t=1.9, produced by MAXENT for each subject are shown in Table 51, together with the mean fraction released ($\bar{F}_R$), the standard deviation (SD) and the standard error of the mean (SEM).

| Subject | $F_R$ | Subject | $F_R$ |
|---|---|---|---|
| 1 | 0.966 | 6 | 0.940 |
| 2 | 0.934 | 7 | 0.933 |
| 3 | 0.974 | 8 | 1.022 |
| 4 | 1.078 | 9 | 1.040 |
| 5 | 1.034 | 10 | 0.985 |
| Mean 0.9906 | SD 0.0505 | SEM 0.0160 | |

**Table 51 :** Fraction of Dose Released predicted by MAXENT for the Controlled Release Input Function with 10% Noise Added to both Weighting and Response Functions

The mean fraction released produced by MAXENT was compared with the true fraction released at t=1.90 (which was 0.970) using a t-test (section 2.4.2) at a probability level of 0.05 and with 9 degrees of freedom. The value 0.970 is the fraction of dose released at t=1.9 calculated from the integral of the true input rate. The $t_s$ value was calculated according to the formula given below, the mean and SEM values were taken from Table 51.

$$t_s = (\bar{F}_R - 0.970) / SEM$$

where $\bar{F}_R$ is the mean fraction released

The value of $t_s$ calculated for MAXENT was (0.9906 - 0.970) / 0.0160 = 1.288

The value of $t_s$ taken from the tables at P=0.05 and 9 degrees of freedom ($t_{0.05(9)}$) was 2.26,

since the calculated value of $t_s$ is less than the critical value taken from the tables there is no significant difference between the mean fraction released predicted by MAXENT and the true value at the 95% probability level.

#### 6.3.2.4 Mean Dissolution Times

The Mean Dissolution Times (MDT) were calculated for each subject, from the input vector produced by MAXENT, according to the method described in section 2.5.1 (using equation (2.49)). These MDT values, together with the mean, standard deviation (SD), and standard error of the mean (SEM) are shown in Table 52.

The mean MDT produced by MAXENT was compared with the true value using the t-test (section 2.4.2) at a probability level of P=0.05 and 9 degrees of freedom. The true

| Subject | $MDT_{1.9}$ | Subject | $MDT_{1.9}$ |
|---|---|---|---|
| 1 | 0.844 | 6 | 0.858 |
| 2 | 0.829 | 7 | 0.855 |
| 3 | 0.838 | 8 | 0.867 |
| 4 | 0.837 | 9 | 0.874 |
| 5 | 0.814 | 10 | 0.868 |
| Mean 0.8484 | SD 0.0193 | SEM 0.0061 | |

**Table 52** Mean Dissolution Times Estimated for the Input Rates predicted by MAXENT for the Controlled Release Input Function with 10% Noise Added to both Weighting and Response Functions

$MDT_{1.9}$ calculated up to t=1.90 was calculated according to equation (2.49) in section 2.5.1 and this gave the value of $MDT_{1.9}$ to be 0.8275. The $t_s$ values were calculated according to the formula given below.

$$t_s = \bar{M}DT - 0.8275 / SEM$$

where $\bar{M}DT$ is the mean MDT.

The value of $t_s$ calculated for MAXENT was (0.8484 - 0.8275) / 0.0061 = 3.426. The value of $t_s$ taken from the table $t_{0.05(9)}$ for P=0.05 and 9 degrees of freedom was 2.26. The calculated value of $t_s$ (3.426) is greater than the critical value obtained from the table therefore there is a significant difference between the mean MDT and the true value, in fact the difference is highly significant, $0.01 > P > 0.001$.

### 6.3.3 Discussion

There was little change in the input rate profiles produced by MAXENT with increasing levels of noise in the source data and the SEM values shown by the mean input rate (Figure 50) are very small, both of these show the stability of the MAXENT method to noise in the data.

The mean input rate predicted by MAXENT gave a good approximation of the true values, except towards the end of the profile where the predicted rate over estimates the true value. Despite this deviation the input rate produced by MAXENT is a better approximation to the true profile than all of those predicted by the different deconvolution methods, although the input rate predicted by the polynomial algorithm is also a good reflection of the true rate.

The mean CFI profile predicted by MAXENT is very close to the true value and little difference is seen between this CFI and those predicted by the deconvolution algorithms. There is no significant difference between the mean predicted $F_R$ and the true value at the 95% probability level.

The mean MDT calculated from the input rates produced by MAXENT is significantly different to the true value ($0.01 > P > 0.001$) this is probably because of the overestimation of the input rate during the declining phase at the later time points. Despite this overestimation the difference between the predicted mean MDT and the true MDT is only 2.5%, but this difference becomes significant because of the very low SEM value associated with it.

## 6.4 CONCLUSIONS

The work in this chapter was designed to subject the MAXENT method to the same challenges to which the deconvolution algorithms were subjected, in order to examine the ability of the MAXENT method to

(a) cope with the presence of noise in the source data and

(b) predict the true form and value of different input functions.

The second aim of this chapter was to compare the results produced by MAXENT with those produced by the four deconvolution methods. Having done this in the discussions shown at the end of each separate input function the following general conclusions can

be drawn about the ability of the MAXENT method to predict release rates.

- For all the input functions used the MAXENT method (which involves no assumptions about the form of the input rate) has been shown to be very stable to the presence of noise in the initial data and in this respect resembles the polynomial and polyexponential deconvolution methods (whose stability to data noise is a consequence of their approximation of the unknown input rate by an empirical function).

- The MAXENT method can predict the correct form of complex input functions. These predictions are not perfect but they do show the general shape of the unknown function correctly. For these more complex functions (e.g. the zero order and controlled release input functions) the MAXENT method provides a better estimate of the true input function than any of the deconvolution methods. The MAXENT method is also able to cope with rapid changes in the input rate with greater facility than shown by the deconvolution algorithms.

- The MAXENT method overestimated the mean MDT values for all the input functions, although this difference was only 2.5% for both the zero order and controlled release input functions but ≈13% for the monoexponential input function. This was due to the overestimation of the input rate at the later time points and which may have arisen from the use of too large an ICF width in the MAXENT program. This is suggested not only by the fact than the function of the ICF is to create a smooth vector but also by the fact that the ICF value used with the monoexponential function was 0.4, whilst those used with the zero order and controlled release functions were 0.1 and 0.06 respectively, implying that the use of the high ICF (0.4) may be contributing to the 13% difference seen.

- The MAXENT method combines the advantages of all the deconvolution methods. It has the stability to data noise seen with the those deconvolution algorithms which involve function approximation (i.e. the polynomial and polyexponential algorithms)

while making no assumptions about the form of the unknown input function, which is the advantage ascribed to the numerical and semi-numerical deconvolution algorithms. Added to this is its ability, demonstrated for the input functions used in this chapter, to show the correct form of an unknown input function, and its ability to cope with rapid changes in the input rate. All these features make in the method of choice if the aim of analysis is to obtain information about the release rate itself.

# 7 *IN VIVO* RELEASE OF CR METOPROLOL TABLETS PREDICTED BY MAXENT

In the previous chapter the ability of the MAXENT method to predict correctly both the form and the values of unknown input functions was examined using pseudo-experimental data. The stability of the MAXENT method to the presence of data noise was also examined.

This chapter is concerned with the practical use of MAXENT to analyze actual clinical data, with the aim of highlighting any problems which may arise from the use of MAXENT in a practical situation. To this end, the clinical data following administration of three different controlled release metoprolol tablets will be analyzed by MAXENT using the plasma concentrations following administration of a bolus solution of 95mg Metoprolol Succinate as the weighting function. This is necessary for the calculation of the predicted plasma concentrations from the current estimate of the dissolution rate in the MAXENT process. By representing the weighting function in this manner the input rate predicted by MAXENT will represent the *in vivo* drug release rate of metoprolol from the controlled release tablets.

The metoprolol data to be used in the analysis is that used previously in chapter 4 where it was analyzed using four deconvolution methods. The use of this data will enable the *in vivo* release characteristics predicted by MAXENT to be compared and contrasted with those produced by deconvolution of the same data, allowing any superiority of methods to become apparent.

Following the application of MAXENT the release process of the CR tablets will by characterised by consideration of the following properties :

(a) The shape and characteristics of the dissolution rate and cumulative fraction released profiles themselves.

(b) The fraction of dose released, $F_R$

(c) The estimated $MDT_{in\ vivo}$

(d) *In vivo -in vitro* Correlation using

  (1) $MDT_{in\ vivo}$ vs $MDT_{in\ vitro}$ Plots

  (2) *In vivo* dissolution rate and *in vitro* dissolution rate plots

Details of the clinical data, the controlled release tablets, the *in vitro* dissolution studies and the justification of linearity have been shown previously in sections 4.1 - 4.4 of chapter 4. The justification of linearity if as important for the use of MAXENT as it is for the application of deconvolution, since the calculation of the predicted plasma concentration from the estimated *in vivo* release rate involves the evaluation of the convolution integral.

## 7.1 METHOD

### 7.1.1 Calculation of *In vivo* Dissolution Rates

Prior to the application of MAXENT to calculate the *in vivo* dissolution rate, the plasma concentrations for each subject following administration of the oral solution (shown in Table D(1)) were fitted to a polyexponential equation of the form shown in equation (4.1) (see section 4.5) using the non-linear least-squares curve fitting routine described in section 2.1.1. The parameters obtained following this curve fitting are shown in Table 31 and these parameters were used to represent the weighting function in the MAXENT process. The dose administered in each CR tablet was 95mg Metoprolol Succinate which was converted to μmoles prior to incorporation into the MAXENT process. The vector used to represent the unknown *in vivo* dissolution rate contained 150 elements each with a width of 0.2hrs.

The analysis was performed over a range of ICF widths for several subjects, for each CR tablet, to find the optimal value for the ICF width. For most subjects this was in the region of 0.8, therefore during the actual analysis the MAXENT process was run at four different ICF widths (0.3, 0.8, 1.5 and 3.5) for each subject and each tablet and the value of **logprob** at convergence was recorded. The predicted *in vivo* dissolution rate for the ICF which corresponded with the maximum value of **logprob** for that subject and that CR tablet was selected. In all except 5 cases this optimal value was 0.8, in 2 subjects the optimal value was 1.5 and in 3 subjects it was 0.3.

The output vector from MAXENT holds the fraction of dose released in each 0.2hr interval. The cumulative total from this vector was used to represent the cumulative fraction released profile and the dissolution rate itself was calculated by dividing each vector element by its width and multiplying by the dose administered.

### 7.1.2 Calculation of *In vitro* Dissolution Rate

The MAXENT method can not only be used to predict the *in vivo* dissolution rate of a CR tablet from the plasma concentrations following its administration, but can be adapted slightly to allow the prediction of *in vitro* dissolution rates from the cumulative fraction dissolved *in vitro*. This is done by representing the weighting function by unity, in which case the convolution equation becomes merely the integral of the *in vitro* dissolution rate (equation (7.1)) and this dissolution rate will be the output from the MAXENT process if the response function is the cumulative fraction released.

$$R(t) = \int_0^t I(\theta)\, d\theta \qquad (7.1)$$

Using this principal the *in vitro* dissolution rate was calculated from the *in vitro* dissolution data shown in Tables D(5)-D(7) using the same conditions as used for the *in vivo* analysis i.e. an ICF width of 0.8 and a vector of 150 elements each with a width of 0.2hrs to represent the *in vivo* dissolution rate.

### 7.1.3 Calculation of the Fraction of Dose Released, $F_R$

The fraction of the dose released at 30hrs was calculated by taking the maximum value reached in the cumulative fraction released (CFI) profile produced following the MAXENT process. This value was calculated for each subject and each CR tablet.

### 7.1.4 Calculation of Mean Dissolution Time *in vivo*, MDT

The MDT was calculated according to the method described in section 2.5.1 and was calculated according to equation (2.49) up to 30hrs and this Mean Dissolution Time ($MDT_{30}$) would be equal to the true MDT only if the release process had been completed by the 30hr interval.

## 7.2 RESULTS

### 7.2.1 *In vivo* Release Characteristics for Individual Subjects

The *in vivo* dissolution rate for each subject and each CR tablet was convolved using the parameters shown in Table 31 to represent the weighting function (oral solution data).

The parameters in Table 31 were used to generate values at 0.2hr intervals and these were used as input for equation (2.43) and these, together with the vector representing the *in vivo* dissolution rate were convolved produce an estimate of the plasma concentrations which would arise if the predicted dissolution rate were true.

Individual graphs were generated for each subject and each tablet to show the following information.

(a) The plasma concentrations following administration of the oral solution, shown in Table D(1) (Appendix D).

(b) The plasma profile predicted by the parameters (Table 31) obtained following curve fitting of the oral solution data for that subject.

(c) The plasma concentrations following administration of the CR tablet in question, CR A (Table D(2)), CR B(Table D(3)) or CR C(Table D(4)).

(d) The *in vivo* dissolution rate predicted by MAXENT.

(e) The *in vivo* CFI profile predicted by MAXENT.

(f) The estimated plasma concentrations, calculated from the *in vivo* dissolution rate predicted by MAXENT.

(g) The *in vitro* dissolution rate in pH 6.8 at 100rpm, predicted by MAXENT.

(h) The cumulative fraction dissolved *in vitro* at pH 6.8 and 100 rpm, shown in Tables D(5), D(6) and D(7).

One set of these individual graphs (subject 1) are shown in Figures 51-53 for CR A, CR B and CR C respectively, the remainder of the individual graphs are shown in Appendix E. Figure E(1)-E(10) show subjects 1-10 for metoprolol CR A, Figures E(11)-E(20) show subjects 1-10 for metoprolol CR B and Figures E(21)-E(30) show subjects 1-10 for metoprolol CR C.

In all subjects, examination of these Figures show that the parameters used to represent the solution data provide an accurate reflection of the true plasma concentrations and, in all tablets and all subjects (except subject 8, CR C) the plasma concentration profiles predicted from the *in vivo* dissolution rate produced by MAXENT are very close to the observed plasma concentrations for that subject and that tablet.

When the individual *in vivo* dissolution rates are examined for each tablet the

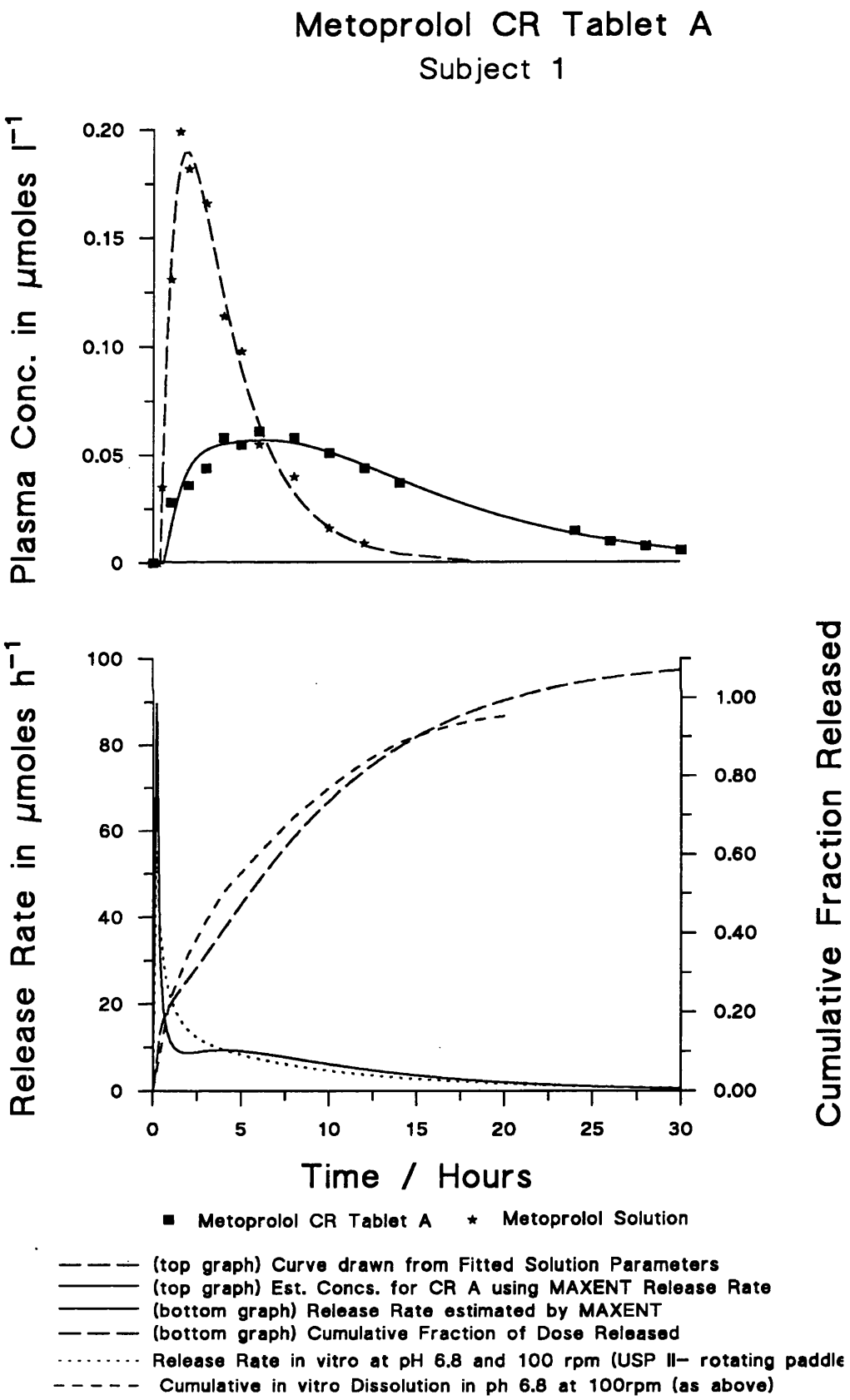


**Figure 51** : Results from MAXENT for Metoprolol CR A, Subject 1

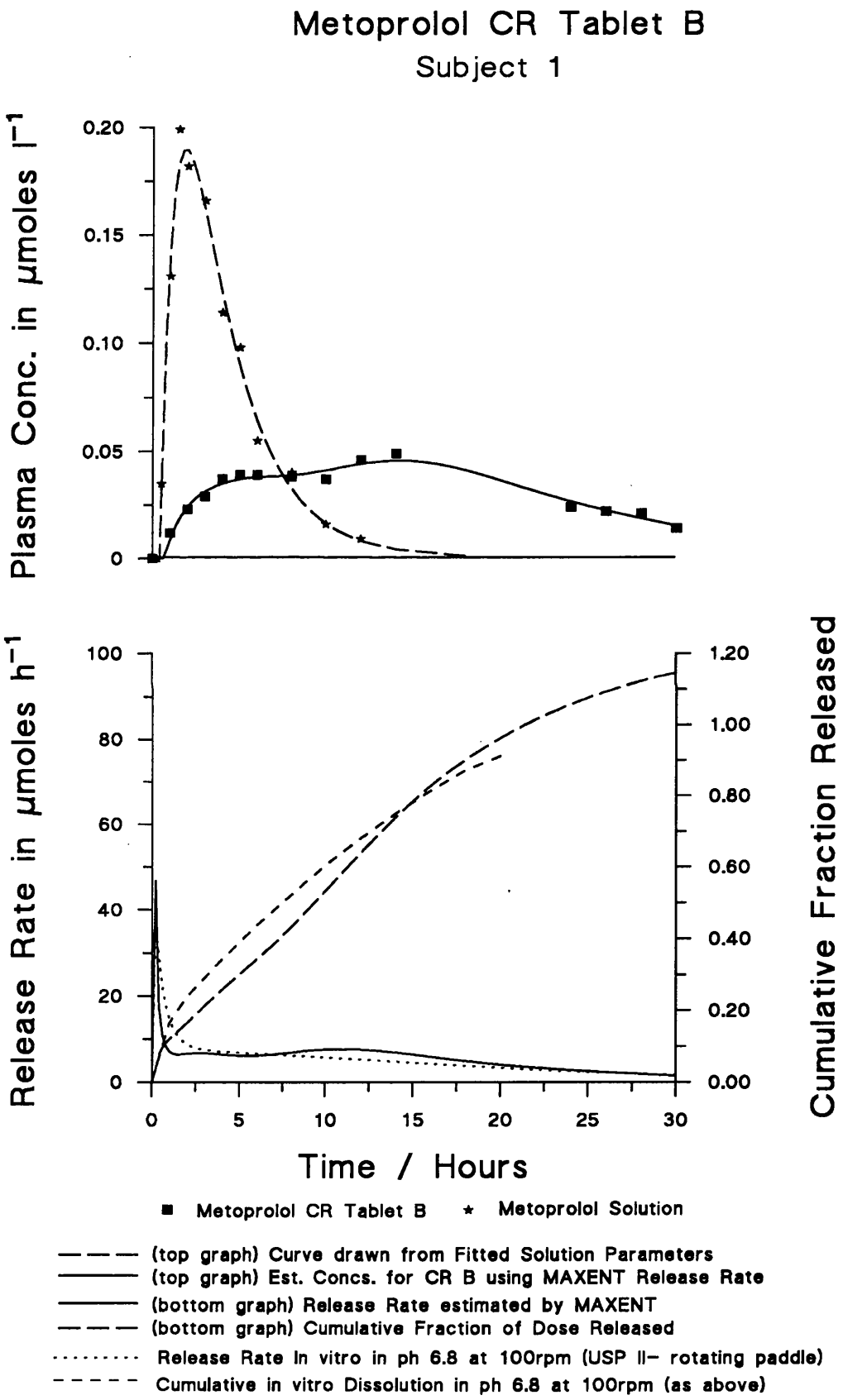


**Figure 52** : Results from MAXENT for Metoprolol CR B, Subject 1

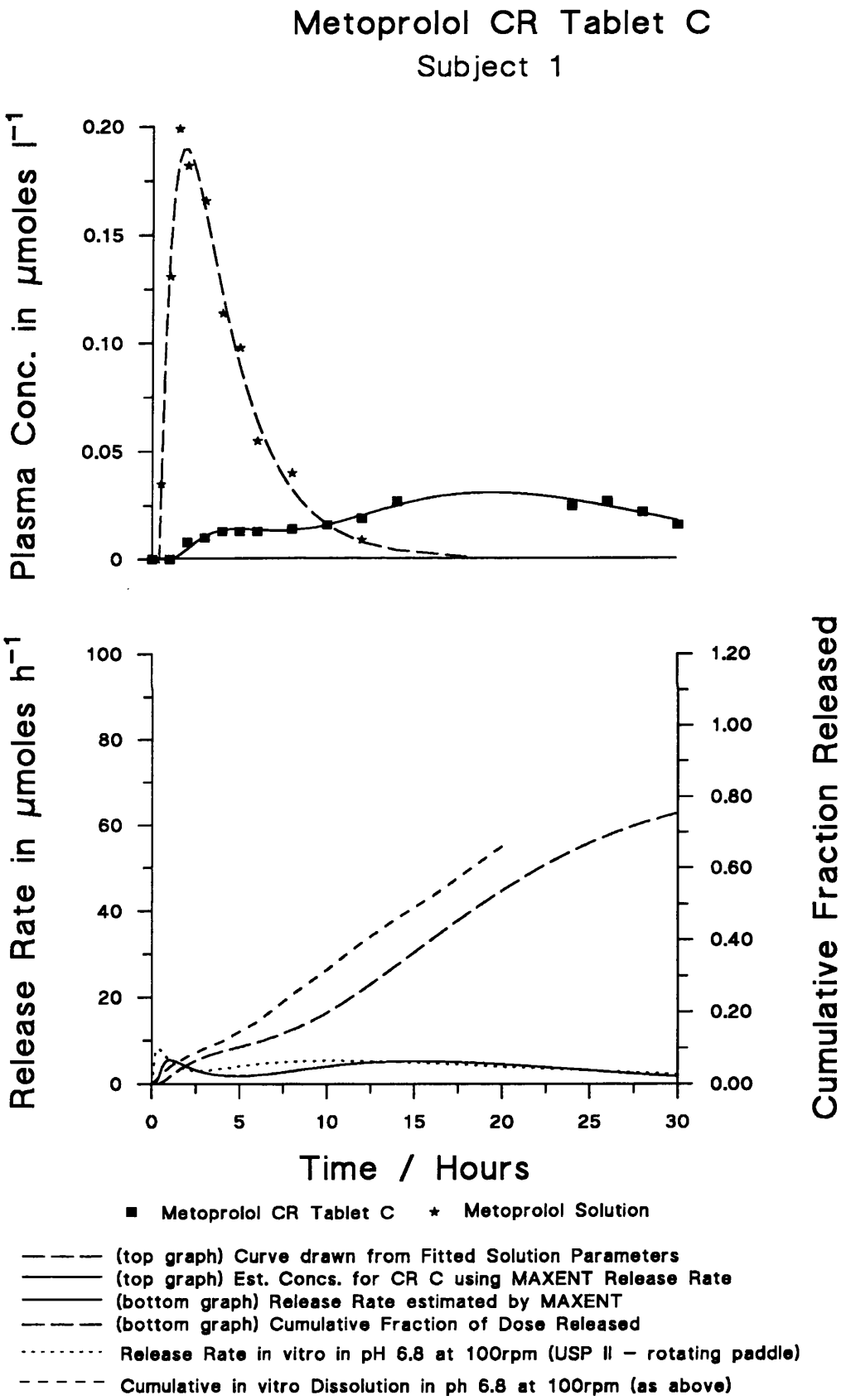


**Figure 53** : Results from MAXENT for Metoprolol CR C, Subject 1

following characteristics can be seen.

#### 7.2.1.1 Metoprolol CR A

All the subjects show a very similar pattern of release, in all cases there is an initial period of very rapid release which occurs in the first 0.5hrs. This is followed by a short period during which the release rate decreases which continues up until about the 5hr interval after which the release rate, in most subjects, becomes constant over the next 10hrs. In only one subject (subject 2) is this pattern not observed, and in this subject the initial spike of release is followed by an **increase** in rate before the gradual decline in rate, which in this subject continues instead of becoming constant.

In all the subjects, except subject 2, the release pattern seen *in vivo* is very similar to that shown *in vitro* (at pH 6.8 and 100rpm) but with the exception of subjects 1,8 and 10 the release rate seen *in vitro* is much more rapid than that seen *in vivo*. This is shown clearly by comparing the CFI profiles seen *in vitro* and *in vivo*.

#### 7.2.1.2 Metoprolol CR B

All the subjects show a similar pattern of release which comprises the initial spike of release during the first 0.5hrs (which was also seen in CR A) followed almost immediately by a period of constant release over the next 10-15 hours. In most subjects the rate of this release is about 5-10 μmoles $h^{-1}$, the only exceptions to this pattern are seen in subjects 2 and 6.

Subject 2 has no initial spike but this is replaced by a slightly broader peak which occurs between 0.5-1hr. There is no period of constant release seen in other subjects, instead the release rate declines gradually and ceases at about 15hrs.

In subject 6 the initial spike is very small and is superimposed on the broader peak seen in subject 2, which makes its presence hard to detect. Unlike subject 2, subject 6 does show the long period of steady release at the later time intervals.

In most subjects the fraction of dose released at 30hrs is in the region of 0.8, however for subjects 2 and 4 this value is substantially lower, ≈0.5. Like the CFI profiles seen in most subjects for CR A the fraction of dose released is always greater *in vitro* than *in vivo* (at equivalent times).

#### 7.2.1.3 Metoprolol CR C

The *in vivo* release pattern seen for CR C is much more consistent from subject to subject than those seen for CR A and B. The initial spike present in the profiles for CR A and CR B is not seen for CR C, either in the *in vitro* dissolution rate or in the *in vivo* dissolution rate, except for subject 6 where a small spike is present.

In all subjects the same pattern of release is seen both *in vivo* and *in vitro* and this profile is comprised of two parts. There is an initial period where a small peak in the release rate is seen during the first 4-5hrs, at the end of which the release rate is very low (1-2 μmoles $h^{-1}$). Following this the release rate begins to increase to ≈5-6 μmoles $h^{-1}$ and it remains constant at this level over the next 10-12 hours after which it begins to decrease.

In all subjects this pattern, although being the same as that seen *in vitro*, appears after about a 1hr time lag, only in subjects 4 and 6 is no time lag seen between the *in vivo* and *in vitro* dissolution rates.

The fraction of dose released for all subjects is always greater *in vitro* than *in vivo* at equivalent times.

### 7.2.2 Mean *in vivo* Dissolution Rates

The mean *in vivo* dissolution rate (n=10) for metoprolol CR tablets A,B and C together with the mean CFI profile for each tablet are shown in Figure 54. The following features of the *in vivo* dissolution rates for the different tablets can be seen from Figure 54.

The mean dissolution rates of CR A and CR B both show the initial spike of rapid release during the first 0.5-1hrs, this spike is not seen for CR C. During the first 10 hours, as would be expected, the rate of release of metoprolol from CR A > CR B > CR C. However after 10 hours this situation becomes reversed and the rate of release from CR C > CR B> CR A. As was seen in the individual graphs the release rate for CR C shows two distinct periods of release but no evidence of the initial spike. The release rate from CR B is largely constant from about 5-18 hours after which it decreases gradually. The mean dissolution rate for CR A shows no plateau of release but the decrease in the release rate is very slow and constant.

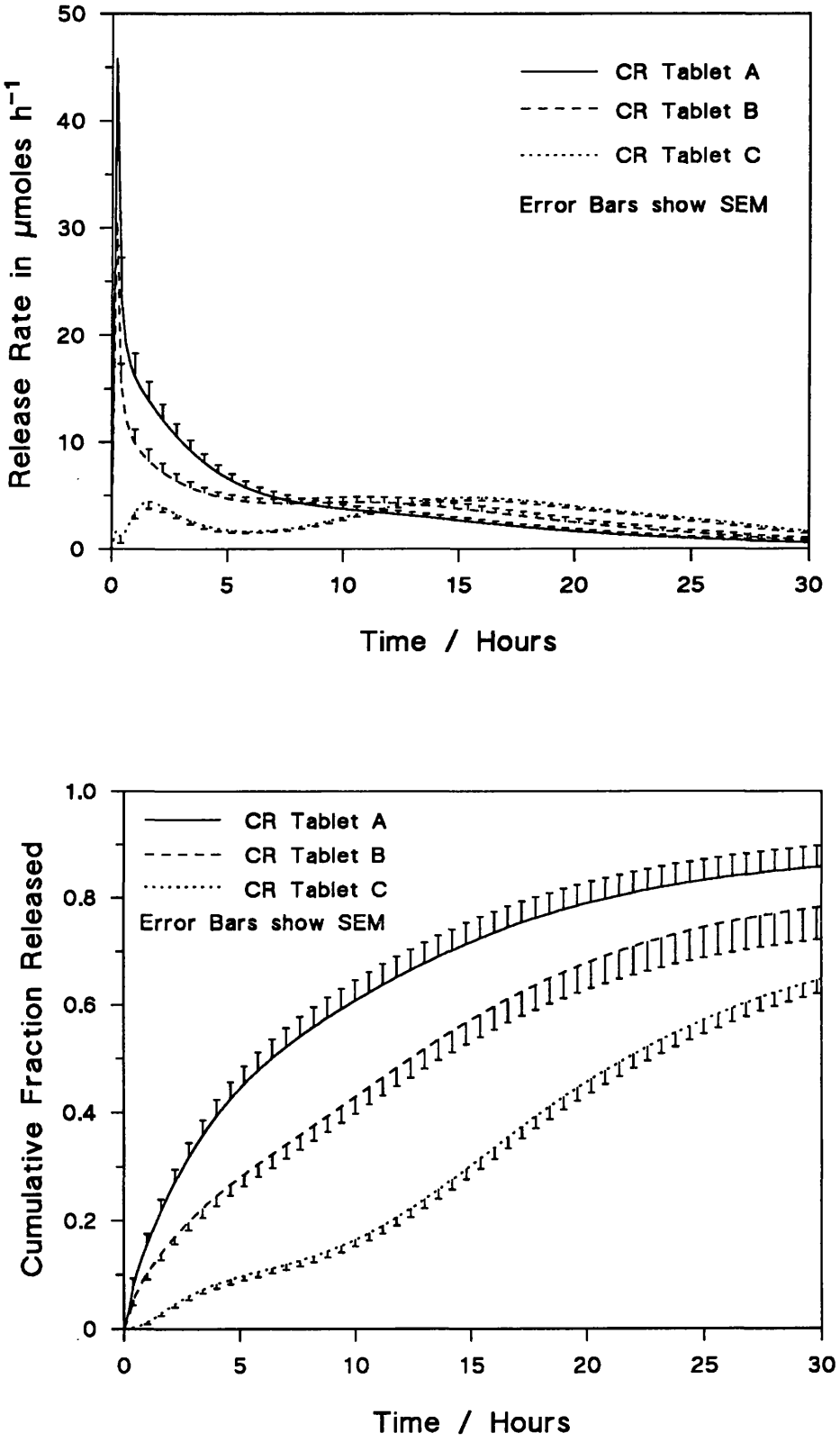


**Figure 54** : Mean Results (n=10) produced by MAXENT for Three Controlled Release Metoprolol 95mg Tablets

The mean CFI profiles for the three tablets are as would be expected, with the fraction of dose released (at all times) being greater for CR A than CR B than CR C. The inflexion seen in the profile for CR C arises from the period of very slow release seen for CR C around the 5 hour interval.

When the mean results shown in Figure 54 are compared with those produced by deconvolution of the same data (Figures 37-40) both similarities and differences can be seen in the results produced by different methods. The initial spike so prominent in the release rates predicted by MAXENT is shown only by the numerical and semi-numerical deconvolution algorithms and even for these, without the further confirmation provided by the MAXENT dissolution rates, it would probably be judged as an oscillation caused by the inherent instability of these methods.

All the methods show the correct ranking of the release rates of the formulations at the early time points and the reversal of this ranking at the later time points. However the definition of detail clearly seen in the MAXENT profiles is not seen by any of the deconvolution methods, especially the numerical and semi-numerical methods in which interpretation of any sort of fine detail is impossible. The distinct bipartite release rate of CR C is missed totally by the polyexponential deconvolution algorithm and its presence is only hinted at by the polynomial method.

When the mean CFI profiles produced by MAXENT (Figure 54) are compared with those produced by deconvolution (shown in Figures 37-40) the same macroscopic features can be seen. The CFI for CR A is always greater than that for CR B which in turn is always greater than that for CR C. The inflexion in the profile for CR C, so clearly seen in the MAXENT method, is also shown very well in the numerical and semi-numerical methods, less well by the polynomial method and not at all for the polyexponential method.

### 7.2.3 Estimated Fraction of Dose Released, $F_R$

The estimated fraction of dose released, calculated at 30hrs, for all subjects and all tablets are shown in Table 53 together with the mean, standard deviation (SD) and standard error of the mean (SEM).

| | Metoprolol CR Tablet | | |
|---|---|---|---|
| Subject | CR A | CR B | CR C |
| 1 | 1.07 | 1.15 | 0.75 |
| 2 | 0.79 | 0.53 | 0.70 |
| 3 | 0.86 | 0.90 | 0.67 |
| 4 | 0.76 | 0.49 | 0.49 |
| 5 | 0.69 | 0.76 | 0.66 |
| 6 | 0.94 | 0.80 | 0.64 |
| 7 | 0.77 | 0.70 | 0.67 |
| 8 | 0.97 | 0.87 | 0.58 |
| 9 | 0.76 | 0.76 | 0.61 |
| 10 | 0.99 | 0.88 | 0.74 |
| Mean | 0.86 | 0.78 | 0.65 |
| SD | 0.126 | 0.189 | 0.078 |
| SEM | 0.040 | 0.060 | 0.025 |

**Table 53 :** Estimated Fraction of Dose Released, $F_R$, in ten subjects, predicted for Three CR Metoprolol Tablets (CR A, CR B and CR C) by MAXENT

In order to test if there is any significant difference between the values of $F_R$ produced by MAXENT and those predicted by the four deconvolution algorithms used previously in chapter 4 to analyze the same data, a paired t-test (Sokal and Rohlf 1981d) was performed between the values of $F_R$ for MAXENT and those for each of the deconvolution methods (shown in Table 35). The test was performed separately for each controlled release tablet, CA A, CR B and CR C.

The paired t-test works on the principle that if the two samples to be tested belong to the same population then the differences between the $F_R$ value for each pair should

$$t_s = \frac{(\bar{F}_{diff} - 0)}{SEM_{F_{diff}}}$$

where $\bar{F}_{diff}$ = mean value of $F_{diff}$ (7.2)

$F_{diff} = (F_{R\ (MAXENT)} - F_{R\ (Deconvolution)})$

$SEM_{F_{diff}}$ = standard error of the mean of the $F_{diff}$ values

| | | $F_{diff} = F_{R\ (MAXENT)} - F_{R\ (Deconvolution)}$ | | | |
|---|---|---|---|---|---|
| Tablet | Subject | Numerical | Semi-Numerical | Polynomial | Poly-exponential |
| CR A | 1 | -0.31 | -0.32 | -0.27 | -0.30 |
| | 2 | -0.12 | -0.20 | -0.11 | -0.09 |
| | 3 | 0.05 | 0.05 | 0.16 | 0.12 |
| | 4 | -0.24 | -0.33 | -0.26 | -0.22 |
| | 5 | 0.04 | -0.01 | 0.06 | -0.01 |
| | 6 | -0.37 | -0.31 | -0.27 | -0.08 |
| | 7 | -0.14 | -0.13 | -0.05 | -0.09 |
| | 8 | -0.35 | -0.42 | -0.31 | -0.41 |
| | 9 | -0.22 | -0.22 | -0.11 | -0.14 |
| | 10 | -0.27 | -0.29 | -0.22 | -0.29 |
| Mean | | -0.19 | -0.22 | -0.14 | -0.15 |
| SD | | 0.149 | 0.149 | 0.158 | 0.156 |
| SEM | | 0.047 | 0.047 | 0.050 | 0.049 |
| CR B | 1 | 0.14 | 0.03 | 0.07 | 0.05 |
| | 2 | -0.05 | -0.08 | -0.02 | -0.03 |
| | 3 | -0.04 | -0.01 | 0.07 | 0.21 |
| | 4 | 0.02 | -0.03 | 0.02 | 0.07 |
| | 5 | 0.05 | 0.00 | 0.04 | 0.02 |
| | 6 | -0.06 | -0.03 | 0.02 | -0.03 |
| | 7 | -0.03 | -0.02 | 0.03 | 0.00 |
| | 8 | 0.02 | -0.04 | 0.06 | 0.00 |
| | 9 | -0.03 | -0.03 | 0.06 | 0.03 |
| | 10 | 0.00 | -0.02 | 0.03 | 0.03 |
| Mean | | 0.00 | -0.02 | 0.038 | 0.035 |
| SD | | 0.060 | 0.028 | 0.028 | 0.069 |
| SEM | | 0.019 | 0.009 | 0.009 | 0.022 |
| CR C | 1 | 0.04 | 0.04 | 0.06 | 0.05 |
| | 2 | 0.04 | 0.02 | 0.04 | -0.03 |
| | 3 | 0.03 | 0.04 | 0.10 | 0.11 |
| | 4 | 0.00 | -0.05 | 0.03 | 0.04 |
| | 5 | 0.09 | 0.07 | 0.06 | 0.07 |
| | 6 | 0.02 | 0.02 | 0.03 | -0.02 |
| | 7 | -0.02 | -0.02 | 0.04 | 0.05 |
| | 8 | -0.04 | -0.08 | -0.06 | -0.10 |
| | 9 | -0.04 | -0.04 | 0.02 | 0.03 |
| | 10 | 0.00 | -0.03 | 0.07 | 0.04 |
| Mean | | 0.01 | 0.00 | 0.04 | 0.02 |
| SD | | 0.040 | 0.048 | 0.042 | 0.059 |
| SEM | | 0.013 | 0.015 | 0.013 | 0.019 |

**Table 54 :** Calculated $F_{diff}$ values, in ten subjects, predicted for Three CR Metoprolol Tablets (CR A,CR B and CR C) by MAXENT.

form a normal distribution with a mean of zero, this forms the null hypothesis for the paired t-test. The differences between the values of each pair are calculated and their mean compared with the expected value (zero) according to the formula shown in equation (7.2).

The difference, $F_{diff}$, calculated between the $F_R$ values produced by MAXENT and those produced by each of the deconvolution algorithms (Table 35) are shown in Table 54, together with the mean, SD and SEM of the $F_{diff}$ values. The values of $t_s$ calculated for each tablet and each method are shown in Table 55.

| | Deconvolution Method | | | |
|---|---|---|---|---|
| Tablet | Numerical | Semi-Numerical | Polynomial | Poly-exponential |
| CR A | -4.09 ** | -4.62 ** | -2.77 * | -3.06 * |
| CR B | 0.11 ns | -2.57 * | 4.26 ** | 1.60 ns |
| CR C | 0.94 ns | -0.20 ns | 2.94 * | 1.28 ns |
| ns = not significant * $P \leq 0.05$ ** $P \leq 0.01$ *** $P \leq 0.001$ | | | | |

**Table 55 :** Values of the $t_s$ statistic, calculated for a Paired t-test between the values of $F_R$ produced by MAXENT and those Produced by Four Deconvolution Methods

Although the differences in the mean $F_R$ values produced by MAXENT and the four deconvolution algorithms appear very small (see Table 56), they have been shown to be significant, in some cases, by the paired t-test.

| | Mean $F_R$ Value | | | | |
|---|---|---|---|---|---|
| Tablet | MAXENT | Numerical Deconvolution | Semi-Numerical Deconvolution | Polynomial Deconvolution | Poly-exponential Deconvolution |
| CR A | 0.86 | 0.84 | 0.87 | 0.79 | 0.80 |
| CR B | 0.78 | 0.78 | 0.81 | 0.75 | 0.75 |
| CR C | 0.65 | 0.64 | 0.65 | 0.61 | 0.63 |
| Values for MAXENT taken from Table 53, other values from Table 35 | | | | | |

**Table 56 :** Mean $F_R$ values predicted for Three Metoprolol CR Tablets by MAXENT and Four Deconvolution Algorithms.

There appears to be no pattern between either the deconvolution methods or the CR tablets and the presence of a significant difference between the mean $F_R$ values. The only trend seems to be that the difference becomes more significant for the more rapidly released tablets (CR A and CR B) and the differences produced with the polynomial deconvolution method are always significant.

### 7.2.4 Mean Dissolution Time, $MDT_{30}$

The $MDT_{30}$ at 30hrs calculated for each subject and each CR tablet are shown in Table 57 together with the mean (n=10), standard deviation (SD) and standard error of the mean (SEM) for each CR tablet.

| | Metoprolol CR Tablet | | |
|---|---|---|---|
| Subject | CR A | CR B | CR C |
| 1 | 7.62 | 11.24 | 14.96 |
| 2 | 5.51 | 4.86 | 14.99 |
| 3 | 9.07 | 11.05 | 14.42 |
| 4 | 9.20 | 10.34 | 14.56 |
| 5 | 4.39 | 8.51 | 14.51 |
| 6 | 6.82 | 9.32 | 13.42 |
| 7 | 8.81 | 12.01 | 16.67 |
| 8 | 5.96 | 9.14 | 16.43 |
| 9 | 8.34 | 11.80 | 17.52 |
| 10 | 6.89 | 8.60 | 14.05 |
| Mean | 7.26 | 9.69 | 15.15 |
| SD | 1.636 | 2.130 | 1.296 |
| SEM | 0.517 | 0.674 | 0.410 |

**Table 57 :** Estimated Mean Dissolution Time / hours, $MDT_{30}$, in ten subjects, predicted for Three CR Metoprolol Tablets (CR A, CR B and CR C) by MAXENT

To test if there is any significant difference between the values of $MDT_{30}$ produced by MAXENT and those predicted by the four deconvolution algorithms used previously in chapter 4 to analyze the same data, a paired t-test (Sokal and Rohlf 1981d) was performed between the values of $MDT_{30}$ for MAXENT and those for each of the

| | | $MDT_{diff} = MDT_{30\ (MAXENT)} - MDT_{30\ (Deconvolution)}$ | | | |
|---|---|---|---|---|---|
| Tablet | Subject | Numerical | Semi-Numerical | Polynomial | Poly-exponential |
| CR A | 1 | 0.29 | 0.29 | -0.04 | -0.28 |
| | 2 | 0.11 | -0.90 | 0.82 | 0.91 |
| | 3 | 4.99 | 5.04 | 4.38 | 4.23 |
| | 4 | 0.52 | -0.15 | -0.26 | -0.46 |
| | 5 | 1.36 | 0.42 | 1.08 | 1.17 |
| | 6 | -1.53 | 0.05 | -0.16 | 0.48 |
| | 7 | -0.11 | 0.20 | 0.23 | 0.41 |
| | 8 | 0.15 | -0.29 | 0.29 | 0.59 |
| | 9 | 0.37 | 0.26 | 0.43 | 1.30 |
| | 10 | -0.06 | -0.02 | 0.02 | 0.39 |
| Mean | | 0.61 | 0.49 | 0.67 | 0.87 |
| SD | | 1.697 | 1.643 | 1.367 | 1.305 |
| SEM | | 0.537 | 0.519 | 0.432 | 0.413 |
| CR B | 1 | 0.50 | 0.18 | 0.06 | -0.18 |
| | 2 | -0.44 | -0.95 | 0.02 | -0.19 |
| | 3 | -0.11 | 0.28 | -0.09 | -0.34 |
| | 4 | 0.52 | -0.10 | 0.03 | -0.45 |
| | 5 | 0.57 | 0.05 | 0.16 | 0.26 |
| | 6 | -0.73 | 0.31 | 0.22 | 0.56 |
| | 7 | 0.31 | 0.52 | 0.34 | 0.48 |
| | 8 | 0.22 | -0.14 | 0.22 | 0.10 |
| | 9 | 0.55 | 0.46 | 0.34 | 0.64 |
| | 10 | 0.17 | 0.07 | -0.11 | -0.29 |
| Mean | | 0.16 | 0.07 | 0.12 | 0.06 |
| SD | | 0.449 | 0.419 | 0.162 | 0.404 |
| SEM | | 0.142 | 0.133 | 0.051 | 0.128 |
| CR C | 1 | 0.68 | 0.48 | 1.09 | 0.26 |
| | 2 | 0.66 | 0.55 | 1.26 | 0.04 |
| | 3 | 0.30 | 0.53 | 1.02 | 0.08 |
| | 4 | 0.83 | 0.39 | 0.04 | 0.47 |
| | 5 | 0.21 | 0.11 | 0.77 | -0.13 |
| | 6 | 0.22 | 0.45 | 0.13 | -0.05 |
| | 7 | 0.66 | 0.78 | 0.65 | 0.72 |
| | 8 | 2.45 | 2.29 | 1.87 | 2.13 |
| | 9 | 1.03 | 0.98 | 0.59 | 0.94 |
| | 10 | 1.31 | 1.14 | 0.57 | 0.29 |
| Mean | | 0.84 | 0.77 | 0.80 | 0.48 |
| SD | | 0.668 | 0.611 | 0.541 | 0.674 |
| SEM | | 0.211 | 0.193 | 0.171 | 0.213 |

**Table 58 :** Calculated $MDT_{diff}$ values for 10 subjects, predicted for Three CR Metoprolol Tablets (CR A,CR B and CR C) by MAXENT.

deconvolution methods (shown in Table 37). The test was performed separately for each controlled release tablet, CA A, CR B and CR C.

The test was performed using the formula given in equation (7.2) only in this case replacing $F_{diff}$ with $MDT_{diff}$, where $MDT_{diff}$ is the difference between $MDT_{30}$ predicted by MAXENT and $MDT_{30}$ predicted by one of the four deconvolution methods. The $SEM_{F_{diff}}$ will therefore become $SEM_{MDT_{diff}}$, the standard error of the mean for $MDT_{diff}$ values. The difference, $MDT_{diff}$, calculated between the $MDT_{30}$ values produced by MAXENT and those produced by each of the deconvolution algorithms (Table 37) are shown in Table 58, together with the mean, SD and SEM of the $MDT_{diff}$ values. The values of $t_s$ calculated for each tablet and each method are shown in Table 59.

| | Deconvolution Method | | | |
|---|---|---|---|---|
| Tablet | Numerical | Semi-Numerical | Polynomial | Poly-exponential |
| CR A | 1.13 ns | 0.94 ns | 1.57 ns | 2.12 ns |
| CR B | 1.10 ns | 0.51 ns | 2.32 * | 0.46 ns |
| CR C | 3.95 ** | 3.98 ** | 4.67 ** | 2.23 ns |
| ns = not significant * $P \leq 0.05$ ** $P \leq 0.01$ *** $P \leq 0.001$ | | | | |

**Table 59 :** Values of the $t_s$ statistic, calculated for a Paired t-test between the values of $MDT_{30}$ produced by MAXENT and those Produced by Four Deconvolution Methods

Unlike the $F_R$ values there appears to be a trend in the difference between the $MDT_{30}$ values produced for the MDT values, and this trend in the significance lies with the tablets and not with the methods. For the faster released tablets, CR A and CR B, there is no significant difference between the results produced by MAXENT and the different deconvolution methods, except for the polynomial result for which the significance was border line ($P_{0.05(9)}$) = 2.26.

However for the slower released tablet, CR C, the difference between the MDT predicted by MAXENT and the deconvolution algorithms becomes significant for all methods, except for the polyexponential method. As was shown in Chapter 6, this overestimation may have been due to the use of too high a ICF width.

### 7.2.5 *In vivo - in vitro* Correlation

#### 7.2.5.1 $MDT_{in\ vivo}$ vs $_{in\ vitro}$ Correlation

The mean *in vivo* MDT values (shown in Table 57) were plotted against the MDT *in vitro* values for different dissolution conditions (shown in Table 39). For each set of values plotted the gradient, Y intercept and correlation coefficient were calculated and these are shown in Table 60 for each set of dissolution conditions.

| | Dissolution Conditions | | | |
|---|---|---|---|---|
| | pH 1.2/100rpm | pH 4.0/100rpm | pH 6.8/100rpm | pH 6.8/50 rpm |
| Gradient | 0.9075 | 0.9978 | 0.9392 | 0.94636 |
| Y Intercept | 2.5934 | 1.3205 | 2.0285 | 1.7419 |
| r | 0.9935 | 0.9960 | 0.9920 | 0.9983 |
| r = XY correlation coefficient | | | | |

**Table 60 :** Parameters obtained following Linear Regression of $MDT_{in\ vivo}$ (produced by MAXENT) against $MDT_{in\ vitro}$ for Three Metoprolol CR Tablets

The critical value for the correlation coefficient, r, for n=3 (1 degree of freedom) is 0.997 for P=0.05, the only set of dissolution conditions which give a value of r greater than 0.997 is pH 6.8 at 50 rpm which shows a significant correlation between $MDT_{in\ vivo}$ and $MDT_{in\ vitro}$. The correlations shown for the other dissolution conditions are not significant, at the 95% probability level.

When these results are compared to those produced by the deconvolution methods (Table 40) it can be seen that whilst the MDT values produced by MAXENT gave a good correlation for only one set of dissolution conditions all the deconvolution algorithms gave significant correlation for all *in vitro* dissolution conditions. The discrepancy between these two results can be explained by the significant difference between the values of the MDT predicted by MAXENT for CR C and those predicted by the deconvolution methods. The MDT for CR C predicted by MAXENT is significantly larger than those produced by the deconvolution methods, and this change in the MDT value provides a poorer $MDT_{in\ vivo}$ - $MDT_{in\ vitro}$ correlation.

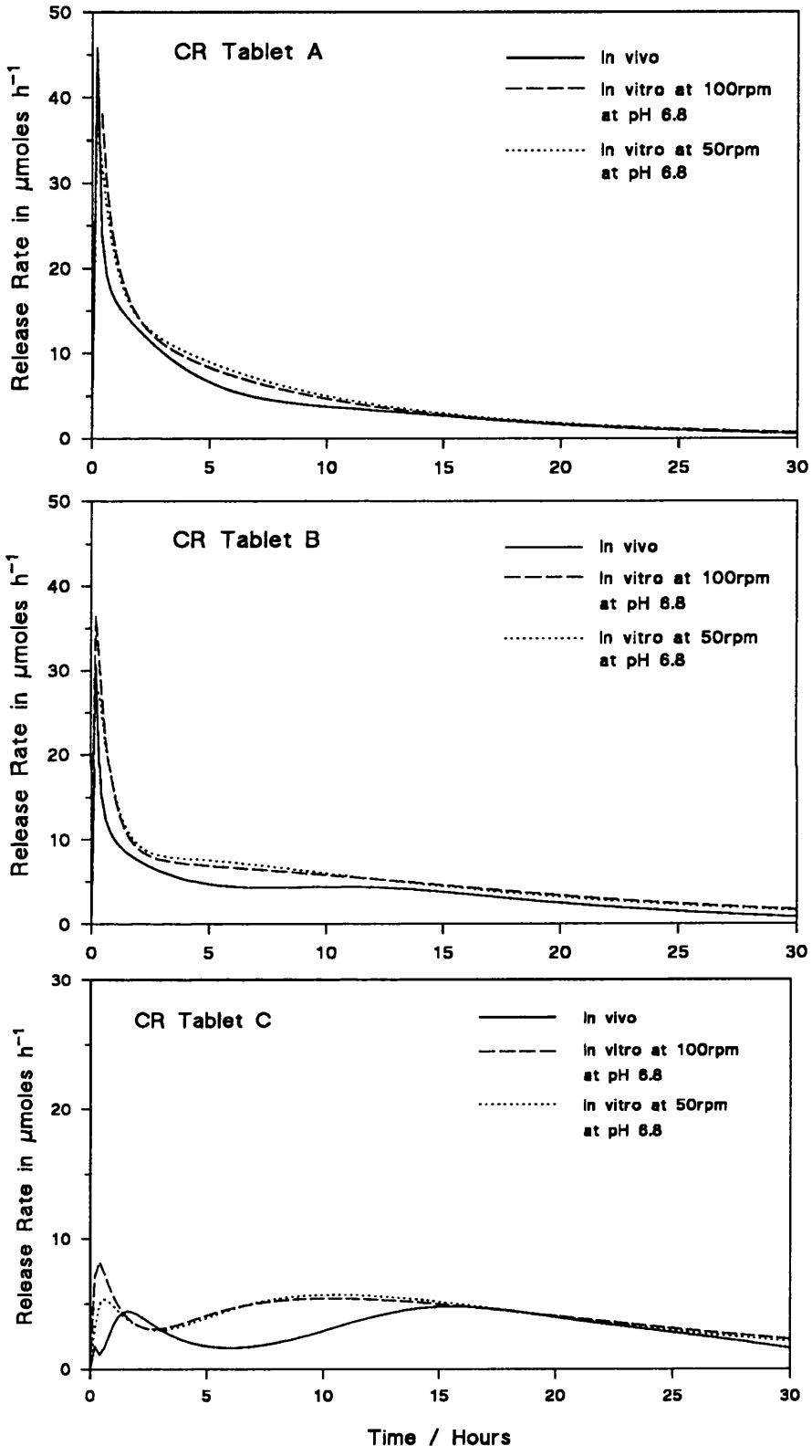


**Figure 55** : Mean *in vivo* (n=10) and *in vitro* (n=6) Dissolution Rates produced by MAXENT for Three Controlled Release Metoprolol 95mg Tablets

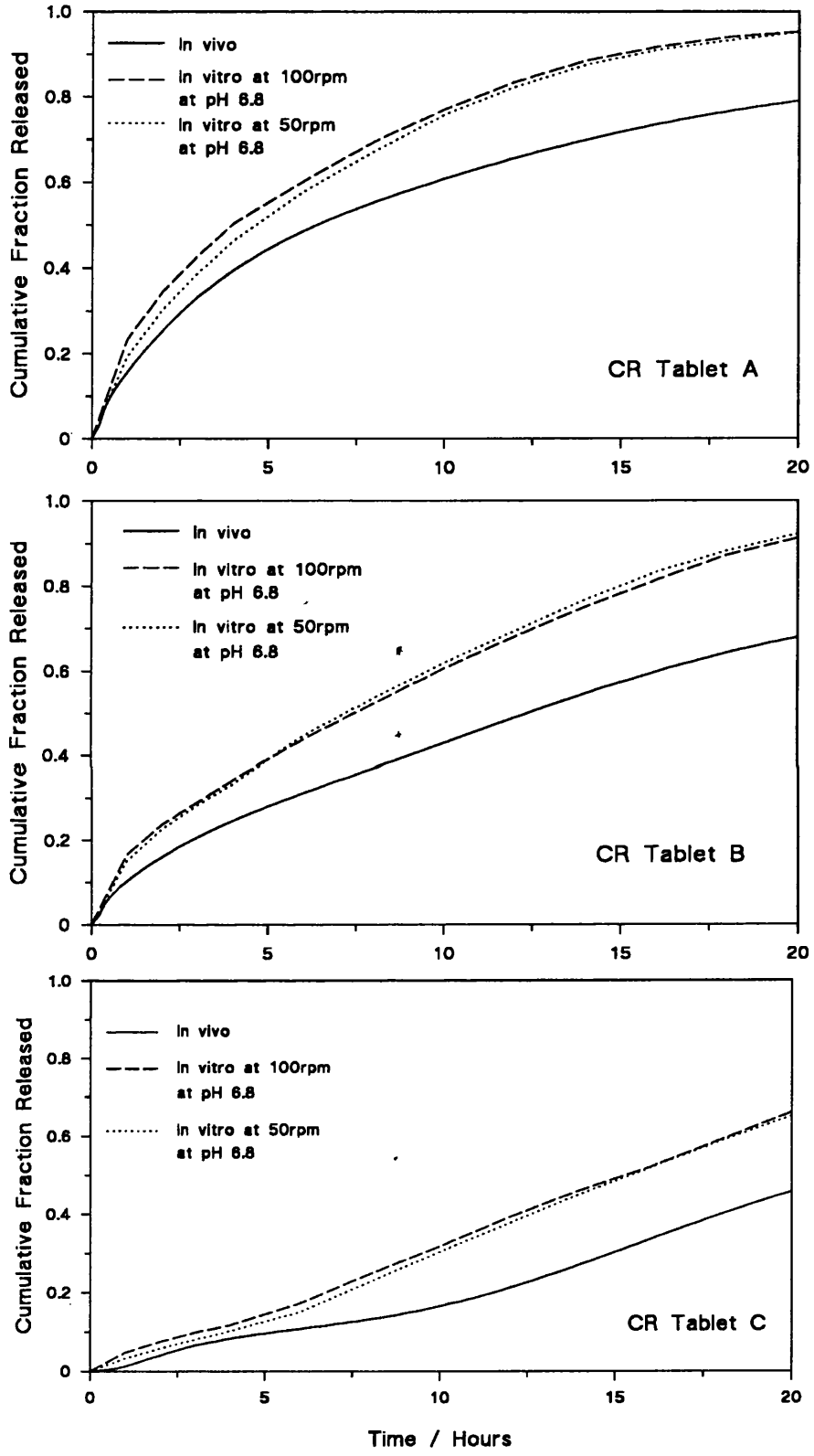


**Figure 56** : Mean *in vivo* (n=10) CFI profiles produced by MAXENT and mean *in vitro* (n=6) CFI profiles for 3 Controlled Release Metoprolol 95mg Tablets

### 7.2.5.2 Comparison of *In vivo* and *In vitro* Dissolution Rates

The mean *in vivo* dissolution rates predicted by MAXENT for each tablet (shown at the top of Figure 54) were plotted against the *in vitro* dissolution rates, predicted by MAXENT, for two sets of dissolution conditions, pH 6.8 at 100rpm and pH 6.8 at 50rpm. These dissolution rates are shown for all CR tablets in Figure 55.

In can be seen from Figure 55 that there is little difference between the dissolution rate predicted for the two *in vitro* conditions in any of the three tablets. There is also a very good parallel between the *in vivo* and *in vitro* dissolution rates for CR tablets A and B, the *in vivo* dissolution rate being very similar in shape but having a slower rate of dissolution than either *in vitro* dissolution rate. The *in vivo* dissolution rate predicted for CR C is similar is shape to both *in vitro* dissolution rates but shows a clearer bipartite nature than either and passes through the same phase of its profile about one hour after the *in vitro* dissolution rates.

The mean CFI profiles produced by MAXENT (shown at the bottom of Figure 54) for the three CR tablets were plotted together with the *in vitro* cumulative dissolution data (Tables D(5)-D(7)) for two sets of dissolution conditions, pH 6.8 at 100rpm and pH 6.8 at 50rpm. These are shown for all three CR tablets in Figure 56.

In can be seen from Figure 56 that the CFI's produced by the two *in vitro* dissolution conditions are very similar to each other for each tablet. It can also be seen that the CFI *in vivo* is very similar in shape to the CFI *in vitro* for each CR tablet, but is always much lower, reflecting the lower dissolution rate *in vivo*. The inflexion seen in the CFI *in vivo* for CR C is also seen *in vitro*, but it occurs earlier and is not quite as pronounced.

## 7.3 DISCUSSION

The *in vivo* dissolution rates predicted by the MAXENT method for the three metoprolol CR tablets are all realistic, smooth and show good agreement with the *in vitro* dissolution rates, as shown in Figure 55. The MAXENT method also shows that it has no difficulty in coping with sudden changes in the dissolution rate as can be seen by the sharp peaks present in the *in vivo* dissolution rate for most subjects for CR A and CR B.

The *in vivo* dissolution rates are realistic in the sense that when they are convolved with the parameters representing the solution data, the estimated plasma concentrations

agree very well with the true values following administration of each tablet.

The macroscopic features seen in the *in vivo* dissolution rates are very similar to those shown by the four deconvolution algorithms, all show similar shapes for the dissolution rate as a function of time, all show the initial rapid release from tablets CR A and CR B, all show the dissolution still continuing at 30 hours for CR C and all show the reversal in the ranking of the dissolution rates for the tablets at later time points. However, the MAXENT method shows the *in vivo* dissolution rates in much finer detail than is managed by any of the deconvolution methods, enabling the form of the dissolution rate profile to be seen more easily and more clearly. This is a major advantage possessed by the MAXENT method for predicting *in vivo* release rates, when compared with the four deconvolution algorithms.

The differences between the $F_R$ values estimated by MAXENT and those estimated by the deconvolution methods showed no strong trend in their significance either among tablets or among methods, and although some differences were shown to be significant, the mean $F_R$ values for all the methods were very similar for equivalent tablets.

The mean $F_R$ values were again all less than one suggesting incomplete release from the tablets, especially from CR C. As has been stated previously (section 4.7) this could be due to the rate of drug release affecting the rate of drug metabolism, and thereby violating the assumption of linearity, and not actually incomplete release.

The differences between the MDT estimated by MAXENT and those estimated from the deconvolution algorithms show no trend in significance from method to method, but do show a clear trend from tablet to tablet. There is a significant difference seen for CR C between the mean MDT estimated from MAXENT and that estimated from the deconvolution algorithms.

The MDT calculated by MAXENT is significantly greater than those calculated by deconvolution and it is this difference which causes the correlation between $MDT_{in\ vivo}$ and $MDT_{in\ vitro}$ to become less significant (for all *in vitro* conditions) than for the deconvolution methods.

This higher value of MDT for CR C could be due to the use of too high an ICF width in the MAXENT program, but without the comparison of this MDT value with those produced by deconvolution, which suggested the MDT was too large, there would

have been no reason to suspect the value had been overestimated. This suggests that one disadvantage to the use of MAXENT is the question of how to find the best possible choice of the ICF width, especially when the **logprob** vs ICF plot shows a broad peak indicating no clear optimal ICF value.

## 7.4 CONCLUSIONS

The aim of this chapter was to highlight any problems to the use of MAXENT in a practical situation, and in the case of the metoprolol data only one real problem was encountered and that was the choice of the ICF width. This led to the following conclusions

- When the **logprob** vs ICF width plot shows a broad peak, indicating that the optimal ICF is not clearly one particular value, then the choice of ICF width must be made with care. If the ICF is too large then the estimated value for MDT may be too high, and for this reason the smallest possible ICF should be selected, without a large fall in the **logprob** value.

- The other conclusion apparent from this chapter is that the MAXENT process produces an *in vivo* dissolution rate profile which is smooth and provides a detailed picture of the form of the dissolution rate, in this respect the MAXENT method has shown itself to be superior to the deconvolution methods. The MAXENT method can also cope with very rapid changes in the dissolution rate without any loss of clarity.

# 8 GENERAL DISCUSSION AND CONCLUSIONS

## 8.1 GENERAL DISCUSSION

The overall aim of the work presented was to be able, at the end, to shed some light on the advantages and disadvantages of different methods of assessing the *in vivo* delivery rate from oral dosage forms, and to find which method of those assessed, gives the optimal results. The methods assessed were all those which could provide information about the whole time course of the delivery process, but which could also differentiate between the *in vivo* drug release and absorption rates. These methods included four different deconvolution algorithms and the Maximum Entropy approach.

The methods were assessed in various ways, firstly using pseudo-experimental data and a variety of different hypothetical release rates, they were tested for both their stability to data noise and their ability to predict the correct release rate. Following this, the methods were assessed on their performance when faced with actual clinical data to analyze.

Since detailed discussions about each point of the assessment have been given at the end of each chapter, and also at the end of sections within each chapter, the aim of this general discussion is to bring together these separate points and to present a clear, concise overview of the results presented.

### 8.1.1 Stability to Data Noise

Of the four deconvolution algorithms, their stability to data noise, found during the assessment, is as would be expected from consideration of the underlying principles of each method. The numerical method (a simple algorithm which makes no assumption as to the form of the underlying input rate) was very susceptible to the presence of noise in the source data and at the higher noise levels provided no useful information about the **rate** of drug release, and even the mean (n=10) rate showed a poor reflection of the true input rate.

The semi-numerical deconvolution algorithm (which also makes no assumptions about the form of the unknown input rate) was expected to be more stable to data noise due to prior smoothing of the weighting function by curve fitting. For none of the different input

functions tested was this shown to be so, in fact, no improvement was seen for the semi-numerical over the numerical method in any of the situations tested, either visually or by any of the statistical comparisons used.

The polynomial and polyexponential algorithms were shown, in all cases, to be very stable to data noise. There was little change seen in their predicted input rate profiles with increasing levels of noise. This is as would be expected since both the polynomial and polyexponential methods represent the unknown input rate using an empirical function.

The Maximum Entropy method also proved to be very stable to the presence of noise in the source data. However, unlike the polynomial and polyexponential methods, this stability does not derive from the policy of representing the input rate by an empirical function. In fact, the Maximum Entropy method imposes no structure upon the input function, except that it must vary smoothly and be non-negative.

If the choice of algorithm merely depended on the stability to data noise, then this choice would be one of the complex methods, either the polynomial or polyexponential deconvolution algorithms or the Maximum Entropy method.

### 8.1.2 The Input Rate Profiles

The picture for the prediction of the correct input rate profiles is more complex than that seen for the levels of added noise. The best method for estimating the delivery rate for error free data, is undoubtedly, the numerical deconvolution method. However, this is not a practical choice, since the experimental data will never be error free, and at the higher levels of error both the numerical and semi-numerical methods show a very poor ability to predict the correct input rate profiles.

Of the two other deconvolution methods, neither showed an ideal approximation to the true input rates at the higher noise levels, especially for the more complex input functions (b) and (c), and both methods had problems in coping with rapid changes in the input rate, but despite this, the polynomial method in particular gave a good reflection of the general shape of the unknown input functions.

The ability of the Maximum Entropy method to predict the true input rate at high noise levels was superior, for the more complex input functions, to any shown by the

deconvolution methods. It was, strangely, not as good for the simple monoexponential input function, which was best approximated by the polynomial method. The poor approximation is thought to be due to the choice of too high an ICF width in the MAXENT program and if the experiment were repeated with a lower ICF width a different result might be seen.

The choice of method from consideration of their ability to produce the correct input rate must be either the polynomial deconvolution method or the Maximum Entropy method, but for the more complex input functions the Maximum Entropy method is the method of choice.

### 8.1.3 Cumulative Fraction Input (CFI) Profiles

It is much more difficult to discriminate between the different methods when the CFI profiles are compared. All the methods, for all the different input functions, give very reasonable approximations to the true CFI profiles. The polynomial and polyexponential deconvolution methods and the Maximum Entropy method do give better profiles than the numerical and semi-numerical methods, but the improvement is from a very good approximation to an excellent approximation. However, the increase in complexity of these methods is hardly balanced by the degree of improvement in the CFI profiles.

### 8.1.4 Fraction of Dose Released, $F_R$

In none of the situations tested was any significant difference seen between the values of $F_R$ produced by the different methods and the true values of $F_R$, either for the deconvolution or Maximum Entropy methods.

### 8.1.5 Mean Dissolution Time, MDT

The only deconvolution method to show no significant difference between the calculated MDT values for the method and the true values was the numerical deconvolution method. The other deconvolution methods all gave a significant difference ($P < 0.05$, in some cases $P < 0.01$) for the MDT values produced for the controlled release

input rate. This difference probably arises from the poor approximation of the true input rate over its period of rapid change.

The MDT values for the Maximum Entropy approach are always significantly different to the true values for all the different input functions considered. However the mean values of the MDT, for the more complex input functions, are only about 2.5% higher than the true values and for the controlled release input function are very close to the values produced by the numerical deconvolution method, which showed no significant difference to the true values. The value of the SEM associated with the mean MDT produced by the Maximum Entropy method (for the controlled release input function) is so small that it is this lack of variation in the predicted MDT which causes the difference to become significant.

From consideration of the $F_R$ and MDT values the choice of method should be the numerical deconvolution method which despite of (or may be because of) its simplicity produces equivalent if not superior results to the more complex methods.

### 8.1.6 Analysis of Metoprolol Data

The sections above, far from clarifying the best choice of method for the assessment of drug delivery, appear to present conflicting answers to the question. Consideration of one aspect leads to one choice and consideration of a second to another, but which is right? A consideration of the performance of the different methods in the analysis of clinical data may aid the decision. The analysis of the metoprolol data gave the following practical considerations to the choice of which of the five methods to use.

Perhaps the most important finding was that the MAXENT method gave a realistic, very detailed *in vivo* dissolution rate profile which showed the same attributes as seen in the *in vitro* dissolution rate profiles, and this could not be claimed by any of the deconvolution methods tested. The profiles produced by polynomial and polyexponential deconvolution, while not providing such fine detail as the MAXENT method, did show the general features of the dissolution rate seen in the profiles predicted by MAXENT.

The CFI profiles produced by all methods, showed little difference, as would be expected from the work done with pseudo-experimental data, and little basis for

differentiation of the different methods can be made on consideration of these profiles alone.

A comparison, by a Model 1 - two way ANOVA, of the mean (n=10) $F_R$ values produced by the four deconvolution methods showed no variation of this value among the different deconvolution methods. However, a comparison of the $F_R$ values (n=10) produced by MAXENT with those produced by deconvolution (using a paired t-test) showed some significant differences between the $F_R$ values, but no obvious trend in significance either between different methods or between different tablets. Despite the significance of some of the differences seen, the mean $F_R$ values produced by MAXENT were very close in value to those produced by the four deconvolution methods. Therefore a consideration of the $F_R$ values does not show the superiority of any one method.

A comparison, by a Model 1 - two way ANOVA, of the mean (n=10) MDT values produced by the four deconvolution algorithms (like that for the $F_R$ values) showed no significant variation of the MDT values between the four deconvolution methods. However, in this case a trend was observed in the differences between the values of MDT produced by MAXENT and those produced by deconvolution. The values of MDT produced by MAXENT for CR C were significantly different to the same values produced by deconvolution ($P \leq 0.01$ for the paired t-test) for three of the four deconvolution methods.

When the $MDT_{in\ vivo}$ values are considered from the perspective of the quality of *in vivo - in vitro* correlation they provide (when plotted against the $MDT_{in\ vitro}$) it was shown that the MDT values produced by all the deconvolution algorithms provided excellent *in vivo - in vitro* correlation for all the *in vitro* dissolution conditions. The $MDT_{in\ vivo}$ values produced by MAXENT provided a satisfactory *in vivo - in vitro* correlation for only one set of *in vitro* dissolution conditions, and this deterioration in the quality of correlation is due to the significantly higher MDT value produced by MAXENT for CR C.

One other practical problem was encountered, and this was the presence of a time-lag in the solution data. The polyexponential algorithm makes no allowance for the existence of a time-lag in the data to be used for the weighting function, and this could preclude the use of this method in a practical situation if the time-lag is large. For the metoprolol

data ignoring this time-lag made no discernable difference in the results produced by the polyexponential method.

It would seem from consideration of the analysis of the metoprolol data that the MAXENT method is, by far, superior to any other method in its ability to give a detailed description of the *in vivo* dissolution process. It is also the only method which can provide a visual comparison of the *in vivo* and *in vitro* dissolution **rates.**

However the numerical deconvolution method is the best choice for the calculation of $F_R$ and MDT, it also gives one of the best *in vivo* - *in vitro* correlations from the MDT values. Since this method is as good as the more complex methods at predicting these values, but is numerically simpler to implement, it becomes the best choice for the calculation of the $F_R$ and MDT values, and for *in vivo* - *in vitro* correlation.

**Considering the analysis of both the pseudo-experimental and real data, the choice of the optimal method for assessment of drug delivery *in vivo* must depend on the end objective of the assessment itself.**

### 8.1.7 Some Other Observations

One observation that was apparent was that throughout all the work presented, there was always a high degree of differentiation seen between the input/dissolution rates produced by the different methods. Once these rates had been integrated, most of the detail apparent in the rate profiles was lost during the integration process. This is one reason why despite the obviously large discrepancies seen between the input/dissolution rates produced by the different methods, there is often no statistical difference seen when the $F_R$ or MDT values are compared for the different methods. Both of these point values involve some form of integration (hence the loss of detail), the $F_R$ value is calculated directly from the integral of the input/dissolution rate and the MDT involves evaluation of integrals in both its numerator and denominator.

To obtain a better comparison, which does not rely on visual inspection, of the different deconvolution and Maximum entropy methods, some statistical comparison of the actual input rate prior to integration is needed. The chi-square value for goodness of

fit would give the same kind of qualitative comparison as the percentage differences did, but since the chi-square test can only be used on frequency distributions it could not be used quantitatively.

Another observation which arises from the analysis of the metoprolol data is that interpretation of *in vivo* dissolution rates should be treated with care and the possibility of the violation of linearity should be considered, especially when an oral solution is being used for the weighting function. In this case there will a positional difference between the site of the weighting function and the site of the response function during the later times of the analysis, which may be the cause of loss of linearity.

Violation of linearity could occur if there is no absorption from the distal regions of the GI tract, in which case lack of absorption will appear as lack of release. This cannot have been true for the metoprolol since it is absorbed equally as well throughout the GI tract (Godbillon et al 1985). Another possibility is that the rate of release from the dosage form may affect the rate of metabolism of the drug, this may apply especially for those drugs which have extensive first pass metabolism, as was suggested for the metoprolol CR tablets (Sandberg et al 1991) and this would manifest as incomplete release from the dosage form.

However, these possibilities should be considered during the interpretation of the *in vivo* drug delivery rate produced by both the deconvolution and the Maximum Entropy methods.

## 8.2 SUGGESTIONS FOR FURTHER WORK

Throughout the work using pseudo-experimental data, only one equation has been used to represent the weighting function ($W(t) = -2e^{-10t} + e^{-5t} + e^{-t}$). This was done to enable the comparison of the predicted input rates to be performed without any consideration of the influence of the weighting function on that predicted input rate.

It is possible that both the shape of the weighting function and the relative magnitudes of the exponents used, as well as the number of terms in the weighting function, may have some effect on the ability of the different methods to predict the correct values for the input function. An assessment of the numerical deconvolution

algorithm (Chan et al 1987) using different ratios of absorption and release rates showed that only when there was a large difference between the absorption and release rate did the method give poor results for error free data. However, this assessment needs to be extended to the other deconvolution methods as well as the Maximum Entropy method and extended to assess their ability to cope with varying forms of weighting functions, focusing not only on the ratios between the absorption and release rates, but also on the ratios between the other exponents present in the weighting function.

Although three different forms of input function were used to test the methods presented, the range is by no means exhaustive and testing further forms of input function may show a continuing superiority for one method, by its ability to cope successfully with a wide range of input functions.

The methods have been assessed throughout for their ability to predict release rates, and while many of the deconvolution methods have been assessed (at least individually) for their ability to predict absorption rates there has been little assessment of the Maximum Entropy method, either using clinical or pseudo-experimental data. Assessment of the Maximum Entropy method for this ability, especially by comparison with the deconvolution methods, would provide a better overall picture of the capabilities of this method.

The assessment of drug delivery by these methods could prove to be a useful tool when trying to study *in vivo* delivery together with transit through the GI tract. With the additional knowledge of the weighting data, the *in vivo* rate of release or absorption can be calculated and this could be correlated with the position of the dosage form within the GI tract, as estimated by such techniques as gamma-scintigraphy.

One other suggestion for further work, is the influence of the ICF width on both the actual rate, $F_R$ and MDT values calculated for the MAXENT method. It has been shown that the MAXENT method often overestimates the MDT value, and that this could be due to a poor choice of ICF width. This occurs especially when the optimum choice of ICF is not clearly one value and some freedom exists for the user to impose their own choice of value.

Work needs to be done not only on the influence of the choice of ICF width on the predicted input rate but also on ways in which the best possible ICF width can be selected without a "try and see" approach.

## 8.3 CONCLUSIONS

In the introduction it was established that the nature of controlled release products is such that their quality, in essence, depends upon their ability to maintain their desired pattern of drug release *in vivo*, and because of this an effective method of monitoring that release rate *in vivo* is required. Ideally this method should be able, provided with the right information, to differentiate between the processes of drug release and drug absorption, it should also be able to provide information about the whole time course of the release/absorption process.

Both the Maximum Entropy and the deconvolution methods satisfy both of these requirements, but their proposed use raised other problems, which in turn gave rise to the objectives given at the end of chapter 1. The wide variety of deconvolution algorithms, of varying complexity, presents a bewildering choice to "would be" users of deconvolution, and it was the aim of the work presented here to narrow that choice to the method which best fits their requirements.

If the desired outcome of the assessment of drug delivery is to obtain information about the release process itself as a function of time, (eg in a situation where it is important to verify that the release itself is zero order) then the best possible choice of method is that of Maximum Entropy. The Maximum Entropy method is both stable to data noise and has shown its ability, when tested, to predict correctly the release rates tested. It has also been shown to provide, in a practical situation, a detailed, realistic profile of the *in vivo* dissolution rate as a function of time, and is the only method which can be used to provide an estimation of the *in vitro* dissolution rate from the cumulative *in vitro* data, enabling a visual comparison of the *in vivo* and *in vitro* dissolution rates.

If the aim of the assessment of drug delivery is to provide an *in vivo - in vitro* correlation using MDT values then the method of choice is the numerical deconvolution algorithm, which provides accurate values with the minimum of computation. The numerical deconvolution algorithm remains the method of choice if the desired result of

the assessment is the cumulative fraction released as a function of time, or merely the final fraction released, $F_R$. Although the profiles produced by numerical deconvolution are not the best, the increase in complexity inherent in the other methods is not compensated by a corresponding increase in accuracy of the CFI profiles, leaving the numerical algorithm the best choice.

Practically speaking care should be taken in the interpretation of the *in vivo* release rates produced using solution data to represent the weighting function, because of the positional change in the point of input within the GI tract during the later time periods. Any violation of linearity will not be apparent from the sole use of deconvolution or Maximum Entropy.

It has been suggested (Breimer 1989) that the concept of controlled release is too often associated with zero order release and that for some drugs a pulsatile or time-programmed delivery may be required to provide an optimal clinical effect. For these systems the delivery process will become even more complex and more critical to the quality of the dosage form. For these sophisticated products a sophisticated means of assessing their drug delivery will be required.

The Maximum Entropy approach is the most sophisticated method currently available for the assessment of drug delivery as a function of time. It has the advantage over the deconvolution algorithms of possessing both stability to data noise (seen by those methods which represent the unknown input rate by empirical functions) and the ability to impose no structure on the unknown input rate (seen in those deconvolution methods which are susceptible to data noise), therefore providing the best of both worlds. Added to this, it provides a detailed, realistic and, in most cases, accurate picture of the required release rate *in vivo*, and despite the problem of selecting the optimal ICF width, the method could prove to be the method of choice in the future when controlled release dosage forms become ever more sophisticated and knowledge of their *in vivo* release rates is essential.

# REFERENCES

Boxenbaum, H. 1988. Commentary to "Linear System Approaches in pharmacokinetics: How much do they have to Offer I General Considerations", *J. Pharmacokinetics and Biopharm.*, 16, 672-681.

Boxenbaum, H.G., Riegelman, S. and Elashoff, R.M. 1973 Statistical Estimations in Pharmacokinetics, *J. Pharmacokinetics and Biopharm.*, 2, 123-148.

Breimer, D.D. 1989. Drug Delivery and Therapeautics in the Future, *Novel Drug Delivery and its Therapeutic Application*, (eds.) L.F.Prescott and W.S.Nimmo, John Wiley & Sons Ltd, 353-355.

Bretthorst, G.L. 1990. An Introduction to Parameter Estimation Using Bayesian Probability Theory, *Maximum Entropy and Bayesian Methods*, 53-79, (ed.) P.F.Fougère, Kluwer Academic Publishers.

Chan, K.K.H., Langenbucher, F. and Gibaldi, M. 1987. Evaluation of *In vivo* Drug Release by Numerical Deconvolution using Oral Solution Data as Weighting Function, *J. Pharm. Sci.*, 76, 446-450.

Charter, M.K. 1990. Drug Absorption in Man, and its Measurement by MaxEnt, *Maximum Entropy and Bayesian Methods*, 325-339, P.F.Fougère (ed.), Kluwer Academic Publishers.

Charter, M.K. 1991. Quantifying Drug Absorption, *Maximum Entropy and Bayesian Methods*, (in print), (ed.) W.T.Grandy, Kluwer Academic Publishers.

Charter, M.K. and Gull, S.F. 1987. Maximum Entropy and its Application to the Calculation of Drug Absorption Rates, *J. Pharmacokinetics and Biopharm.*, 15, 645-655.

Chiou, W.L. 1980. New Compartmental and Model Independent Method for Rapid Calculation of Drug Absorption Rates, *J. Pharm. Sci.*, 69, 57-62.

Cox, R,T. 1946 Probability, Frequency and Reasonable Expectation, *American Journal of Physics*, 14, 1-13.

Cutler, D.J. 1978a Numerical Deconvolution by Least Squares, Use of Prescribed Input Functions, *J. Pharmacokinetics and Biopharm.*, 6, 227-241.

Cutler, D.J. 1978b Numerical Deconvolution by Least Squares. Use of Polynomials to Represent the Input Function *J. Pharmacokinetics and Biopharm.*, 6, 243-263.

Cutler, D.J. 1978c. Linear Systems Analysis in Pharmacokinetics *J. Pharmacokinetics and Biopharm.*, 6, 265-282.

Cutler, D.J. 1986 Assessment of Rate and Extent of Drug Absorption, *Pharmacokinetics : Theory and Methodology*, 369-406 eds. M.Rowland and G.T.Tucker, Pergamon Press.

Cutler, D.J. 1987. Definition of Mean Residence Times in Pharmacokinetics *Biopharm. and Drug Disp.*, 8, 87-97.

Firsov, A.A. and Piotrovskii, V.K. 1986a. Methods for Estimating Drug Bioavailability Parameters. Part 2. Methods for Estimating Absorption Rate, *Die Pharmazie*, 41, 369-377.

Firsov, A.A. and Piotrovskii, V.K. 1986b. Methods for Estimating Drug Bioavailability Parameters. Part 3. Peculiarities of Pharmacokinetic Analysis in Assessment of Bioavailability, *Die Pharmazie*, 41, 457-465.

Gillespie, W.R. and Veng-Pederson, P. 1985a. The Determination of Mean Residence Time using Statistical Moments. It is Correct. *J. Pharmacokinetics and Biopharm.*, 1985, 13 549-554.

Gillespie, W.R. and Veng-Pederson, P. 1985b. A Polyexponential Deconvolution Method. Evaluation of "Gastrointestinal Bioavailability" and Mean *in vivo* Dissolution Time of some Ibuprofen Dosage Forms, *J. Pharmacokinetics and Biopharm.*, 13, 289-307.

Godbillon, J., Evard, D., Vidon, N., Duval, M., Schoeller, J.P, Bernier, J.J and Hirtz, J. 1985. Investigation of Drug Absorption from the Gastrointestinal Tract of Man. III Metoprolol in the Colon, *Br. J. Clin. Pharmac.*, 19, 1135-1185.

Gull, S.F. 1989. Developements in Maximum Entropy Data Analysis, *Maximum Entropy and Bayesian Methods*, 53-71, J.Skilling (ed.), Kluwer Academic Publishers.

Gull, S.F. and Skilling. J. 1984. Maximum Entropy Method in Image Processing, *IEE Proc 131F*, 646-659.

Iga, K., Ogawa, Y., Yashiki, T. and Shimamoto, T. 1986 Estimation of Drug Absorption Rates Using a Deconvolution Method with Non-Equal Sampling Times, *J. Pharmacokinetics and Biopharm.*, 14, 213-225.

Jaynes, E.T. 1983. *Papers on Probability, Statistics and Statistical Physics*, 210-314, (ed.)R.D.Rosenkrantz, D.Riegel, Dordrect.

Kendall, M.J., Brown, D., Grieve, A. and John, V.A. 1977. Pharmacokinetic and Pharmacodynamic Studies of Single Oral Doses of Metoprolol in Normal Volunteers, *Eur. J. Drug Metab. and Pharmacokinetics*, 2, 73-80.

Langenbucher, F. 1982. Numerical Convolution/Deconvolution as a Tool for Correlating *in vitro* with *in vivo* Drug Availability, *Pharm. Ind.*, 44, 1166-1172.

Langenbucher, F. and Möller, H. 1983a. Correlation of *in vitro* Drug Release with *in vivo* Response Kinetics. Part I. Mathematical Treatment of Time Functions, *Pharm. Ind.*, 45, 623-628.

Langenbucher, F. and Möller, H. 1983b. Correlation of *in vitro* Drug Release with *in vivo* Response Kinetics. Part II. Use of Function Parameters, *Pharm. Ind.*, 45, 629-633.

Langenbucher, F. and Mysicka, J 1985. *In vitro* and *in vivo* Deconvolution Assessment of Drug Release Kinetics from Oxprenolol Oros Preparations, *British J. of Clinical Pharmacology*, 19, 151S - 162S.

Loo, J.C.K. and Riegelman, S. 1968. New Method for Calculating the Intrinsic Absorption of Drugs, *J. Pharm. Sci.*, 57, 918-916.

Louis, T.A. 1991. Using Empirical Bayes Method in Biopharmaceutical Research, *Statistics in Medicine*, 10, 881-829.

Metzler, C.M. 1988. Commentary to "Linear and Non-Linear System Approaches. How much do they have to Offer? II The Response Mapping Operator" *J. Pharmacokinetics and Biopharm.*, 16, 682-694.

Nicklasson, M., Ellstrom, K., Sjoquvist, R. and Sjovall, J. 1984 Linear Systems Analysis and Moment Analysis in the Evaluation of Bacampicillin Bioavailability from Microcapsule Suspensions, *J. Pharmacokinetics and Biopharm.*, 12, 467-478.

Press, W., Flannery, B., Teukolsky, S. and Vetterling, W. 1988a. *Numerical Recipes in C : The Art of Scientific Computing*, 540-547, Cambridge University Press.

Press, W., Flannery, B., Teukolsky, S. and Vetterling, W. 1988b. *Ibid.*, 28-45, Cambridge University Press.

Press, W., Flannery, B., Teukolsky, S. and Vetterling, W. 1988c. *Ibid.*, 528-539, Cambridge University Press.

Press, W., Flannery, B., Teukolsky, S. and Vetterling, W. 1988d, *Ibid*, 94-98, Cambridge University Press.

Press, W., Flannery, B., Teukolsky, S. and Vetterling, W. 1988e. *Ibid.*, 528-538, Cambridge University Press.

Press, W., Flannery, B., Teukolsky, S. and Vetterling, W. 1988f, *ibid.*, 279-282, Cambridge University Press.

Regårdh, C. and Johnsson, G. 1980. Clinical Pharmacokinetics of Metoprolol, *Clin. Pharmacokinetics*, 5, 557-569.

Rescigno and Segre 1966. *Drug and Tracer Kinetics*, 1966, Blaisdell, Waltham, Mass.

Riegelman, S. and Collier, P. 1980. The Application of Statistical Moment Theory to the Evaluation of *in vivo* Dissolution Time and Absorption Time, *J. Pharmacokinetics and Biopharm.*, 8, 509-534.

Rohlf, F.J. and Sokal, R.R. 1981. *Statistical Tables, 2nd Edition*, W.H. Freeman and Co., New York.

Sandberg, A., Abrahamsson, B. and Sjögren, J. 1991. Influence of Dissolution Rate on the Extent and Rate of Bioavailability of Metoprolol, *Int. J. Pharmaceutics*, 68, 167-177.

Sandberg, A., Ragnarsson, G., Jonsson, U.E. and Sjögren, J. 1988. Design of a New Multiple-Unit Controlled-Release Formulation of Metoprolol - Metoprolol CR, *Eur. J. Clin. Pharmacol.*, 33 Suppl S3-S7.

Saunders, L. and Natunen, T. 1973. A Stable Method for Calculating Oral Drug Absorption Rate Constants with Two Compartment Disposition, *J. Pharm. Pharmacol.*, 25, 44p-51p.

Shannon, C.E. 1948. *Bell System Journal*, 27, 379-623, Reprinted in C.E.Shannon and W.Weaver, The Mathematical Theory of Communication, University of Illinois Press, Urbana, 1949.

Siegel, R.A. 1988. Commentary to "Linear and Non-Linear System Approaches. How much do they have to offer? I General Considerations", *J. Pharmacokinetics and Biopharm.*, 16, 667-672.

Silverman, M. and Burden, A. 1961. *Journal Appl. Physiol.*, 16, 911.

Skilling, J. 1989. Classic Maximum Entropy, *Maximum Entropy and Bayesian Methods*, 45-52, J.Skilling (ed.), Kluwer Academic Publishers.

Smolen, V.F. 1976a. Theoretical and Computational Basis for Drug Bioavailability Determinations using Pharmacological Data. I. General Considerations and

Procedures, *J. Pharmacokinetics and Biopharm.*, 4, 337-353.

Smolen, V.F. 1976b. *ibid.* II. Drug Input ⇔ Response Relationships, *J. Pharmacokinetics and Biopharm.*, 4, 355-375.

Sokal, P.R. and Rohlf, F.J. 1981a. *Biometry*, W.H.Freeman & Co, New York, 174-175.

Sokal, P.R. and Rohlf, F.J. 1981b. *Biometry*, W.H.Freeman & Co, New York, 321-344.

Sokal, P.R. and Rohlf, F.J. 1981c. *Biometry*, W.H.Freeman & Co, New York, 402-412.

Sokal, P.R. and Rohlf, F.J. 1981d. *Biometry*, W.H.Freeman & Co, New York, 359.

Tanigawara, Y., Yamaoka, K., Nakagawa, T. and Uno, T. 1982 New Method for the Evaluation of *in vitro* Dissolution Time and Disintergration Time, *J. Chem. Pharm. Bull.*, 30, 1088-1090.

Thron, C.D. 1974. Linearity and Superposition in Pharmacokinetics, *Pharmacol. Review*, 26, 3-31.

Tucker, G.T. 1983 The Determination of *in vivo* Absorption Rates, *Acta Pharmaceutica Technologica*, 29, 159-164

Tucker, G.T. and Jackson, P.R. 1989. Pharmacokinetic Evaluation of Novel Delivery Systems: Assessment of Rate, *Novel Drug Delivery and its Therapeutic Application*, 1989, 113-120, eds. L.F.Prescott and W.S.Nimmo, John Wiley & Sons Ltd.

Vajda, S., Godfrey, K. and Valko, P. 1988. Numerical Deconvolution Using System Identification Methods, *J. Pharmacokinetics and Biopharm.*, 16, 85-107.

Vaughan, D.P. 1981. Approximations in Point-Area Deconvolution Algorithm as Mathematical Basis of Empirical Instantaneous Mid-Point Input Deconvolution Method, *J. Pharm. Sci.*, 70, 831-832.

Vaughan, D.P. and Dennis, M. 1978. Mathematical Basis of Point-Area Deconvolution

Method for Determining *in vivo* Input Functions, *J. Pharm. Sci.*, 67, 663-665.

Vaughan, D.P. and Dennis, M. 1980. Mathematical Basis and Generalisation of the Loo-Riegelman Method for the Determination of *in vivo* Drug Absorption, *J. Pharmacokinetics and Biopharm.*, 8,83-98.

Veng-Pederson, P. 1980a. Model-Independant Method of Analysing Input in Linear Pharmacokinetic Systems having Polyexponential Impulse Response. I. Theoretical Analysis, *J. Pharm. Sci.*, 69, 298-304.

Veng-Pederson, P. 1980b. Model Independant Method of Analysing Input in Linear Systems having Polyexponential Impulse Response. II. Numerical Evaluation, *J. Pharm. Sci.*, 69, 305-312.

Veng-Pederson, P. 1980c. An Algorithm and Computer Program for Deconvolution in Linear Pharmacokinetics, *J. Pharmacokinetics and Biopharm.*, 8, 463-481.

Veng-Pederson, P. 1980d. Novel Deconvolution Method for Linear Pharmacokinetic Systems with Polyexponential Impulse Response, *J. Pharm. Sci.*, 69, 312-318.

Veng-Pederson, P. 1981. Pharmacokinetic Analysis by Linear System Approach. I. Cimetidine Bioavailability and Second Peak Phenomenon, *J. Pharm. Sci.*, 70, 32-38.

Veng-Pederson, P. 1988a. Linear and Non-Linear System Approaches in Pharmacokinetics: How much do they have to offer. I. General Considerations, *J. Pharmacokinetics and Biopharm.*, 16, 413-473.

Veng-Pederson, P. 1988b. Linear and Non-Linear System Approaches in Pharmacokinetics: How much do they have to Offer II. The Response Mapping Operator (RMO) Approach, *J. Pharmacokinetics and Biopharm.*, 16, 543-571.

Veng-Pederson, P. and Gillespie, W.R. 1988. A System Approach to Pharmacodynamics. I. Theoretical Framework, *J. Pharm. Sci.*. 77, 39-47.

Veng-Pederson, P. and Tillman, L.G. 1989. Centre of Gravity of Drug Level Curves: A

Model-Independent Parameter useful in Bioavailability Studies, *J. Pharm. Sci.*, 78, 848-854.

Verotta, D. 1989 An Inequality-constrained Least-Squares Deconvolution Method, *J. Pharmacokinetics and Biopharm.*, 17, 269-289.

Wagner, J.G. and Nelson, E. 1963. Per Cent Absorbed Time plots derived from Blood Level and/or Urinary Excretion Data, *J. Pharm. Sci.*, 52, 610-611.

Wagner, J.G. 1974. Application of the Wagner-Nelson Absorption Method to the Two-compartment Open Model, *J. Pharmacokinetics and Biopharm.*, 2, 469-486.

Wagner, J.G. 1975. Application of the Loo-Riegelman Absorption Method, *J. Pharmacokinetics and Biopharm.*, 3, 51-67.

Wagner, J.G. 1988. Types of Mean Residence Times, *Biopharm. and Drug Disp.*, 9, 41-57.

Yamaoka, K., Nakagawa, T. and Uno, T. 1978. Statistical Moments in Pharmacokinetics, *J. Pharmacokinetics and Biopharm.*, 6, 547-558.

Yeh, K.C. and Kwan, K.C. 1978. A Comparison of Numerical Integrating Algorithms by Trapeziodal, Lagrange and Spline Interpolation, *J. Pharmacokinetics and Biopharm.*, 6, 79-98.

# APPENDIX A :

## DERIVATION OF AN EQUATION FOR THE RESPONSE FUNCTION WHEN THE INPUT FUNCTION IS REPRESENTED BY A POLYNOMIAL AND THE WEIGHTING FUNCTION BY A POLYEXPONENTIAL

The convolution integral can be written as follows :

$$R(t) = \int_0^t W(t-\theta) I(\theta)\, d\theta$$

where $W(t)$ = Weighting Function $I(t)$ = Input Function

and $R(t)$ = Response Function

Convolution Integral (A.1)

If the Laplace transform of the convolution integral is taken then equation (A.1) can be expressed by the following equation in which R(s) is the Laplace transform of the Response function R(t), W(s) is the Laplace transform of the Weighting function W(t) and I(s) is the Laplace transform of the Input function I(t).

$$R(s) = W(s)\, I(s)$$

The Laplace Transform of the Convolution Integral (A.2)

When the Weighting function is represented by a polyexponential as shown in equation (A.3), where $A_i$ and $\alpha_i$ are constants and D is the dose administered to produce the weighting function, and the Input function is represented by a polynomial as shown in equation (A.4) where $C_j$ are constants and t=time, then the response function can be evaluated by Laplace transformation.

$$W(t) = \frac{1}{D} \sum_{i=1}^{n} A_i\, e^{-\alpha_i t}$$

Weighting Function Represented by a Polyexponential (A.3)

$$I(t) = \sum_{j=0}^{m} C_j t^j$$

Input Function Represented by a Polynomial (A.4)

Taking Laplace transforms of the weighting function and the input function leads to equations (A.5) and (A.6) respectively.

$$W(s) = \frac{1}{D} \sum_{i=1}^{n} \frac{A_i}{(s + \alpha_i)}$$

Laplace Transform of the Weighting Function (A.5)

$$I(s) = \sum_{j=0}^{m} \frac{C_j j!}{s^{j+1}}$$

Laplace Transform of the Input function (A.6)

Substituting equations (A.5) and (A.6) into equation (A.2) equation (A.7) is obtained, which is the Laplace transform of the response function.

$$R(s) = \frac{1}{D} \sum_{i=1}^{n} \frac{A_i}{(s + \alpha_i)} \cdot \sum_{j=0}^{m} \frac{C_j j!}{s^{j+1}}$$

Laplace Transform of the Response Function (A.7)

The equation for the Laplace transform of the response function (A.7) can be expanded term by term to give equation (A.8).

$$R(s) = \frac{1}{D} \sum_{i=1}^{n} \frac{A_i}{(s + \alpha_i)} \left( \frac{C_0 0!}{s} + \frac{C_1 1!}{s^2} + \frac{C_2 2!}{s^3} + \ldots + \frac{C_m m!}{s^{m+1}} \right)$$

Equation (A.7) expanded (A.8)

If equation (A.8) is itself expanded, then the response function can be built up term by term.

$$\text{Term 1} = \frac{1}{D}\frac{C_0 0!}{s}.\sum_{i=1}^{n}\frac{A_i}{(s+\alpha_i)} = \frac{1}{D}C_0 0!\sum_{i=1}^{n}\left(\frac{A_i}{\alpha_i}\left(\frac{1}{s}-\frac{1}{s+\alpha_i}\right)\right)$$

Term 1 from equation (A.8) expanded (A.9)

Equation (A.9) is the Laplace transform of the first term of the response function (A.8). If the inverse Laplace transform of equation (A.9) is taken then the first term of the response function is obtained (A.10).

$$\boxed{\text{Term 1} = \frac{1}{D}C_0 0!\sum_{i=1}^{n}\frac{A_i}{\alpha_i}(1-e^{-\alpha_i t})}$$

Inverse Laplace Transform of Term 1 (A.10)

If this process is repeated for the second and third terms the equations (A.11-A.14) are obtained.

$$\text{Term 2} = \frac{1}{D}\frac{C_1 1!}{s^2}\sum_{i=1}^{n}\frac{A_i}{(s+\alpha_i)} = \frac{1}{D}C_1 1!\sum_{i=1}^{n}\frac{A_i}{\alpha_i^2}\left(\frac{\alpha_i}{s^2}-\frac{1}{s}+\frac{1}{(s+\alpha_i)}\right)$$

Term 2 from Equation (A.8) expanded (A.11)

$$\boxed{\text{Term 2} = \frac{1}{D}C_1 1!\sum_{i=1}^{n}\frac{A_i}{\alpha_i^2}\left(\frac{\alpha_i.t}{1!}-1+e^{-\alpha_i t}\right)}$$

Inverse Laplace Transform of Term 2 (A.12)

$$\text{Term3} = \frac{1}{D}\,\frac{C_2 2!}{s^3}\sum_{i=1}^{n}\frac{A_i}{(s+\alpha_i)} = \frac{1}{D}\,C_2 2!\sum_{i=1}^{n}\frac{A_i}{\alpha_i^3}\left(\frac{\alpha_i^2}{s^3} - \frac{\alpha_i}{s^2} + \frac{1}{s} - e^{-\alpha_i t}\right)$$

Term 3 from Equation (A.8) expanded (A.13)

$$\boxed{\text{Term 3} = \frac{1}{D}\,C_2 2!\sum_{i=1}^{n}\frac{A_i}{\alpha_i^3}\left(\frac{\alpha_i^2 t^2}{2!} - \frac{\alpha_i t}{1!} + 1 - e^{-\alpha_i t}\right)}$$

Inverse Laplace Transform of Term 3 (A.14)

If equations (A.10), (A.12) and (A.14) are gathered together the first three terms of the progression for the response function can be seen (equation (A.15)).

$$\text{Term 1} = \frac{C_0}{D}\,0!\sum_{i=1}^{n}\frac{A_i}{\alpha_i}(1 - e^{-\alpha_i t})$$

$$\text{Term 2} = \frac{C_1}{D}\,1!\sum_{i=1}^{n}\frac{A_i}{\alpha_i^2}\left(\frac{\alpha_i . t}{1!} - 1 + e^{-\alpha_i t}\right)$$

$$\text{Term 3} = \frac{C_2}{D}\,2!\sum_{i=1}^{n}\frac{A_i}{\alpha_i^3}\left(\frac{\alpha_i^2 t^2}{2!} - \frac{\alpha_i t}{1!} + 1 - e^{-\alpha_i t}\right)$$

First three terms of the Response Function (A.15)

From the first three terms the progression of the response function can be shown to be equation (A.16).

$$R(t) = \frac{1}{D} \sum_{j=0}^{m} C_j j! \sum_{i=1}^{n} \frac{A_i}{\alpha_i^{j+1}} \left( (-1)^{j+1} e^{-\alpha_i t} + \sum_{k=0}^{k=j} (-1)^{j-k} \frac{\alpha_i^k t^k}{k!} \right)$$

Response Function (A.16)

If the weighting function instead of being represented by a polyexponential is adapted to include a time lag then the weighting function will now be represented by equation (A.17).

$$W(t) = \frac{1}{D} H(t - tlag) \sum_{i=1}^{n} A_i e^{-\alpha_i (t - tlag)}$$

Weighting Function now Incorporating a Time Lag (A.17)

H(t-tlag) is known as the Unit step function and takes a value of 0 for t < tlag and a value of 1 for t ≥ tlag. Equation (A.17) can be expressed in the form

H(t-tlag)W(t-tlag)

where $W(t) = 1/D.\Sigma_{i=1}^{n} A_i e^{-\alpha t}$, and the Laplace transform of H(t-tlag)W(t-tlag) is equal to $e^{-s.tlag}.W(s)$ where W(s) is the Laplace transform of the function W(t). If this is applied to equation (A.5) then the Laplace transform of the weighting function can be calculated (equation (A.18)).

$$W(s) = \frac{e^{-tlags}}{D} \sum_{i=1}^{n} \frac{A_i}{(s + \alpha_i)}$$

Laplace Transform of the Weighting Function (A.18)

This leads to an expression for R(s), the Laplace transform of the Response Function, as given in equation (A.19).

$$R(s) = \frac{e^{-s\,tlag}}{D} \sum_{i=1}^{n} \frac{A_i}{(s+\alpha_i)} \left( \frac{C_0 0!}{s} + \frac{C_1 1!}{s^2} + \frac{C_2 2!}{s^3} + \ldots + \frac{C_m m!}{s^{m+1}} \right)$$

Laplace Transform of the Response Function (A.19)

A corollary of the Laplace transform of a unit step function is that if the Laplace transform of a function R(t) is in the form $e^{-s.tlag}R(s)$ then the function R(t) is of the form $H(t-t_{lag})R(t-t_{lag})$, where R(s) is the Laplace transform of R(t). From this theory the inverse transform of equation (A.19) i.e. the response function (R(t)), will be as shown in equation (A.20).

$$\boxed{R(t) = \frac{1}{D} H(t-tlag) \sum_{j=0}^{m} C_j j! \sum_{i=1}^{n} \frac{A_i}{\alpha_i^{j+1}} \left( (-1)^{j+1} e^{-\alpha_i (t-tlag)} + \sum_{k=0}^{k=j} (-1)^{j-k} \frac{\alpha_i^k (t-tlag)^k}{k!} \right)}$$

Response Function (A.20)

# APPENDIX B :

## DERIVATION OF AN EQUATION FOR THE RESPONSE FUNCTION WHEN THE INPUT FUNCTION IS REPRESENTED BY VARIOUS EQUATIONS AND THE WEIGHTING FUNCTION IS REPRESENTED BY A POLYEXPONENTIAL.

The convolution integral can be represented as shown in Appendix A in equation (A.1). Taking the Laplace transform of the convolution integral leads to the following expression :

$$R(s) = W(s).I(s)$$

where R(s) is the Laplace transform of the response function, W(s) is the Laplace transform of the weighting function and I(s) is the Laplace transform of the Input function. The weighting function, W(t), is represented by a polyexponential (equation (B.1)) and the Laplace transform of the weighting function is shown in equation (B.2).

$$W(t) = \sum_{i=1}^{n} A_i e^{-\alpha_i t}$$

Weighting Function represented by a Polyexponential (B.1)

$$W(s) = \sum_{i=1}^{n} \frac{A_i}{s + \alpha_i}$$

Laplace Transform of the Weighting Function (B.2)

When the Input function is a monoexponential representing a first order release process, as shown in equation (B.3), where k is the first order rate constant and D is the dose given, then the Laplace transform of this Input function is as shown in equation (B.4).

$$I(t) = kD\,e^{-kt}$$

Monoexponential Input Function (B.3)

$$I(s) = \frac{kD}{k + s}$$

Laplace Transform of the Input Function (B.4)

Multiplication of the Laplace transform of the weighting function (B.2) with that of the input function (B.4) results in an equation for the Laplace transform of the response function (equation (B.5)). Re-arrangement of equation (B.5) gives equation (B.6).

$$R(s) = W(s).I(s) = \frac{kD}{s + k} \sum_{i=1}^{n} \frac{A_i}{s + \alpha_i}$$

Laplace Transform of the Response Function (B.5)

$$R(s) = kD \sum_{i=1}^{n} A_i \left( \frac{1}{(s + k)} \cdot \frac{1}{(s + \alpha_i)} \right)$$

$$= kD \sum_{i=1}^{n} \frac{A_i}{k - \alpha_i} \left( \frac{1}{(s + \alpha_i)} - \frac{1}{(s + k)} \right)$$

(B.6)

Taking the inverse Laplace transform of equation (B.6) gives an expression for the response function, R(t), shown in equation (B.7).

$$\boxed{R(t) = kD \sum_{i=1}^{n} \frac{A_i}{k - \alpha_i} \left(e^{-\alpha_i t} - e^{-kt}\right)}$$

Response Function (B.7)

If the input function, instead of being represented by a monoexponential, takes the form of a zero order function changing to first order at time $t_c$, then the input function can be expressed as shown in equation (B.8) (where $k_0$ is the zero order rate constant, $D_r$ is the dose remaining at time $t_c$, k is the first order rate constant and $H(t - t_c)$ is the unit step function which takes the value 0 at $t < t_c$ and 1 when $t \geq t_c$).

$$I(t) = k_0 - H(t - t_c)k_0 + H(t - t_c)\,kD_r e^{-k(t - t_c)}$$

Input Function (B.8)

Taking the Laplace transform of equation (B.8) gives equation (B.9) and multiplication of this equation with the Laplace transform of the weighting function (equation (B.2)) gives an expression for the Laplace transform of the response function, (B.10).

$$I(s) = \frac{k_0}{s} - e^{-t_c s}.\frac{k_0}{s} + e^{-t_c s}\frac{kD}{s + k}$$

Laplace transform of the Input Function (B.9)

$$R(s) = W(s).I(s) = \sum_{i=1}^{n} \frac{A_i}{s + \alpha_i}\left(\frac{k_0}{s} - e^{-t_c s}.\frac{k_0}{s} + e^{-t_c s}\frac{kD}{s + k}\right)$$

(B.10)

Re-arrangement of equation (B.10) gives (B.11) for which the inverse transformation can be taken to give an expression for the response function as shown in equation (B.12).

$$R(s) = k_0\sum_{i=1}^{n}\frac{A_i}{\alpha_i}\left(\frac{1}{s} - \frac{1}{s+\alpha_i}\right) - e^{-t_c s}.k_0\sum_{i=1}^{n}\frac{A_i}{\alpha_i}\left(\frac{1}{s} - \frac{1}{s+\alpha_i}\right)$$

$$+ \; kDe^{-t_c s}\sum_{i=1}^{n}\frac{A_i}{k-\alpha_i}\left(\frac{1}{s+\alpha_i} - \frac{1}{s+k}\right)$$

Laplace Transform of the Response Function (B.11)

$$\boxed{\begin{aligned} R(t) &= k_0\sum_{i=1}^{n}\frac{A_i}{\alpha_i}(1 - e^{-\alpha_i t}) - H(t-t_c)\,k_0\sum_{i=1}^{n}\frac{A_i}{\alpha_i}(1 - e^{-\alpha_i(t-t_c)}) \\ &+ H(t-t_c)\,kD\sum_{i=1}^{n}\frac{A_i}{k-\alpha_i}(e^{-\alpha_i(t-t_c)} - e^{-k(t-t_c)}) \end{aligned}}$$

Response Function (B.12)

| Time | True W(t) | 1% noise | 5% noise | 10% noise |
|---|---|---|---|---|
| 0.05 | 0.5170 | 0.5156 | 0.5223 | 0.4926 |
| 0.10 | 0.7756 | 0.7700 | 0.7487 | 0.6939 |
| 0.15 | 0.8868 | 0.8948 | 0.8894 | 0.7694 |
| 0.20 | 0.9159 | 0.9093 | 0.9161 | 0.9660 |
| 0.30 | 0.8644 | 0.8550 | 0.8859 | 1.0089 |
| 0.40 | 0.7690 | 0.7660 | 0.7824 | 0.7808 |
| 0.60 | 0.5936 | 0.6006 | 0.6119 | 0.6057 |
| 0.80 | 0.4670 | 0.4698 | 0.4877 | 0.4784 |
| 1.00 | 0.3745 | 0.3714 | 0.3975 | 0.4074 |
| 1.20 | 0.3037 | 0.3075 | 0.3320 | 0.3354 |
| 1.40 | 0.2475 | 0.2514 | 0.2320 | 0.2206 |
| 1.60 | 0.2022 | 0.1978 | 0.2099 | 0.2070 |
| 2.00 | 0.1354 | 0.1360 | 0.1462 | 0.1579 |

**Table C(1a) :** Pseudo-Experimental Weighting Function Values used in Chapter 3 with Increasing Levels of Added Noise and Generated from the Equation $W(t) = -2e^{-10t} + e^{-t} + e^{-5t}$.

| Time | True R(t) | 1% noise | 5% noise | 10% noise |
|---|---|---|---|---|
| 0.05 | 0.0166 | 0.0166 | 0.0168 | 0.0160 |
| 0.10 | 0.0530 | 0.0526 | 0.0511 | 0.0621 |
| 0.15 | 0.0959 | 0.0960 | 0.0962 | 0.0969 |
| 0.20 | 0.1386 | 0.1386 | 0.1386 | 0.1410 |
| 0.30 | 0.2110 | 0.2120 | 0.2162 | 0.1646 |
| 0.40 | 0.2615 | 0.2624 | 0.2660 | 0.2687 |
| 0.60 | 0.3081 | 0.3100 | 0.3176 | 0.3352 |
| 0.80 | 0.3100 | 0.3126 | 0.3236 | 0.3074 |
| 1.00 | 0.2899 | 0.2935 | 0.3077 | 0.3174 |
| 1.20 | 0.2607 | 0.2655 | 0.2850 | 0.2816 |
| 1.40 | 0.2287 | 0.2258 | 0.2143 | 0.1952 |
| 1.60 | 0.1973 | 0.1988 | 0.2048 | 0.1958 |
| 2.00 | 0.1422 | 0.1445 | 0.1536 | 0.1562 |

**Table C(1b) :** Pseudo-Experimental Response Function Values used in Chapter 3 with Increasing Levels of Added Noise and Generated from the Equations $W(t) = -2e^{-10t} + e^{-t} + e^{-5t}$ and $I(t) = 1.2e^{-2t}$ according to the Method Described in Secion 2.3.2

| Subject / Time | 1 | 2 | 3 | 4 | 5 | 6 | 7 | 8 | 9 | 10 |
|---|---|---|---|---|---|---|---|---|---|---|
| 0.05 | 0.5224 | 0.4990 | 0.4864 | 0.5253 | 0.5379 | 0.5311 | 0.5219 | 0.5058 | 0.4932 | 0.5185 |
| 0.10 | 0.6233 | 0.7593 | 0.6780 | 0.7888 | 0.8361 | 0.7795 | 0.9214 | 0.7671 | 0.7184 | 0.7810 |
| 0.15 | 0.9080 | 0.8307 | 0.7711 | 0.9465 | 0.8258 | 0.8195 | 0.9375 | 0.8815 | 0.9928 | 0.8957 |
| 0.20 | 0.8283 | 0.9202 | 0.9767 | 0.9751 | 0.8910 | 0.9071 | 1.0783 | 0.8414 | 1.0713 | 0.9047 |
| 0.30 | 0.6195 | 0.8254 | 0.9583 | 0.7550 | 0.9480 | 0.9746 | 0.8461 | 0.7961 | 0.8041 | 0.7360 |
| 0.40 | 0.7757 | 0.7572 | 0.8044 | 0.7430 | 0.7618 | 0.7294 | 0.8524 | 0.7476 | 0.6374 | 0.7334 |
| 0.60 | 0.5645 | 0.6816 | 0.5706 | 0.5233 | 0.6665 | 0.6421 | 0.5463 | 0.6909 | 0.6637 | 0.4491 |
| 0.80 | 0.4658 | 0.4537 | 0.4034 | 0.5081 | 0.5041 | 0.4621 | 0.4557 | 0.3932 | 0.4208 | 0.4115 |
| 1.00 | 0.3947 | 0.3975 | 0.3802 | 0.3373 | 0.4351 | 0.3882 | 0.4115 | 0.3598 | 0.3343 | 0.3405 |
| 1.20 | 0.3108 | 0.3006 | 0.3234 | 0.2845 | 0.3303 | 0.2964 | 0.2826 | 0.3051 | 0.3355 | 0.2871 |
| 1.40 | 0.2715 | 0.2426 | 0.2467 | 0.2276 | 0.2300 | 0.2666 | 0.2339 | 0.2778 | 0.2559 | 0.2793 |
| 1.60 | 0.2010 | 0.1952 | 0.1618 | 0.2184 | 0.2110 | 0.2006 | 0.2094 | 0.2246 | 0.2040 | 0.1813 |
| 2.00 | 0.1275 | 0.1414 | 0.1109 | 0.1429 | 0.1168 | 0.1405 | 0.1323 | 0.1654 | 0.1315 | 0.1457 |

**Table C(2) :** Pseudo-Experimental Weighting Function Values used in Chapter 3 with a Noise Level of 10% and Generated from the Equation $W(t) = -2e^{-10t} + e^{-t} + e^{-5t}$

| Subject / Time | 1 | 2 | 3 | 4 | 5 | 6 | 7 | 8 | 9 | 10 |
|---|---|---|---|---|---|---|---|---|---|---|
| 0.05 | 0.0162 | 0.0156 | 0.0171 | 0.0168 | 0.0160 | 0.0167 | 0.0173 | 0.0165 | 0.0159 | 0.0168 |
| 0.10 | 0.0500 | 0.0463 | 0.0556 | 0.0630 | 0.0507 | 0.0534 | 0.0462 | 0.0530 | 0.0620 | 0.0563 |
| 0.15 | 0.0933 | 0.0835 | 0.0872 | 0.1015 | 0.0868 | 0.0970 | 0.0879 | 0.0945 | 0.1011 | 0.0802 |
| 0.20 | 0.1208 | 0.1478 | 0.1509 | 0.1632 | 0.1387 | 0.1369 | 0.1399 | 0.1199 | 0.1167 | 0.1536 |
| 0.30 | 0.2469 | 0.2339 | 0.2314 | 0.2065 | 0.2167 | 0.1797 | 0.2456 | 0.1994 | 0.2258 | 0.2550 |
| 0.40 | 0.2687 | 0.2735 | 0.2536 | 0.2899 | 0.2130 | 0.2494 | 0.2596 | 0.2720 | 0.1991 | 0.2705 |
| 0.60 | 0.2690 | 0.2962 | 0.2625 | 0.2836 | 0.3024 | 0.2331 | 0.2967 | 0.2875 | 0.3292 | 0.3149 |
| 0.80 | 0.3229 | 0.2678 | 0.3297 | 0.3025 | 0.3339 | 0.2732 | 0.2943 | 0.3386 | 0.3153 | 0.2839 |
| 1.00 | 0.3001 | 0.2943 | 0.2663 | 0.3185 | 0.3390 | 0.2636 | 0.2993 | 0.2759 | 0.2608 | 0.2448 |
| 1.20 | 0.2772 | 0.2776 | 0.2532 | 0.3426 | 0.2928 | 0.2464 | 0.2852 | 0.2675 | 0.2642 | 0.2865 |
| 1.40 | 0.2460 | 0.2279 | 0.2152 | 0.2161 | 0.2479 | 0.2580 | 0.2245 | 0.2703 | 0.2161 | 0.2188 |
| 1.60 | 0.1952 | 0.1578 | 0.1939 | 0.2044 | 0.1904 | 0.1769 | 0.1951 | 0.2057 | 0.2198 | 0.2178 |
| 2.00 | 0.1552 | 0.1164 | 0.1454 | 0.1389 | 0.1450 | 0.1530 | 0.1461 | 0.1585 | 0.1599 | 0.1359 |

**Table C(3) :** Pseudo-Experimental Response Function Values used in Chapter 3 (section 3.1) with a Noise Level of 10% and Generated from the Equations $W(t) = -2e^{-10t} + e^{-t} + e^{-5t}$ and $I(t) = 1.2e^{-2t}$ according to the Method Described in Section 2.3.2

| Time | True W(t) | 1% noise | 5% noise | 10% noise |
|---|---|---|---|---|
| 0.05 | 0.5170 | 0.5152 | 0.5212 | 0.5219 |
| 0.10 | 0.7756 | 0.7740 | 0.7822 | 0.9214 |
| 0.15 | 0.8868 | 0.8812 | 0.9167 | 0.9375 |
| 0.20 | 0.9159 | 0.9163 | 0.9455 | 1.0783 |
| 0.30 | 0.8644 | 0.8605 | 0.8097 | 0.8461 |
| 0.40 | 0.7690 | 0.7678 | 0.7560 | 0.8524 |
| 0.60 | 0.5936 | 0.5919 | 0.6197 | 0.5793 |
| 0.80 | 0.4670 | 0.4699 | 0.4438 | 0.5131 |
| 1.00 | 0.3745 | 0.3741 | 0.3627 | 0.3484 |
| 1.20 | 0.3037 | 0.3061 | 0.2944 | 0.2898 |
| 1.40 | 0.2475 | 0.2467 | 0.2574 | 0.2564 |
| 1.60 | 0.2022 | 0.2031 | 0.2078 | 0.1975 |
| 2.00 | 0.1354 | 0.1357 | 0.1349 | 0.1348 |

**Table C(4a) :** Pseudo-Experimental Weighting Function Values used in Chapter 3 with Increasing Levels of Added Noise and Generated from the Equation $W(t) = -2e^{-10t} + e^{-t} + e^{-5t}$.

| Time | True R(t) | 1% noise | 5% noise | 10% noise |
|---|---|---|---|---|
| 0.05 | 0.0072 | 0.0072 | 0.0070 | 0.0074 |
| 0.10 | 0.0237 | 0.0236 | 0.0222 | 0.0249 |
| 0.15 | 0.0447 | 0.0446 | 0.0418 | 0.0406 |
| 0.20 | 0.0674 | 0.0665 | 0.0696 | 0.0734 |
| 0.30 | 0.1123 | 0.1142 | 0.1184 | 0.1231 |
| 0.40 | 0.1531 | 0.1535 | 0.1566 | 0.1485 |
| 0.60 | 0.2209 | 0.2218 | 0.2059 | 0.2349 |
| 0.80 | 0.2735 | 0.2745 | 0.2756 | 0.2513 |
| 1.00 | 0.3037 | 0.3056 | 0.3136 | 0.2950 |
| 1.20 | 0.2967 | 0.2989 | 0.2962 | 0.2792 |
| 1.40 | 0.2696 | 0.2693 | 0.2426 | 0.2649 |
| 1.60 | 0.2356 | 0.2378 | 0.2143 | 0.2104 |
| 2.00 | 0.1698 | 0.1702 | 0.1728 | 0.1589 |

**Table C(4b) :** Pseudo-Experimental Response Function Values used in Chapter 3 with Increasing Levels of Added Noise and Generated from the Equations $W(t) = -2e^{-10t} + e^{-t} + e^{-5t}$ and $I(t) = 0.5$ for $t \leq 0.8$ and $I(t) = 0.5e^{-2.5(t-0.8)}$ for $t > 0.8$ according to the Method Described in Secion 2.3.2

| Subject / Time | 1 | 2 | 3 | 4 | 5 | 6 | 7 | 8 | 9 | 10 |
|---|---|---|---|---|---|---|---|---|---|---|
| 0.05 | 0.5224 | 0.4990 | 0.4864 | 0.5253 | 0.5379 | 0.5311 | 0.5219 | 0.5058 | 0.4932 | 0.5185 |
| 0.10 | 0.6233 | 0.7593 | 0.6780 | 0.7888 | 0.8361 | 0.7795 | 0.9214 | 0.7671 | 0.7184 | 0.7810 |
| 0.15 | 0.9080 | 0.8307 | 0.7711 | 0.9465 | 0.8258 | 0.8195 | 0.9375 | 0.8815 | 0.9928 | 0.8957 |
| 0.20 | 0.8283 | 0.9202 | 0.9767 | 0.9751 | 0.8910 | 0.9071 | 1.0783 | 0.8414 | 1.0713 | 0.9047 |
| 0.30 | 0.6195 | 0.8254 | 0.9583 | 0.7550 | 0.9480 | 0.9746 | 0.8461 | 0.7961 | 0.8041 | 0.7360 |
| 0.40 | 0.7757 | 0.7572 | 0.8044 | 0.7430 | 0.7618 | 0.7294 | 0.8524 | 0.7476 | 0.6374 | 0.7334 |
| 0.60 | 0.5920 | 0.5767 | 0.5127 | 0.6458 | 0.6407 | 0.5873 | 0.5793 | 0.4998 | 0.5349 | 0.5231 |
| 0.80 | 0.4922 | 0.4957 | 0.4740 | 0.4206 | 0.5425 | 0.4840 | 0.5131 | 0.4487 | 0.4168 | 0.4246 |
| 1.00 | 0.3833 | 0.3707 | 0.3988 | 0.3509 | 0.4073 | 0.3656 | 0.3484 | 0.3763 | 0.4137 | 0.3540 |
| 1.20 | 0.3364 | 0.3006 | 0.3057 | 0.2821 | 0.2850 | 0.3304 | 0.2898 | 0.3443 | 0.3171 | 0.3460 |
| 1.40 | 0.2460 | 0.2390 | 0.1980 | 0.2673 | 0.2383 | 0.2455 | 0.2564 | 0.2750 | 0.2500 | 0.2219 |
| 1.60 | 0.1904 | 0.2111 | 0.1656 | 0.2134 | 0.1744 | 0.2099 | 0.1975 | 0.2470 | 0.1964 | 0.2176 |
| 2.00 | 0.1194 | 0.1380 | 0.1402 | 0.1344 | 0.1430 | 0.1425 | 0.1348 | 0.1472 | 0.1301 | 0.1358 |

**Table C(5) :** Pseudo-Experimental Weighting Function Values used in Chapter 3 with a Noise Level of 10% and Generated from the Equation $W(t) = -2e^{-10t} + e^{-t} + e^{-5t}$

| Subject / Time | 1 | 2 | 3 | 4 | 5 | 6 | 7 | 8 | 9 | 10 |
|---|---|---|---|---|---|---|---|---|---|---|
| 0.05 | 0.0073 | 0.0070 | 0.0068 | 0.0073 | 0.0075 | 0.0073 | 0.0070 | 0.0069 | 0.0072 | 0.0074 |
| 0.10 | 0.0191 | 0.0232 | 0.0207 | 0.0241 | 0.0256 | 0.0282 | 0.0234 | 0.0220 | 0.0239 | 0.0238 |
| 0.15 | 0.0458 | 0.0419 | 0.0389 | 0.0477 | 0.0416 | 0.0473 | 0.0444 | 0.0501 | 0.0452 | 0.0413 |
| 0.20 | 0.0610 | 0.0677 | 0.0719 | 0.0718 | 0.0656 | 0.0794 | 0.0619 | 0.0788 | 0.0666 | 0.0668 |
| 0.30 | 0.0805 | 0.1072 | 0.1245 | 0.0981 | 0.1232 | 0.1099 | 0.1034 | 0.1045 | 0.0956 | 0.1266 |
| 0.40 | 0.1544 | 0.1507 | 0.1602 | 0.1479 | 0.1517 | 0.1697 | 0.1488 | 0.1269 | 0.1460 | 0.1452 |
| 0.60 | 0.2203 | 0.2146 | 0.1908 | 0.2403 | 0.2384 | 0.2156 | 0.1860 | 0.1991 | 0.1947 | 0.2186 |
| 0.80 | 0.2883 | 0.2903 | 0.2776 | 0.2464 | 0.3177 | 0.3005 | 0.2628 | 0.2441 | 0.2486 | 0.2835 |
| 1.00 | 0.3108 | 0.3006 | 0.3234 | 0.2845 | 0.3303 | 0.2826 | 0.3051 | 0.3355 | 0.2871 | 0.2964 |
| 1.20 | 0.3254 | 0.2908 | 0.2957 | 0.2729 | 0.2757 | 0.2804 | 0.3331 | 0.3068 | 0.3348 | 0.3196 |
| 1.40 | 0.2680 | 0.2603 | 0.2158 | 0.2912 | 0.2814 | 0.2793 | 0.2995 | 0.2720 | 0.2417 | 0.2674 |
| 1.60 | 0.2219 | 0.2460 | 0.1929 | 0.2487 | 0.2033 | 0.2301 | 0.2878 | 0.2288 | 0.2535 | 0.2445 |
| 2.00 | 0.1497 | 0.1730 | 0.1759 | 0.1686 | 0.1796 | 0.1690 | 0.1846 | 0.1632 | 0.1703 | 0.1787 |

**Table C(6) :** Pseudo-Experimental Response Function Values used in Chapter 3 (section 3.1) with a Noise Level of 10% and Generated from the Equations $W(t) = -2e^{-10t} + e^{-t} + e^{-5t}$ and $I(t) = 0.5$ for $t \leq 0.8$ and $I(t) = 0.5e^{-2.5(t-0.8)}$ according to the Method Described in Section 2.3.2

| Time | True W(t) | 1% noise | 5% noise | 10% noise |
|---|---|---|---|---|
| 0.05 | 0.5170 | 0.5156 | 0.5223 | 0.4926 |
| 0.10 | 0.7756 | 0.7700 | 0.7487 | 0.6939 |
| 0.15 | 0.8868 | 0.8948 | 0.8894 | 0.7694 |
| 0.20 | 0.9159 | 0.9093 | 0.9161 | 0.9660 |
| 0.30 | 0.8644 | 0.8550 | 0.8859 | 1.0089 |
| 0.40 | 0.7690 | 0.7660 | 0.7824 | 0.7808 |
| 0.60 | 0.5936 | 0.6006 | 0.6119 | 0.6057 |
| 0.80 | 0.4670 | 0.4698 | 0.4877 | 0.4784 |
| 1.00 | 0.3745 | 0.3714 | 0.3975 | 0.4074 |
| 1.20 | 0.3037 | 0.3075 | 0.3320 | 0.3354 |
| 1.40 | 0.2475 | 0.2514 | 0.2320 | 0.2206 |
| 1.60 | 0.2022 | 0.1978 | 0.2099 | 0.2070 |
| 2.00 | 0.1354 | 0.1360 | 0.1462 | 0.1579 |

**Table C(7a) :** Pseudo-Experimental Weighting Function Values used in Chapter 3 with Increasing Levels of Added Noise and Generated from the Equation $W(t) = -2e^{-10t} + e^{-t} + e^{-5t}$.

| Time | True R(t) | 1% noise | 5% noise | 10% noise |
|---|---|---|---|---|
| 0.05 | 0.0000 | 0.0000 | 0.0000 | 0.0000 |
| 0.10 | 0.0052 | 0.0052 | 0.0049 | 0.0058 |
| 0.15 | 0.0155 | 0.0153 | 0.0162 | 0.0160 |
| 0.20 | 0.0303 | 0.0302 | 0.0317 | 0.0291 |
| 0.40 | 0.1125 | 0.1123 | 0.1152 | 0.1112 |
| 0.60 | 0.1886 | 0.1876 | 0.1839 | 0.1960 |
| 0.80 | 0.2480 | 0.2518 | 0.2517 | 0.2529 |
| 1.00 | 0.2948 | 0.2924 | 0.3074 | 0.3025 |
| 1.20 | 0.3307 | 0.3310 | 0.3359 | 0.3617 |
| 1.40 | 0.3462 | 0.3450 | 0.3384 | 0.3881 |
| 1.60 | 0.3314 | 0.3336 | 0.3431 | 0.3220 |
| 1.80 | 0.2982 | 0.3029 | 0.2877 | 0.2716 |
| 2.00 | 0.2591 | 0.2583 | 0.2685 | 0.2578 |

**Table C(7b) :** Pseudo-Experimental Response Function Values used in Chapter 3 with Increasing Levels of Added Noise and Generated from the Equations $W(t) = -2e^{-10t} + e^{-t} + e^{-5t}$ and the Controlled Release Input Function according to the Method Described in Secion 2.3.2

| Subject / Time | 1 | 2 | 3 | 4 | 5 | 6 | 7 | 8 | 9 | 10 |
|---|---|---|---|---|---|---|---|---|---|---|
| 0.05 | 0.5035 | 0.5277 | 0.4972 | 0.5224 | 0.5430 | 0.5052 | 0.5493 | 0.4989 | 0.5207 | 0.4927 |
| 0.10 | 0.7191 | 0.7277 | 0.9099 | 0.6233 | 0.7800 | 0.7324 | 0.8489 | 0.9593 | 0.7785 | 0.6939 |
| 0.15 | 0.9663 | 0.8919 | 0.8959 | 0.9080 | 0.9267 | 0.8615 | 0.8194 | 0.8307 | 0.8452 | 0.7694 |
| 0.20 | 0.8490 | 0.9163 | 0.9322 | 0.8284 | 0.8550 | 0.7984 | 1.0086 | 0.9203 | 0.9426 | 0.9660 |
| 0.30 | 0.7705 | 0.9074 | 0.6744 | 0.6195 | 0.9405 | 1.0115 | 0.8299 | 0.8254 | 0.7753 | 1.0089 |
| 0.40 | 0.7391 | 0.7957 | 0.7902 | 0.7757 | 0.6988 | 0.7903 | 0.8669 | 0.7572 | 0.7619 | 0.7807 |
| 0.60 | 0.6629 | 0.6301 | 0.6459 | 0.5645 | 0.5925 | 0.5183 | 0.6170 | 0.6816 | 0.5993 | 0.6057 |
| 0.80 | 0.4956 | 0.5084 | 0.4632 | 0.4657 | 0.4094 | 0.4864 | 0.4676 | 0.4537 | 0.3985 | 0.4784 |
| 1.00 | 0.3431 | 0.4204 | 0.4100 | 0.3948 | 0.4145 | 0.3876 | 0.4036 | 0.3975 | 0.4394 | 0.4074 |
| 1.20 | 0.3417 | 0.3603 | 0.3280 | 0.3108 | 0.3290 | 0.3229 | 0.2925 | 0.3006 | 0.2599 | 0.3354 |
| 1.40 | 0.2864 | 0.2164 | 0.2113 | 0.2715 | 0.2980 | 0.2662 | 0.1995 | 0.2426 | 0.2331 | 0.2206 |
| 1.60 | 0.1576 | 0.2176 | 0.2006 | 0.2010 | 0.2156 | 0.2001 | 0.2101 | 0.1953 | 0.2497 | 0.2070 |
| 2.00 | 0.1417 | 0.1570 | 0.1487 | 0.1275 | 0.1393 | 0.1477 | 0.1357 | 0.1414 | 0.1006 | 0.1579 |

**Table C(8) :** Pseudo-Experimental Weighting Function Values used in Chapter 3 with a Noise Level of 10% and Generated from the Equation $W(t) = -2e^{-10t} + e^{-t} + e^{-5t}$

| Subject / Time | 1 | 2 | 3 | 4 | 5 | 6 | 7 | 8 | 9 | 10 |
|---|---|---|---|---|---|---|---|---|---|---|
| 0.05 | 0.0000 | 0.0000 | 0.0000 | 0.0000 | 0.0000 | 0.0000 | 0.0000 | 0.0000 | 0.0000 | 0.0000 |
| 0.10 | 0.0054 | 0.0049 | 0.0043 | 0.0050 | 0.0055 | 0.0053 | 0.0051 | 0.0055 | 0.0048 | 0.0052 |
| 0.15 | 0.0149 | 0.0142 | 0.0145 | 0.0169 | 0.0161 | 0.0157 | 0.0167 | 0.0157 | 0.0160 | 0.0143 |
| 0.20 | 0.0331 | 0.0298 | 0.0376 | 0.0304 | 0.0283 | 0.0290 | 0.0278 | 0.0334 | 0.0267 | 0.0293 |
| 0.40 | 0.1175 | 0.1314 | 0.0990 | 0.1112 | 0.1182 | 0.0939 | 0.1080 | 0.1107 | 0.1066 | 0.1295 |
| 0.60 | 0.1663 | 0.1998 | 0.1544 | 0.1767 | 0.1906 | 0.1822 | 0.2012 | 0.2182 | 0.1825 | 0.1860 |
| 0.80 | 0.2088 | 0.2463 | 0.2679 | 0.2249 | 0.3039 | 0.2249 | 0.2717 | 0.2601 | 0.2356 | 0.2554 |
| 1.00 | 0.2825 | 0.2634 | 0.3095 | 0.3201 | 0.3721 | 0.3041 | 0.2815 | 0.2740 | 0.3163 | 0.2663 |
| 1.20 | 0.3417 | 0.3226 | 0.3478 | 0.3708 | 0.3408 | 0.3172 | 0.3268 | 0.3436 | 0.3372 | 0.3393 |
| 1.40 | 0.3972 | 0.3590 | 0.3819 | 0.3787 | 0.3881 | 0.3363 | 0.3153 | 0.3444 | 0.3617 | 0.3328 |
| 1.60 | 0.3206 | 0.3489 | 0.3342 | 0.3623 | 0.3460 | 0.2923 | 0.2790 | 0.3176 | 0.3424 | 0.3802 |
| 1.80 | 0.2994 | 0.2934 | 0.3353 | 0.2885 | 0.2994 | 0.3180 | 0.2810 | 0.3243 | 0.3243 | 0.2937 |
| 2.00 | 0.2763 | 0.2681 | 0.2453 | 0.3160 | 0.2962 | 0.2664 | 0.2909 | 0.3092 | 0.2934 | 0.3086 |

**Table C(9) :** Pseudo-Experimental Response Function Values used in Chapter 3 (section 3.1) with a Noise Level of 10% and Generated from the Equations $W(t) = -2e^{-10t} + e^{-t} + e^{-5t}$ and the Controlled Release Input Function according to the Method Described in Section 2.3.2

| Subject / Time (h) | 1 | 2 | 3 | 4 | 5 | 6 | 7 | 8 | 9 | 10 |
|---|---|---|---|---|---|---|---|---|---|---|
| 0.00 | 0.000 | 0.000 | 0.000 | 0.000 | 0.000 | 0.000 | 0.000 | 0.000 | 0.000 | 0.000 |
| 0.25 | 0.000 | 0.100 | 0.038 | 0.036 | 0.005 | 0.130 | 0.044 | 0.014 | 0.134 | 0.115 |
| 0.50 | 0.035 | 0.690 | 0.179 | 0.323 | 0.114 | 0.469 | 0.331 | 0.047 | 0.493 | 0.282 |
| 1.00 | 0.131 | 0.850 | 0.212 | 0.610 | 0.334 | 0.680 | 0.410 | 0.254 | 0.441 | 0.580 |
| 1.50 | 0.199 | 0.880 | 0.174 | 0.461 | 0.362 | 0.750 | 0.331 | 0.375 | 0.379 | 0.690 |
| 2.00 | 0.182 | 0.810 | 0.165 | 0.395 | 0.384 | 0.820 | 0.301 | 0.418 | 0.318 | 0.690 |
| 3.00 | 0.166 | 0.710 | 0.126 | 0.312 | 0.303 | 0.780 | 0.307 | 0.400 | 0.299 | 0.660 |
| 4.00 | 0.114 | 0.700 | 0.078 | 0.253 | 0.259 | 0.770 | 0.189 | 0.311 | 0.220 | 0.510 |
| 5.00 | 0.098 | 0.660 | 0.064 | 0.189 | 0.200 | 0.750 | 0.170 | 0.276 | 0.157 | 0.456 |
| 6.00 | 0.055 | 0.580 | 0.043 | 0.143 | 0.148 | 0.740 | 0.128 | 0.198 | 0.120 | 0.435 |
| 8.00 | 0.040 | 0.490 | 0.024 | 0.084 | 0.106 | 0.610 | 0.078 | 0.135 | 0.087 | 0.335 |
| 10.00 | 0.016 | 0.384 | 0.020 | 0.053 | 0.060 | 0.530 | 0.048 | 0.082 | 0.046 | 0.259 |
| 12.00 | 0.009 | 0.342 | 0.008 | 0.045 | 0.042 | 0.430 | 0.030 | 0.046 | 0.028 | 0.199 |
| 24.00 | nd | 0.105 | nd | nd | 0.008 | 0.156 | nd | 0.007 | nd | 0.041 |

0.00 = concentration not dectectable, treated as 0 nd = concentration not dectectable

**Table D(1) :** Individual Plasma Concentrations (μmol/l) after Oral Administration of Metoprolol Succinate Solution 95mg.

| Subject / Time (h) | 1 | 2 | 3 | 4 | 5 | 6 | 7 | 8 | 9 | 10 |
|---|---|---|---|---|---|---|---|---|---|---|
| 0.00 | 0.000 | 0.000 | 0.000 | 0.000 | 0.000 | 0.000 | 0.000 | 0.000 | 0.000 | 0.000 |
| 1.00 | 0.028 | 0.035 | 0.031 | 0.066 | 0.045 | 0.090 | 0.037 | 0.032 | 0.055 | 0.025 |
| 2.00 | 0.036 | 0.070 | 0.042 | 0.069 | 0.090 | 0.191 | 0.067 | 0.109 | 0.066 | 0.173 |
| 3.00 | 0.044 | 0.221 | 0.047 | 0.072 | 0.129 | 0.339 | 0.070 | 0.141 | 0.085 | 0.229 |
| 4.00 | 0.058 | 0.377 | 0.047 | 0.076 | 0.159 | 0.419 | 0.091 | 0.168 | 0.107 | 0.308 |
| 5.00 | 0.055 | 0.353 | 0.042 | 0.071 | 0.128 | 0.413 | 0.086 | 0.177 | 0.100 | 0.296 |
| 6.00 | 0.061 | 0.428 | 0.037 | 0.079 | 0.115 | 0.417 | 0.082 | 0.179 | 0.099 | 0.290 |
| 8.00 | 0.058 | 0.348 | 0.030 | 0.077 | 0.080 | 0.450 | 0.069 | 0.156 | 0.074 | 0.306 |
| 10.00 | 0.051 | 0.357 | 0.025 | 0.073 | 0.075 | 0.420 | 0.061 | 0.115 | 0.059 | 0.281 |
| 12.00 | 0.044 | 0.341 | 0.024 | 0.074 | 0.065 | 0.403 | 0.052 | 0.089 | 0.057 | 0.248 |
| 14.00 | 0.037 | 0.336 | 0.019 | 0.085 | 0.042 | 0.382 | 0.053 | 0.083 | 0.066 | 0.242 |
| 24.00 | 0.015 | 0.184 | nd | 0.031 | 0.011 | 0.281 | 0.033 | 0.028 | 0.025 | 0.132 |
| 26.00 | 0.010 | 0.116 | nd | 0.026 | nd | 0.246 | 0.028 | 0.021 | 0.023 | 0.098 |
| 28.00 | 0.008 | 0.108 | nd | 0.021 | nd | 0.246 | 0.021 | 0.015 | 0.017 | 0.088 |
| 30.00 | 0.006 | 0.085 | nd | 0.016 | nd | 0.206 | 0.020 | 0.013 | 0.014 | 0.073 |

0.00 = concentration not dectectable, treated as 0 nd = concentration not dectectable

**Table D(2) :** Individual Plasma Concentrations (µmol/l) after Oral Administration of CR A ; Metoprolol Succinate CR Tablet 95mg.

| Subject / Time (h) | 1 | 2 | 3 | 4 | 5 | 6 | 7 | 8 | 9 | 10 |
|---|---|---|---|---|---|---|---|---|---|---|
| 0.00 | 0.000 | 0.000 | 0.000 | 0.000 | 0.000 | 0.000 | 0.000 | 0.000 | 0.000 | 0.000 |
| 1.00 | 0.012 | 0.029 | 0.023 | 0.029 | 0.022 | 0.036 | 0.023 | 0.016 | 0.030 | 0.082 |
| 2.00 | 0.023 | 0.142 | 0.033 | 0.032 | 0.050 | 0.101 | 0.042 | 0.057 | 0.044 | 0.111 |
| 3.00 | 0.029 | 0.186 | 0.031 | 0.039 | 0.067 | 0.188 | 0.044 | 0.079 | 0.059 | 0.156 |
| 4.00 | 0.037 | 0.229 | 0.032 | 0.042 | 0.088 | 0.224 | 0.047 | 0.099 | 0.070 | 0.182 |
| 5.00 | 0.039 | 0.194 | 0.025 | 0.041 | 0.082 | 0.253 | 0.049 | 0.099 | 0.062 | 0.173 |
| 6.00 | 0.039 | 0.238 | 0.027 | 0.043 | 0.078 | 0.285 | 0.051 | 0.101 | 0.057 | 0.193 |
| 8.00 | 0.038 | 0.275 | 0.023 | 0.042 | 0.080 | 0.295 | 0.052 | 0.102 | 0.051 | 0.216 |
| 10.00 | 0.037 | 0.245 | 0.024 | 0.043 | 0.080 | 0.324 | 0.047 | 0.084 | 0.045 | 0.215 |
| 12.00 | 0.046 | 0.238 | 0.026 | 0.051 | 0.069 | 0.299 | 0.042 | 0.080 | 0.051 | 0.210 |
| 14.00 | 0.049 | 0.254 | 0.030 | 0.058 | 0.066 | 0.321 | 0.051 | 0.094 | 0.062 | 0.216 |
| 24.00 | 0.024 | 0.106 | 0.018 | 0.024 | 0.034 | 0.277 | 0.036 | 0.047 | 0.042 | 0.151 |
| 26.00 | 0.022 | 0.082 | 0.018 | 0.018 | 0.028 | 0.229 | 0.040 | 0.035 | 0.042 | 0.118 |
| 28.00 | 0.021 | 0.065 | 0.015 | 0.017 | 0.020 | 0.246 | 0.036 | 0.030 | 0.036 | 0.091 |
| 30.00 | 0.014 | 0.059 | 0.008 | 0.012 | 0.016 | 0.221 | 0.032 | 0.019 | 0.028 | 0.080 |

0.00 = concentration not dectectable, treated as 0 nd = concentration not dectectable

**Table D(3) :** Individual Plasma Concentrations (μmol/l) after Oral Administration of CR B ; Metoprolol Succinate CR Tablet 95mg.

| Subject / Time (h) | 1 | 2 | 3 | 4 | 5 | 6 | 7 | 8 | 9 | 10 |
|---|---|---|---|---|---|---|---|---|---|---|
| 0.00 | 0.000 | 0.000 | 0.000 | 0.000 | 0.000 | 0.000 | 0.000 | 0.000 | 0.000 | 0.000 |
| 1.00 | 0.000 | 0.000 | 0.000 | 0.008 | 0.000 | 0.018 | 0.000 | 0.023 | 0.000 | 0.000 |
| 2.00 | 0.008 | 0.014 | 0.019 | 0.015 | 0.011 | 0.039 | 0.009 | 0.017 | 0.009 | 0.043 |
| 3.00 | 0.010 | 0.029 | 0.013 | 0.016 | 0.016 | 0.061 | 0.011 | 0.032 | 0.012 | 0.052 |
| 4.00 | 0.013 | 0.078 | 0.015 | 0.013 | 0.026 | 0.089 | 0.025 | 0.041 | 0.020 | 0.060 |
| 5.00 | 0.013 | 0.086 | 0.013 | 0.020 | 0.028 | 0.101 | 0.023 | 0.036 | 0.018 | 0.071 |
| 6.00 | 0.013 | 0.090 | 0.012 | 0.021 | 0.025 | 0.107 | 0.021 | 0.039 | 0.017 | 0.059 |
| 8.00 | 0.014 | 0.102 | 0.011 | 0.022 | 0.025 | 0.130 | 0.021 | 0.039 | 0.019 | 0.082 |
| 10.00 | 0.016 | 0.111 | 0.011 | 0.029 | 0.028 | 0.137 | 0.024 | 0.037 | 0.020 | 0.085 |
| 12.00 | 0.019 | 0.130 | 0.014 | 0.037 | 0.035 | 0.158 | 0.022 | 0.038 | 0.022 | 0.093 |
| 14.00 | 0.027 | 0.159 | 0.018 | 0.057 | 0.045 | 0.192 | 0.041 | 0.048 | 0.035 | 0.159 |
| 24.00 | 0.025 | 0.259 | 0.020 | 0.038 | 0.062 | 0.258 | 0.053 | 0.062 | 0.058 | 0.187 |
| 26.00 | 0.027 | 0.247 | 0.019 | 0.029 | 0.063 | 0.277 | 0.054 | 0.066 | 0.057 | 0.152 |
| 28.00 | 0.022 | 0.240 | 0.016 | 0.031 | 0.043 | 0.245 | 0.054 | 0.060 | 0.052 | 0.116 |
| 30.00 | 0.016 | 0.204 | 0.010 | 0.029 | 0.026 | 0.225 | 0.049 | 0.048 | 0.054 | 0.114 |

0.00 = concentration not dectectable, treated as 0 nd = concentration not dectectable

**Table D(4) :** Individual Plasma Concentrations (μmol/l) after Oral Administration of CR C ; Metoprolol Succinate CR Tablet 95mg.

| Time | pH 6.8 / 100 rpm | | pH 1.2 / 100 rpm | | pH 4.0 / 100 rpm | | pH 6.8 / 50 rpm | | pH 6.8 / 150 rpm | |
|---|---|---|---|---|---|---|---|---|---|---|
| | Mean | SD | Mean | SD | Mean | SD | Mean | SD | Mean | SD |
| 0 | 0.0 | | 0.0 | | 0.0 | | 0.0 | | 0.0 | |
| 1 | 23.3 | 2.3 | 28.5 | 2.9 | 23.7 | 3.9 | 19.3 | 2.8 | 26.2 | 3.2 |
| 2 | 34.5 | 3.1 | 39.3 | 3.9 | 35.5 | 5.0 | 30.3 | 3.7 | 37.5 | 4.2 |
| 3 | 42.8 | 3.1 | 47.0 | 4.5 | 44.7 | 5.2 | 38.8 | 3.9 | 45.7 | 4.9 |
| 4 | 50.3 | 4.7 | 53.0 | 4.5 | 51.8 | 6.0 | 46.3 | 3.7 | 52.3 | 5.2 |
| 6 | 60.2 | 3.8 | 62.7 | 4.9 | 63.7 | 6.3 | 57.8 | 4.0 | 63.0 | 5.8 |
| 8 | 69.5 | 3.3 | 71.2 | 5.2 | 73.5 | 6.3 | 67.2 | 3.6 | 72.0 | 6.2 |
| 10 | 77.0 | 3.7 | 78.3 | 5.4 | 81.0 | 6.4 | 75.8 | 4.0 | 79.2 | 6.5 |
| 12 | 83.5 | 3.4 | 84.0 | 5.2 | 87.2 | 6.7 | 82.3 | 3.8 | 85.7 | 6.5 |
| 14 | 88.5 | 3.4 | 88.3 | 5.2 | 91.0 | 6.4 | 87.5 | 4.0 | 90.7 | 7.1 |
| 16 | 91.7 | 3.6 | 91.8 | 5.3 | 94.3 | 6.6 | 91.0 | 3.7 | 93.7 | 7.1 |
| 18 | 94.0 | 3.5 | 94.2 | 5.2 | 96.0 | 6.4 | 93.2 | 4.0 | 95.7 | 7.1 |
| 20 | 95.3 | 3.4 | 94.5 | 5.4 | 97.0 | 6.4 | 95.2 | 4.0 | 97.0 | 7.1 |
| SD = standard variation | | | | | | | | | | |

**Table D(5) :** Mean and SD (n=6) per cent Metoprolol released *in vitro* at Different Times for CR A ; Metorolol Succinate CR 95mg

| Time | pH 6.8 / 100 rpm | | pH 1.2 / 100 rpm | | pH 4.0 / 100 rpm | | pH 6.8 / 50 rpm | | pH 6.8 / 150 rpm | |
|---|---|---|---|---|---|---|---|---|---|---|
| | Mean | SD | Mean | SD | Mean | SD | Mean | SD | Mean | SD |
| 0 | 0.0 | | 0.0 | | 0.0 | | 0.0 | | 0.0 | |
| 1 | 16.5 | 1.0 | 19.8 | 1.7 | 17.8 | 2.7 | 15.0 | 1.7 | 16.8 | 1.7 |
| 2 | 23.8 | 1.5 | 27.7 | 1.6 | 24.3 | 2.9 | 22.7 | 2.4 | 24.2 | 2.0 |
| 3 | 29.0 | 1.4 | 32.5 | 2.1 | 29.2 | 3.2 | 28.3 | 2.8 | 29.0 | 2.1 |
| 4 | 34.2 | 1.9 | 36.5 | 2.1 | 33.7 | 3.2 | 33.3 | 2.8 | 34.0 | 2.1 |
| 6 | 43.7 | 2.3 | 44.7 | 2.7 | 42.2 | 3.4 | 44.5 | 3.4 | 43.2 | 2.1 |
| 8 | 52.2 | 2.5 | 52.8 | 3.1 | 49.7 | 3.0 | 53.5 | 3.6 | 51.7 | 1.8 |
| 10 | 60.5 | 2.8 | 60.0 | 3.4 | 56.7 | 3.0 | 61.8 | 3.8 | 59.3 | 1.5 |
| 12 | 68.0 | 3.3 | 67.3 | 3.7 | 63.3 | 3.1 | 69.3 | 3.7 | 66.2 | 1.7 |
| 14 | 75.0 | 3.5 | 74.3 | 3.7 | 39.7 | 2.9 | 76.7 | 3.9 | 73.2 | 1.3 |
| 16 | 81.3 | 3.9 | 80.3 | 3.7 | 75.5 | 3.0 | 83.2 | 4.3 | 79.2 | 1.3 |
| 18 | 87.2 | 4.2 | 84.8 | 3.2 | 80.7 | 2.9 | 88.2 | 4.3 | 84.5 | 1.8 |
| 20 | 91.2 | 4.2 | 90.3 | 4.2 | 85.3 | 3.3 | 92.2 | 4.3 | 88.0 | 2.0 |
| SD = standard variation | | | | | | | | | | |

**Table D(6) :** Mean and SD (n=6) per cent Metoprolol released *in vitro* at Different Times for CR B ; Metorolol Succinate CR 95mg

| Time | pH 6.8 / 100 rpm | | pH 1.2 / 100 rpm | | pH 4.0 / 100 rpm | | pH 6.8 / 50 rpm | | pH 6.8 / 150 rpm | |
|---|---|---|---|---|---|---|---|---|---|---|
| | Mean | SD | Mean | SD | Mean | SD | Mean | SD | Mean | SD |
| 0 | 0.0 | | 0.0 | | 0.0 | | 0.0 | | 0.0 | |
| 1 | 4.7 | 0.8 | 6.4 | 1.3 | 4.8 | 0.4 | 3.2 | 0.4 | 5.8 | 0.8 |
| 2 | 7.5 | 0.6 | 9.4 | 0.9 | 8.0 | 0.7 | 5.8 | 0.8 | 8.8 | 1.2 |
| 3 | 9.8 | 1.0 | 11.6 | 1.1 | 10.4 | 1.1 | 8.0 | 0.6 | 11.5 | 1.4 |
| 4 | 11.7 | 1.0 | 13.8 | 1.3 | 12.4 | 1.1 | 10.2 | 1.0 | 14.0 | 1.6 |
| 6 | 17.2 | 1.5 | 17.2 | 1.1 | 19.4 | 1.1 | 15.0 | 1.3 | 19.5 | 1.9 |
| 8 | 24.7 | 1.9 | 21.4 | 1.3 | 27.6 | 1.3 | 22.7 | 2.0 | 27.5 | 1.9 |
| 10 | 31.7 | 1.9 | 27.4 | 1.3 | 36.4 | 2.0 | 30.3 | 2.3 | 35.5 | 1.9 |
| 12 | 39.2 | 2.3 | 34.0 | 1.6 | 45.0 | 2.0 | 37.7 | 2.6 | 43.0 | 2.3 |
| 14 | 46.0 | 2.5 | 40.6 | 1.8 | 52.4 | 2.8 | 45.0 | 2.7 | 51.0 | 2.3 |
| 16 | 52.0 | 3.0 | 47.0 | 2.1 | 60.4 | 3.4 | 51.8 | 3.4 | 58.3 | 2.5 |
| 18 | 59.0 | 3.0 | 53.4 | 2.1 | 67.8 | 3.8 | 58.7 | 3.3 | 65.5 | 2.4 |
| 20 | 66.0 | 3.7 | 58.8 | 2.8 | 74.4 | 4.0 | 65.0 | 3.5 | 72.0 | 2.6 |
| SD = standard variation | | | | | | | | | | |

**Table D(7) :** Mean and SD (n=6) per cent Metoprolol released *in vitro* at Different Times for CR C ; Metorolol Succinate CR 95mg

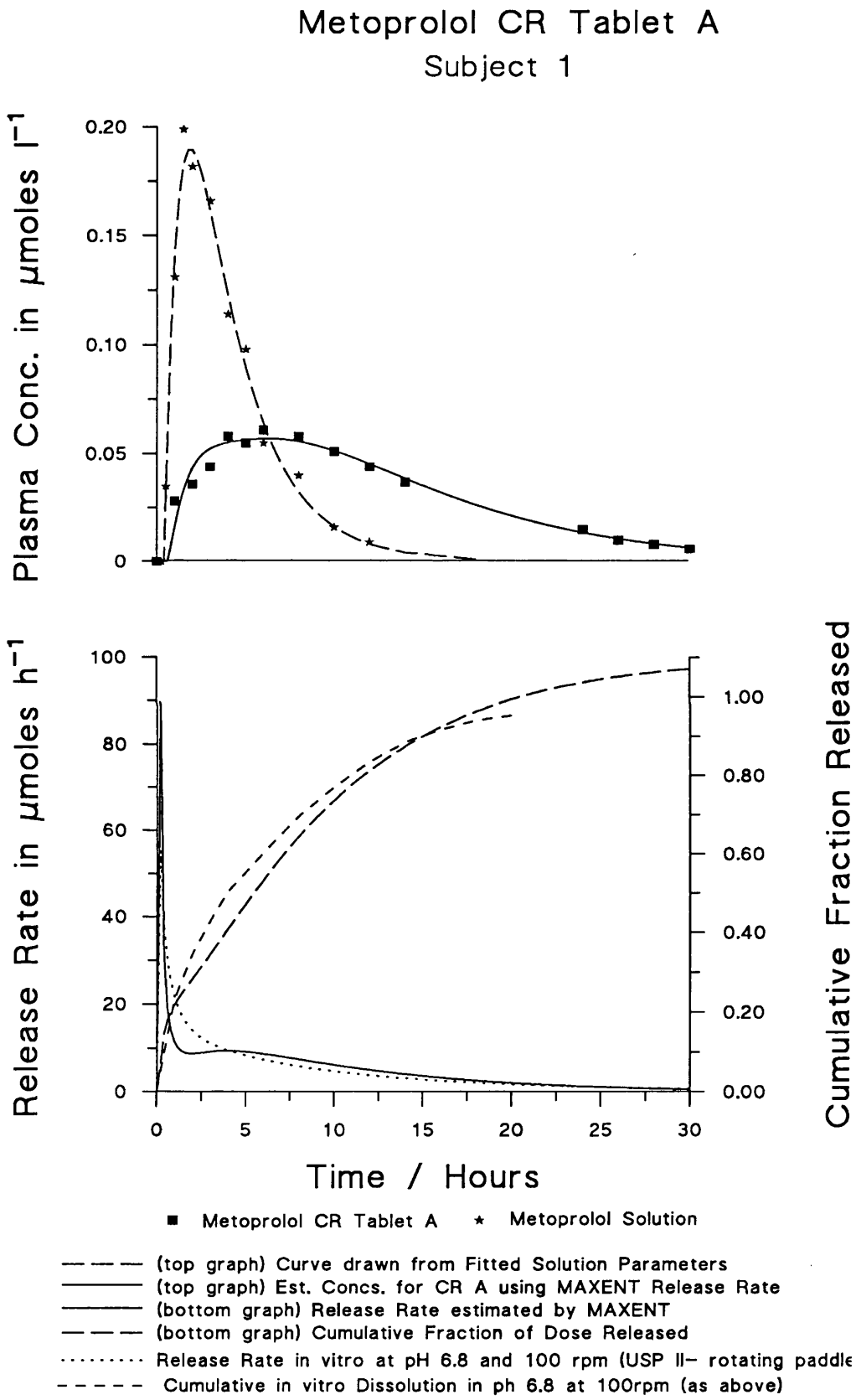


**Figure E.1** : Results from MAXENT for Metoprolol CR A, Subject 1

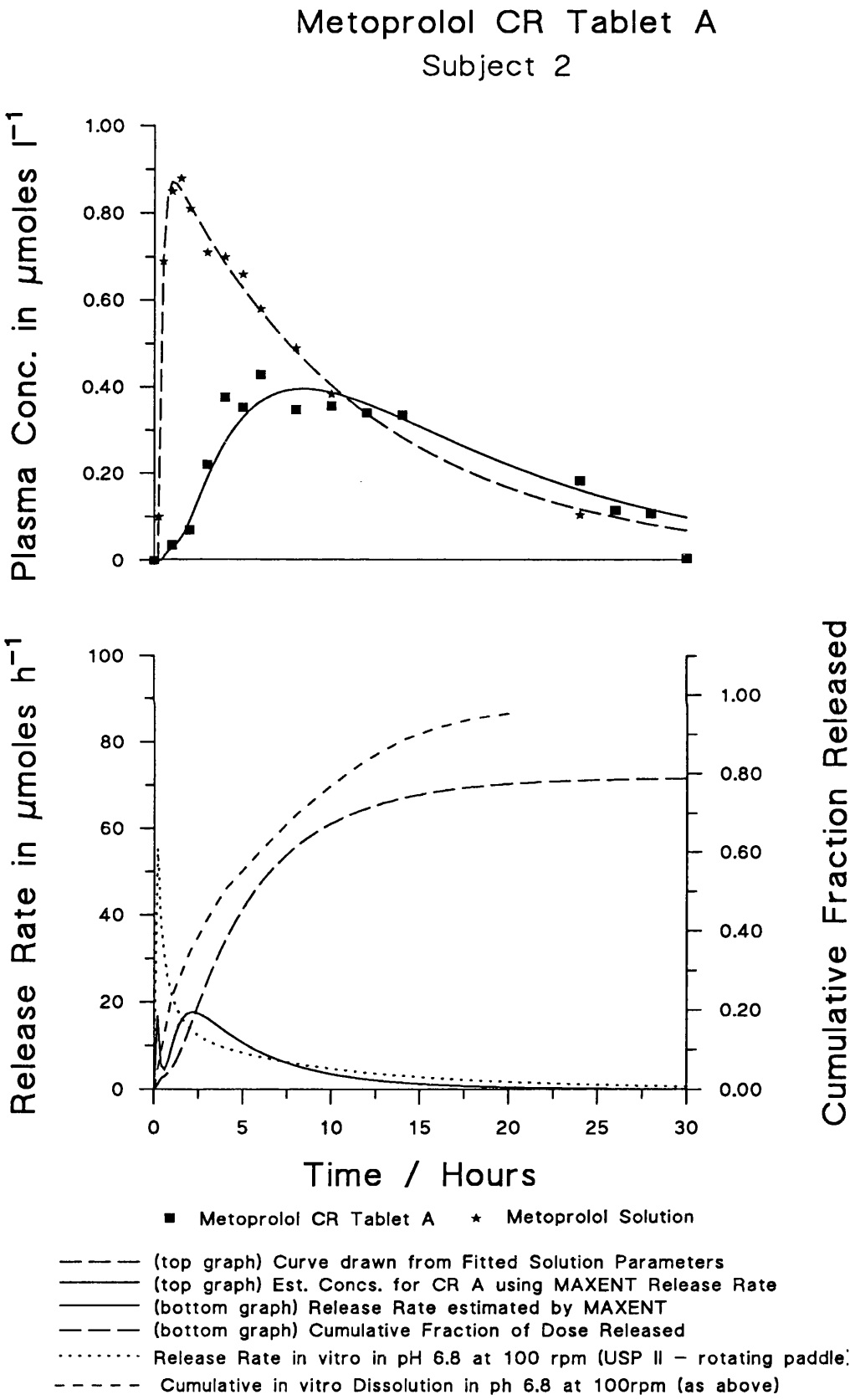


**Figure E.2** : Results from MAXENT for Metoprolol CR A, Subject 2

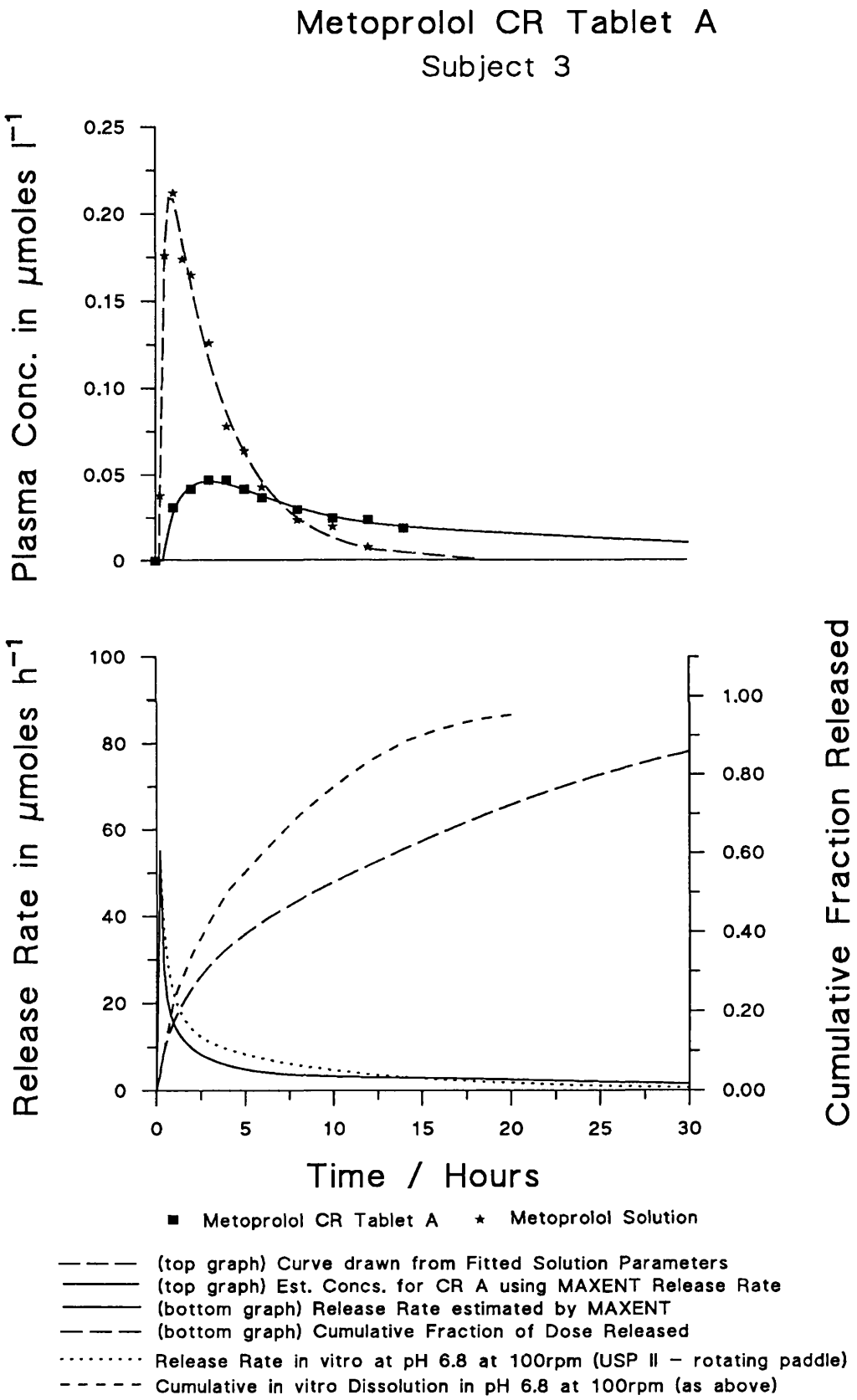


**Figure E.3** : Results from MAXENT for Metoprolol CR A, Subject 3

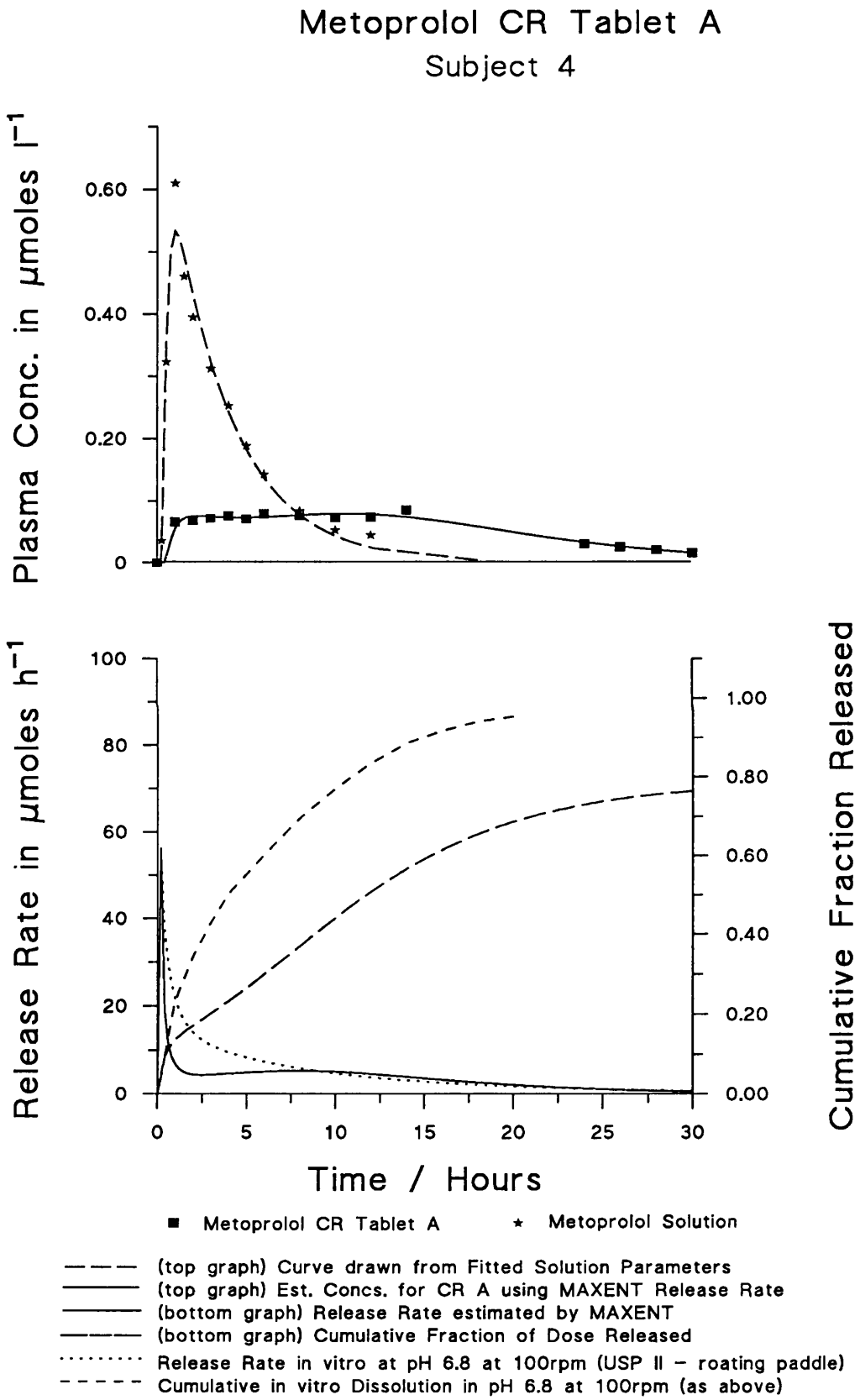


**Figure E.4** : Results from MAXENT for Metoprolol CR A, Subject 4

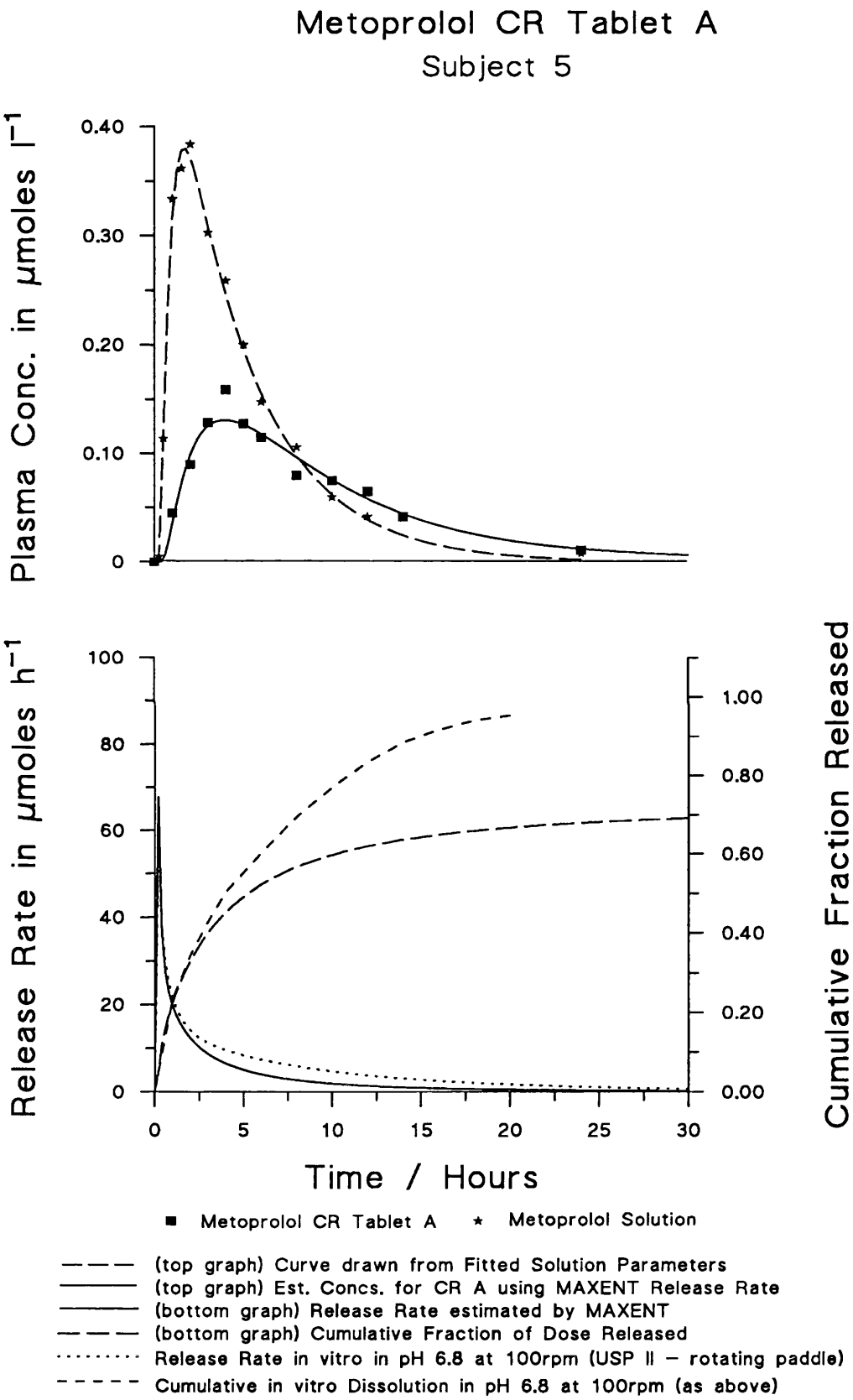


**Figure E.5** : Results from MAXENT for Metoprolol CR A, Subject 5

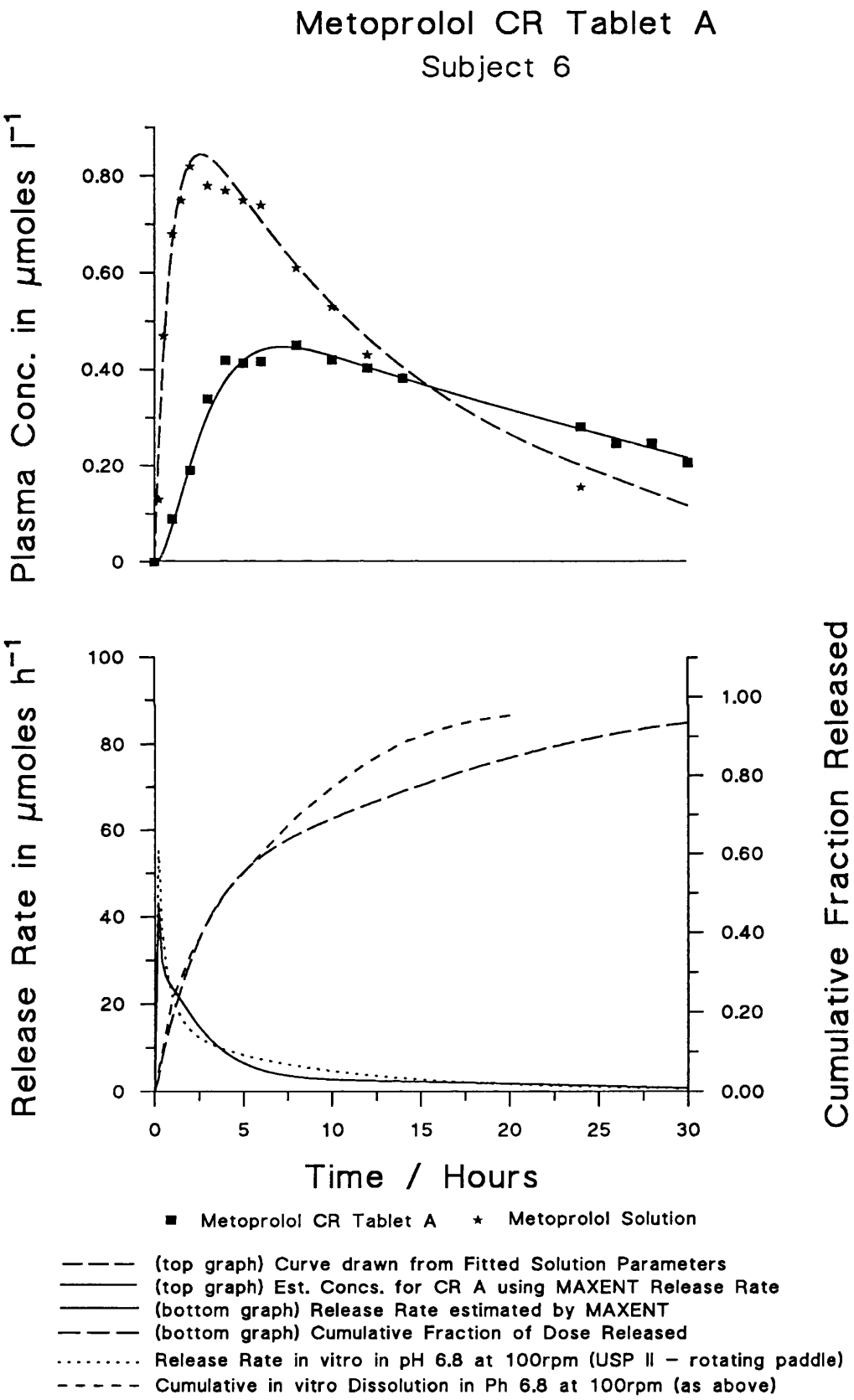


**Figure E.6** : Results from MAXENT for Metoprolol CR A, Subject 6

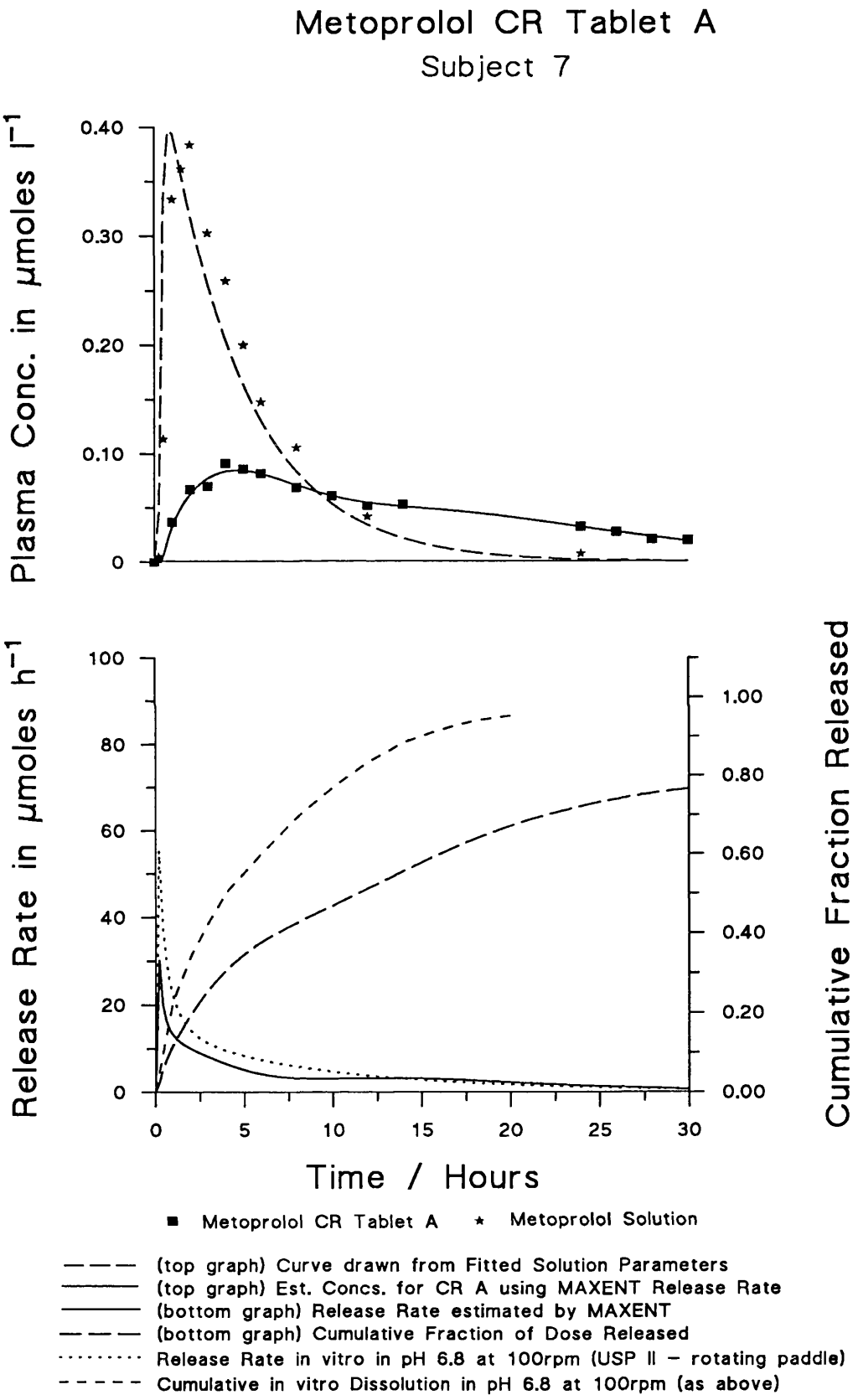


**Figure E.7** : Results from MAXENT for Metoprolol CR A, Subject 7

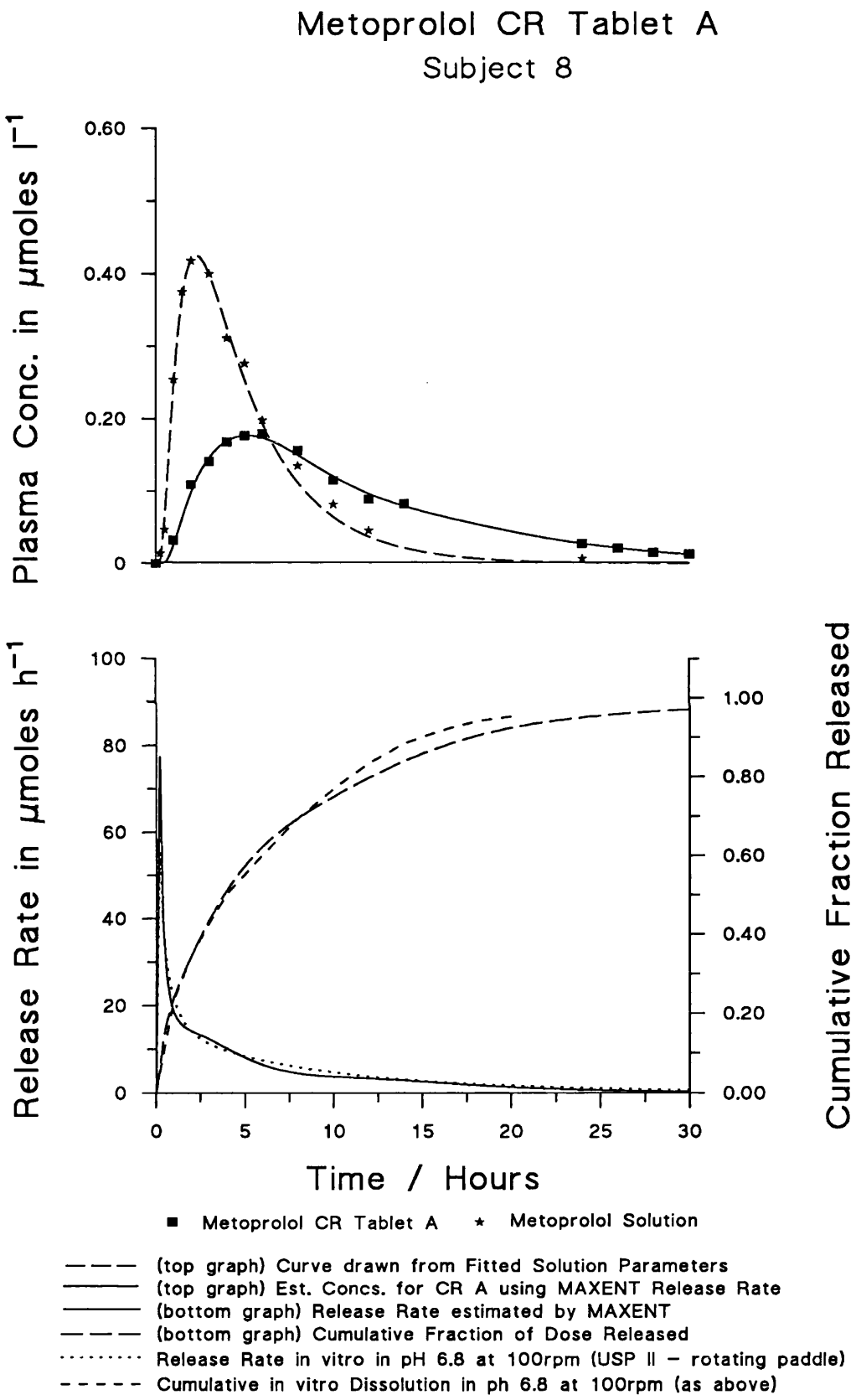


**Figure E.8** : Results from MAXENT for Metoprolol CR A, Subject 8

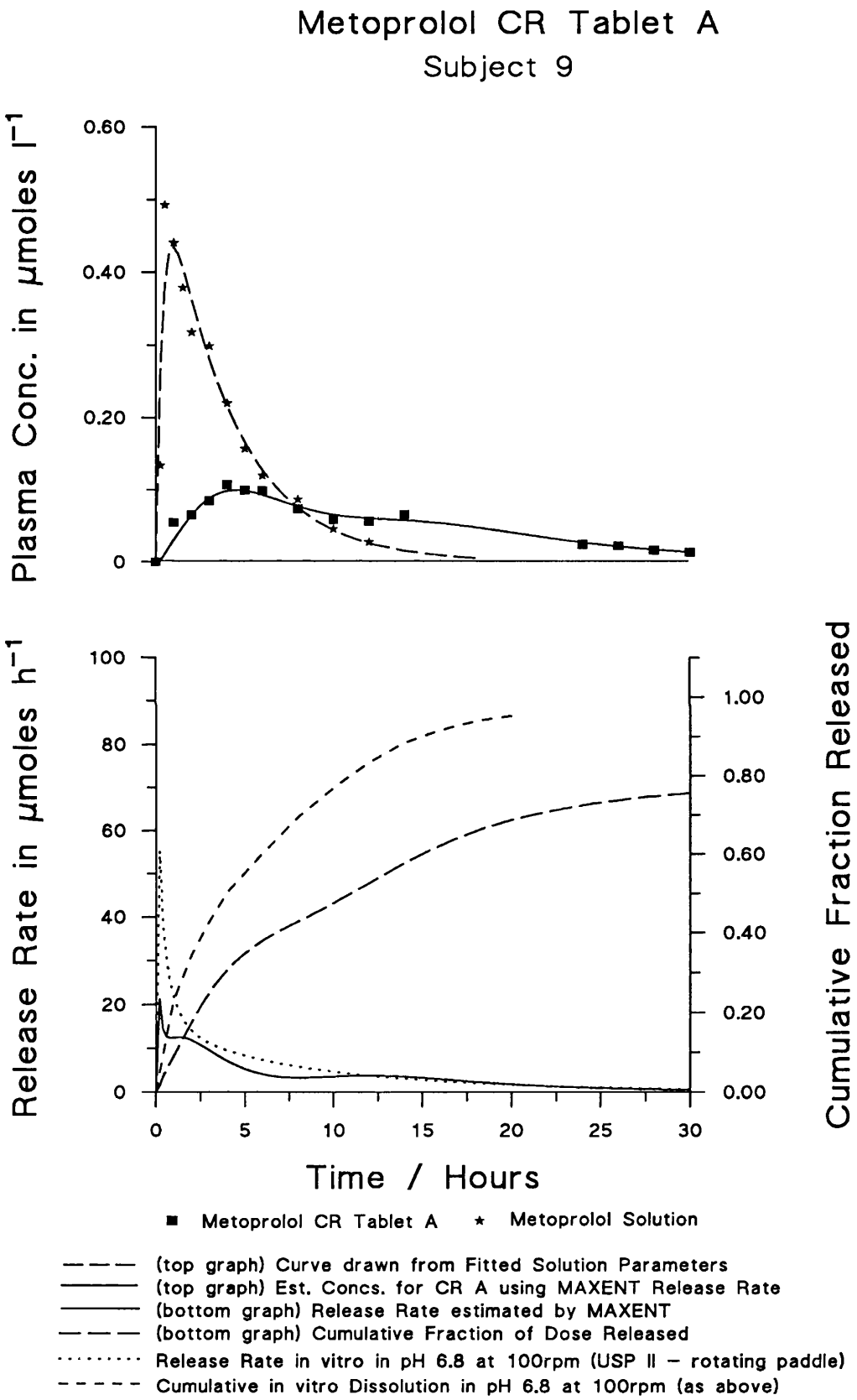


**Figure E.9** : Results from MAXENT for Metoprolol CR A, Subject 9

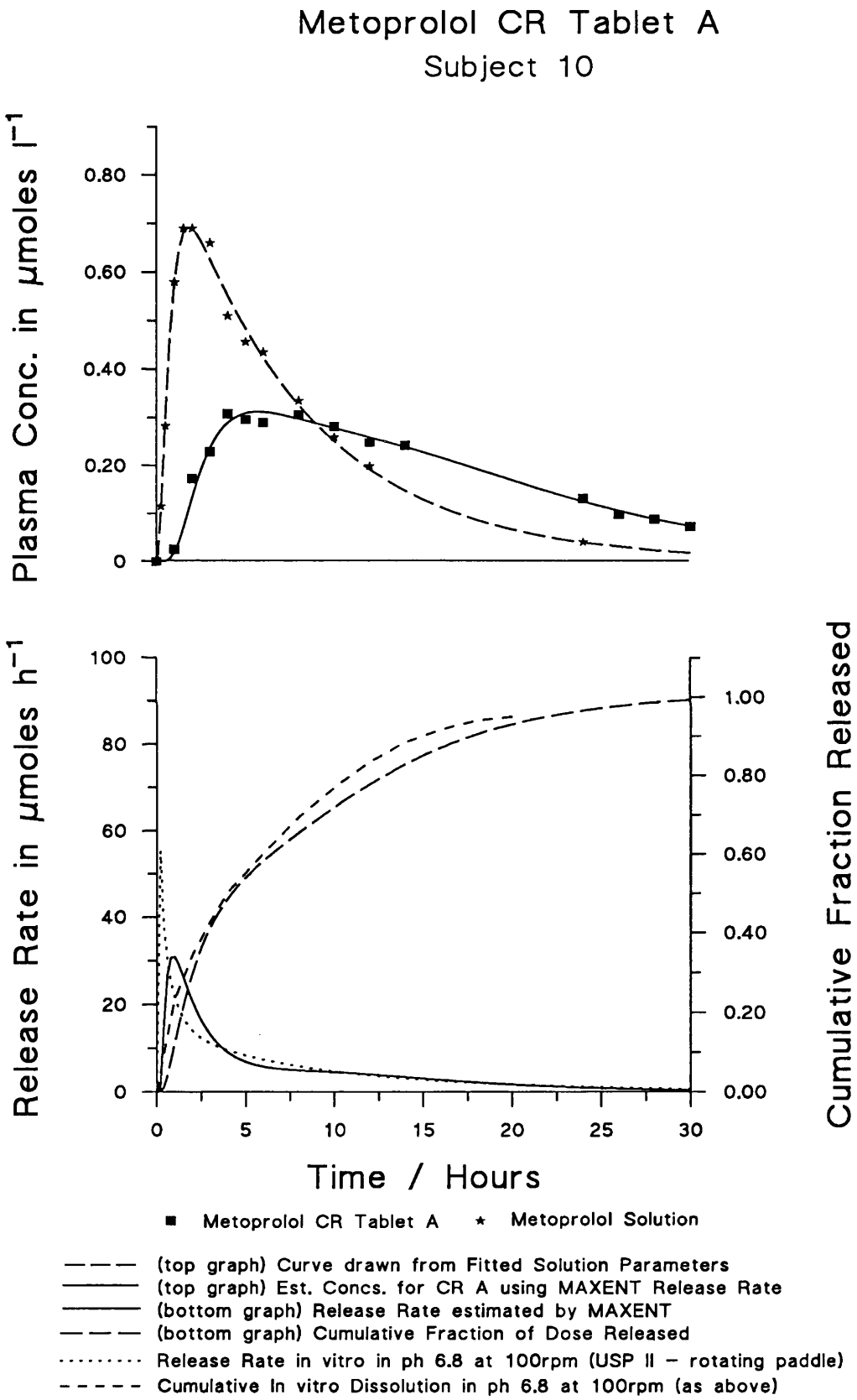


**Figure E.10** : Results from MAXENT for Metoprolol CR A, Subject 10

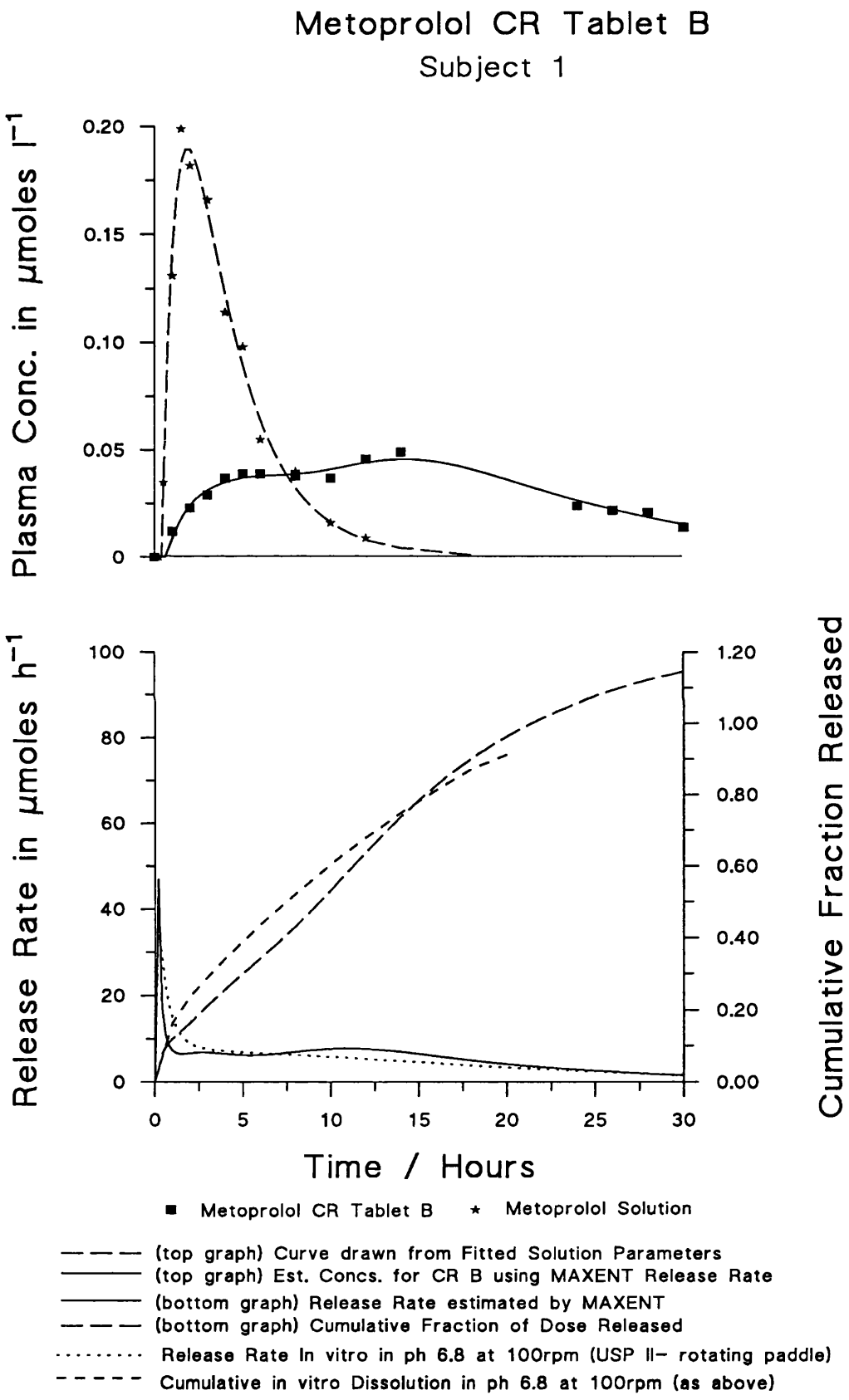


**Figure E.11** : Results from MAXENT for Metoprolol CR B, Subject 1

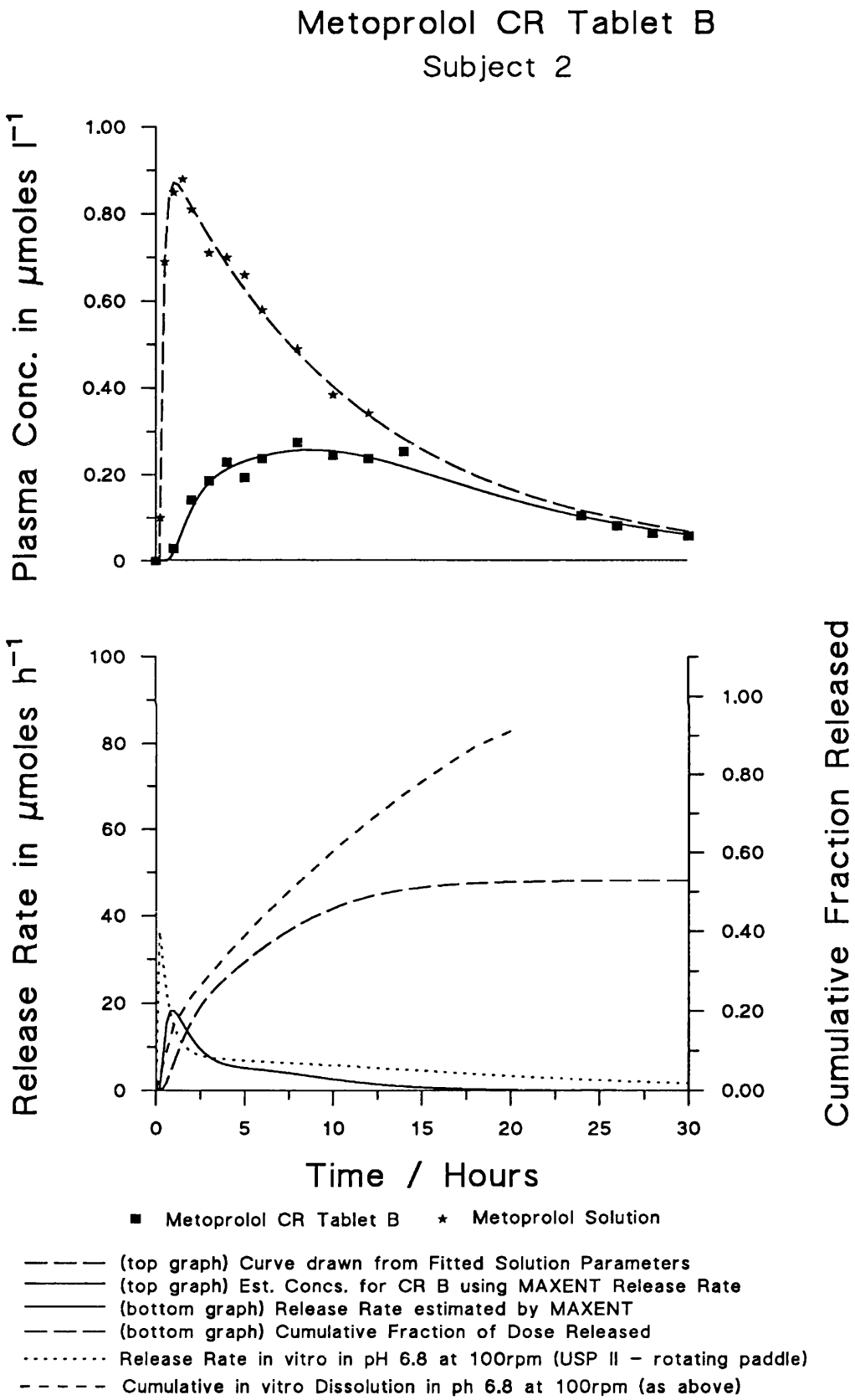


**Figure E.12** : Results from MAXENT for Metoprolol CR B, Subject 2

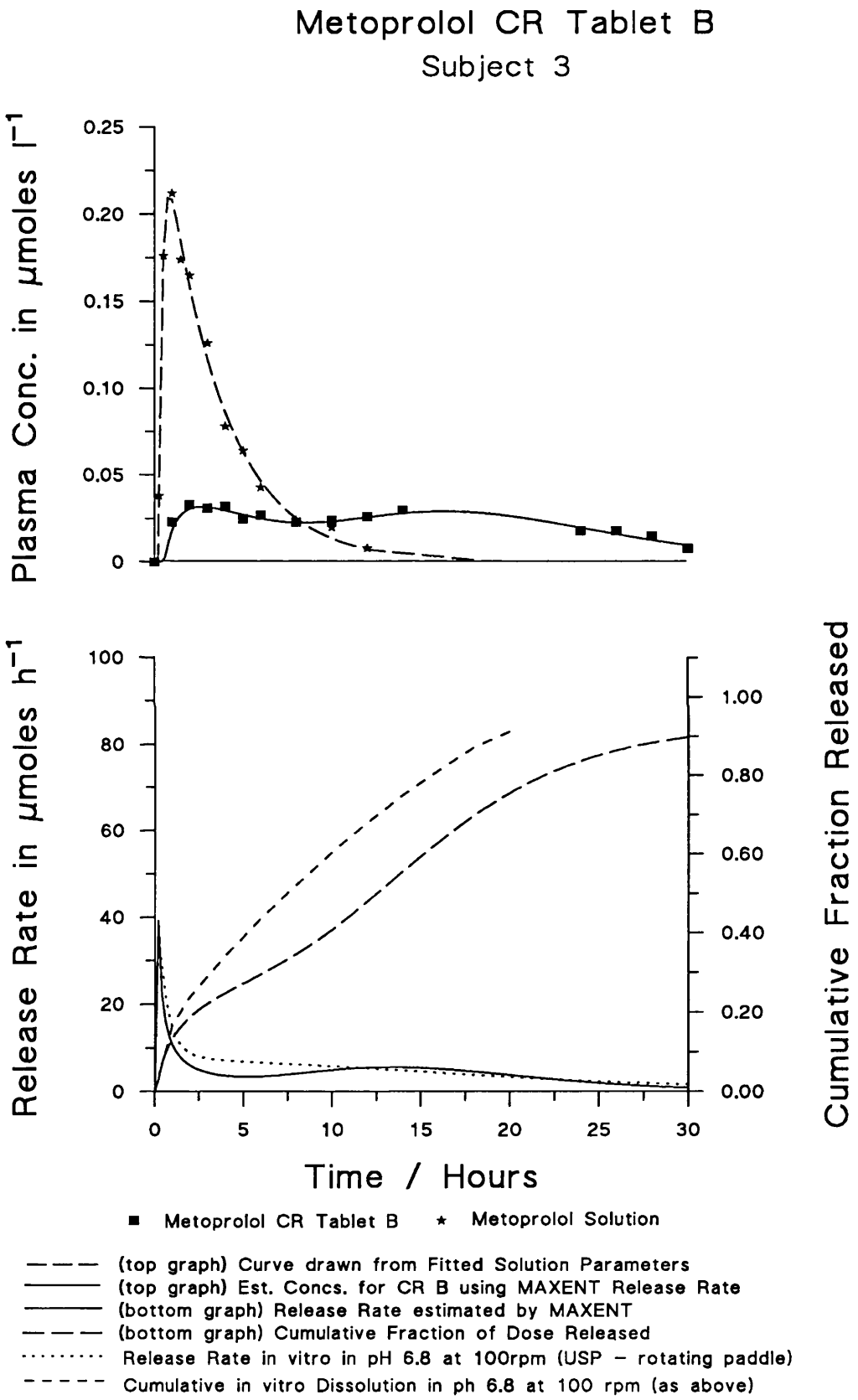


**Figure E.13** : Results from MAXENT for Metoprolol CR B, Subject 3

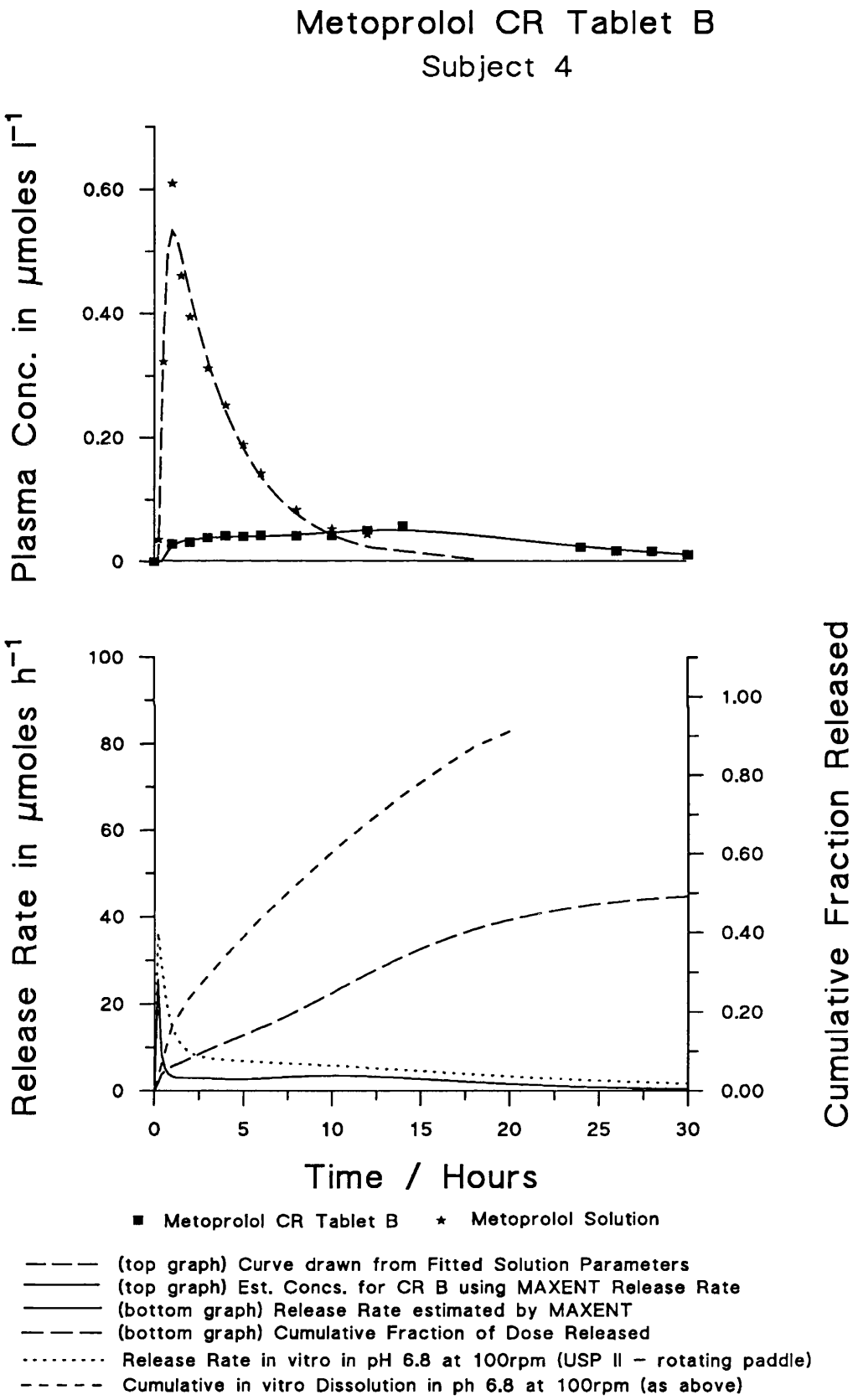


**Figure E.14** : Results from MAXENT for Metoprolol CR B, Subject 4

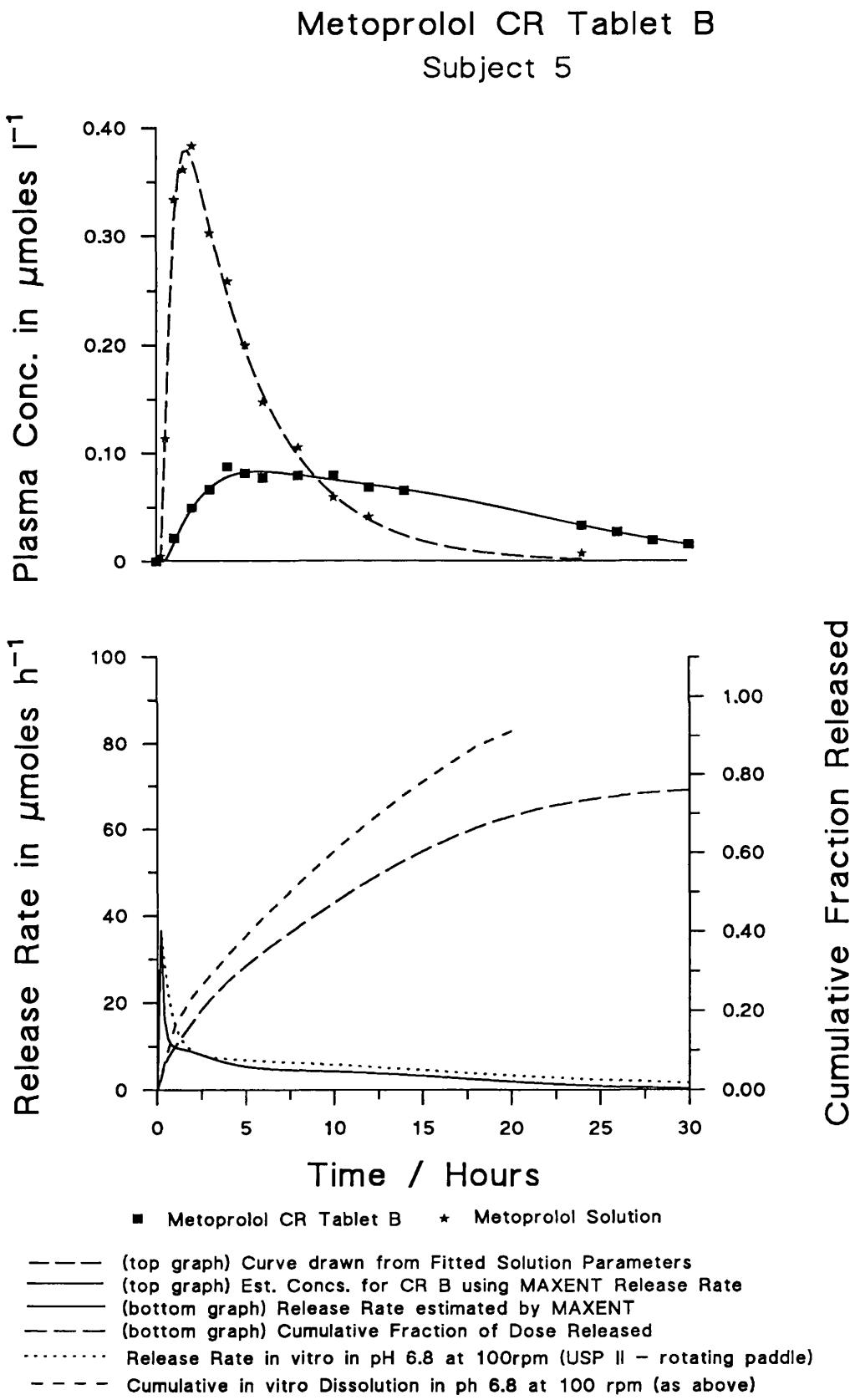


**Figure E.15** : Results from MAXENT for Metoprolol CR B, Subject 5

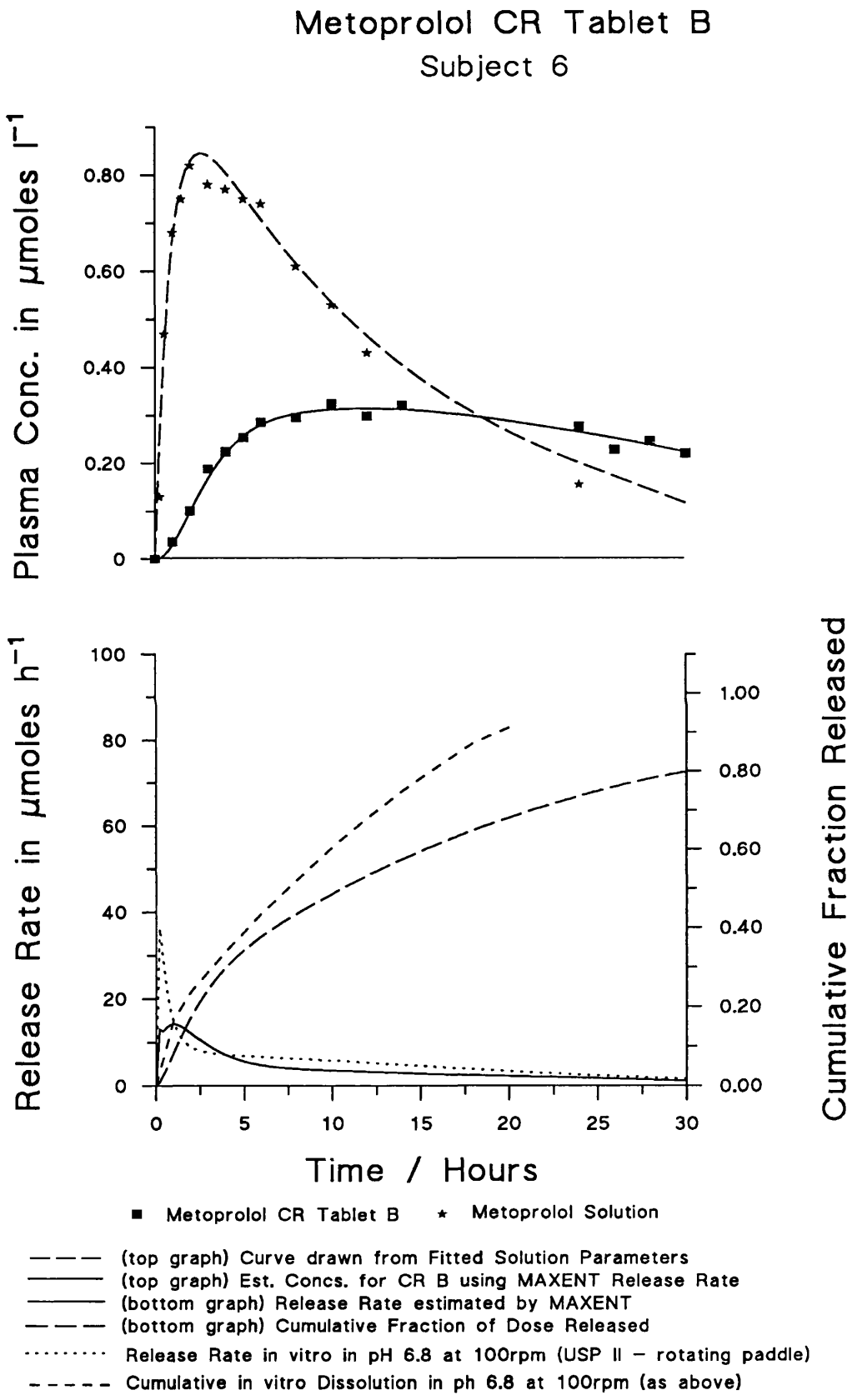


**Figure E.16** : Results from MAXENT for Metoprolol CR B, Subject 6

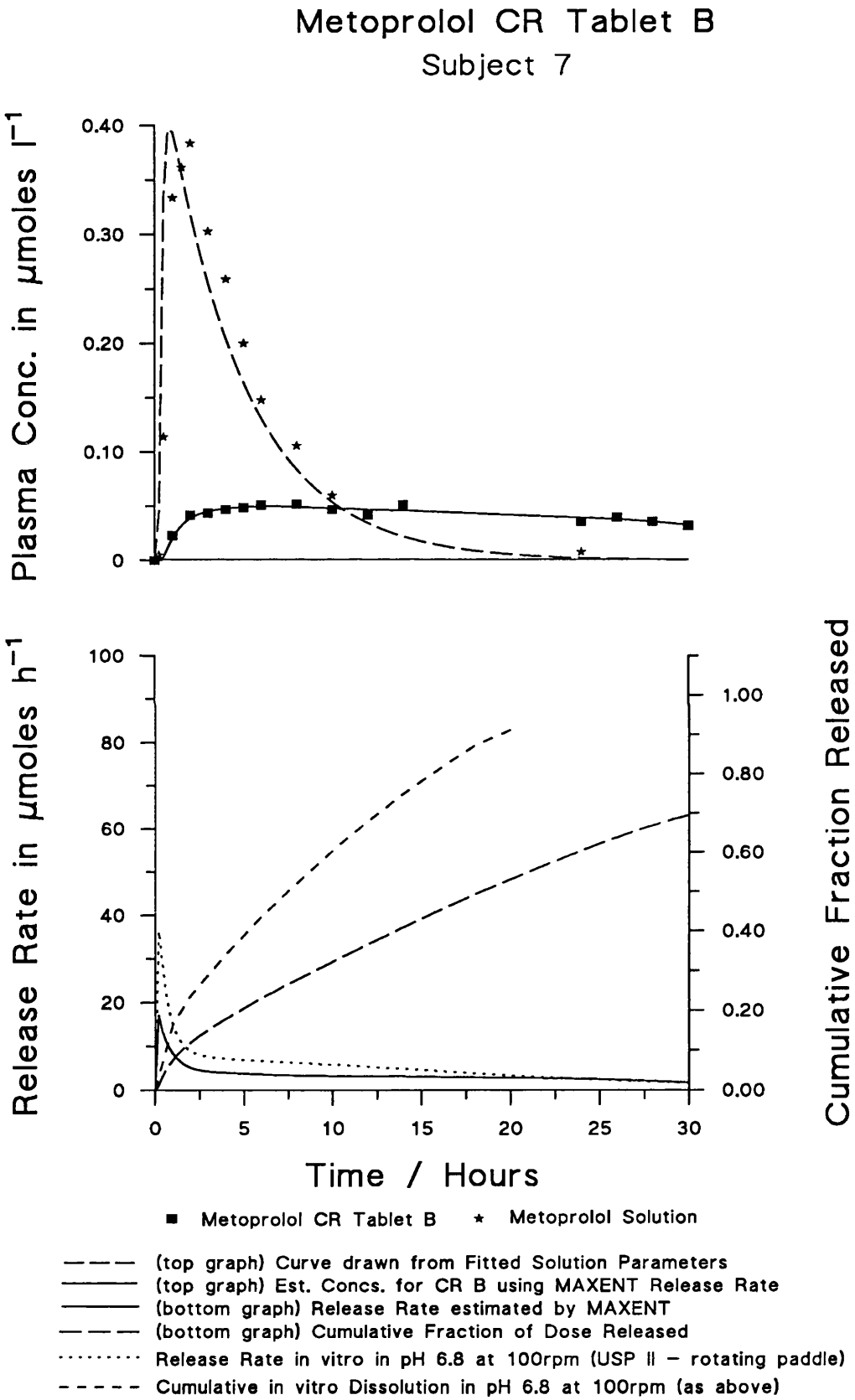


**Figure E.17** : Results from MAXENT for Metoprolol CR B, Subject 7

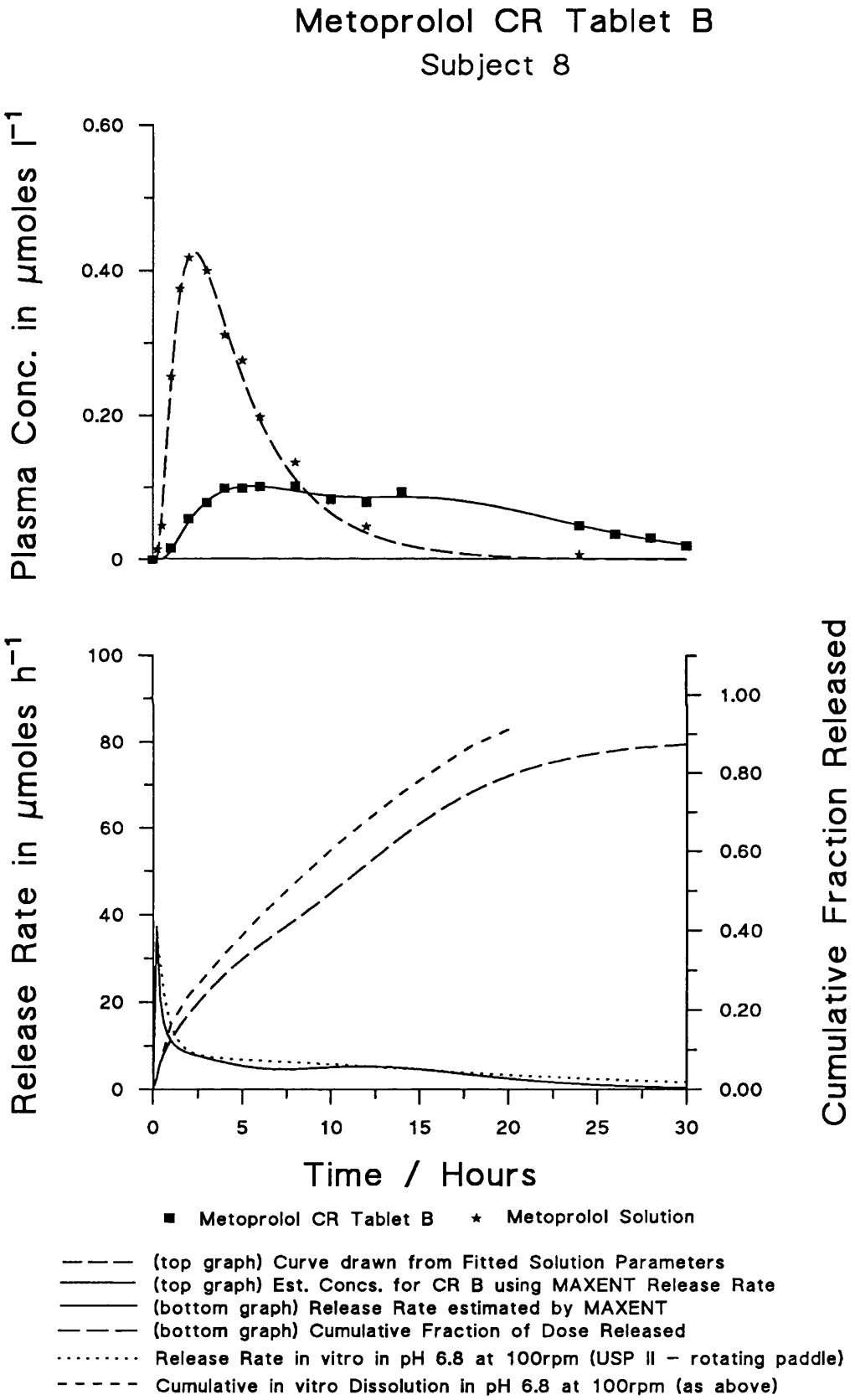


**Figure E.18** : Results from MAXENT for Metoprolol CR B, Subject 8

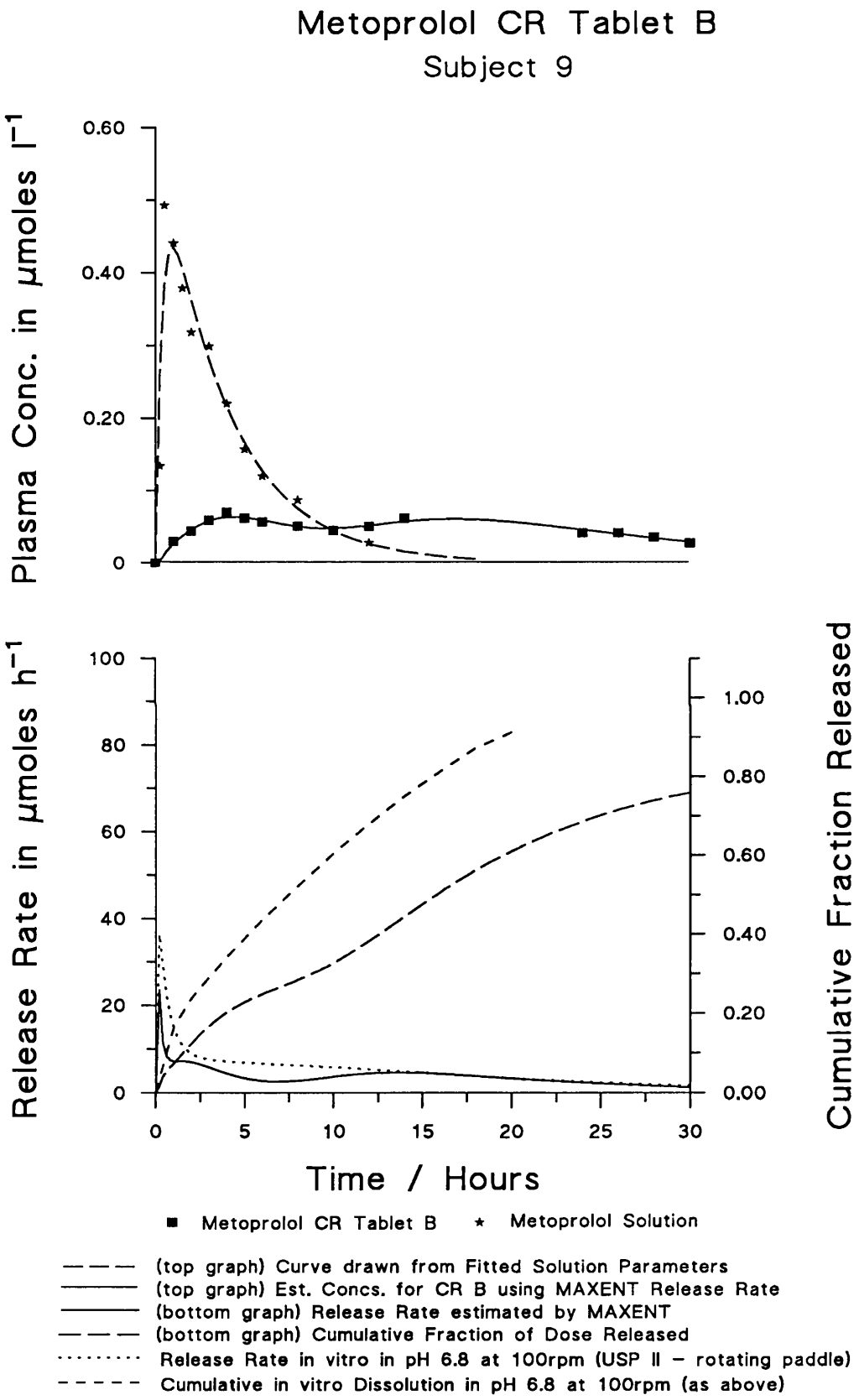


**Figure E.19** : Results from MAXENT for Metoprolol CR B, Subject 9

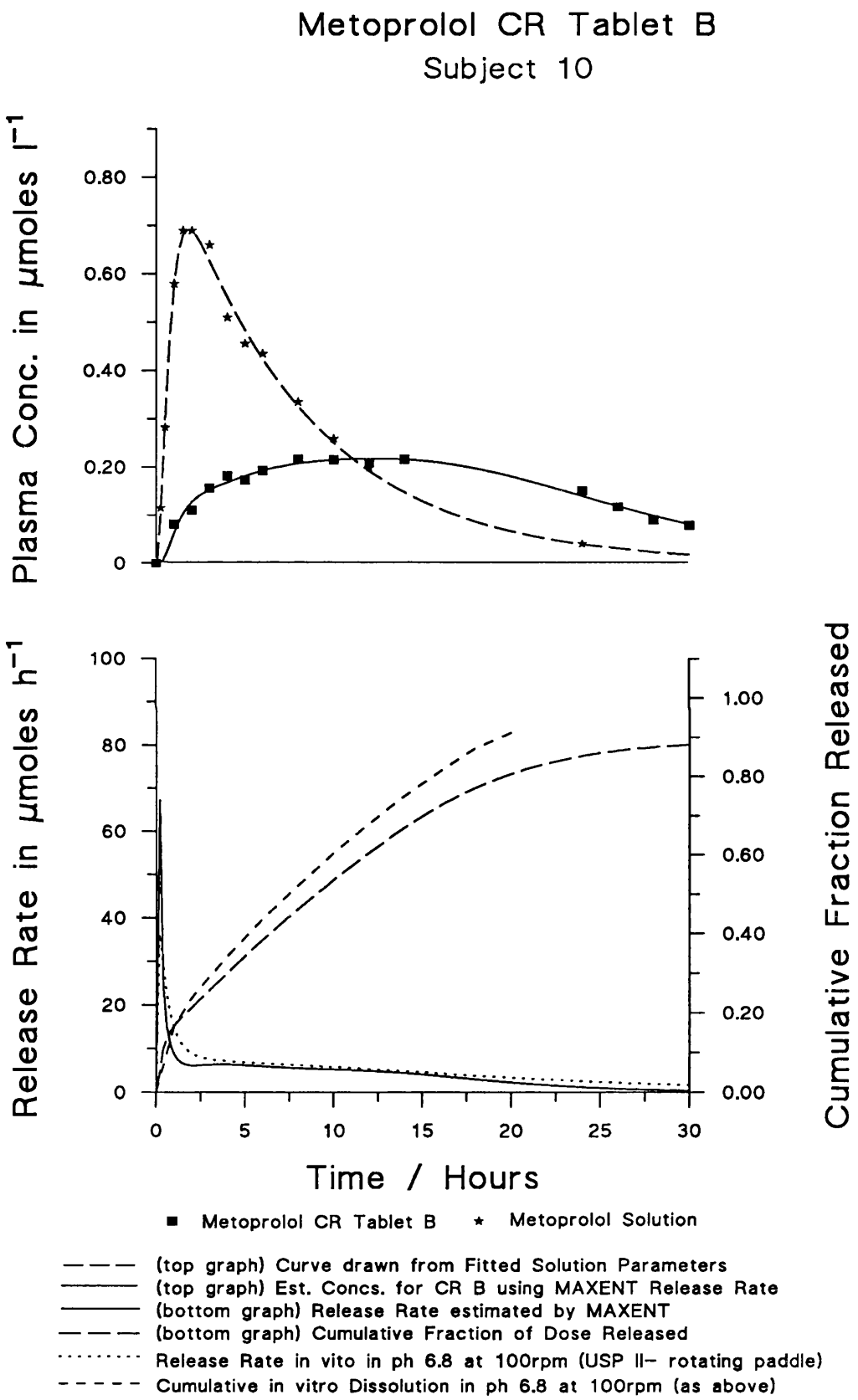


**Figure E.20** : Results from MAXENT for Metoprolol CR B, Subject 10

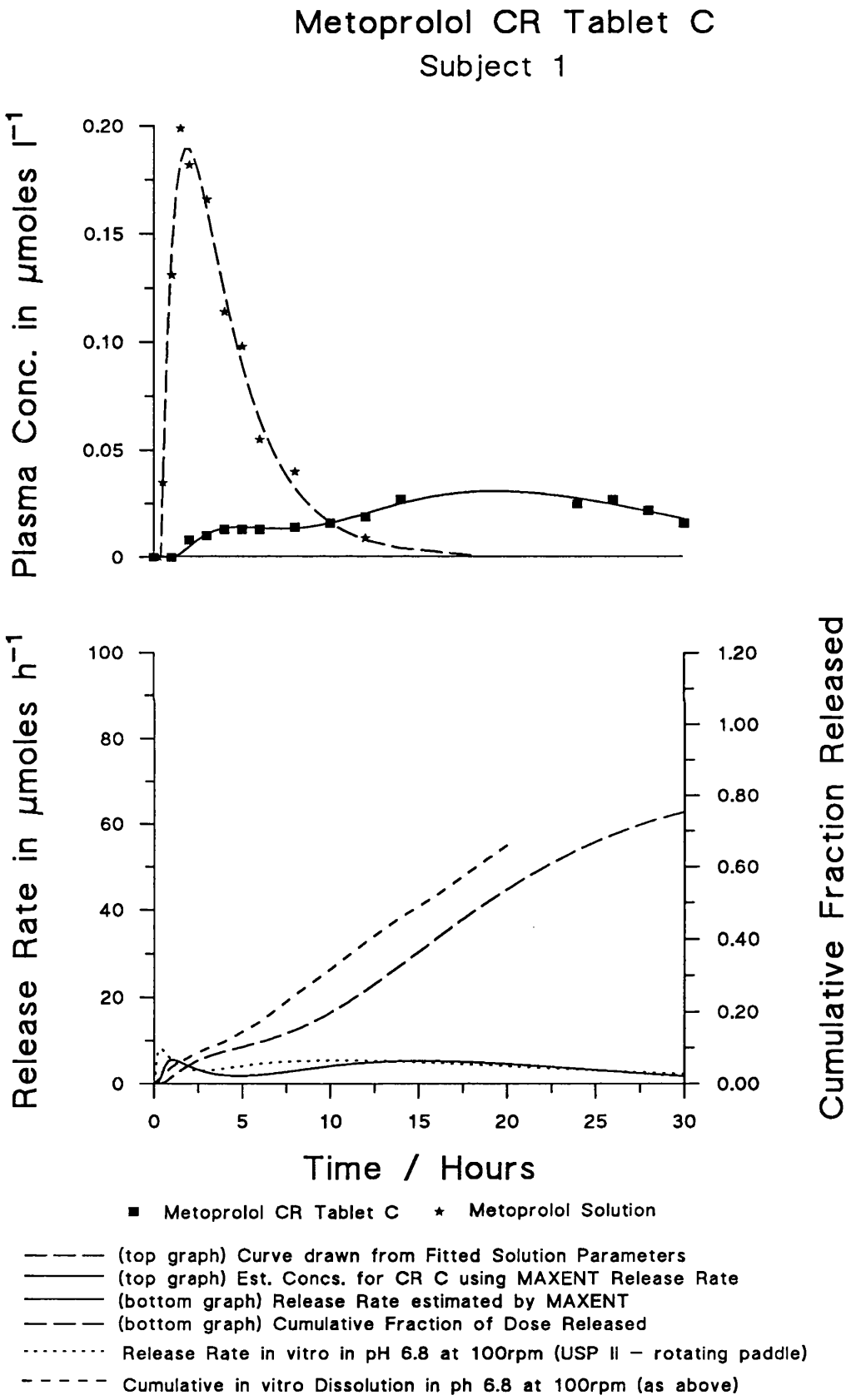


**Figure E.21** : Results from MAXENT for Metoprolol CR C, Subject 1

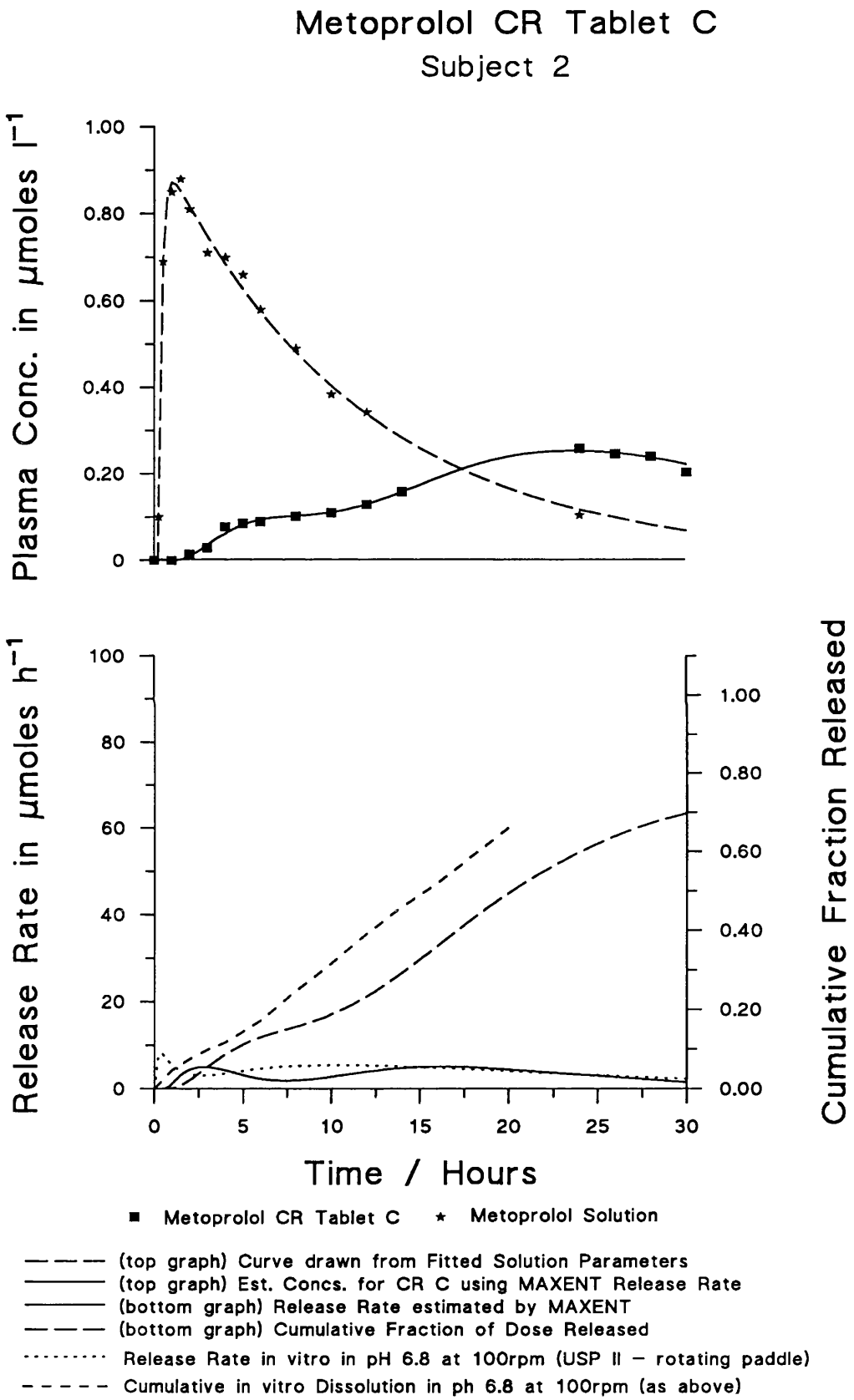


**Figure E.22** : Results from MAXENT for Metoprolol CR C, Subject 2

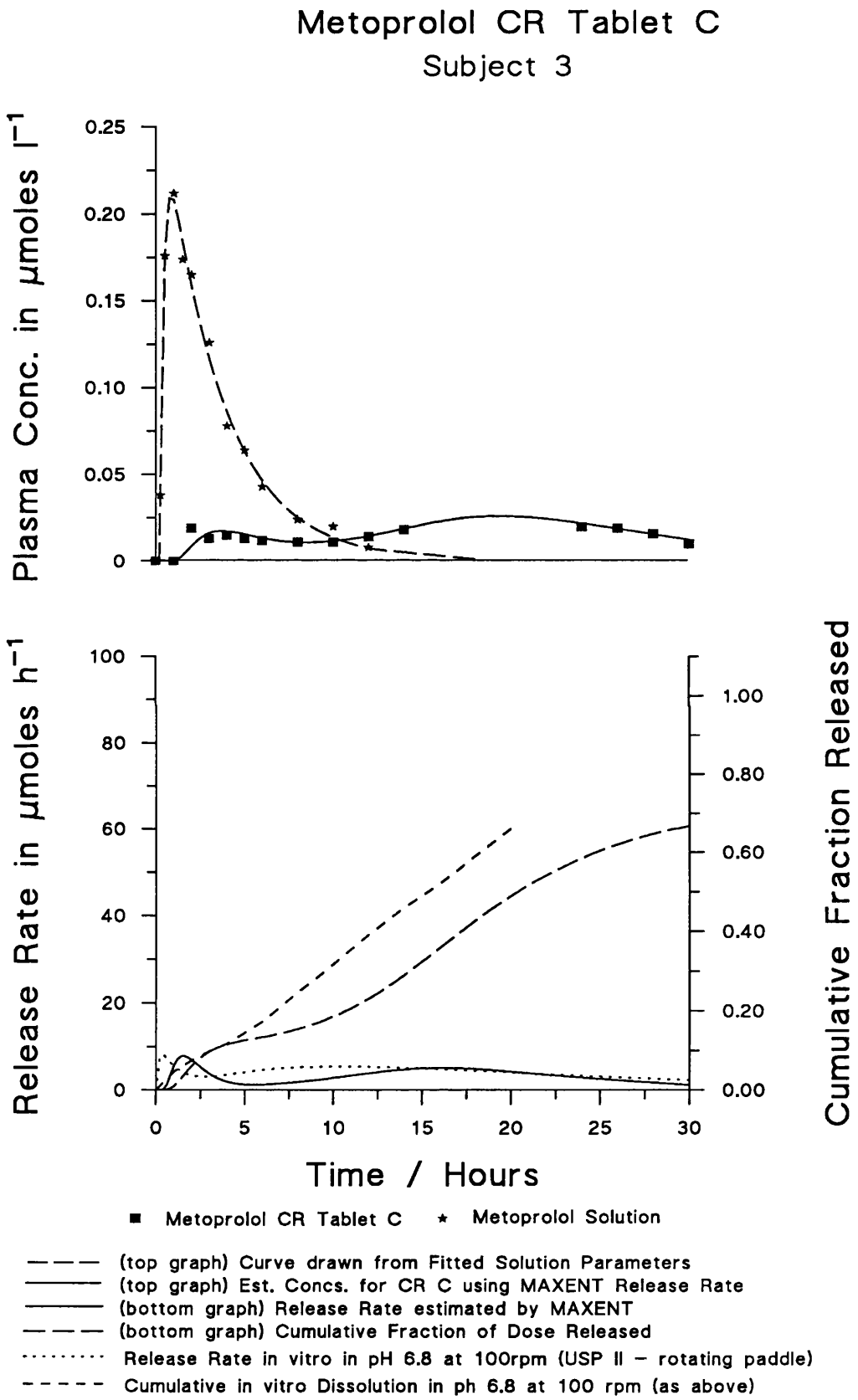


**Figure E.23** : Results from MAXENT for Metoprolol CR C, Subject 3

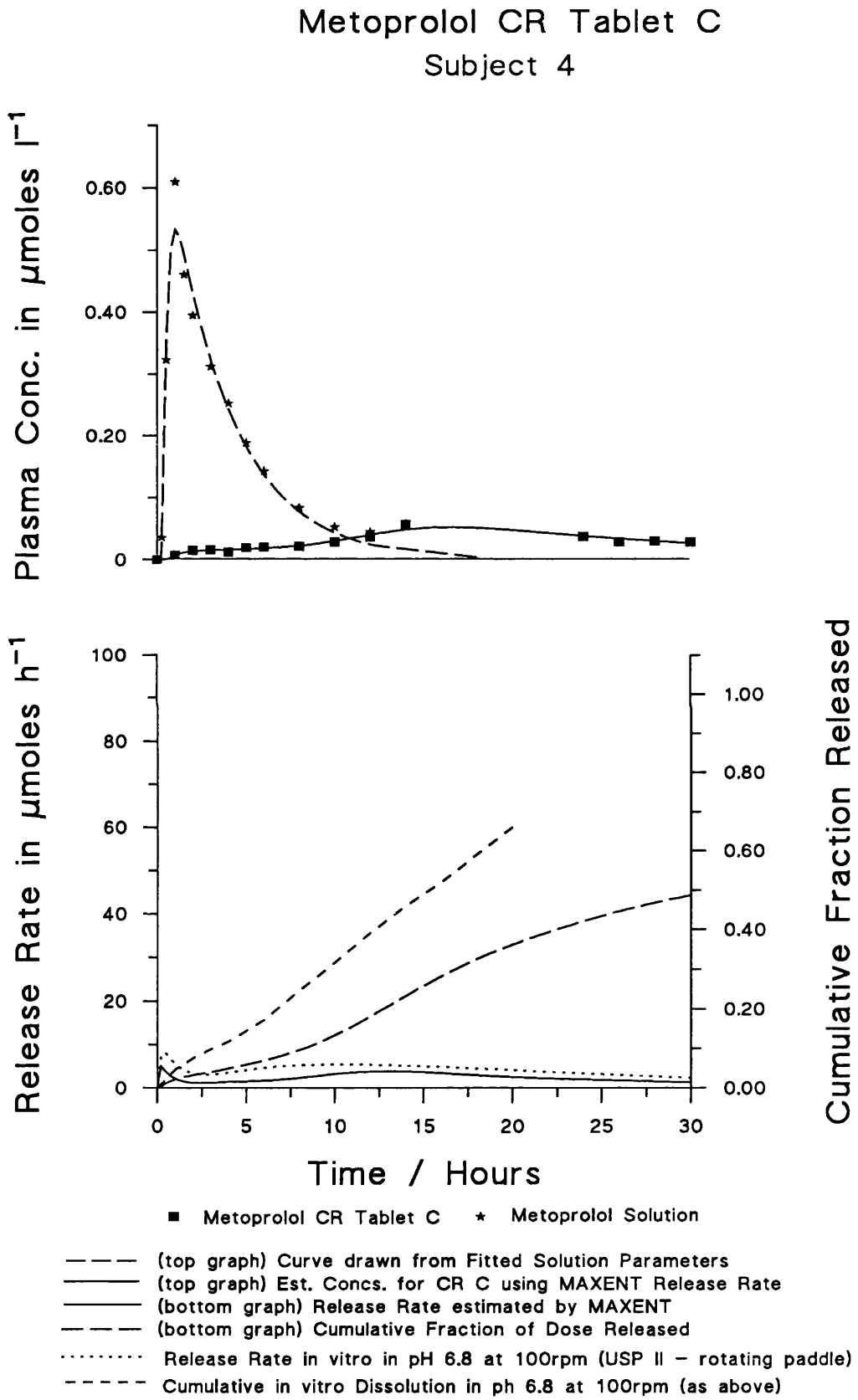


**Figure E.24** : Results from MAXENT for Metoprolol CR C, Subject 4

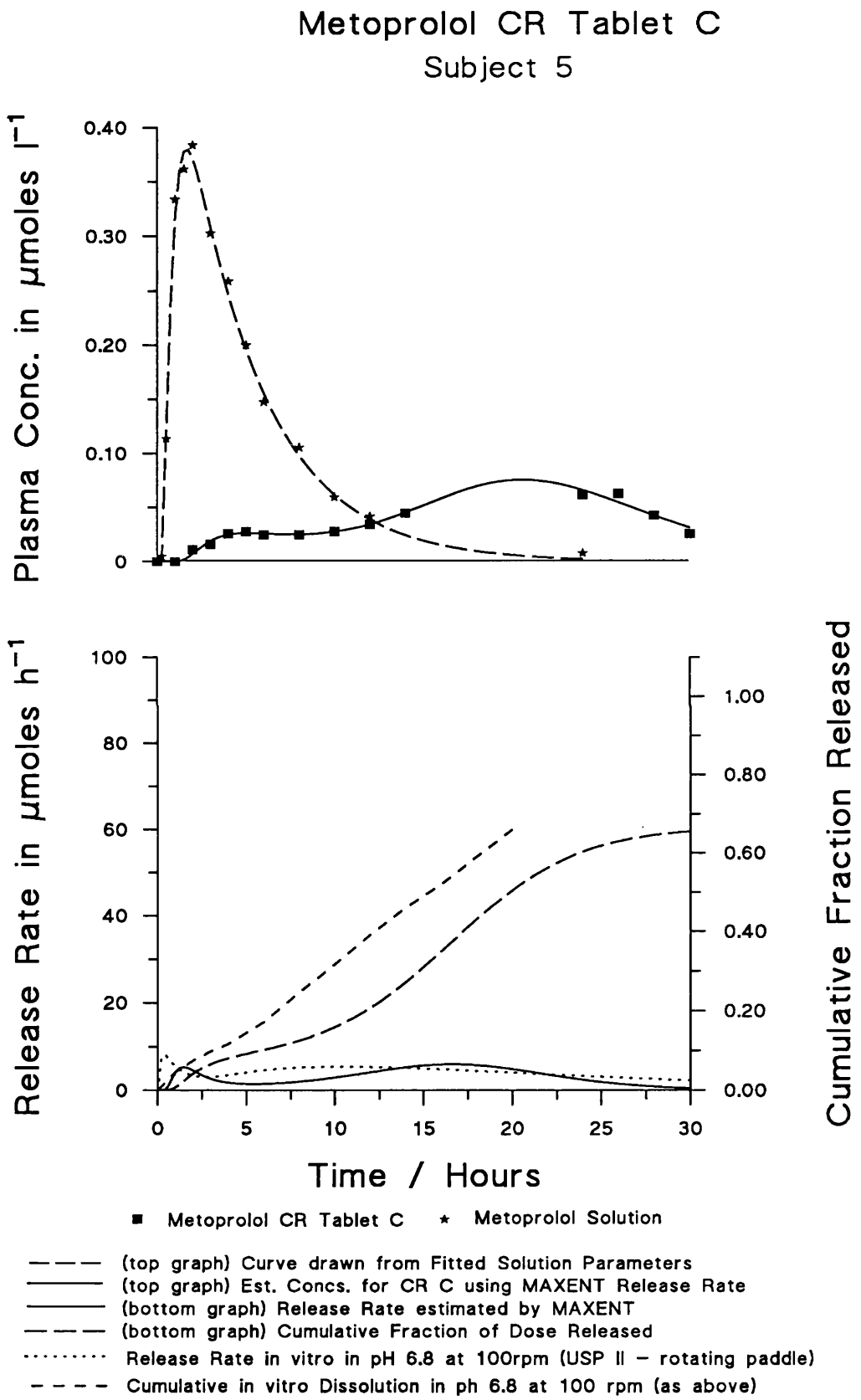


**Figure E.25** : Results from MAXENT for Metoprolol CR C, Subject 5

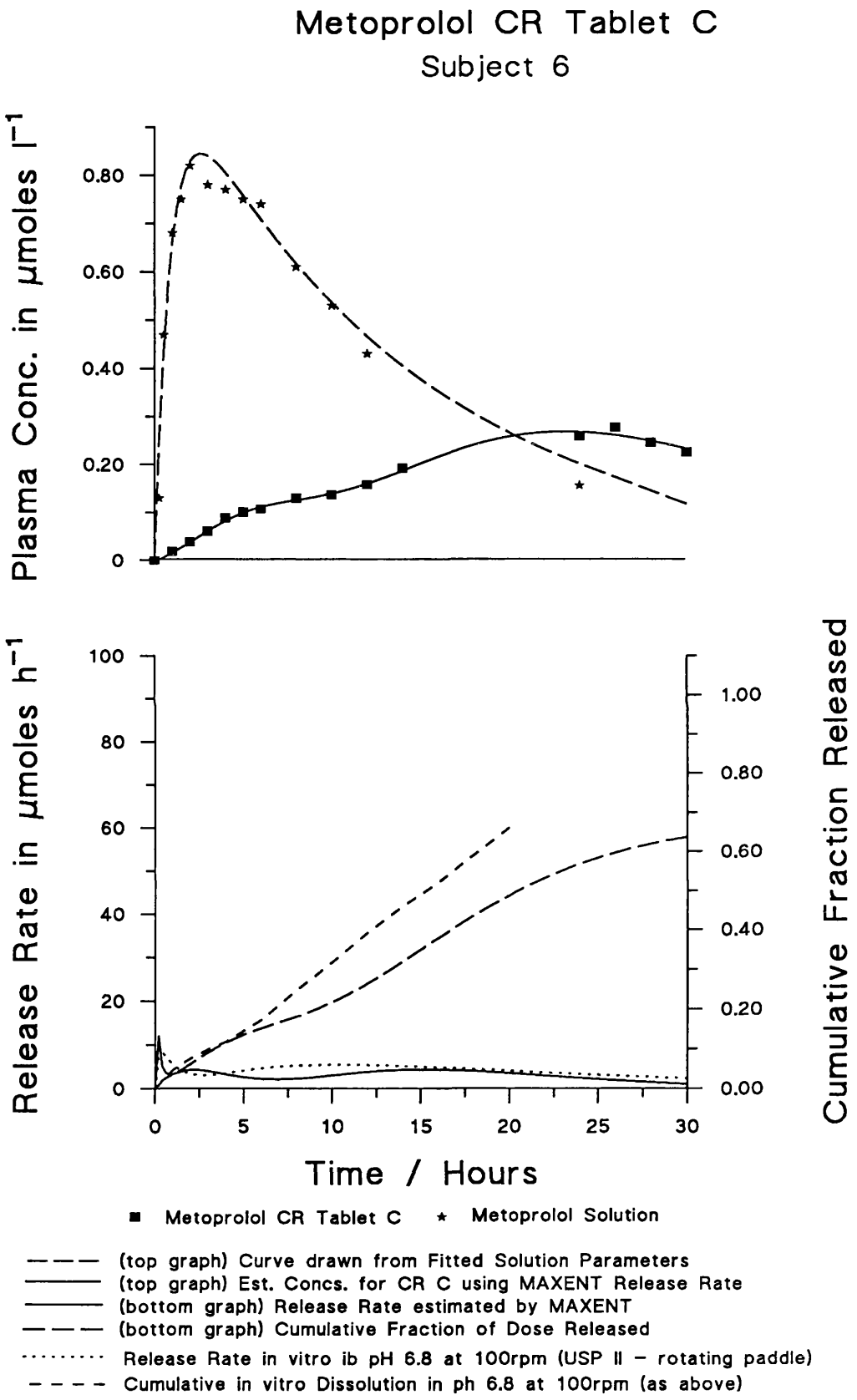


**Figure E.26** : Results from MAXENT for Metoprolol CR C, Subject 6

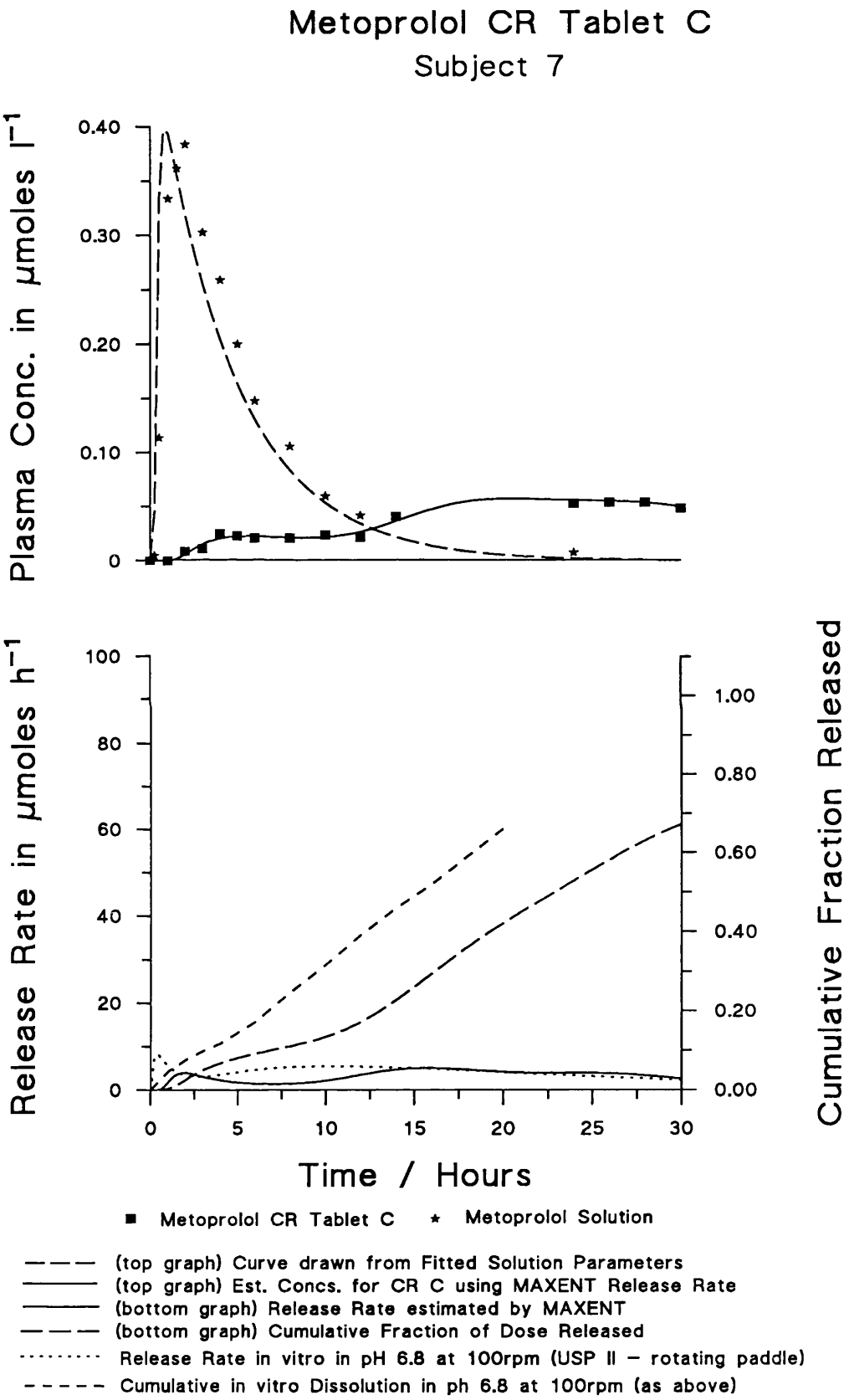


**Figure E.27** : Results from MAXENT for Metoprolol CR C, Subject 7

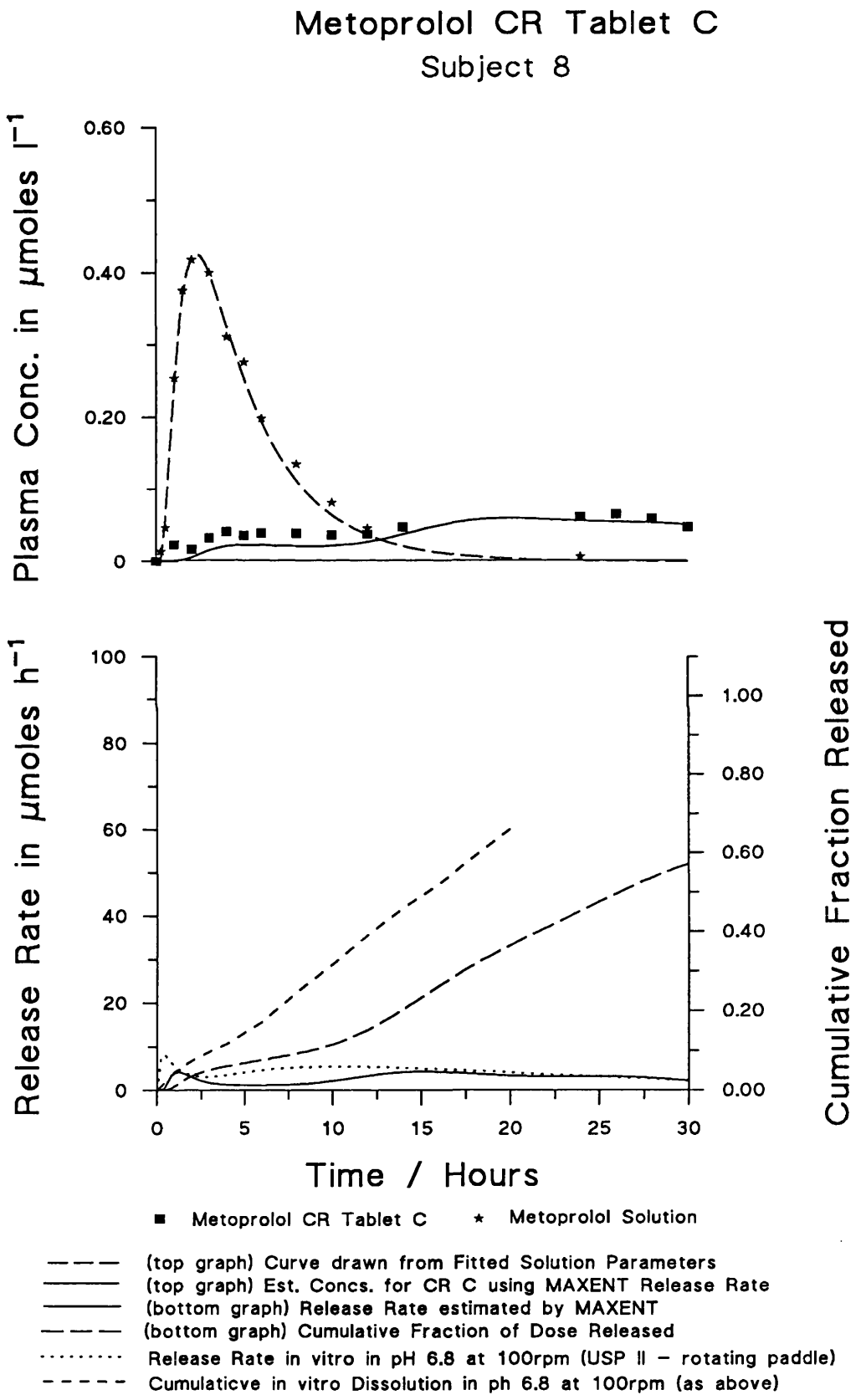


**Figure E.28** : Results from MAXENT for Metoprolol CR C, Subject 8

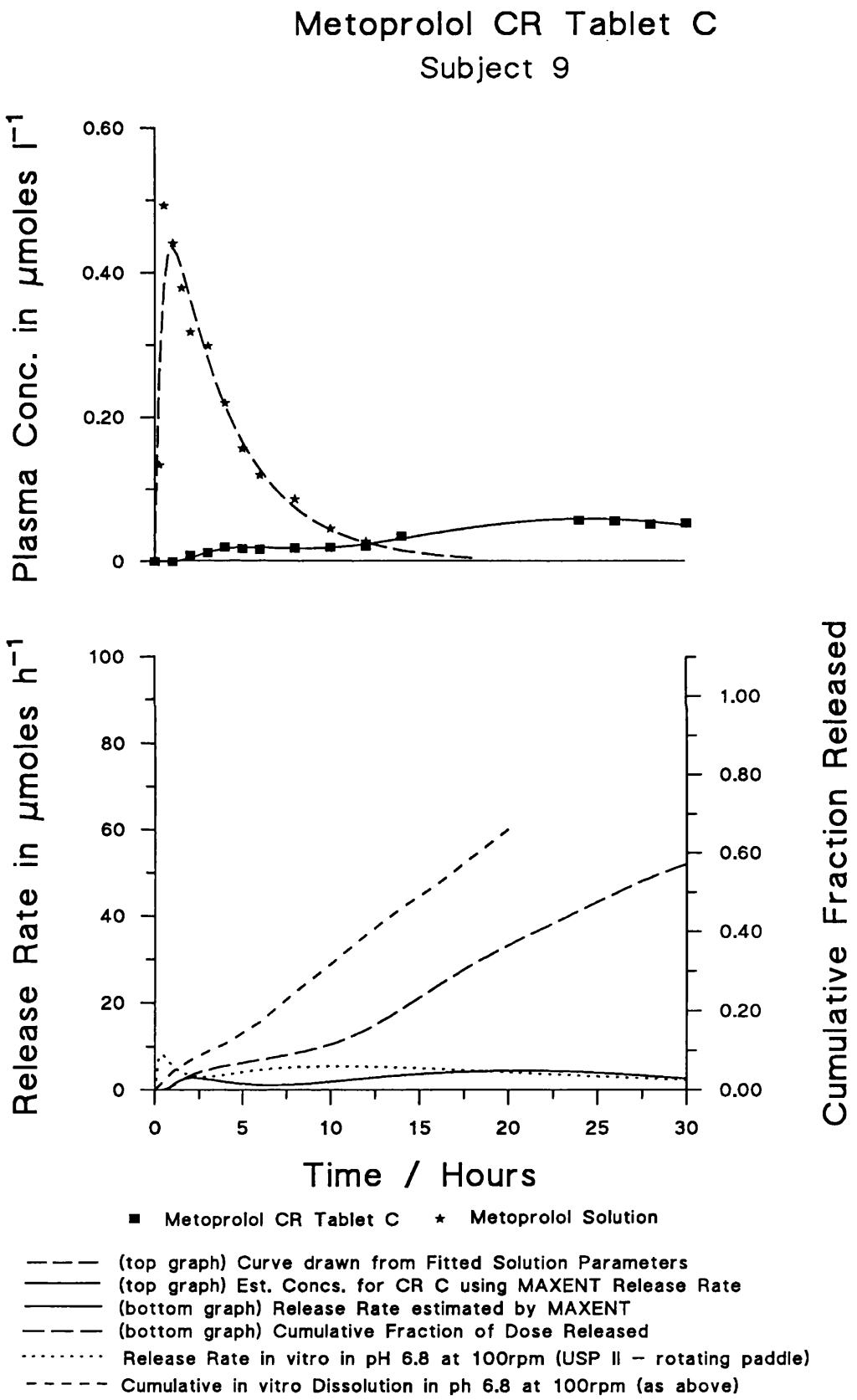


**Figure E.29** : Results from MAXENT for Metoprolol CR C, Subject 9

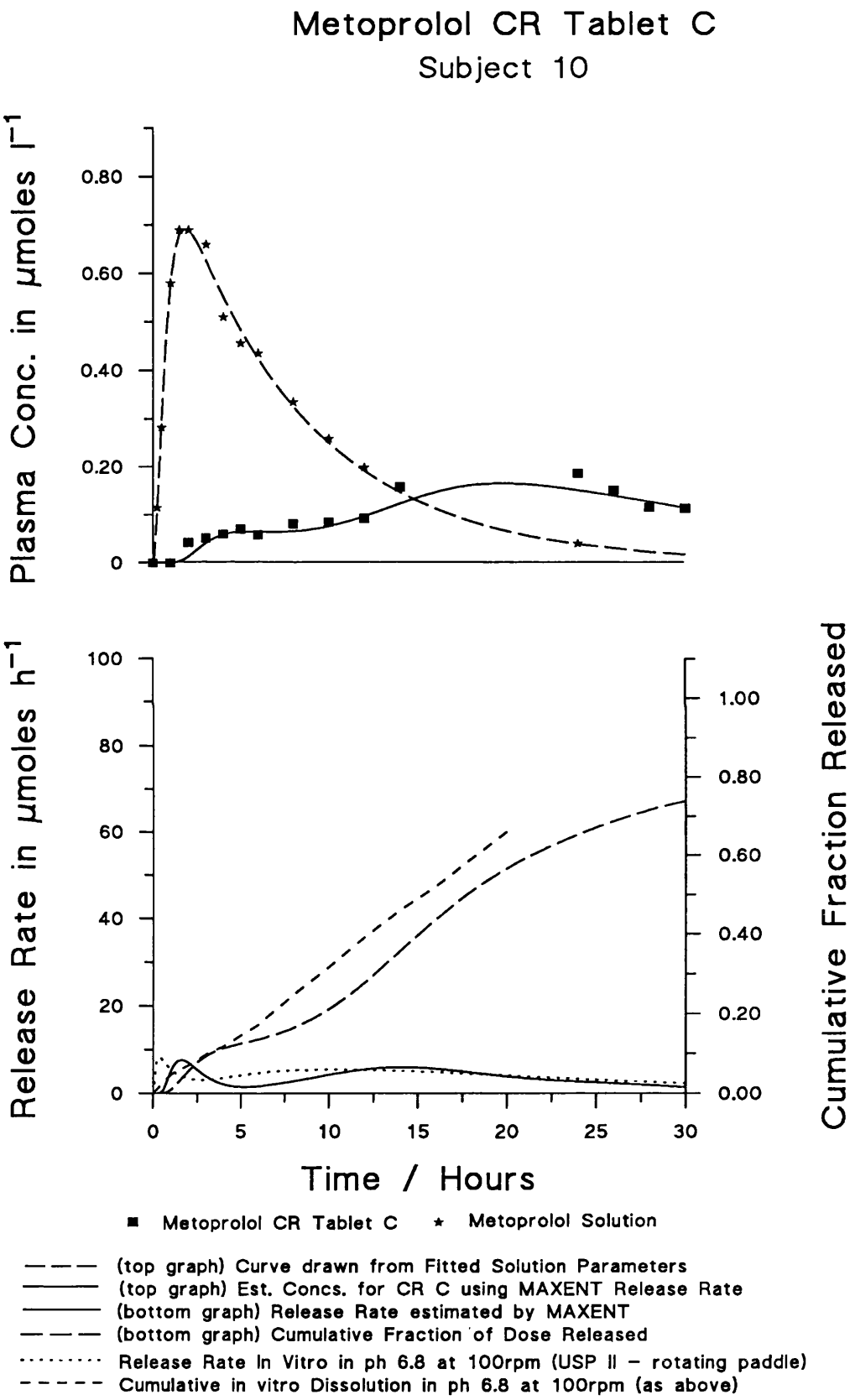


**Figure E.30** : Results from MAXENT for Metoprolol CR C, Subject 10